AN INVESTIGATION OF SCLERAL BIOMECHANICS AND MYOPIA IN THE MOUSE

A Dissertation
Presented to
The Academic Faculty

By

Dillon M. Brown

In Partial Fulfillment
of the Requirements for the Degree
Doctor of Philosophy in Bioengineering in the
Wallace H. Coulter Department of Biomedical Engineering

Georgia Institute of Technology

December 2022

AN INVESTIGATION OF SCLERAL BIOMECHANICS AND MYOPIA IN THE MOUSE

Approved by:

Dr. Machelle T. Pardue
Wallace H. Coulter Department of Biomedical Engineering
Georgia Institute of Technology and Emory University

Dr. J. Brandon Dixon
George W. Woodruff School of Mechanical Engineering
Georgia Institute of Technology

Dr. C. Ross Ethier
Wallace H. Coulter Department of Biomedical Engineering
Georgia Institute of Technology and Emory University

Dr. Wilbur A. Lam
Wallace H. Coulter Department of Biomedical Engineering
Georgia Institute of Technology and Emory University

Dr. Rafael G. Grytz
Heersink School of Medicine
University of Alabama at Birmingham

Date approved: August 10, 2022

To my family, Fiona, and friends.

ACKNOWLEDGMENTS

I would like to thank those who co-mentored me and supervised this dissertation - Machelle Pardue, who demonstrates an enviable mixture of conscientiousness, compassion, and drive to improve that tends to bring out the best in those around her, and Ross Ethier, with whom conversations were always incredibly thought provoking and formative to my own approach to problems. Without either of these two, the final product of this dissertation would be incredibly different. I would also like to thank the other members of my thesis committee for their help in preparation of this work – Rafael Grytz, whose work and writing inspired much of my own, Brandon Dixon, who helped to shed new light on many of my ideas, and Wilbur Lam, who offered a unique and important perspective to the project.

I was fortunate enough to collaborate with some incredibly talented and kind individuals on this highly disciplinary dissertation - Jay Patel, who was always eager to share his expertise, and Maureen Kane, whose knowledge and capabilities enabled much of this work.

Special thanks are, of course, due to the many friends and colleagues who made this work possible. Thomas Read, an incredibly skilled scientist and researcher. Bailey Hannon Gussler, with whom I shared many late nights in the lab. Andrew Feola, an invaluable source of feedback. I was fortunate enough to be involved in two great labs, so thank you Erica, Kelleigh, Reece, Katie, Rachael, Monica, Ryan, Pooja, Cara, Kyle, Mike, Stephen, Eric, and Babak for not only any direct contributions, but making the experience an enjoyable one.

The author gratefully acknowledges the support for this work offered by the NIH via the NEI T32 training grant (Grant no.). Any views and conclusions contained herein are those of the author, and do not necessarily represent the official positions, express or implied, of the funders.

TABLE OF CONTENTS

LIST OF TABLES

LIST OF FIGURES

LIST OF ACRONYMS

7-Mx 7-methylxanthine

AC adenyl cyclase

ACD anterior chamber depth

Ado adenosine

AdoR adenosine receptor

AL axial length

apoA-1 apolipoprotein A-1

ARVO Association for Research in Vision and Ophthalmology

atRA all-trans retinoic acid

BCLE biphasic conewise linear elastic

C-4-S chondroitin-4-sulfate

C-4-S chondroitin A

C-6-S chondroitin-6-sulfate

C-6-S chondroitin C

cAMP cyclic adenosine monophosphate

CC corneal curvature

CCT central corneal thickness

ChAC chondroitinase AC

ChB chondroitinase B

CLE conewise linear elasticity

CREAM Consortium for Refractive Error and Myopia

D diopters

DA dopamine

DAC dopaminergic amacrine cell

DAergic dopaminergic

DMMB 1,9-dimethylmethylene blue

DOPAC 3,4-dihydroxyphenylacetic acid

DRD1 dopamine receptor 1 gene

DS chondroitin B

DS dermatan sulfate

ECM extracellular matrix

ERG electroretinography

FD form-deprivation

FDM form-deprivation myopia

GAG glycosaminoglycan

GJD2 gap junction delta-2 protein

GLMM generalized linear mixed effects model

GWAS genome-wide association study

Hif-1α hypoxia-inducible factor 1-α

IHC immunohistochemistry

IMI International Myopia Institute

IOD interocular difference (treated - contralateral eye)

IOP intraocular pressure

LC-MS/MS liquid chromatography-tandem mass spectrometry

LIM lens-induced myopia

LT lens thickness

mRGC melanopsin retinal ganglion cell

OCT spectral domain optical coherence tomography

PBS phosphate-buffered saline

PG proteoglycan

PPAR peroxisome proliferator-activated receptor

R/C/S RPE, choroid, and sclera

RA retinoic acid

RALDH(1/2/3) retinaldehyde dehydrogenases

RAR retinoic acid receptor

RBP retinoid binding protein

RDH5 retinol dehydrogenase 5

RE refractive error

RGR retinal G protein-coupled receptor

ROL retinol

RORβ receptor-related orphan receptor β

RPE retinal pigment epithelium

RT retinal thickness

RXR retinoid-X receptor

sGAG sulfated GAG

SNP single nucleotide polymorphism

TBS-T tris-buffered saline with 0.1% Triton X-100

TGF-β transcription growth factor β

tRE total retinyl esters

UCT unconfined compression testing

VCD vitreous chamber depth

SUMMARY

The prevalence of myopia, or ”nearsightedness” is on the rise globally, set to affect about half of the global population by 2050. A myopic eye is characterized by a mismatch between the focal point of incoming light and the position of the photosensitive retina, most commonly due to excessive axial elongation of the eye (axial myopia). Axial myopia is thought to be driven by remodeling of the scleral microstructure and altered biomechanics. Certain types of visual cues drive or protect against myopigenic axial elongation, coupling retinal signaling to scleral remodeling via a complex ”retinoscleral” signaling cascade. However, the key signaling molecules that may propagate retinal signal(s) through the choroid to the sclera are largely unknown. All-trans retinoic acid (atRA) has been suggested to be both capable of trans-choroidal signaling and influencing scleral remodeling of glycosaminoglycans, biomechanically relevant extracellular matrix components known to change rapidly upon presentation of visual cues.

The mouse can be an excellent model organism for causal studies of myopigenesis, yet its small eye makes confirming axial elongation and scleral changes technically challenging. The central hypothesis of this work was that visual cues will lead to scleral remodeling and altered biomechanics comparable to other species. Additionally, we hypothesized that artificially increasing atRA concentration in the eye leads to a myopic phenotype.

To address these hypotheses, we developed a method to quantify the material properties of the mouse sclera using compression testing and a poroelastic material model, permitting the first characterizations of mouse scleral compressive/tensile stiffness and hydraulic permeability. In the mouse model of form-deprivation myopia, we then showed that the extensibility and permeability of the mouse sclera are greatly increased during myopigenesis, even without measurable axial elongation. We then characterized the ocular phenotype of mice treated with atRA, showing that atRA is myopigenic in the mouse and that scleral biomechanics are altered in a manner similar to that seen in visually mediated myopigene-

sis. These results implicate retinoic acid in the myopigenic retinoscleral signaling cascade and lay the groundwork for future studies of myopigenesis in the mouse.

Note: the bulk of this thesis document is made up of published/submitted papers, as follows:

- Section 1.2: **Brown, D. M.** et al. Candidate pathways for retina to scleral signaling in refractive eye growth. *Experimental Eye Research* 219, 109071 (2022).
- Chapter 3: **Brown, D. M.**, Pardue, M. T., & Ethier, C. R. A biphasic approach for characterizing tensile, compressive and hydraulic properties of the sclera. *Journal of The Royal Society Interface* 18, (2021).
- Chapter 4: **Brown, D. M.** et al. Altered structure and function of murine sclera in form-deprivation myopia. *Investigative Ophthalmology & Visual Science* (Accepted for publication; November, 2022).
- Chapter 5: **Brown, D. M.** et al. Exogenous all-trans retinoic acid induces myopia and alters scleral biomechanics in mice. *Investigative Ophthalmology & Visual Science* (In review; October, 2022).

CHAPTER 1

INTRODUCTION AND BACKGROUND

1.1 Myopia

1.1.1 Vision and Refractive Errors

Vision is a complex sensory process, relying on layers of highly networked neurons in the eye and the brain to process and perceive visual information. To enable high acuity vision, the eye must first capture well-focused light, a process dependent on the optical geometry of the eye. When the optics of the eye are tuned such that incoming light is refracted by the anterior eye to be focused precisely on the photosensitive retina in the posterior eye, the eye is in a state of emmetropia, i.e. is without refractive error (Figure 1.1a). If the position of the retina becomes discordant with the optical power, a refractive error is introduced that degrades visual acuity via a defocus aberration.

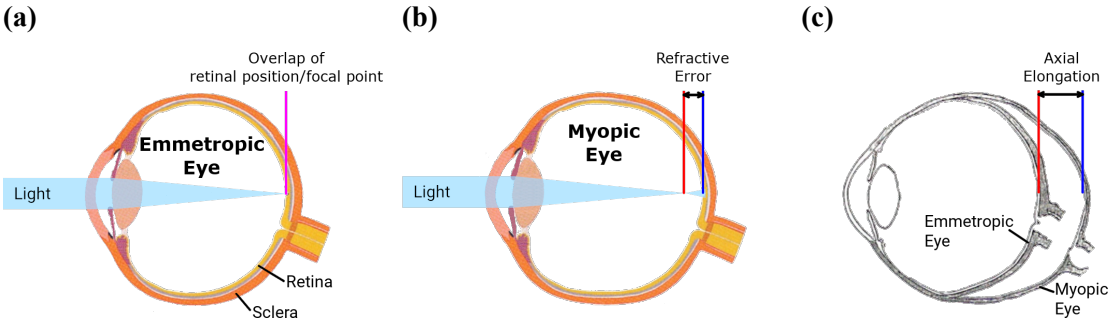

Figure 1.1: Comparison of emmetropia and axial myopia. (a) An emmetropic eye with no refractive error. Light refracted through the optical components (cornea, lens) is focused precisely on the retina. (b) An emmetropic eye with a negative or myopic refractive error. Light focuses in front of the retina and has diverged by the time it reaches the retina. (c) A comparison of a myopic and emmetropic eye from the same subject. Alignment of the eyes shows virtually no differences in the anterior eye. Image adapted from Grytz, 2018

Myopia is the refractive state in which the eye is ”too long” for its optics (Figure 1.1b). An eye can become myopic by erroneous development of the anterior tissues, e.g., developing an excessively steep cornea (keratoconus), and myopia that occurs in this manner has been termed ”refractive myopia”. However, the majority of myopia is not refractive in nature; it is instead due to excessive axial elongation of the eye and has thus been labeled ”axial myopia”[1](Figure 1.1c) (Flitcroft et al., 2019).

1.1.2 The Myopia Epidemic

The prevalence of myopia is rapidly approaching epidemic levels. The average axial length of the adult eye has been steadily increasing over the last 100 years (Figure 1.2a, Tideman et al., 2016). This increase is predicted to result in nearly 50% of the global population being classified as myopic by 2050 and an even higher prevalence in adults (Figure 1.2b, Holden et al., 2016). The burden of myopia is pernicious, and its magnitude is only recently being recognized. In no small part this is because it is a straightforward and mature practice to optically correct refractive errors, e.g., using powered lenses or manipulating of the corneal power. Optical corrections cannot be relied upon to combat the growing epidemic, despite the maturity of the practice. For one, optical approaches require access to individualized care and maintenance from specialists, infrastructure that is not present in many parts of the world. Even today, uncorrected myopia is the second most common cause of blindness (Holden et al., 2016) and has been estimated be responsible for losses in global annual productivity totaling ∼$202 billion USD in 2007 and ∼$244 billion USD in 2015 (Naidoo et al., 2019; Smith, Frick, et al., 2009).

[1]Throughout this body of work, ”myopia” will refer to ”axial myopia” unless otherwise specified.

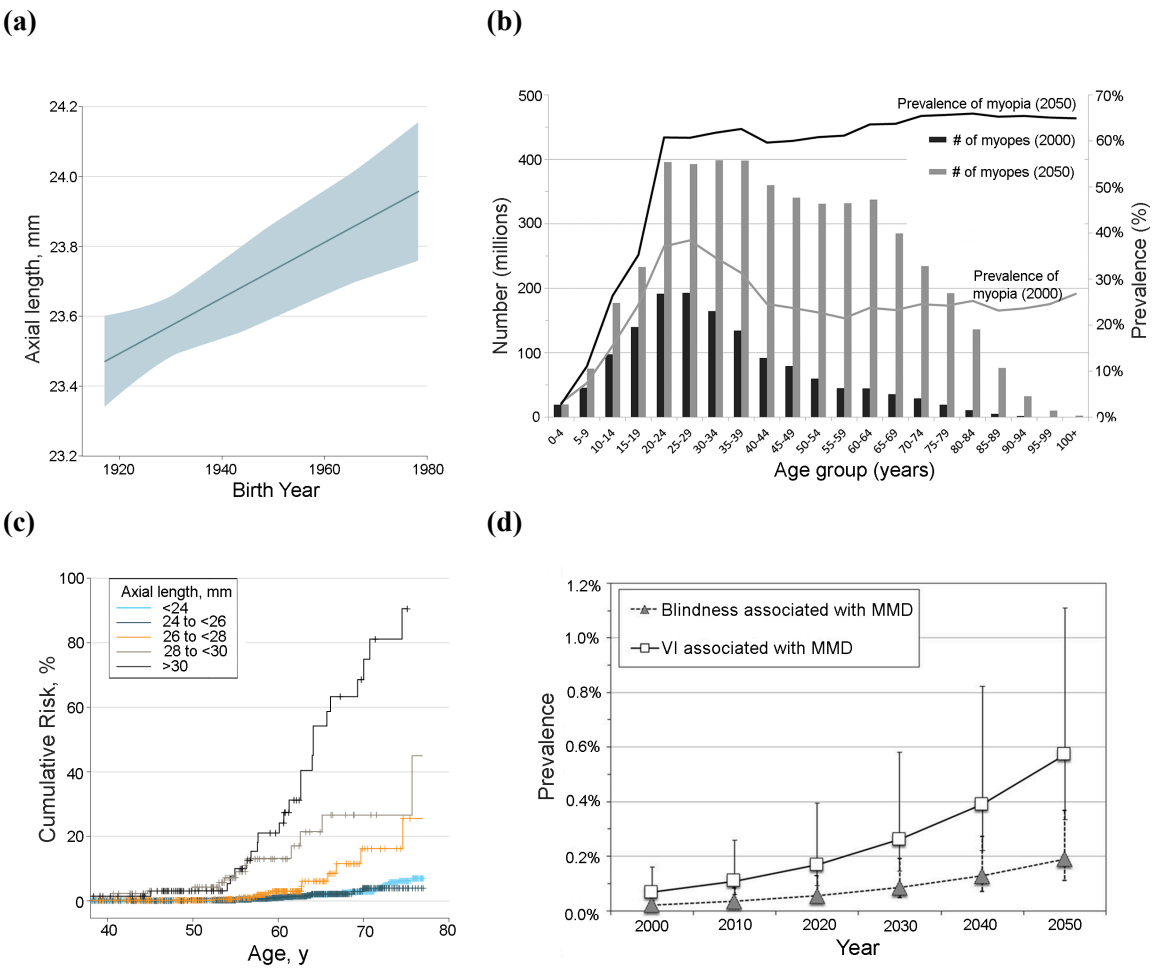

Figure 1.2: (a) Axial length of the adult eye has been increasing since at least the 1920s. Shaded region shows a 95% confidence interval. (b) The prevalence of myopia in nearly every age group is projected to increase over the next few decades, affecting more than half of the world by 2050. (c) Increased axial length is associated with higher risk of developing additional blinding disorders. (d) Number of people blinded or visually impaired (VI) from myopic macular degeneration (MMD) is estimated to significantly increase with myopia. Panels reprinted from (a,c) Tideman et al., 2016, (b) Holden et al., 2016, (d) Fricke et al., 2018.

Perhaps more importantly, optical approaches do not address the pathology underlying the refractive error, i.e., axial elongation, which appears to have broader implications for visual impairment. Increased size of the eye is broadly associated with greater risk of developing uncorrectable visual impairment or blindness (Figure 1.2c). In a large, cross-sectional study of ~16,000 people, visual impairment by 75 years of age was only found in

$\sim$4 % of eyes shorter than 26 mm, compared to 25 % in eyes 26 mm or greater and $>$90 % in eyes 30 mm or greater (Tideman et al., 2016). For instance, myopic macular degeneration, is estimated to increase the prevalence of visual impairment and blindness nearly 10-fold by 2050 (Figure 1.2d), impacting close to 100 million people (Fricke et al., 2018). Thus, it is critical to improve our understanding of the basic mechanistic pathways regulating the size of the eye to develop more effective interventions/treatments that can mitigate the projected global burden.

1.1.3 Animal Models of Myopia

Since Wiesel and Raviola reported the generation of experimental axial myopia in macaque monkeys (Wiesel & Raviola, 1977), animal models have become imperative to advancing our mechanistic understanding of myopia. An abundance of evidence has since accumulated supporting the existence of a homeostatic process coupling the size of the eye to visual cues, a process named ”emmetropization” (Troilo et al., 2019). This process has been demonstrated across a wide variety of species (fish, birds, and mammals) with many important features broadly conserved (Table 1.1; Schaeffel and Feldkaemper, 2015). Here I am going to highlight the most commonly used myopia model, the chicken, and compare it to the mouse model which is used in this thesis.

1.1.3.a The Chicken

The chicken has played an outsized role since it was introduced by Wallman, Turkel, and Trachtman (Wallman et al., 1978). Many findings central to our current understanding of myopia and emmetropization have been made in the chicken, such as the ability for visual

cues to cause axial elongation (Schaeffel et al., 1988) and that these cues are propagated locally within the eye from the retina to the sclera via a ”retinoscleral” signaling cascade (Troilo et al., 1987; Wildsoet & Pettigrew, 1988a). In Section 1.3, the role of the sclera is discussed as the endpoint of retinoscleral signaling, and it is clear that the sclera largely dictates the size of the eye.

The scleral regulation of eye size introduces issues with relying on results from avian species. The anatomy of the avian eye, and specifically the sclera, is quite different from that of human/mammalian eyes (Schaeffel & Feldkaemper, 2015). Mammals have a fibrous sclera primarily composed of collagen; the avian sclera is made up of both a fibrous and cartilagenous layer. In mammals, axial elongation results from scleral remodeling and thinning, whereas in chickens, the cartilagenous sclera grows, i.e., increases in volume (Gottlieb et al., 1990). Presumably stemming from these differences, some results in the chicken choroid and sclera are opposite that to those found in humans and other mammals, motivating the increased use of mammalian models.

1.1.3.b The Mouse

While there are disadvantages to mammalian models in studying mechanisms of myopigenesis compared to avian models, e.g., slower myopigenesis and less accurate emmetropization, the ocular anatomy is more representative of the human eye making findings more directly translatable. A disadvantage common to most models, mammalian or otherwise, is the inability to probe the genome, which has clear benefits for studying a complex signaling mechanism like myopigenic retinoscleral signaling.

The mouse is uniquely situated as a mammalian species in which signaling pathways can

be both probed with genetic precision and interpreted in a broad genomics context. While there are significant anatomical differences between the human and mouse eye, retinal signaling appears to be broadly conserved. The gestational period is short, allowing larger, cheaper, and faster studies in which both the environment and genome can be precisely manipulated to study genome-environment interactions (Pardue et al., 2013).

However, the small size of the mouse eye ($\sim$3 mm) introduces significant technical challenges not yet addressed. While evidence suggests that the mouse may develop myopia similarly to primates (Pardue et al., 2013; Tkatchenko et al., 2010), this is not yet settled. Visual cues have been reported to cause axial elongation, but inconsistently and with widely varying magnitudes (Pardue et al., 2013). Axial elongation is achieved via retinoscleral signaling, and many of the choroidal and scleral changes common to most other mammals have yet to be studied in the mouse (Table 1.1). Thus, despite its significant potential advancing our understanding of retinoscleral signaling, basic phenotypic characterization that is straightforward in other species and necessary to its adoption as a standard model has been slow in the mouse.

1.1.4 Summary

Our understanding of the mechanism of myopia eye growth have increased greatly over the last 50 years due to the use of experimental models of myopia. In the following sections, I review emmetropization and the potential retinoscleral signaling pathways involved in the process in detail, summarizing findings primarily from species other than the mouse (Section 1.2). I then discuss the scleral changes that occur with myopia (Section 1.3). Many of the unknowns surrounding the retinoscleral pathways and scleral remodeling could be

more directly explored in the mouse.

Table 1.1: Summary of major myopia findings and the species in which they have been confirmed. Findings confirmed in the mouse are bolded. Adaptation from Schaeffel and Feldkaemper, 2015.

Experimental Findings	Species
Visual cues influencing eye size:	
Form deprivation	Chick; tree shrew; guinea pig; **mouse**; marmoset; rhesus monkey; fish; rabbit; kestrel
Negative Lens	Chick; tree shrew; guinea pig; **mouse**; marmoset; rhesus monkey; fish
Positive Lens	Chick; tree shrew; guinea pig; marmoset; rhesus monkey
Local control of eye growth:	
Neurotoxins blocking retinal output or optic nerve cut	Chick; tree shrew
Locally-imposed defocus	Chick; tree shrew; guinea pig; marmoset; rhesus monkey
Factors influencing emmetropization to imposed defocus:	
Accommodation is not required	Chick; tree shrew
Accommodation has a role	Chick; tree shrew
Chromatic cues are necessary	**Mouse**; fish
Chromatic cues are not necessary	Chick; guinea pig
Signaling pathways/molecules involved:	
Dopamine	Chick; tree shrew; guinea pig; **mouse**; rhesus monkey
Egr-1/ZENK	Chick; tree shrew; **mouse**; rhesus monkey
Vasoactive peptide	Chick; tree shrew; guinea pig; rhesus monkey
Antimuscarinics	Chick; tree shrew; guinea pig; **mouse**; rhesus monkey
Retinoic acid	Chick; guinea pig; marmoset
Nitric oxide	Chick; tree shrew; guinea pig
Inhibition of myopia by high ambient illumination:	
Deprivation myopia	Chick; tree shrew; rhesus monkey
Lens-induced myopia	Chick; tree shrew; **mouse**; guinea pig; rhesus monkey
Choroidal thinning/thickening in response to imposed defocus	Chick; tree shrew; guinea pig; marmoset; rhesus monkey
Scleral metabolism changes in the fibrous sclera of myopic eyes:	
Thinning of the fibrous sclera	Chick; tree shrew; guinea pig; rhesus monkey; rabbit
Decreased proteoglycan synthesis	Chick; tree shrew; marmoset

1.2 Candidate pathways for retina to scleral signaling in refractive eye growth

Authors: **Dillon M. Brown**, Reece Mazade, Danielle Clarkson-Townsend, Kelleigh Hogan, Pooja M. Datta Roy, Machelle T. Pardue

Status: Published in *Experimental Eye Research* **219**, 109071 (2022)

1.2.1 Abstract

The global prevalence of myopia, or nearsightedness, has increased at an alarming rate over the last few decades. An eye is myopic if incoming light focuses prior to reaching the retinal photoreceptors, which indicates a mismatch in its shape and optical power. This mismatch commonly results from excessive axial elongation. Important drivers of the myopia epidemic include environmental factors, genetic factors, and their interactions, e.g., genetic factors influencing the effects of environmental factors. One factor often hypothesized to be a driver of the myopia epidemic is environmental light, which has changed drastically and rapidly on a global scale.

In support of this, it is well established that eye size is regulated by a homeostatic process that incorporates visual cues (emmetropization). This process allows the eye to detect and minimize refractive errors quite accurately and locally over time by modulating the rate of elongation of the eye via remodeling its outermost coat, the sclera. Critically, emmetropization is not dependent on post-retinal processing. Thus, visual cues appear to influence axial elongation through a retina-to-sclera, or retinoscleral, signaling cascade, capable of transmitting information from the innermost layer of the eye to the outermost layer.

Despite significant global research interest, the specifics of retinoscleral signaling path-

ways remain elusive. While a few pharmacological treatments have proven to be effective in slowing axial elongation (most notably topical atropine), the mechanisms behind these treatments are still not fully understood. Additionally, several retinal neuromodulators, neurotransmitters, and other small molecules have been found to influence axial length and/or refractive error or be influenced by myopigenic cues, yet little progress has been made explaining how the signal that originates in the retina crosses the highly vascular choroid to affect the sclera.

Here, we compile and synthesize the evidence surrounding three of the major candidate pathways receiving significant research attention — dopamine, retinoic acid, and adenosine. All three candidates have both correlational and causal evidence backing their involvement in axial elongation and have been implicated by multiple independent research groups across diverse species. Two hypothesized mechanisms are presented for how a retina-originating signal crosses the choroid — via 1) all-trans retinoic acid or 2) choroidal blood flow influencing scleral oxygenation. Evidence of crosstalk between the pathways is discussed in the context of these two mechanisms.

1.2.2 Introduction

Myopia, commonly known as “nearsightedness”, describes a mismatch between an eye’s optical power and its geometry where the eye is too long for its optics. This mismatch results in light focusing in front of the retina instead of directly on it (i.e., a refractive error) and is typically the result of excessive axial elongation of the eye rather than improper development of optical power (Flitcroft et al., 2019). While myopic refractive errors are commonly treated by correcting the optical power of the eye via spectacles or contact lenses, these opti-

cal interventions do not slow axial elongation or myopia progression (Wildsoet et al., 2019). In the United States, myopia prevalence increased from about 25% in 1970 to 40% in 2000 (Vitale et al., 2009), and in Singapore, myopia reportedly affects more than 80% of young adults (Morgan et al., 2012). Predictions estimate that about 50% of the global population will be myopic by 2050 unless more effective preventative interventions or treatments of the underlying biological cause are identified (Holden et al., 2016). With excessive elongation being a risk factor for many additional sight-threatening disorders (Grytz et al., 2020), this epidemic requires additional study of the mechanisms of myopigenesis to develop interventions capable of resolving the underlying biological mismatch.

The rapid rise in prevalence is thought to be real, not due to increased identification, and driven primarily by environmental factors rather than drifting population genetics (Dolgin, 2015; Goldschmidt & Jacobsen, 2014; Vitale et al., 2009). While polygenic risk scores obtained from genome-wide association study (GWAS) can be modestly predictive for severe myopia, they do not perform well for mild and moderate myopia (Ghorbani Mojarrad et al., 2020), which make up the vast majority of cases. Instead, the pathogenesis of myopia is thought to be environmentally driven by "myopigenic" cues, a hypothesis dating back to at least the late 16th century, when near work was first proposed as causing myopia (de Jong, 2018). In the last century, the types of environmental visual cues presented to an eye during adolescence have been found to be highly influential over its mature size, with the homeostatic process linking vision and eye size being termed emmetropization (Troilo et al., 2019). Thus, the global increase in myopia throughout the 20th century occurring during a period of increasing urbanization and widespread adoption of artificial electric lighting is likely not coincidental. Indoor environments are known to contain very differ-

ent visual cues than outdoor, natural environments, e.g., different luminance, spatial, and spectral properties (Flitcroft et al., 2020; French et al., 2013).

The rise in time spent indoors and in urban environments is a likely driver of the myopia epidemic (Flitcroft, 2013), supported by the often-repeated finding that increasing time spent outdoors displays protective effects against myopigenesis. A study of monozygotic twins in the United Kingdom (n=64 pairs), where each pair had a $\geq$2 diopters (D) difference in refractive error between them, found that the less myopic of the pair tended to spend more time outdoors or doing outdoor sports, while the more myopic individuals more often lived in an urban area, performed more near work, and had greater professional status (Ramessur et al., 2015). Other studies have shown that children who spent more time outdoors (assessed via questionnaire or objective light measurement) showed modest, but significant, slowing of myopia progression (Jin et al., 2015; Read et al., 2014; Rose et al., 2008; Wu et al., 2013). The protective effect also appears to be quite variable. A study of monozygotic twins in China (n=490 pairs) found that near work and time outdoors only explained roughly 3% of the discordance in refractive error between twins (Ding et al., 2018). These discrepancies could possibly be explained by low sensitivity of questionnaire data for exposure measurements; however, it is also possible that variation in outdoor visual environments (outdoors in a city around buildings versus outdoors in a forest) and/or genetic factors that influence susceptibility to myopigenic cues could influence the amount of protection conferred.

Significant progress has been made in not only identifying myopigenic/protective visual cues, but also interventions capable of slowing myopigenesis, including optical, behavioral, and pharmacological methods (Smith & Walline, 2015; Wildsoet et al., 2019). Despite this,

our understanding of the signaling mechanisms underlying myopigenesis is still limited. This is exemplified with the clinical use of topical atropine; atropine has been the most common pharmacological intervention for myopia control for over a century now, yet little consensus has been reached regarding its mechanism of action in the eye (Galvis et al., 2016; Mathis et al., 2020; Upadhyay & Beuerman, 2020).

Nevertheless, much has still been learned about general characteristics and requirements of myopigenic signaling. The mature eye size is influenced by visual cues detected by the retina. Remodeling of the sclera, the white outermost layer of the posterior eye, is causal to modulating eye size and occurs during myopigenesis (Boote et al., 2020; Grytz, 2018). The signaling does not appear to require post-retinal processing of the visual stimulus and thus is largely contained to the posterior eye wall (McFadden & Wildsoet, 2020; Norton et al., 1994; Troilo & Wallman, 1991; Troilo et al., 1987; Wildsoet & Wallman, 1995; Wildsoet & Pettigrew, 1988b; Wildsoet, 2003). Myopigenic visual cues presented to the retina therefore result in a signal, likely chemical in nature (e.g., signaling molecules), capable of 1) propagating across the retinal pigment epithelium (RPE) and vascular choroid and 2) influencing remodeling processes in the sclera. How environmental visual cues interact with genetics to induce myopigenesis in some people but not others and what molecules are involved in the retina-to-sclera (retinoscleral) signaling pathways are currently open questions and the subject of active research (de Jong, 2018; Dirani et al., 2009; Huang et al., 2015; Jones-Jordan et al., 2012; Rose et al., 2008).

This review aims to summarize and contextualize recent findings related to a subset of signaling molecules and pathways (dopamine, retinoic acid, and adenosine), as opposed to serving as a fully comprehensive review of every molecule involved in retinoscleral sig-

naling (for a broader review, see (Summers et al., 2021)). These signaling pathways were selected as the most likely to directly regulate myogenesis due to each having been correlated with and causally linked to axial length and myopia numerous times across many different research groups and species. Additionally, each has been suggested to act in multiple tissues throughout the retinoscleral cascade.

1.2.3 Emmetropization and homeostasis of eye size

The size of a mature eye is determined by a combination of growth and elongation, both of which appear to involve the sclera. Here, growth is defined as an increase in scleral tissue volume, which leads to an overall increase in ocular dimensions. In contrast, axial elongation is a process that modulates the axial length of the eye without increasing scleral tissue volume, which in mammals is believed to be determined primarily by remodeling of the sclera (Lim et al., 2011). This remodeling includes both the reorganization of existing tissue components (primarily collagen) and altered synthesis/degradation of others (collagen and proteoglycans/glycosaminoglycans). During remodeling, the sclera is more extensible, permitting elongation with either no change or a small decrease in overall volume (Backhouse & Gentle, 2018) and leading to a thinner sclera (for recent reviews, see Boote et al., 2020; Grytz, 2018).

In the human prenatal period, eye size increases rapidly via growth, closely matching the general growth curve of the body (Mutti et al., 2005; Watanabe et al., 1999). Upon birth, infants typically have mismatches in the power and geometry of their eyes (i.e., refractive errors), biased towards the eyes being too short for their optical power, a state termed hyperopia (Chakraborty et al., 2020; Mutti et al., 2005; Watanabe et al., 1999). Growth of the

eye may only occur for about two years (Shen, You, et al., 2016); however, eyes continue to elongate for many years, initially quite rapidly but slowing exponentially, reaching mature size around the teenage years (Fledelius & Christensen, 1996; Fledelius et al., 2014). By the age of 6, significant emmetropization of the population has generally occurred (characterized by a significant decrease in variance of refractive errors) (Chakraborty et al., 2020); however, eyes that will continue on to be emmetropic later in life are still on average hyperopic by about 1 diopter (Figure 1.3). The remaining hyperopic refractive errors are corrected over the next decade while the eye continues to elongate and the optical components mature (Gordon & Donzis, 1985; Hagen et al., 2019; Jones et al., 2005; Mutti et al., 2005). Thus, throughout the first nearly two decades of life, eye development occurs in a complex yet highly coordinated manner, evidenced by the fact that only a minority (albeit a rapidly growing one) develop signififcant refractive errors.

The homeostatic process responsible for this coordinated development is called emmetropization, and it appears to function via controlling the rate of axial elongation. Emmetropic eyes can properly coordinate their rate of axial elongation such that the length of the eye matches the optical power and results in little to no refractive error. In most adult human populations, emmetropes are overrepresented, leading to a non-Gaussian leptokurtic distribution of refractive errors (Figure 1.3B,C) (Flitcroft, 2013). While refractive errors follow a mostly Gaussian distribution at birth and through early adolescence (Flitcroft, 2013), the number of myopes continue to increase. These statistical features, among others, reflect a tightly controlled homeostatic mechanism that is now understood to incorporate visual signals, primarily, blur.

Interestingly, many features that differ between indoor and outdoor visual environments

have been demonstrated to be disruptive to achieving or maintaining emmetropia (for in-depth review see (Lingham et al., 2020; Norton, 2016; Rucker, 2019; Schaeffel & Feldkaemper, 2015)). Sunlight is significantly brighter than most indoor environments, and this increased luminance has been shown to be protective in chicks (Ashby et al., 2009; Ashby & Schaeffel, 2010; Chen et al., 2017), tree shrews (Norton & Siegwart, 2013), guinea pigs (Li et al., 2014), and macaques (Smith et al., 2013; Smith et al., 2012) compared to typical indoor lighting. Additionally, emmetropic children have been observed to spend more time in these bright light levels (Read et al., 2014). However, a recent re-analysis of the study by Read et al. found that children with myopia spent less time in both bright and dim light (Landis et al., 2018), and both luminance conditions were demonstrated to be protective in mice (Landis et al., 2021). Additionally, when chicks were exposed to sunlight daily, they had shorter myopic axial elongation (Ashby et al., 2009), but when they were reared outdoors, acute myopic protection did not last (Stone et al., 2016).

Sunlight also contains a broader spectrum of wavelengths than indoor light, including a larger proportion of shorter wavelengths (Krutmann et al., 2014; Thorne et al., 2009). Visual stimulation with violet light slowed myopia progression in human clinical studies (Torii et al., 2017), and short-wavelength light protected mice (Jiang et al., 2021; Strickland et al., 2020), guinea pigs (Yu et al., 2021), and chicks (Torii et al., 2017; Wang et al., 2018) from induced myopia. However, in tree shrews and rhesus monkeys, long-wavelength red light was protective, suggesting potential species differences (Gawne et al., 2017; Smith et al., 2015; Ward et al., 2018).

The protective effect of the outdoors could also be related to the spatial frequency content of the environment since outdoor environments contain more mid-level ($\sim$10cpd) and

higher spatial frequencies than artificial environments (Flitcroft et al., 2020). Manipulating the visual experience to degrade (Howlett & McFadden, 2006; Norton & Rada, 1995; Pardue et al., 2013; Shen et al., 2005; Troilo & Nickla, 2005; Wallman et al., 1978) or reduce mid-high spatial frequencies leads to axial elongation in chicks (Bartmann & Schaeffel, 1994; Tran et al., 2008), guinea pigs (Bowrey et al., 2015), mice (Pardue et al., 2008), and monkeys (Smith & Hung, 2000), and evidence exists that extends this effect to humans. Adolescents with cataracts, which significantly reduce sensitivity to high spatial frequencies (Lewis & Maurer, 2005), often develop severe myopia (He et al., 2017). More directly, it has recently been shown that movies carefully low-pass filtered to match spatial frequency spectra of imposed optical defocus can acutely influence axial length in emmetropic and myopic humans (Swiatczak & Schaeffel, 2021). Thus, axial blur, luminance, chromaticity, and spatial frequency content have all been demonstrated to be myopigenic cues. Most animal studies of myopia impose one or more of these visual cues on the animal, commonly axial blur via powered lenses (lens-induced myopia (LIM)) or diffuser goggles (form-deprivation myopia (FDM)).

Myopic eyes have failed to either properly emmetropize or maintain emmetropia, and it is now well established that these failures cannot be traced back to a single source. The variable age of myopia onset in adolescents and the much larger variance in the distribution of refractive errors in myopic populations (Flitcroft, 2013) (Figure 1.3) supports many distinct origins of a disrupted homeostatic process. Visual environments contain many types of myopigenic visual cues, some of which may drive myopigenesis to differing degrees. However, the retinal circuitry used to sense these cues is highly complex, involving many distinct cell types and signaling pathways and thus has many points at which one's genetics

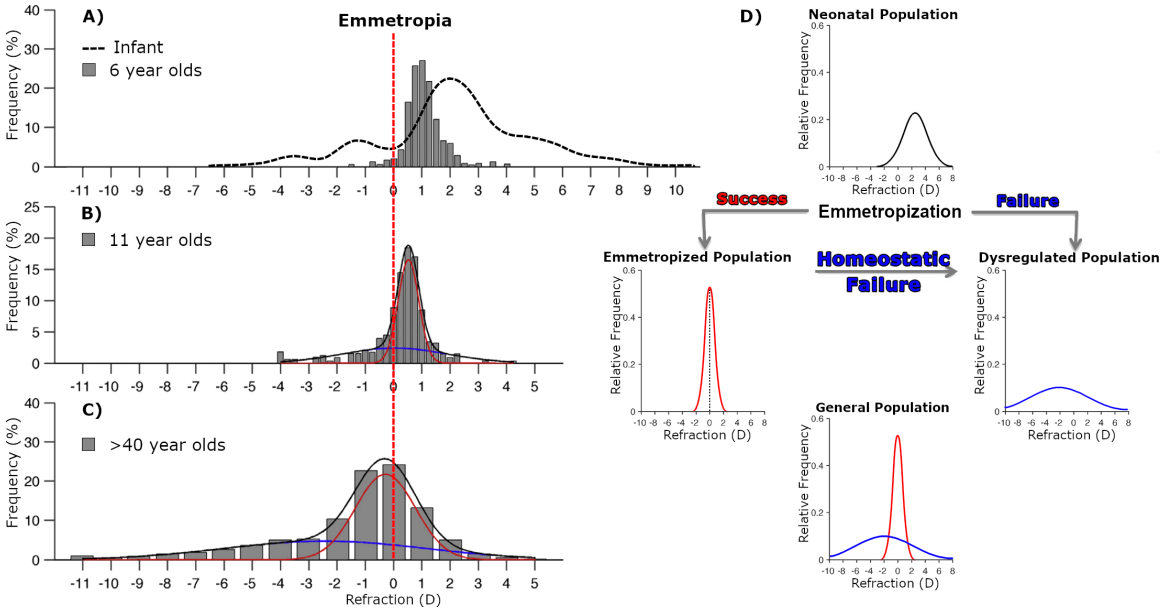

Figure 1.3: Population distributions of refractive error development. Vertical red dashed line indicates no refractive error. A) Infant populations approximately Gaussian distributions of refractive error, the majority hyperopic on average (dashed line). By age 6, emmetropization has reduced the variance. (B,C) As populations age, refractive errors become increasingly leptokurtic and can be well described by fitting two separate Gaussian distributions, representing properly emmetropized (red) and dysregulated (blue) populations. D) Hypothetical paths of refractive development. Dysregulated populations could be explained by a combination of failure to initially emmetropize (A), or failure maintain emmetropia (B,C). Modified from Flitcroft, 2013 and Chakraborty et al., 2020.

could drive myopia or influence susceptibility to myopigenic cues.

While many genetic abnormalities have been demonstrated to disrupt emmetropization and confer a degree of heritability to myopia (with estimates ranging from 15% to 98%) (Tedja et al., 2019), the types and durations of visual cues presented to the eye appear especially critical to emmetropization and its maintenance. Thus, it is important to study the mechanisms by which these myopigenic cues signal to increase axial elongation.

1.2.4 Retinoscleral signaling

In mammals, myopigenic visual cues appear to influence eye size primarily by increasing the rate of axial elongation through altering scleral remodeling (Troilo et al., 2019),

as opposed to the avian model in which the cartilaginous layer of the sclera grows. The influence of visual cues on the sclera occurs quite locally — myopigenic visual cues can influence eye size unilaterally (if only one eye is presented the stimulus), without a functioning connection to the visual cortex (Norton et al., 1994; Troilo et al., 1987; Wildsoet & Pettigrew, 1988b; Wildsoet, 2003), and regionally within an eye (if presented a spatially nonuniform myopigenic stimulus, e.g., hemi-diffusers) (Diether & Schaeffel, 1997; Norton & Siegwart, 1995; Smith et al., 2014; Smith, Huang, et al., 2009; Smith et al., 2010; Wallman et al., 1987). Thus, the retina senses and encodes visual cues and initiates a signaling cascade that propagates to regions of the sclera located posterior to the region of the retina that sense the cue, ultimately leading to scleral remodeling and modulation of eye size.

While this general framework for retinoscleral signaling is well supported, the specifics of the process are still unknown. Many types of retinal signaling molecules and pathways have been associated with myopigenesis, and the signaling dynamics of some have been studied in detail (most notably, dopamine). However, efforts to incorporate retinal research into a pathway spanning the entire ocular wall have been much less successful. Additionally, different myopigenic cues may have differing retinal mechanisms, evidenced by retinal interventions that protect against lens-induced myopia but not form-deprivation (or vice versa) (Bitzer et al., 2000; Dong et al., 2011; Wang et al., 2014). However, there is no evidence to date showing different myopigenic cues result in different outcomes in scleral remodeling. Thus, various types of retinal signaling may converge at or before the choroid, resulting in a graded signal that combines various myopigenic cues and determines if the eye will increase, maintain, or slow its axial elongation (sometimes referred to as a GO, STAY, STOP signal (Guo et al., 2019)).

In the following sections, we focus on the roles and influence of dopamine, retinoic acid, and adenosine in myopigenesis (Figure 1.4). While these represent only a subset of the many signaling molecules reported in the literature, we focus on these three due to 1) robust reports of causal influence on and correlations with refractive development, 2) localization of the signaling molecule/receptor in multiple ocular tissues, 3) evidence from a variety of species (especially mammalian), and 4) corroboration by multiple independent research groups. While little direct evidence currently exists linking these three pathways in the eye, we suggest that these pathways likely represent key components of the signaling cascade that warrant future study. Additionally, two possible points of signal convergence are discussed alongside supporting evidence.

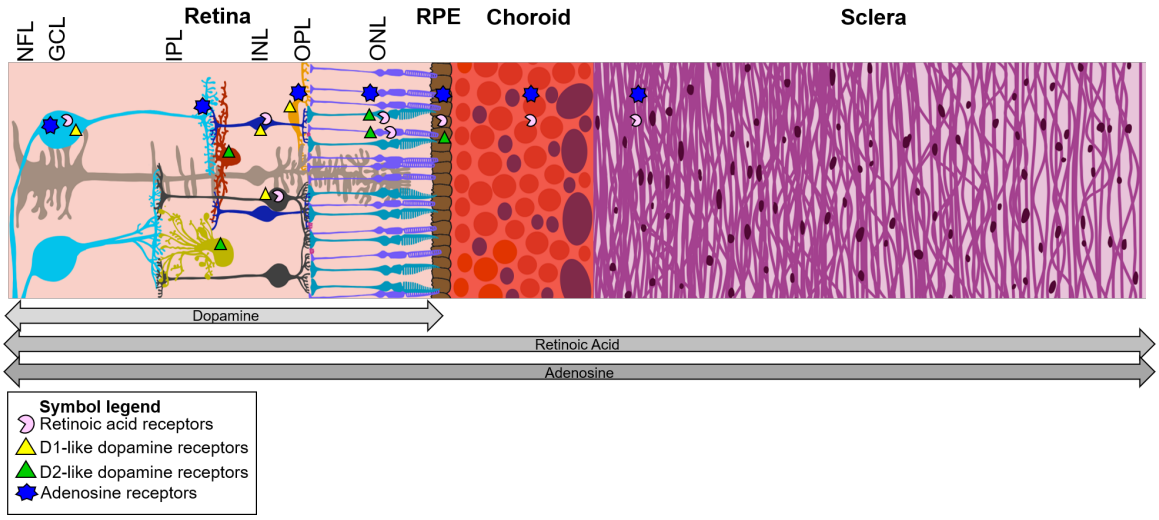

Figure 1.4: Cartoon representation of the human posterior eye wall and the path of a hypothetical retinoscleral signal. Arrows below the diagram signify where each molecule has been implicated as a potential signaling molecule. The proportions of each layer are approximately to scale. NFL: nerve fiber layer, GCL: ganglion cell layer, IPL: inner plexiform layer, INL: inner nuclear layer, OPL: outer plexiform layer, ONL: outer nuclear layer, RPE: retinal pigment epithelium.

1.2.4.a Dopamine (DA)

The role of retinal dopamine (DA) in myopigenesis has been an active area of research for the last 30 years since the first report that DA may link visual signals with myopic axial elongation (Stone et al., 1989). In this report, Stone and colleagues discovered that levels of DA and its metabolite, 3,4-dihydroxyphenylacetic acid (DOPAC), were significantly reduced in retinas of chickens with experimental myopia (FDM or LIM). This study suggested that retinal dopaminergic (DAergic) signaling could be a principal modulator of myopic changes in the retina. Since then, extensive effort has been spent investigating DAergic signaling (Table 1.2), mostly through measurements of DA and its metabolites, in retinas of myopic eyes or those exposed to myopigenic stimulus (for a recent in-depth review, see Zhou et al., 2017). In this section, we will present evidence for DA as the starting point for the retinoscleral signaling cascade that leads to myopic axial elongation.

1.2.4.a.1 Dopamine signaling pathway

Retinal DA is produced and released by a subset of dopaminergic amacrine cells (DACs) that are sparsely tiled across the retina (Witkovsky, 2004). Despite their low numbers, DACs have long dendrites that can span millimeters of the retina and can extend from the inner plexiform layer to the outer plexiform layer and ganglion cell layer (Witkovsky, 2004). DA can act through local synaptic release from DAC varicosities and dendritic spines (Dacey, 1990) or extra-synaptically through paracrine diffusion (Puopolo et al., 2001) across the retina to activate multiple types of postsynaptic and extra synaptic receptors. DA receptors are located on almost all retinal cells and fall into two families, D1-like

	C.1	C.2	C.3	C.4			C.5	C.6	
	Visual Cue	*Effect*	*Outcome*	*Retina (+)*			*RPE (+)*	*Choroid (-)*	
A) Endogenous	A1) FD/NL	↑ *Elongation*	Conc.	↓ Conc.	No effect		No effect		
			Synth.	↓ Synth.	No effect				
			Receptor	No effect			↓ Expr.		
	A2) *Rec/PL*	↓ *Elongation*	Conc.	↑ Conc.					
			Synth.	↑ Synth					
			Receptor						
	Drug Delivery	*Signaling*	*Outcome*	*Intravitreal*			*Oral/Gavage/ IP*	*Subconj./ Topical*	
B) Exogenous	B1) *Molecule/ Precursor*	↑ *Signaling*	Axial Length	↓ AL			↓ AL	↓ AL	
	B2) *Reuptake Inhibitor*	↑ *Signaling*	Axial Length	↓ AL					
	B3) *Receptor Agonist*	↑ *Signaling*	Axial Length	↓ AL	No effect		↓ AL	↓ AL	No effect (With NL)
	B4) *Synthesis Inhibitor*	↓ *Signaling*	Axial Length	↓ AL (Ablated DACs)	No effect				
	B5) *Receptor Antagonist*	↓ *Signaling*	Axial Length	↓ AL & Blocks agonist	No effect	↑ AL	No effect	↓ AL & Blocks agonist	
	Gene Knockout	*Signaling*	*Outcome*	*Retina-KO*			*RPE-KO*	*Nonspecific-KO*	
C) Genetic	C1) *mGluR6*$^{-/-}$	↔ *DA* ↓ *DOPAC*	Axial Length	↑ AL					
	C2) *rTH-KO*	↓ *DA* ↓ *DOPAC*	Axial Length	↑ AL					
	C3) *D2R-KO*	↓ *Signaling*	Axial Length					↓ AL	
	C4) *D1R-KO*	↓ *Signaling*	Axial Length					No effect	
	C5) *Vsx1*$^{-/-}$	↑ $\frac{DOPAC}{DA}$	Axial Length	No effect					

Table 1.2: **Potential of dopamine to be a retinoscleral signal in refractive eye growth.** Column C.1: Treatments given to animals. C.2: General description of main effect of treatment. Columns C.3-6: Additional outcomes (C.3) studied with corresponding treatments. In A) Endogenous, C.4-6 are locations of measurements, and (±) represent whether receptors are expressed. In B) Exogenous and C) Genetic, C.4-6 are different locations of the treatment. Cells are shaded to highlight trends. Orange/blue shading indicate an increase/decrease in signaling or elongation. Gray indicates inconclusive or no effect. Table cells are split when studies came to different conclusions. AL: Axial Length, Conc: Concentration, Expr: Expression, Synth: Synthesis, FD: FormDeprivation, NL: Negative Lens, PL: Positive Lens, Rec: Recovery from myopia, DA: Dopamine, DOPAC: 3,4-Dihydroxyphenylacetic acid, DAC: Dopaminergic amacrine cell. See Supplemental Table 1 for associated references.

receptors (D1 and D5) and D2-like receptors (D2, D3, and D4), which respectively increase and decrease cyclic adenosine monophosphate (cAMP) (Witkovsky, 2004). D1 receptors are located on bipolar, horizontal, amacrine, and ganglion cells, D2 receptors on DACs, D4 receptors on rod and cone photoreceptors, and D1, D2, D4, and D5 receptors on the RPE (Baba et al., 2017; Witkovsky, 2004). After DA binds to its receptor, it is metabolized to DOPAC (Cohen et al., 1983) which reflects DA release and turnover (Megaw et al., 2001).

DA release and synthesis is light-dependent, increasing with continuous diffuse and flickering light stimulation (Bauer et al., 1980; Boelen et al., 1998; Cohen et al., 2012; Godley & Wurtman, 1988; Iuvone et al., 1978; Kramer, 1971; Proll et al., 1982) and regulated by circadian rhythms (Doyle et al., 2002). Consequently, DACs are activated by light onset visual signals through three potential pathways: 1) rod photoreceptor-mediated input through the rod-rod bipolar-AII amacrine-ON cone bipolar circuit 2) direct cone photoreceptor-ON cone bipolar cell connection, and 3) melanopsin retinal ganglion cell (mRGC) axon collateral input (Boelen et al., 1998; Dumitrescu et al., 2009; Prigge et al., 2016; Zhang et al., 2012; Zhang et al., 2008; Zhao et al., 2017). Therefore, DACs can release DA from stimulation of multiple ON pathways (Qiao et al., 2016) that are active under different environmental conditions. The actions of DA on retinal signaling is widespread and occurs at multiple levels from photoreceptors to ganglion cells (Roy & Field, 2019). Therefore, the extensive functions that DA has in retinal signaling supports its potential role in the development of myopia due to altered visual input, as was first noted by Stone et al. (Stone et al., 1989).

1.2.4.a.2 Evidence for dopamine signaling in experimental myopia

DA is generally understood to be a 'stop' signal in myopic axial elongation (Feldkaemper & Schaeffel, 2013). In chickens, guinea pigs, and monkeys, DA and DOPAC levels are reduced after form-deprivation (Dong et al., 2011; I. Papastergiou et al., 1998; Iuvone et al., 1989; Stone et al., 1989; Sun et al., 2018) and lens defocus (Guo et al., 1995; Ohngemach et al., 1997). Interestingly, the reduction in DOPAC was specific to only the region of the retina deprived of form vision (Ohngemach et al., 1997; Stone et al., 2006), matching the property of regional specificity observed in visually-mediated axial elongation. However, altered DA metabolism associated with myopigenic stimuli may not be conserved across species, as form-deprivation did not alter retinal DA levels in mice (Chakraborty et al., 2014; Chakraborty et al., 2015; Park et al., 2014; Wu et al., 2015). However, mice, as well as rabbits and guinea pigs, show inhibited FDM (Gao et al., 2006; Landis et al., 2020; Mao & Liu, 2017; Mao et al., 2016; Mao et al., 2010) following injections of L-DOPA, the precursor to DA, or other DAergic activators. These findings suggest that while direct measurements of DA levels in mice were not different in FDM, activation of the whole Daergic system could still slow myopic eye growth.

Furthermore, in multiple species, DA receptor agonists prevent FDM, but do not appear to be as effective for LIM (Ashby et al., 2007; Dong et al., 2011; Iuvone et al., 1991; McCarthy et al., 2007; Rohrer et al., 1993; Schmid & Wildsoet, 2004; Stone et al., 1989; Yan et al., 2015), and it is still unclear the reason for this difference. One explanation could be that the visual cues that cause FDM and LIM initiate two distinct pathways that are differently influenced by dopamine; however, this cannot yet be concluded. Direct

comparisons between the two models may be confounded by other unmatched features of the visual cues, e.g., the spatial frequency spectra or optical aberrations introduced by the lenses.

Surprisingly, reduced axial elongation associated with increased DA is only effective when visual input is disrupted (e.g., form deprivation, lens defocus) and not during normal vision (Dong et al., 2011; Landis et al., 2020; Mao et al., 2010; Rohrer et al., 1993; Yan et al., 2015). These findings suggest that the activation of DA pathways is important but not sufficient to affect eye growth. One hypothesis is that visual environments deficient in certain features change activation of pathways that drive DAergic signaling (e.g., ON pathways). Recent work shows that stimuli which overstimulate ON pathways lead to anti-myopigenic outcomes, e.g., choroid thickening (Aleman et al., 2018) and increased vitreal DA (Wang et al., 2019). However, the direct connections between environmental stimulation of ON pathways, DA, and myopia susceptibility are still not fully elucidated.

Unlike activation of DA pathways, depletion of DA pathways prevents FDM but has no effect on LIM in chickens and fish (Kröger et al., 1999; Li et al., 1992; Schaeffel et al., 1994; Schaeffel et al., 1995) (Table 1.2). In contrast, decreasing DA with 6-hydroxydopamine in mice results in a myopic refractive shift with normal vision and increased FDM (Wu et al., 2016). Additionally, when retinal tyrosine hydroxylase, the rate-limiting enzyme in DA synthesis, is conditionally knocked out, mice have reduced DA levels and develop spontaneous myopia in normal conditions, while responding like wild-type mice to FDM (Bergen et al., 2016).

Interestingly, the dopamine receptor pathways involved in the protective effects of dopamine and bright light in myopia depends on the animal model (Zhou et al., 2017). For example, in

chickens, D2 receptor activation inhibited FDM and LIM (Nickla et al., 2010; Rohrer et al., 1993; Schmid & Wildsoet, 2004; Stone et al., 1989) while blocking D2 receptors inhibited the protective effect of light on FDM and LIM (Ashby & Schaeffel, 2010; McCarthy et al., 2007). Additionally, blocking D2, but not D1, receptors attenuated the inhibitory effects of levodopa and dopamine on FDM and LIM (Thomson, Karouta, et al., 2020a; Thomson, Morgan, Karouta, et al., 2020). Likewise, activation of primarily D2 receptor pathways reduced FDM in tree shrews (Ward et al., 2017). However, in the guinea pig, D1 receptor activation inhibited myopic refractive development and FDM while D2 receptor activation tended to do the opposite; however, this modulation varied with the DA receptor agonist (Zhang et al., 2018). In the mouse, it appears to be more complicated. Blocking D1 receptors attenuated the protective effect of bright light exposure during FDM (Chen et al., 2017). Additionally, activation of all DA receptors in wild-type mice and D2, but not D1, receptor knockout mice inhibited FDM (Huang et al., 2018) supporting a D1 receptor mechanism for myopigenesis in the mouse model. However in other studies, D2 receptor agonists and antagonists altered FDM in a dose-dependent manner and the protective effects of a D2 antagonist disappeared in D2 receptor knockout mice (Huang et al., 2022; Huang et al., 2020; Huang et al., 2014). Lastly, a D1 receptor mechanism is further supported in human genetic studies; a GWAS utilizing data from the Consortium for Refractive Error and Myopia (CREAM) cohort and the 23andMe, Inc. participants reported that a single nucleotide polymorphism (SNP) located near the dopamine receptor 1 gene (DRD1), a type of D1-like receptor, was significantly associated with refractive error (untransformed spherical equivalent) (Tedja et al., 2018).

1.2.4.a.3 Influence of dopamine signaling on ocular tissues

There is strong evidence showing a clear but complicated relationship between DAergic pathways and myopia. Retinal DA appears to have a profound influence over axial length under certain conditions. For example, in chicks, topical or intravitreal application of DA, DA receptor agonists, or levodopa reduced axial length in form-deprived or negative lens-treated eyes compared to control eyes (Nickla et al., 2019; Thomson, Karouta, et al., 2020a, 2020b; Thomson, Morgan, Karouta, et al., 2020; Thomson et al., 2021). Moreover, in mice, intravitreal injections of the DA agonist apomorphine attenuated axial length changes after form-deprivation (Huang et al., 2018). Additionally, D1 receptor antagonist blocked the protective effect of bright light on axial length changes in FDM (Chen et al., 2017). Likewise, intravitreal injections of high doses of D2 DA receptor agonists or antagonists reduced vitreous chamber elongation in the form-deprived tree shrew eye (Ward et al., 2017). However, modulation of DAergic signaling by DA, DA receptor agonists or antagonists, and levodopa did not affect axial length in otherwise untreated eyes (Thomson, Karouta, et al., 2020a; Thomson, Morgan, Karouta, et al., 2020; Zhang et al., 2018), further supporting the notion that DA effects on axial elongation and myopia require altered visual input.

Despite the significant effects of DA on axial length changes, DA has not been associated with scleral signaling, and there is no evidence that DA itself reaches the sclera to affect structural remodeling. However, choroidal thickness is well established to change with myopia and correlated with axial elongation (for a recent review see Liu et al., 2021), and there is strong evidence that dopamine also affects choroidal thickness. In chickens, choroidal thickness is regulated through D2 receptors, where D2 receptor agonists increase

thickness after brief periods of unaltered vision following LIM and D2 receptor antagonists inhibit this increase after FDM (Nickla & Totonelly, 2011; Nickla et al., 2010). However, in rabbits, dopamine-induced vasodilation of the choroid was mediated through D1 receptors (Reitsamer et al., 2004). Based on the previous evidence, it is likely that the interaction between DA and choroidal thickness occurs outside of the neural retina and not within the choroid. While tyrosine hydroxylase has been localized to the choroid (Klooster et al., 1996), no evidence to date shows significant choroidal expression of DA receptors. This leaves the RPE as a tissue potentially able to translate dopaminergic signaling to choroidal changes, that ultimately may influence axial elongation.

The RPE is a single layer of pigmented cells whose apical surface is embedded between photoreceptor outer segments and whose basal surface is lined with Bruch's membrane, separating it from the vascular choroid. The RPE carries out diverse and important set of roles for visual function, but most relevant is its role in ionic transport (Strauss, 2005), which 1) may affect fluid flow into the choroid/choroidal thickness (Zhang & Wildsoet, 2015) and 2) is altered during myopigenesis. Both the gene for chloride channels and expression of chloride channels and transporters were down-regulated after lens defocus (Seko et al., 2000; Zhang et al., 2011). Moreover, during recovery from FDM in chickens, sodium and chloride ions decrease in the RPE and increase in the choroid, which correlates temporally with a thickening of the choroid (Liang et al., 2004). Ionic flow across the retina, particularly with regards to chloride, sodium, and potassium, have been implicated in and are affected by experimental myopia (Crewther et al., 2006; Crewther et al., 2008) and hypothesized to regulate fluid flow that could change the size of various ocular layers. Since changes in cell size and transporters can affect fluid balance across cells, regulation at the RPE provides an

intriguing potential link between the retina and the classical changes in choroidal thickness associated with myopia reported more than 20 years ago (Wallman et al., 1995; Wildsoet & Wallman, 1995).

DA is a promising signal that could link the RPE to changes in the choroid due to RPE expression of D1, D2, D4, and D5 DA receptors in chicks and mice, likely on both the apical and basolateral membranes (Baba et al., 2017; Rymer & Wildsoet, 2005). When DA is applied to the basolateral surface, chicken RPE cells depolarize, due to the opening of chloride channels (Gallemore & Steinberg, 1990). This response is dependent on DA concentration and likely involves interaction effects with other receptors, possibly adrenergic receptors. For example, with low DA concentrations, DA receptors and B-adrenergic receptors are active, reducing the probability of chloride channels opening. However, when DA concentrations are high, alpha-adrenergic receptors become active which may also contribute to chloride channel opening (Rymer & Wildsoet, 2005). These findings on chloride channel activity in vitro are supported by in vivo electroretinography (ERG) using intravitreal injections of DA or DA receptor antagonists and measuring the chloride channel-mediated component (Gallemore & Steinberg, 1990; Sato et al., 1987; Wioland et al., 1990). Regardless of the specific pathway, these data suggest that DAergic activity has the potential to regulate ionic flow and thus fluid transfer across the RPE into the choroid. However, whether or not this effect is large enough to significantly impact choroidal thickness and myopigenesis has not been directly shown.

1.2.4.a.4 Summary

In summary, DA has long been known to be causally involved in myopigenesis and is likely the starting point linking at least some types of myopigenic cues to scleral remodeling. However, its direct influence via receptor binding appears to be limited to the retina and RPE. It is possible that the RPE serves as the link between myopigenic stimuli, DA, and choroidal thickness by regulating choroidal swelling via dopamine receptors. Additional research is necessary to elucidate signaling occurring at the RPE and how it may propagate and influence the choroid.

1.2.4.b Retinoic acid (RA)

Retinoic acid (RA) is a metabolite of vitamin A and a critical signaling molecule involved in numerous autocrine and paracrine developmental and physiological processes (Cvekl & Wang, 2009), regulating the transcription of over 100 genes (Balmer & Blomhoff, 2002). With advances in retinoid measurement technologies, evidence suggests that all-trans retinoic acid (atRA) is important in postnatally regulating the growth of many organ systems, including the eye (Summers, 2019). It is a promising candidate in signaling myopic axial elongation for many reasons: it is present in all eye wall tissues, bidirectionally modulated by the direction of blur (Mao et al., 2012; McFadden et al., 2004), and is known to stimulate catabolic remodeling processes (Bonassar et al., 1997; Mertz & Wallman, 2000). However, despite significant evidence linking RA to myopia development, several discrepancies remain, complicated by the breadth of its biological roles and the spatial and temporal variability in its action.

	C.1	C.2	C.3	C.4	C.5			C.6		
	Visual Cue	*Effect*	*Outcome*	*Retina (+)*	*RPE/Choroid (+)*			*Sclera (+)*		
A) Endogenous	A1) FD/NL	↑ *Elongation*	Conc.	↑ Conc.	↑ Conc.		**No Effect**			
			Synth.	↑ Synth.	↑ Synth.	↓ **Synth.**	**No Effect**			
			Receptor	↑ Expr.				↑ Expr.	No Effect	↓ Expr.
	A2) *Rec/PL*	↓ *Elongation*	Conc.	↓ Conc.	↓ Conc.	No Effect	↑ **Conc.**			
			Synth.	↓ Synth.	↓ Synth.		↑ **Synth.**			
			Receptor	↑ **Expr.**				No Effect		
	Drug Delivery	*Effect*	*Outcome*	*Intravitreal*	*Oral/Gavage/IP*			*Culture*		
B) Exogenous	B1) *Molecule/ Precursor*	↑ *Signaling*	Axial Length		↑ AL			↓ Prolif. (Fibroblasts)	↑ **Prolif. (Chondrocytes)**	
	B2) *Receptor Agonist*	↑ *Signaling*	Axial Length		↑ **AL**					
	B3) *Synthesis Inhibitor*	↓ *Signaling*	Axial Length	↓ AL						
	B4) *Receptor Antagonist*	↓ *Signaling*	Axial Length	↓ **AL**	↓ AL					

Table 1.3: **Potential of atRA to be a retinoscleral signal in refractive eye growth.** Column C.1: Treatments given to animals. C.2: General description of main effect of treatment. Columns C.3-6: Additional outcomes (C.3) studied with corresponding treatments. In A) Endogenous, C.4-6 are locations of measurements, and (±) represent whether receptors are expressed. In B) Exogenous, C.4-6 are different locations of the treatment. Cells are shaded to highlight trends. Orange/blue shading indicate an increase/decrease in signaling or elongation. Gray indicates inconclusive or no effect. Table cells are split when studies came to different conclusions. Bolded text indicates non-mammalian species used in study. AL: Axial Length, Conc: Concentration, Expr: Expression, Prolif: Proliferation, Synth: Synthesis, FD: Form-Deprivation, NL: Negative Lens, PL: Positive Lens, Rec: Recovery from myopia. See Supplemental Table 2 for associated references.

1.2.4.b.1 RA signaling pathway

Retinal RA is thought to be synthesized primarily by RPE cells as a byproduct of phototransduction (Weiler et al., 1998); however, subpopulations of amacrine (Milam et al., 1997; Saari et al., 1995) and Müller cells (Edwards et al., 1992; Milam et al., 1990) have been shown to either synthesize or express enzymes that synthesize RA. Currently, the canonical pathway by which RA appears to exert its effects involves the all-trans form

(Balmer & Blomhoff, 2002). The synthesis of atRA occurs in two steps: all-trans retinaldehyde is synthesized from all-trans retinol (vitamin A) via alcohol dehydrogenases (ADHs), which is subsequently oxidized into atRA via cytosolic retinaldehyde dehydrogenases (RALDH(1/2/3)). A dimer of a nuclear retinoic acid receptor (RAR) and retinoid-X receptor (RXR) binds atRA, subsequently binding DNA and influencing transcription (Balmer & Blomhoff, 2002). After synthesis, atRA can be bound by one of many retinoid binding proteins (RBPs) to facilitate intra- or extracellular transport or metabolized by CYP26 (Summers, 2019).

In vertebrates, retinal atRA concentration and synthesis have been demonstrated to be visually mediated. It is increased in response to both myopigenic cues (Mao et al., 2012; McFadden et al., 2004; Seko et al., 1998; Troilo et al., 2006) and greater luminance (McCaffery et al., 1996), although these increases may occur through different pathways. Together, this implies that the regulation of many retinal processes by light may occur at the transcriptional level via atRA, including light adaptation of horizontal cells (Pottek & Weiler, 2000; Weiler et al., 1999; Weiler et al., 2000; Weiler et al., 1998) and the transcription of arrestin, a critical phototransduction protein (Wagner et al., 1997).

1.2.4.b.2 Evidence for RA signaling in experimental myopia

Retinal atRA has been demonstrated to be increased after FDM and LIM in the guinea pig (Huang et al., 2011; Mao et al., 2012; McFadden et al., 2004) and chicken (Bitzer et al., 2000; Seko et al., 1998). It has also been observed to decrease with positive defocus (either via powered lenses or recovery from myopia) (McFadden et al., 2004). The significance of this bidirectional modulation of atRA in the retina is still not known. While recent genomics

studies suggest that the sign of blur may be encoded through two distinct sets of genes (Tkatchenko et al., 2018), this does not imply distinct signaling pathways between the retina and the RPE.

Recently, atRA has been demonstrated to modulate the protective effect of short wavelength light against myopigenesis. A study in guinea pigs exposed to different wavelengths of light showed a retinal atRA dependence on chromatic content, with the retinal atRA concentrations decreasing in the shorter wavelength (blue) light. Additionally, guinea pigs given unilateral LIM and reared in white light had significantly more retinal atRA in the myopic eyes than the contralateral eyes. However, when reared in blue light, there was no difference between the treated and control eyes, and both eyes had less atRA than those reared in white light (Yu et al., 2021). Finally, inhibition of RA-synthesizing enzymes in the retina has also been demonstrated as protective against myopia development (Bitzer et al., 2000; Yu et al., 2021), suggesting that the influence of atRA on axial elongation may begin in the retina.

As has been found in the retina, choroidal atRA concentrations appear to be bidirectionally influenced by the direction of blur imposed on the retina (Table 1.3). This choroidal atRA is likely choroidally-derived, as it has been demonstrated that the choroid synthesizes a large amount of atRA, more than the retina and liver (Mertz & Wallman, 2000). Three sets of co-culture experiments have important implications regarding atRA and retinoscleral signaling. When eyes from chickens were exposed to hyperopic defocus/diffusers or myopic defocus (conditions that influence choroidal thickness) and the choroids subsequently dissected and cultured, atRA production was bidirectionally altered (Mertz & Wallman, 2000) (similar bidirectional modulation of atRA synthesis, although opposite trends, were

found in marmosets (Troilo et al., 2006)). Second, a more complex experiment was carried out which exposed chicken eyes to various visual cues and co-cultured different combinations of tissues, assessing scleral remodeling when cultured with choroids from different visual conditions (form-deprived or recovering from myopia) (Marzani & Wallman, 1997). Scleral remodeling (quantified by glycosaminoglycan incorporation) was influenced by the visual condition from which the choroid came. Finally, Mertz and Wallman also showed that when sclera and choroid were cultured together, the choroid would rapidly release atRA into medium, and the sclera had the tendency to concentrate significantly more atRA than would be predicted by diffusion (the scleral tissue accumulated over 50% of the atRA released by the choroid, despite only making up 1% of the volume in culture) (Mertz & Wallman, 2000). Together, these studies make a compelling case that atRA can be produced in the choroid, has the tendency to be transported to the sclera, and can influence scleral remodeling. However, the exact source of the atRA is still unclear. A recent study aiming to characterize cells positive for RALDH2, an atRA synthesis enzyme, in the choroid of both humans and chicks found that choroidal atRA concentrations were partially controlled by proliferation of RALDH2+ cells (Summers et al., 2020). Yet, protein levels of RALDH2 were only found to be altered in chicks recovering from myopia, not in those with myopia (Rada et al., 2012; Summers et al., 2020).

The association of retinoids with specific RBPs that influence transport may be another means by which atRA could reach the sclera. Recently, Summers and colleagues showed that apolipoprotein A-1 (apoA-1) may act as a RBP in the eye that can traverse the choroid. apoA-1 is produced by the chick choroid and is also upregulated by atRA (Summers et al., 2016). In the same study, it was found that despite cultured sclera not synthesizing apoA-1

at detectable levels, cultured sclera releases significant amounts of apoA-1 into the medium, implying transport from choroid to sclera (Summers et al., 2016) and possibly explaining the previously discussed finding from Mertz and Wallman showing the tendency for the sclera to concentrate choroidally-derived atRA. Together, these results suggest a directionality to the transport of atRA and may overcome one of the primary limiting factors of retinoscleral signaling.

In humans, multiple GWAS studies of refractive error and myopia have also identified SNPs in genes related to atRA signaling. For example, multiple studies have reported associations between refractive error and the retinol dehydrogenase 5 (RDH5) gene (Kiefer et al., 2013; Tedja et al., 2018; Verhoeven et al., 2013), which encodes the enzyme 11-cis retinol dehydrogenase and is expressed in the RPE. GWAS findings have also implicated the RPE-retinal G protein-coupled receptor (RGR) (Kiefer et al., 2013; Tedja et al., 2018), expressed in the RPE and Müller glia (Pandey et al., 1994), and the atRA receptor-related orphan receptor β (RORβ) (Tedja et al., 2018), expressed in retinal tissue (Jia et al., 2009) and a component of the circadian clock system (André et al., 1998).

While retinoscleral signaling by atRA appears to be well supported, many nuances remain to be studied. Perhaps the greatest discrepancy is in the opposite effects of axial elongation and atRA in mammals and chickens. In both, retinal atRA increases with myopigenic stimuli while choroidal and scleral atRA concentrations are negatively correlated with axial elongation in the chick but positively correlated in mammals (Table 1.3). A likely factor contributing to this are the different scleral compositions of the two species: mammals have a fibrous sclera and chicks have both a cartilaginous and fibrous sclera. The different resident cell types of the two tissues have been demonstrated to respond differently to atRA in

the presence of transcription growth factor β (TGF-β), arresting the proliferation of fibroblasts but not chondrocytes (Seko et al., 1996). Additionally, co-culturing the choroid with fibrous sclera and cartilaginous sclera also lead to opposite outcomes on scleral remodeling (Marzani & Wallman, 1997). Thus, it is possible that there are significant differences in the physiological function of atRA as a retinoscleral signal. For example, in guinea pigs, RALDH2 was not found to be expressed in the choroid (Mao et al., 2012). Additional study of the function of atRA in mammalian models is required to determine the extent of species differences.

1.2.4.b.3 Influence of RA on ocular tissues

Unlike DA, atRA displays the ability to affect scleral remodeling processes that underly myopic axial elongation. While atRA is not produced in the sclera, scleral fibroblasts have atRA receptors and remodeling processes are influenced by atRA (Li et al., 2010; Troilo et al., 2006). In marmosets, RA concentration in retina, choroid, and sclera were found to be positively correlated with rate of axial elongation and negatively correlated to the rate of proteoglycan synthesis (Troilo et al., 2006). Systemic treatment of guinea pigs with atRA also led to axial elongation and an altered scleral microstructure with similarities to the outcome of myopigenic visual cues (McFadden et al., 2004), and treatment of mice led to myopic refractive errors, axial elongation, and altered scleral biomechanics (Brown, Ethier, et al., 2021).

However, exogenous atRA treatment has also been observed to lead to significant ocular growth without refractive errors in both chickens and guinea pigs, proportionally growing the eye and causing the lens of these animals to thicken instead of just causing axial elonga-

tion (McFadden et al., 2004; McFadden et al., 2006). One possible explanation could be a dual role for atRA in signaling proportional eye growth and axial elongation, with younger animals more susceptible to growth rather than elongation.

1.2.4.b.4 Summary

In summary, atRA is one of the few chemical signals with evidence supporting the capacity to cross the choroid. However, its role in myopigenesis is still unclear. While exogenous atRA causes myopia to develop in some cases, in others it leads to excessive proportional growth of the eye. Additional mammalian research is required to make more general conclusions due to previous work being avian-specific, such as the role of apoA-1 as an RBP. However, with multiple genes related to atRA signaling and myopia implicated in GWAS studies, this is a promising pathway for further investigation.

1.2.4.c Adenosine (Ado)

Adenosine (Ado) is one of the most widely occurring organic compounds. It is a purine and is a basic building block of life as one of four nucleosides of DNA and RNA with a role in energy transport. Ado's role as an extracellular signaling molecule was discovered in the early 20th century (Drury & Szent-Györgyi, 1929). It has since been observed to modulate many cellular processes and act as a neuromodulator, exerting its actions through four types of membrane-bound, G-protein coupled adenosine receptors (AdoRs) - AdoRA1, AdoRA2A, AdoRA2B, AdoRA3 (Eltzschig, 2013). Similar to DA, AdoRs have opposing effects on cAMP production, with AdoA1 and AdoRA3 decreasing cAMP and AdoRA2A, AdoRA2B increasing cAMP by inhibiting or activating adenyl cyclase (AC), respectively

(Spinozzi et al., 2021).

	C.1	C.2	C.3	C.4	C.5	C.6	C.7	
	Visual Cue	*Effect*	*Outcome*	*Retina (+)*	*RPE (+)*	*Choroid (+)*	*Sclera (+)*	
A) Endogenous	A1) *FD/NL*	↑ *Elongation*	Receptor	↑ Expr ↓ Expr				
	A2) *Rec/PL*	↓ *Elongation*	Receptor					
	Drug Delivery	*Effect*	*Outcome*	*Intravitreal*	*Culture*	*Subconj./ Topical*	*Oral/Gavage/IP*	
B) Exogenous	B1) *Downstream activation*	↑ *Signaling*	Axial Length				↑ AL	
	B2) *Downstream Inhibition*	↓ *Signaling*	Axial Length			↓ AL		
	B3) *Synthesis Inhibitor*	↓ *Signaling*	Axial Length					
	B4) *Receptor Antagonist*	↓ *Signaling*	Axial Length	No effect	No effect	↓ AL	↓ AL	No effect
	Gene Knockout	*Effect*	*Outcome*	*Retina-KO*	*RPE-KO*	*Choroid-KO*	*Nonspecific-KO*	
C) Genetic	C1) *$AdoRA_{2A}$*	↓ *Signaling*	Axial Length				↑ AL	

Table 1.4: **Potential of adenosine to be a retinoscleral signal in refractive eye growth.** Column C.1: Treatments given to animals. C.2: General description of main effect of treatment. Columns C.3-7: Additional outcomes (C.3) studied with corresponding treatments. In A) Endogenous, C.4-7 are locations of measurements, and (±) represent whether receptors are expressed. In B) Exogenous and C) Genetic, C.4-7 are different locations of the treatment. Cells are shaded to highlight trends. Orange/blue shading indicate an increase/decrease in signaling or elongation. Gray indicates inconclusive or no effect. Table cells are split when studies came to different conclusions. AL: Axial Length, Expr: Expression, FD: Form-Deprivation, NL: Negative Lens, PL: Positive Lens, Rec: Recovery from myopia. See Supplemental Table 3 for associated references.

1.2.4.c.1 Adenosine signaling pathway

The exact mechanisms by which Ado reaches extracellular targets are complex and multivariate. Cells and interstitial fluids in tissues have basal concentrations of Ado in the nanomolar range (Fredholm, 2007). Many types of cells, including neurons and glial cells,

have been demonstrated to release some amount of Ado from intracellular stores into the extracellular space (Brundege & Dunwiddie, 1998; Cotrina et al., 1998; Pascual et al., 2005), which appears to be increased by glutamate binding to N-methyl-D-aspartate (NMDA) receptors (Brambilla et al., 2005).

In general, extracellular Ado tends to dramatically increase with tissue activity, hypoxia, and other pathological states and biological stressors, increasing to the micromolar range (Fredholm, 2014; Haskó et al., 2018). However, this increase appears to be due to leakage or controlled release of adenosine triphosphate, which is subsequently degraded into adenosine monophosphate and then Ado (Antonioli et al., 2013; Eltzschig, 2013). Additionally, the extent to which these changes affect signaling is not clear, as Ado signaling is highly dynamic. Ado is rapidly metabolized to inosine and hypoxanthine, exhibiting a half-life of only $\sim$1.5 seconds (Spinozzi et al., 2021), and equilibrative nucleoside transporters rapidly equilibrate imbalances in intra- and extracellular Ado (Lovatt et al., 2012).

In many cases, AdoRs are significantly activated by basal levels of Ado (Fredholm, 2007) and significantly blocked by commonly consumed amounts of caffeine, a nonselective inhibitor of AdoRs (Fredholm et al., 1999). However, the sensitivity of the cell or tissue to the ligands are highly dependent on the expression of the receptor, which has also been noted to vary significantly with diseased states and presence of stressors, most notably of which are related to the immune system and hypoxia. Hypoxic conditions have been shown to increase expression of AdoRA2B (Kong et al., 2006) without affecting AdoRA2A (Fredholm et al., 2007) and may influence trafficking of the receptors to the membrane (Arslan et al., 2002).

It is critical to note that these effects are very much cell type-dependent, and only a

small fraction of the work on Ado signaling has occurred in ocular tissues. In the retina, it has been demonstrated that extracellular Ado signaling is controlled by light intensity and circadian rhythms, both of which have been implicated in myopigenesis (Ribelayga & Mangel, 2005).

1.2.4.c.2 Evidence for adenosine signaling in experimental myopia

The first connection of purinergic Ado signaling to myopigenesis was made with the discovery that 7-methylxanthine (7-Mx), a metabolite of caffeine and a nonselective inhibitor of AdoRs, influenced scleral collagen and proteoglycan content in rabbits, opposite to that occurring with myopigenesis (Trier et al., 1999). Following this finding, many additional studies have also found a causal role of Ado on refractive state, axial elongation, and scleral remodeling (see paragraph 1.2.4.c.3 and Table 1.4).

Despite significant experimental evidence, most details of the role of purinergic signaling in myopigenesis are still unclear. All four subtypes of AdoRs have been found to be expressed in all layers of the posterior eye wall of rhesus monkeys and guinea pigs (Beach et al., 2018; Cui et al., 2010) and in human scleral fibroblasts (Cui et al., 2008). A small epigenetic study of youth with high myopia (n=18 cases, 18 controls) reported hypermethylation of the AdoA2A receptor gene (ADORA2A) in peripheral blood samples (Vishweswaraiah et al., 2019), suggesting Ado signaling may be influenced by myopia. Additionally, when guinea pigs were deprived of form vision, protein levels of AdoA1 / AdoA2B in the retina were elevated (Cui et al., 2010).

The poor ability of other methylated xanthines like 7-MX to pass the blood-brain/blood-retina barrier (Hung et al., 2018; Shi & Daly, 1999) would suggest that the target tissue of

these systemic treatments is not likely to be the retina. Neither AdoA2A gene expression (in tree shrew) nor protein levels (in guinea pigs) are affected in choroid or sclera (Cui et al., 2010; He et al., 2014). However, scleral cAMP, known to influence collagen remodeling, has been demonstrated to be influenced by visual cues (Tao et al., 2013), and pharmacologically activating AC led to myopic refractive errors, and inhibiting AC led to attenuation of myopigenesis in guinea pigs (Tao et al., 2013). Yet, it is not clear if altered collagen metabolism is critical to myopigenesis, or if it occurs in response to the elongated eye, since significant myopia can develop in tree shrews with little change in collagen remodeling (McBrien, Cottriall, et al., 2001).

1.2.4.c.3 Influence on ocular tissues

7-Mx treatment has been demonstrated to reduce the progression of myopia in children (Trier et al., 2008) and in rabbits, chickens, guinea pigs, and macaques subjected to myopigenic visual stimuli (Cui et al., 2011; Hung et al., 2018; Nie et al., 2012; Wang et al., 2014). Despite these findings, oral 7-MX had only a minor protective effect with lens defocus and no effect on form-deprivation in chickens and tree shrews (Khanal et al., 2020; Liu et al., 2020; Wang et al., 2014) (Table 1.4). Together, these data may indicate significant species differences in myopigenic signaling and/or bioavailability of the 7-MX. Additionally, AdoR inhibition often only leads to partial protection against myopia development, which may suggest Ado influences myopia development either through a separate parallel and opposing pathway to myopigenic signaling or a pathway that contributes to retinoscleral signaling. In contrast to the pharmacological findings, transgenic mice lacking AdoA2A developed relative myopia, both in terms of refractive error and axial length, compared to

littermate wildtype controls (Zhou et al., 2010).

1.2.4.c.4 Summary

Ado is a highly dynamic and ubiquitous type of signaling with clear connections to scleral remodeling. While present in all tissues of the posterior eye wall, there is little evidence suggesting it connects any two layers and relatively little evidence showing altered signaling with myopigenesis, both in animal and human GWAS studies. However, thus far scleral Ado has not been ruled out as integral to myopigenesis, if influenced by another pathway capable of transmitting information through the choroid.

1.2.4.d Other signals

It is known that retinoscleral signaling involved in emmetropization and myopigenesis involves many distinct signaling molecules and pathways. In addition to the signaling molecule candidates featured above, a few other signaling pathways are of particular interest due to their bidirectional modulation with visual stimulus (retinal glucagon) and successful clinical use as a pharmacological treatment for slowing myopia (atropine, a nonselective metabotropic muscarinic acetylcholine receptor antagonist). For in depth review of these and other chemical signaling molecules, see the recent review (Troilo et al., 2019).

Beyond these commonly studied signaling molecules, the thickness of the choroid has long been hypothesized to be involved in directing eye growth. It is bidirectionally modulated by visual cues, thinning with myopigenic cues and thickening in response to positive lenses or recovery from myopia. The consequences of these changes have been hypothesized to influence the scleral oxygen content and thus potentially function as a signal (Wu

et al., 2018).

1.2.4.d.1 Hypoxia-inducible factor 1-alpha (Hif-1α)

It is well established that the choroid rapidly thins in response to myopigenic cues. It has been proposed that this thinning may be the result of decreased blood flow, and thus may decrease the oxygenation of the sclera (Liu et al., 2021). Retinoscleral signaling via oxygenation appears to be potentially viable, requiring that: 1) visual cues presented to the retina are able to influence the choroid, 2) decreased blood flow in the choroid underlies the choroidal thinning and results in graded degrees of scleral hypoxia, and 3) hypoxia in the sclera affects remodeling processes. Additionally, if oxygenation of the sclera explains myopigenesis, choroidal thickening should either elicit an opposite response in the sclera, or an additional pathway is required to signal slowing of axial elongation.

In support of this hypothesis, recent studies have found scleral hypoxia-inducible factor 1-α (Hif-1α) to be correlated to myopigenesis. Hif-1α protein levels in the sclera, but not the retina, were associated with FDM in mice and guinea pigs and LIM in guinea pigs (Pan et al., 2021; Wu et al., 2018). Additionally, analysis of human gene databases revealed a moderate association with scleral Hif-1α signaling pathway in individuals with high myopia (Wu et al., 2018; Zhao et al., 2020). However, in tree shrews, scleral Hif-1α mRNA expression was not altered with form-deprivation, lens defocus, or recovery from lens-defocus (Guo et al., 2013; Guo et al., 2019). And in contrast to all, one study reported scleral Hif-1α mRNA expression decreased with lens defocus in guinea pigs (Guo et al., 2013).

Furthermore, experimentally manipulating hypoxia signaling appears to influence re-

fractive state. Simultaneous treatment of guinea pigs with lens defocus and anti-hypoxia drugs resulted in reduced Hif-1α levels and partially suppressed myopic refractive error development and axial elongation (Wu et al., 2018). Additionally, two treatments used to experimentally reduce choroidal blood perfusion (and presumably decrease oxygenation of the sclera) were found to also induce myopia in guinea pigs (Zhou et al., 2021). These studies suggest a relationship between hypoxia, Hif-1α and development of myopia; however, the strength of this connection and whether scleral hypoxia is solely responsible for trans-choroidal propagation of myopigenic signaling is not clear. Additionally, whether the signal can encode both signs of defocus is not clear; the choroid has been shown to thicken with positive defocus and recovery from myopia, but how this translates to oxygen diffusion to the sclera and Hif-1α is not known.

1.2.5 Pathway crosstalk

Each of the primary signaling molecules discussed in the previous section are implicated to some degree in myopigenic retinoscleral signaling (Figure 1.4). Currently, the only retina-derived signal with any evidence to reach and act on the sclera is atRA, and more evidence suggests atRA acting on the sclera may be derived from the choroid. Thus, DA and other retinal signaling molecules known to affect myopigenesis acting anterior to the choroid, suggest that the choroid is a likely point of crosstalk between various pathways. Two mechanisms by which information can traverse the choroid have been presented: 1) changes to choroidal thickness/blood flow 2) a RA-based signal propagated across the choroid, possibly involving RBPs.

Many visual cues and retinal signaling molecules are known to influence choroidal

thickness. Retina-originating signals (DA, Ado, atRA, glucagon, insulin, vasoactive intestinal peptide, monamines) could interact in the retina. While the genetic evidence for DA and Ado in human cohorts is limited, one of the most robust and repeated GWAS findings are the associations between refractive error and the gap junction delta-2 protein (GJD2) gene (Cheng et al., 2013; Fan et al., 2016; Hysi et al., 2020; Miyake et al., 2015; Solouki et al., 2010; Tedja et al., 2018; Verhoeven et al., 2013), which encodes connexin-36. As connexin-36 is dephosphorylated by DA and phosphorylated by Ado (Li et al., 2013), connexin-36 may be a conduit for these neuromodulators to affect eye growth. While not yet evaluated in the context of myopia, DA has also been found to act as an epigenetic histone marker in a process termed "dopaminylation" (Lepack et al., 2020), which may provide a future explanation linking the influence of the visual environment on genetic contribution to eye growth.

It is likely that many retina-originating signals are relayed by the RPE, due to the presence of many receptor types. With many distinct myopigenic cues similarly affecting choroidal thickness, and choroidal thickness possibly influenced by the RPE, many distinct retinal signals could be summed and influence choroidal thickness in a graded manner at the RPE. If choroidal thickness does in fact influence the oxygen environment of the sclera, further study into the role of the RPE on choroidal thickness could help elucidate these connections.

apoA-1 expression is known to be at least partially regulated by peroxisome proliferator-activated receptors (PPARs) (Gervois et al., 2000), which may be downregulated under hypoxic conditions. Intravitreal injections of the PPARα agonist GW6747, upregulated retinal and scleral apoA-I expression and suppressed experimental myopia in chickens (Bertrand

et al., 2006). This increased protein expression of apoA-1 in the sclera could be from the choroid, since the sclera has not been shown to synthesize apoA-1 (Summers et al., 2016). However, GW6747 had no effect on choroidal apoA-1 mRNA expression (Summers et al., 2016).

Evidence suggests that hypoxic conditions may inhibit PPAR subtypes, possibly linking the effects of hypoxia to apoA-1 and atRA. When guinea pigs were treated with PPAR α/γ antagonists, Hif-1α increased and the animals developed myopic refractive errors and axial elongation (Pan et al., 2018). The opposite effect was found for animals treated with agonists (Pan et al., 2018). This bidirectionality of the influence of PPAR would further support the possibility of hypoxia as a cue for signaling increased/decreased axial elongation. However, PPAR activation has not yet been demonstrated to occur with choroidal thickening/hyperoxia or recovery from myopia. It is also not clear if scleral hypoxia and PPAR expression would influence apoA-1 that has presumably been transported from the choroid.

1.2.6 Conclusions and Future Directions

All of the major signaling pathways identified in this paper contribute in some way to myopigenesis and retinoscleral signaling. While DAergic signaling appears to be primarily restricted to the retina and RPE, the consequences of the signaling are known to influence both choroidal thickness and axial length. Ado is ubiquitous through the posterior eye wall and influences scleral remodeling; however, whether it is involved in signaling between tissues is not clear. RA is a promising candidate, ubiquitous to all posterior eye wall tissues, bidirectionally modulated with positive/negative defocus and has a plausible hypothesized

transport mechanism by which it could cross the choroid. However, much of the work surrounding this molecule has been performed in the chicken model, which displays significant differences in scleral composition compared to mammalian species and necessitates further study in mammalian models. While many pathways play a role in myopigenesis, signaling across the choroid appears to be a bottleneck before which crosstalk likely occurs. Identified here are two main mechanisms by which information originating in the retina may reach the sclera: via an atRA-driven mechanism and/or oxygenation of the sclera. Future studies should be performed in mammalian models in order to better understand which findings are general mechanisms of myopigenesis. Additionally, directing research effort towards the use of inducible knockout mouse models could help to elucidate additional details of some of these difficult to study signaling mechanisms, such as: the role of adenosine in the retina, how dopamine influences the RPE, whether myopigenesis can occur in apoA-1 deficient animals, and how the various pathways influence choroidal apoA-1.

1.3 The scleral endpoint of retinoscleral signaling

While there is still much that is unknown about the process and mechanisms by which signals can propagate from the retina to the sclera, there is an abundance of evidence that suggests that ultimately the sclera significantly influences the overall shape and size of the eye. Yet, the exact manner by which the sclera remodels to influence biomechanics and how the biomechanics of the sclera in turn influence the dimensions of the eye remain uncertain.

1.3.1 Anatomy of the sclera

The sclera is a tough, highly collagenous connective tissue, maintained by fibroblasts, which serves many functions in the eye and is thus involved in many ocular pathologies. As the white, outer coat forming ~85% of the surface of the human eye, its primary role is often thought to be protecting the delicate internal tissues from mechanical insult; however, its role in determining overall shape and size of the eye is of arguably more importance to daily life (Grytz & Siegwart, 2015; Rada et al., 2006). Due to the mammalian eye being made up entirely of soft tissue, the eye requires an intraocular pressure (IOP) to maintain its essentially spherical shape. The sclera must be able to resist this dynamic IOP that spans multiple orders of magnitude, while also withstanding externally applied forces (Campbell et al., 2014). Failure in either of these roles would decrease visual acuity by altering the retina's position relative to the optical focal point and possibly damaging the integrity of other ocular tissues critical to vision, e.g., the retina and optic nerve. To fulfil these functions, the sclera has evolved a complex structure that imparts similarly complex biomechanical functions.

1.3.2 Scleral Biomechanics and Structure

The sclera can be considered as an active, triphasic (solid, fluid, and ion) material formed from a hydrated, intrinsically viscoelastic (Mow et al., 1984; Shen et al., 2011), and anisotropic solid matrix. It is active in that it responds to mechanical stimuli, and does so at different timescales. There are a subset of contractile fibroblasts appear to respond acutely to strain (Harper & Summers, 2015; Phillips & McBrien, 2004), but also longer term, fibroblast lineage and remodeling influencing by mechanical strain (Qiu et al., 2018; Zhang et al., 2017). The sclera demonstrates spatially and temporally heterogeneous properties and ion distributions. The complex tissue-level biomechanics of the sclera are due to its biochemical composition and structure, and the interaction of its various phases.

The human sclera is approximately 70% water by weight imbibed into a solid matrix. This matrix is primarily composed of collagen fibrils ($\sim$90% by dry weight) arranged into many lamellae or layers (Figure 1.5). The high collagen content gives the sclera significant tensile stiffness and strength. Proteoglycans (PGs) and glycosaminoglycans (GAGs) ($<$1% wet weight (Grytz, 2018)) interact with and connect lamellae, while also fixing charge within the solid matrix, imparting electromechanical properties to the sclera.

Aggrecan, a large proteoglycan, concentrates most of the fixed charges within the sclera. Each molecule of aggrecan has over 100 charged, sulfated GAGs (sGAGs) covalently bound to its core protein, compared to 1 or 2 sGAGs on decorin and biglycan, the two most common scleral proteoglycans. These fixed charges introduce a host of mechano-electrochemical phenomena, such as the sequestering of water and ions within the matrix, a Donnan osmotic swelling pressure, and streaming potentials and currents that together

influence scleral compressive properties, hydraulic properties, and possibly cell signaling processes (Mow et al., 1999). The orientation (Gogola et al., 2018) and quantity (Rada, Achen, Penugonda, et al., 2000) of proteoglycans and collagen vary spatially in the sclera. Contractile fibroblasts confer active properties to the tissue by mechanically interfacing with the extracellular matrix (ECM) (McBrien et al., 2009). This high degree of complexity and heterogeneity allows the sclera to tailor its properties to the local needs of its environment, such as reinforcing the optic nerve head or regions of the scleral shell compromised by vessels. However, it also makes it challenging to mechanically characterize the tissue and to determine the causes and effects of altered remodeling processes and biomechanics.

1.3.3 The Sclera and Myopia

1.3.3.a Scleral biomechanics and eye size

Many studies have observed a correlation between scleral biomechanics and eye size during myopigenesis (Grytz & Siegwart, 2015; Levy et al., 2018; Lin et al., 2019; McBrien et al., 2009). Structurally, the mammalian sclera thins during myopigenesis, which would cause the eye to become more extensible all else being equal (McBrien et al., 2009). However, there is significant evidence of intrinsic changes to the material properties of the sclera in myopigenesis, which is indicative of altered organization and/or relative concentrations of its constituent components. Both the scleral elastic tensile modulus (Lin et al., 2019; Phillips & McBrien, 1995) and viscoelastic properties (time-dependent response to loading, e.g., creep rate) are altered during myopigenesis (Levy et al., 2018; Moring et al., 2007; Phillips et al., 2000; Siegwart & Norton, 1999), in the direction of increasing the ex-

tensibility of the eye. Therefore, in response to both instantaneous and sustained pressure changes, myopic scleral samples elongate more than non-myopic samples.

While it is possible that scleral biomechanics change in response to ocular globe elongation, biomechanical changes instead appear to cause eye size changes. The effect of scleral biomechanics on eye size can be observed experimentally by changing scleral properties. For example, scleral reinforcement surgeries are one of the few direct treatments for myopia; in this treatment, the sclera is stiffened to reduce axial elongation/eye size (Wang & Chen, 2012; Yan et al., 2010; Zhu et al., 2018). Additionally, collagen crosslinking, a procedure known to stiffen the sclera and change its tensile properties in a manner opposite to the changes observed in myopic eyes, has been successfully applied to reduce/ameliorate myopigenesis in various animal models (Levy et al., 2018; Lin et al., 2019).

Thus, the evidence to date supports altered scleral biomechanics as causal to myopic eye growth; however, how altered scleral biomechanics cause changes in ocular size is still unclear. While altered elastic properties of the sclera have been measured in myopic eyes, these altered properties have rarely predicted accurate eye size. Similarly, while altered scleral creep rates have been measured, these also fail to accurately predict overall rates of ocular elongation measured in myopia (Grytz & Siegwart, 2015; McBrien et al., 2009; Phillips & McBrien, 1995). Thus, there is still much to be explored regarding the connection between scleral biomechanics and ocular size.

1.3.3.b Scleral remodeling in myopia

Emerging evidence over the last few decades implicates scleral remodeling (change in structure), as opposed to growth (increased in tissue mass) as the primary process causing my-

opic ocular globe elongation (Grytz, 2018). Due to collagen's role as the primary tension-resisting biological molecule (Harper & Summers, 2015), and the IOP imposing primarily tensile stresses in the eye wall (Campbell et al., 2014), collagen has been one of the most-studied scleral molecules in myopia. It was hypothesized early on that altered collagen could lead to a decreased ability to resist eye wall tensile loading and thus lead to increased eye size (Greene & McMahon, 1979). While there is substantial evidence that collagen is altered in myopia, the most significant changes in bulk collagen content seem to occur in long-term myopia after the eye has already elongated (McBrien, Cornell, et al., 2001), suggesting major changes to collagen ultrastructure may be a consequence of myopic elongation rather than a cause. Thus, the cause of elongation is likely more nuanced, involving other biomechanically relevant scleral proteins.

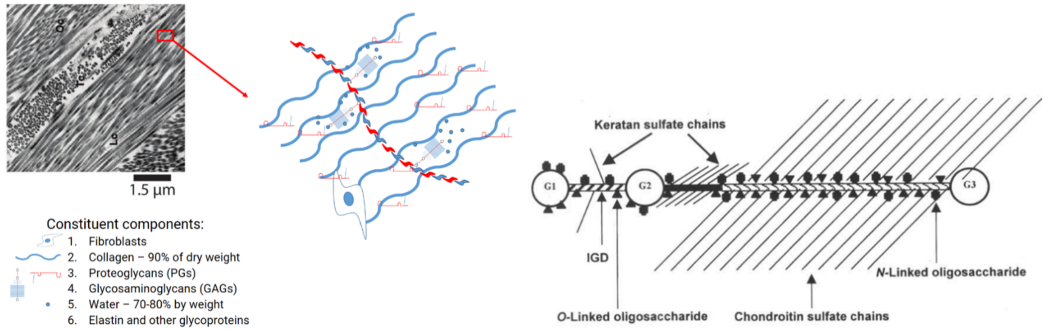

(a) **(b)**

Figure 1.5: Microstructure of the sclera and aggrecan. (a) Representative image of a sclera displaying the lamellar structure. (Right) Within these lamellar structures, collagen is highly aligned. Proteoglycans are resident within and between the lamellae, sequestering water and ions. (b) Schematic representation of aggrecan. The core protein has three globular domains, to which keratin sulfate and over 100 chondroitin sulfate GAGs are attached. Adapted from (a) Watson and Young, 2004 (top left panel) (b) Kiani et al., 2002.

One candidate protein likely to be involved in myopia development is aggrecan, which is most extensively studied as a primary biomechanical constituent of cartilage. Aggrecan is a highly charge-dense molecule; each core aggrecan protein fixes more than 100 charged,

sGAGs 10-15 angstroms apart within the collagen matrix (Mow et al., 1999) (Figure 1.5b), imparting electromechanical properties to the tissue. The GAGs/fixed charges are best understood in their role in conferring compressive stiffness to tissue due to the majority of aggrecan research being performed in cartilage; however, there are now many (conflicting) reports that detail varying effects of aggrecan/glycosaminoglycans on tissue level mechanics in a number of tissues (Hatami-Marbini & Pachenari, 2020; Mattson et al., 2017; Midgett et al., 2018; Murienne et al., 2016; Murienne et al., 2015; Yasmin et al., 2018). The seemingly complex and/or context-dependent nature of the role of aggrecan and GAGs in tissue biomechanics makes it all the more important to aggrecan study in the sclera.

Aggrecan has been implicated in the myopia signaling pathway in both humans and animal models. In humans, a single nucleotide polymorphism in the aggrecan gene has recently been associated with high myopia in the Chinese population (Yang et al., 2014). In tree shrews, it has been demonstrated that aggrecan and related factors are modulated within days of imposed defocus. Aggrecan mRNA has been shown to decrease with presentation of myopigenic stimulus and increase upon removal, while the opposite is observed for its main proteases, ADAMTS4 and ADAMTS5 (aggrecanase-1 and -2) (Guo et al., 2013; Guo et al., 2014; Moring et al., 2007; Siegwart & Strang, 2007). Further, in guinea pigs treated with atRA, scleral aggrecan protein content was observed to decrease concurrent with increased axial length (Huo et al., 2013). A better understanding of the role aggrecan plays in scleral biomechanics and the signaling pathways that ultimately regulate its levels in the sclera could lead to pharmacological treatments that block the effects of myopigenic visual stimulus and reduce myopia.

CHAPTER 2

SPECIFIC AIMS

2.1 Aim 1: Evaluate the efficacy of poroelastic theory for characterizing scleral biomechanics.

The sclera is a highly complex mechanical tissue that can be described as multiphasic and anisotropic. It is often idealized as uniphasic and linear or hyperelastic, and uni-/biaxial tensile tests or inflation tests are performed to measure its stiffness. However, these standard tests are not easily translatable to the small mouse eye. **Approach:** We will relax the uniphasic idealization and utilize the multiphasic nature of the sclera to characterize its material properties. A poroelastic material model will be used to analyze unconfined compression of sclera and obtain tensile and hydraulic properties. To validate the methodology, porcine sclera will be tested and retested, and the resulting properties compared between tests and to literature values. This method will then be applied to the mouse sclera to measure its intrinsic material properties for the first time. **Impact:** The results are the first measurements of material properties of the mouse sclera, the biomechanics of which are understood to be central to at least glaucoma and myopia, and permit a robust characterization of mouse myopia models in the following aims.

2.2 Aim 2: Quantify biomechanical and related biochemical changes in myopic murine sclera.

Altered scleral structure and biomechanics are believed to underlie the axial elongation responsible for most mammalian myopia, but there are significant uncertainties in how comparable mouse myopigenesis is to other species, as the small eye makes axial measurements challenging. Additionally, there is significant evidence linking retinoic acid, glycosaminoglycans, and scleral biomechanics; however, it is spread across many species and none is from the mouse. **Approach:** Using the methodology developed in Chapter 3[Aim 1], we will first determine how scleral biomechanics change in eyes deprived of form vision, a common model for myopia. We will then quantify scleral sulfated glycosaminoglycans (via the metachromatic 1,9-dimethylmethylene blue (DMMB) assay and immunohistochemistry (IHC)) and ocular retinoids (via specialized liquid chromatography-tandem mass spectrometry (LC-MS/MS) methods) in the normal and myopic mouse sclera. **Impact:** These results will provide important and previously unobtainable evidence on whether the mouse develops axial myopia, as scleral biomechanical changes are understood to be necessary preconditions to axial elongation. These results will not only inform the subsequent Aim, but also provide important context to interpreting previous findings using the mouse model.

2.3 Aim 3: Determine the effect of retinoic acid on refractive development and scleral biomechanics.

AtRA has been implicated at various points of the myopia pathway as a potential bi-directional regulator of ocular size; however, there are conflicting reports as to whether or not it is re-

sponsible for scleral changes and the development of refractive error. **Approach:** To isolate and study its role as a myopigenic signal in the mouse, retinoic acid will be fed to mice. Refractive development will be monitored in these animals to compare their ocular phenotype with control and with form-deprived eyes. Techniques introduced in the previous aims will be used to characterize the scleral phenotype induced by atRA via biomechanics and sGAG content. **Impact:** The results of this aim will permit a direct comparison between visually-mediated myopigenesis with the atRA phenotype across structural and functional outcomes, providing evidence for or against a role of atRA in myopigenic retinoscleral signaling.

CHAPTER 3

A BIPHASIC APPROACH FOR CHARACTERIZING TENSILE, COMPRESSIVE AND HYDRAULIC PROPERTIES OF THE SCLERA

Authors: **Dillon M. Brown**, Machelle T. Pardue, C. Ross Ethier

Status: Published in *Journal of the Royal Society Interface* **18**(174): 20200634. (2020)

3.1 Abstract

Measuring the biomechanical properties of the mouse sclera is of great interest: altered scleral properties are features of many common ocular pathologies, and the mouse is a powerful tool for studying genetic factors in disease, yet the small size of the mouse eye and its thin sclera make experimental measurements in the mouse difficult. Here, a poroelastic material model is used to analyse data from unconfined compression testing of both pig and mouse sclera, and the tensile modulus, compressive modulus and permeability of the sclera are obtained at three levels of compressive strain. Values for all three properties were comparable to previously reported values measured by tests specific for each property. The repeatability of the approach was evaluated using a test–retest experimental paradigm on pig sclera, and tensile stiffness and permeability measurements were found to be reasonably repeatable. The intrinsic material properties of the mouse sclera were measured for the first time. Tensile stiffness and permeability of the sclera in both species were seen to be dependent on the state of compressive strain. We conclude that unconfined compression

testing of sclera, when analysed with poroelastic theory, is a powerful tool to phenotype mouse scleral changes in future genotype–phenotype association studies.

3.2 Introduction

The eye captures, refracts, and senses light, and the sclera, the outer white coat of the eye, has an important role in supporting these three functions. Specifically, the sclera resists the stresses imposed on the eye wall by the intraocular pressure, making its structure and biomechanical properties critical to overall ocular shape and size (Song et al., 2016). Scleral biomechanics also directly impact the biomechanical loading imposed on the other more delicate tissues of the eye, including the retina and optic nerve head (Boote et al., 2020; Coudrillier et al., 2012; Norman et al., 2011). Pathological remodeling and altered material properties of the sclera have been implicated in a number of ocular pathologies, including myopia and glaucoma (Grytz & Siegwart, 2015; Pijanka et al., 2014; Rada et al., 2006). Thus, more research on scleral biomechanics and how scleral microstructure influences its biomechanics is warranted.

The sclera is primarily made up of collagen, proteoglycans, water, ions, and cells. The mammalian sclera consists of a hydrated, highly collagenous solid matrix sparsely cellularized by scleral fibroblasts. The collagen, primarily type I, is organized into lamellae embedded in a proteoglycan matrix. A similar matrix has been found to impart complex triphasic biomechanics to articular cartilage by influencing hydration and ion distributions throughout the tissue (Mow et al., 2002), and it is likely to generally function in a similar capacity within the sclera. The proteoglycan-collagen matrix is maintained by scleral

fibroblasts and imbibes fluid, making sclera ∼70% water by weight (Boote et al., 2020).

Despite its microstructural complexity, most biomechanical studies treat the sclera as a uniphasic material and use linear elastic, hyperelastic, or viscoelastic material models to characterize the tissue. These studies have primarily been concerned with determining scleral response to tensile loads through uniaxial, biaxial, and inflation tests (Cruz Perez et al., 2014; Eilaghi et al., 2010; Grytz & Siegwart, 2015) and are generally performed in species well suited to ocular biomechanical studies due to the large size of their eyes e.g. pigs, cattle, and monkeys (Campbell et al., 2014), unfortunately, these same species are poorly suited to studying connections between microstructure, biomechanics, and molecular factors due to limited availability of molecular reagents and difficulties in directly manipulating genetic factors. On the other hand, the mouse is well suited to molecular studies; however, current methods of characterizing tissue-level material properties do not scale down well to the small mouse eye (∼3 mm diameter).

Saint Venant's principle, which states that arbitrary stress distributions due to loading become uniform a sufficient distance from the applied load, is normally utilized in the design and analysis of these experiments to account for stress concentrations that arise from the mechanical interaction of the testing device gripping the sample. With a sufficiently large sample, this uniform stress distribution assumption can be easily met and the effect of the grips is likely negligible; however, in the case of the mouse sclera, acquiring enough tissue in the area of interest is not feasible (Legerlotz et al., 2010). The small eye size imposes further technical constraints and challenges that would need to be overcome to employ a standard tensile test. The small diameter would also cause any strips of tissue cut from the sphere to be significantly curved, imposing bending stresses during straightening that

would be difficult to account for. The mouse sclera is also extremely thin ($<100\,\mu m$) and this thickness is spatially heterogeneous (Myers et al., 2010; Norman et al., 2010), making analysis of a tensile tests difficult and resulting properties prone to an additional source of measurement error.

For these reasons, the mouse has only been involved in a handful of ocular biomechanics studies (Myers et al., 2010; Nguyen et al., 2013; Wang et al., 2017; Wang & Larin, 2014). While a few displacement-imaging studies have been performed on the mouse sclera, the results are still prone to large measurement errors due to the eye size (Myers et al., 2010). More importantly even, the biomechanical outcome measures available in these previous studies did not separate the effect of sample geometry from material properties. Thus, the use of these methods is of limited use for the study of ocular pathologies that involve altered anatomy, e.g., myopia and glaucoma.

Compression testing is well suited to small and limited tissue samples due to the lack of necessary mechanical attachment of the sample to the apparatus. However, compression testing of uniphasic materials typically only yields compressive properties, which are likely of secondary importance to the tensile properties in the context of the sclera due to the nature of the loading imposed by the intraocular pressure (IOP). By relaxing the uniphasic idealization of the sclera, a biphasic formulation of poroelastic theory can be applied to the analysis of compression testing to obtain compressive, tensile, and hydraulic properties simultaneously. Poroelastic theory has been used to characterize the biomechanical response of many biological tissues, including cartilage (Armstrong et al., 1984), bone (Cowin, 1999), vasculature (Johnson & Tarbell, 2001), ligaments, tendons (Atkinson et al., 1997), and cornea (Hatami-Marbini & Etebu, 2013); however, it is still utilized infrequently compared to other

material models, such as the linear elastic and hyperelastic theories, and it has never been applied to the analysis of the sclera.

Our goal was to develop methodology for quantifying material properties of the mouse sclera. To do so, we performed unconfined compression experiments and took advantage of the microstructural complexity of the sclera by analyzing the experiments with a biphasic poroelastic model. We show that this approach can reliably characterize material properties of porcine sclera and obtain results comparable to other methods in the literature. We further show that compression testing can biomechanically interrogate the much smaller mouse sclera, and we report its intrinsic material properties for the first time. The ability to accurately measure the properties of the mouse sclera is desirable as it allows for a more direct exploration of genetic contributions to scleral biomechanics and associated ocular disorders through the use of transgenic animals and other technologies.

3.3 Materials and Methods

3.3.1 Animals

All animals were treated according to the Association for Research in Vision and Ophthalmology (ARVO) Statement for the Use of Animals in Ophthalmic and Vision Research and relevant Institutional Animal Care and Use Committee-approved protocols at the Atlanta Veteran Affairs Healthcare System. Male C57BL/6J mice were ordered from Jackson Laboratory (Bar Harbor, Maine, USA) and housed on a 12 hr:12 hr light:dark cycle in the Atlanta Veterans Affairs Healthcare System animal facility. A total of 7 mice from 3 litters were used in the study, with a mean age of $\sim$4 months. Mice were sacrificed by CO_2 asphyx-

iation and eyes were immediately enucleated, marked for orientation, and stored in 0.1M (1X) phosphate-buffered saline (PBS) (Thermo Fisher Scientific, Waltham, MA). Porcine eyes were obtained from a local abattoir (Holifield Farms, Covington, GA) and stored in a solution of Hanks balanced salt solution (MP Biomedicals) with antibiotics. A total of 4 pig eyes were tested from pigs of approximately 6 months of age. All eyes were maintained at 4 °C until use and used the day of animal sacrifice, except where otherwise stated.

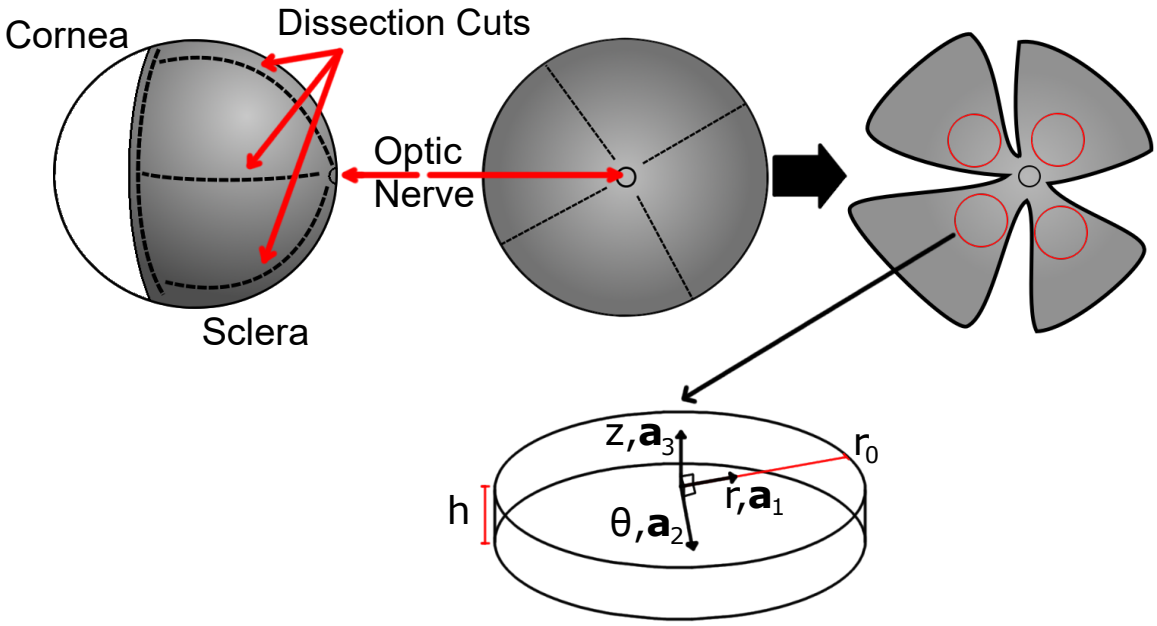

Figure 3.1: Schematic detailing the dissection procedure in a mouse eye. Top: Cornea was removed at the corneoscleral junction and intraocular tissues were removed. The resulting scleral shells were opened into four regions. Red circles show the typical punch locations in the mouse eyes; dashed lines show dissection cuts. Pig eyes were dissected similarly. Bottom: Punched samples were assumed to be cylindrical and a cylindrical coordinate system was assigned as shown. Scleral samples were always taken such that the axial cylindrical axis z and the material symmetry axis a_3 were coincident. r_0 and h are the sample radius and thickness in the reference configuration.

3.3.2 Sample Preparation

Porcine eyes were dissected in open air with periodic application of PBS to prevent dehydration; mouse eyes were dissected while submerged in PBS. Orbital muscle, fat, and con-

junctiva were cleaned from the outer coat and then eyes were bisected at the corneoscleral junction, and the intraocular tissues were removed to create a scleral shell. This shell was then opened to create four oriented regions (Figure 3.1).

A 1mm diameter sample was harvested from the posterior region of the scleral shell using a biopsy punch immediately prior to testing. Due to the higher likelihood of failure in the mouse samples, four samples were taken from each eye (one sample per quadrant). Porcine and mouse samples were taken approximately 5 mm and 0.5 mm away from the optic nerve head, respectively, to avoid excessive circumferential alignment of collagen around the optic nerve head while remaining primarily in the posterior sclera (Boote et al., 2020). Graphite powder was applied to scleral samples to reduce friction between samples and compression platens.

Eyes were rejected prior to testing if they were grossly abnormal, e.g., had cataracts or evident damage to the sclera from enucleation or dissection. Mouse samples were rejected prior to testing if the biopsy did not cleanly remove the sample or if the samples were noticed to fold prior to being placed between the compression platens.

3.3.3 Unconfined Compression Testing

A cantilever-based compression testing apparatus (CellScale Microsquisher, Waterloo, ON, Canada) was used to perform unconfined axial compression tests on scleral samples. This device controls the position of the base of a cantilevered tungsten beam with known geometry, and a calibrated camera measures the beam tip position (resolution: 0.6155 μm/px). A glass platen is fixed to the beam by cyanoacrylate adhesive (Figure 3.2). Software (Squisherjoy v5.34) calculates the deflection of the beam, which is then used to calculate the force

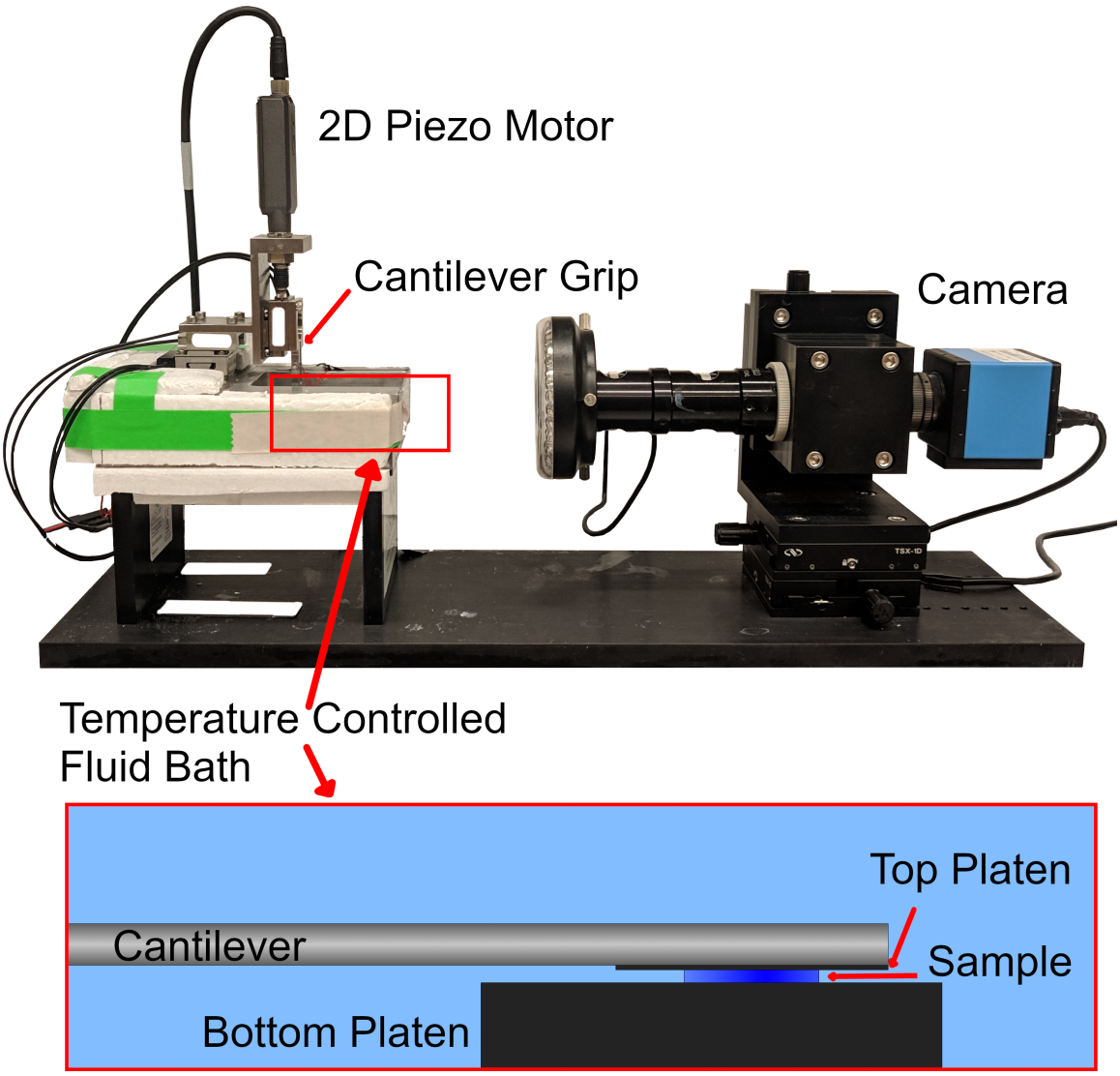

Figure 3.2: CellScale Microsquisher Compression Device. Top: Side view of the device. A piezo motor controls the gripped base position of a cantilevered beam. Tip position of the beam is measured by a camera and image processing software. Bottom: Side view of the interior of the fluid bath. The top platen is affixed to the cantilevered beam by cyanoacrylate adhesive.

applied to the sample in real time throughout the test. Data was collected at the compression system's maximum sampling rate of 5Hz.

Both pig and mouse samples were submerged in a temperature-controlled bath set to 37°C and underwent the same preconditioning protocol, including a period of cyclic loading followed by the application of the same static tare load (Figure 3.3). 500 µN (636 Pa

engineering stress) was chosen for the magnitude of the tare load, in order to flatten the samples and ensure good contact between the sample and platens, as is standard in compression tests (Hatami-Marbini & Etebu, 2013; Soltz & Ateshian, 2000). The magnitude of tare loading was comparable to loads previously used (Battaglioli & Kamm, 1984; Hatami-Marbini & Etebu, 2013) and allowed the total applied compressive stress at final equilibrium (including the tare load) to approximate the physiological IOP (2.16±0.31kPa). Samples were allowed to creep under this tare load until equilibration ($\sim$ 30 min). In preliminary experiments on mouse sclera where only the tare loading portion of the preconditioning protocol was performed, the time taken to equilibrate under the tare load was variable, which likely added additional variability in measured scleral material properties. The thickness of each sample at equilibrium was measured optically using the testing device's calibrated camera. The equilibrated configuration was used as the reference for calculations of stress and strain.

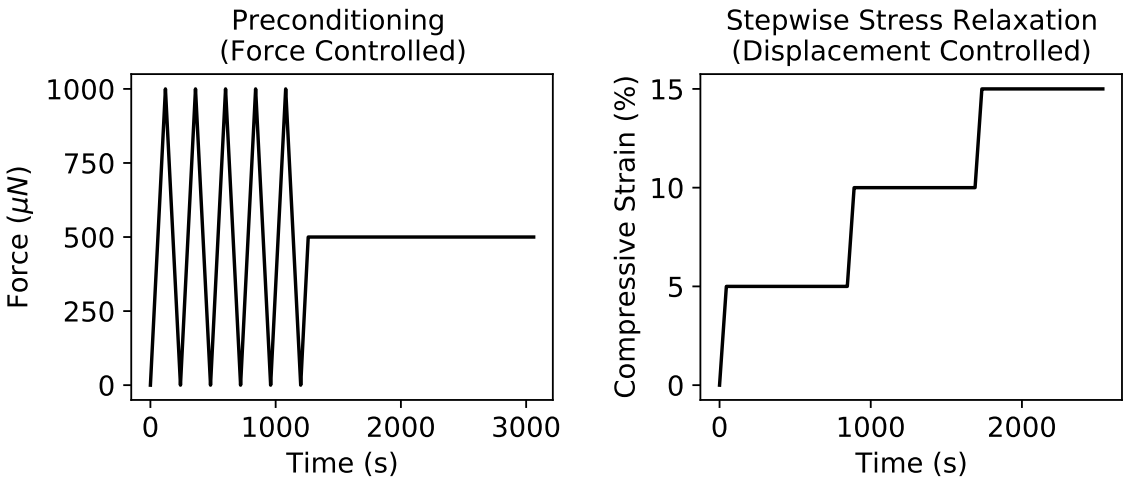

Figure 3.3: Preconditioning and stress relaxation protocol for unconfined compression. (a) Preconditioning protocol applied to all samples under force-controlled mode of the compression device. (b) Representative stepwise stress relaxation experiment applied under displacement-controlled mode. Exact duration of relaxation phase and ramp time varied by sample.

Stepwise stress relaxation experiments were performed on tare-loaded samples. 15% compressive strain was applied over three 5% strain ramp-hold steps, allowing stress to relax and equilibrate before initiating the subsequent step. 15% compressive strain was chosen as the maximum applied strain in order to conform to the assumption of small strains used to formulate the material model. Mouse and porcine sclera were compressed at $\sim$0.01 1/s and 0.001 1/s, respectively, with the difference being due to the vastly different sample dimensions and device limitations (see Discussion). However, all samples equilibrated to a similar state of compression (5.01 ± 0.28% strain per step).

Samples were rejected after testing if all three strain steps were not successfully applied (3 samples), if the cyanoacrylate glue failed to sufficiently fix the glass platen to the beam throughout the entirety of the test (3 samples), or if significant stress relaxation was still occurring when the next step in an experiment began (1 sample).

Porcine samples were used to determine the test-retest reliability, or repeatability, of the experimentally measured material properties. After the initial stress relaxation test, porcine samples were stored in PBS at 4°C until retesting the following day. Mouse samples were not used for test-retest studies due to their extremely small size, which made extended handling difficult due to their tendency to fold on themselves.

3.3.4 Biphasic Poroelastic Theory

A modified formulation of the biphasic conewise linear elastic (BCLE) theory of Soltz and Ateshian (Soltz & Ateshian, 2000) was used to model the unconfined compression response of cylindrical scleral samples. The theory considers a material composed of two phases, a solid matrix and an imbibing fluid, each individually assumed incompressible but with no

assumptions made on the compressibility of the mixture. The solid matrix is postulated to be bimodular, i.e., it responds differently to tension and compression. The samples are assumed to be cylindrical and have frictionless interfaces with the platens applying the compression, together resulting in a shear-free state of deformation and a uniform axial strain field.

Under these conditions, compressive strains will occur in the z-direction (the through-plane) and tensile strains will occur in the r- and θ-directions (the in-plane). Due to the separation of tensile and compressive strains into orthogonal directions in this configuration, a cubic symmetry assumption combined with tension-compression nonlinearity is similar in practice to a transverse isotropy assumption, in that both assign the in-plane and through-plane directions different stiffnesses. This assumption is reasonable for the sclera since scleral collagen fibers are preferentially aligned in-plane (Boote et al., 2020).

The total second Piola-Kirchoff stress $\boldsymbol{S}$ experienced by a biphasic poroelastic material can be decomposed into the stress that results from the solid matrix deformation, $\boldsymbol{S^e}$, and an isotropic normal stress due to the interstitial fluid pressure,

$$\boldsymbol{S} = -p\boldsymbol{I} + \boldsymbol{S^e} \tag{3.1}$$

This model is governed by two equations - the mixture momentum equation, assuming negligible inertial and body forces

$$div\,(\boldsymbol{S}) = 0 \tag{3.2}$$

and the mixture continuity equation,

$$div\left(\boldsymbol{v^s} + \boldsymbol{w}\right) = 0 \tag{3.3}$$

where $\boldsymbol{w}$ is the flux of the fluid relative to the solid and $\boldsymbol{v^s}$ is the solid phase velocity.

3.3.4.a Constitutive Relations

Two constitutive relations are assumed. First, fluid flux in the tissue is linearly related to the pressure gradient, i.e. Darcy's law holds

$$\boldsymbol{w} = -\boldsymbol{k}\nabla p \tag{3.4}$$

where $\boldsymbol{k}$ is the permeability tensor and ∇p is the pressure gradient.

Second, conewise linear elasticity (CLE) of Curnier et al (Curnier et al., 1995) is assumed for the solid matrix, valid for small strains. In brief, this model describes a material with 3 principal material directions (orthotropic) with identical properties in the three orthogonal directions (cubic symmetry) but which responds differently to tensile and compressive strains (bimodular). The strain-energy density function, $W\left(\boldsymbol{E}\right)$, for this material is given as

$$W\left(\boldsymbol{E}\right) = \sum_{a=1}^{3}\left\{\frac{\lambda_1[\boldsymbol{A}_a:\boldsymbol{E}]}{2}tr^2\left(\boldsymbol{A}_a\boldsymbol{E}\right) + \mu tr\left(\boldsymbol{A}_a\boldsymbol{E}^2\right) + \sum_{\substack{b=1\\b\neq a}}^{3}\frac{\lambda_2}{2}tr\left(\boldsymbol{A}_b\boldsymbol{E}\right)tr\left(\boldsymbol{A}_a\boldsymbol{E}\right)\right\} \tag{3.5}$$

which relates $\boldsymbol{S}^e$ to the Green-Lagrange material strain tensor $\boldsymbol{E}$ by

$$\boldsymbol{S}^{e}\left(\boldsymbol{E}\right)=\sum_{a=1}^{3}\left\{\lambda_{1}\left[\boldsymbol{A}_{a}:\boldsymbol{E}\right]tr\left(\boldsymbol{A}_{a}\boldsymbol{E}\right)\boldsymbol{A}_{a}+\sum_{\substack{b=1\\b\neq a}}^{3}\lambda_{2}tr\left(\boldsymbol{A}_{a}\boldsymbol{E}\right)\boldsymbol{A}_{b}\right\}+2\mu\boldsymbol{E} \tag{3.6}$$

where $[\boldsymbol{A}_a : \boldsymbol{E}]$ and λ_2 are the elastic constants, μ is the shear constant, $\boldsymbol{A_a}$ are three texture tensors that define the unit normals describing three orthogonal hyperplanes of material symmetries, $\boldsymbol{A_a} = \boldsymbol{a_a} \bigotimes \boldsymbol{a_a}$, $\bigotimes$ denotes the dyadic product of two vectors, and $tr\left(\ \right)$ is the trace operator.

This model captures tension-compression nonlinearity through the discontinuity of λ_1 across tensile and compressive deformations, represented by

$$\left[\boldsymbol{A}_{a}:\boldsymbol{E}\right]:=\begin{cases}\lambda_{-1}\ , & \boldsymbol{A}_{a}:\boldsymbol{E}<0\\ \lambda_{+1}\ , & \boldsymbol{A}_{a}:\boldsymbol{E}>0\end{cases} \tag{3.7}$$

λ_{-1} and λ_{+1} can be mapped to more physically meaningful constants by the following relations

$$H_{-A}=\lambda_{-1}+2\mu \tag{3.8a}$$

$$H_{+A}=\lambda_{+1}+2\mu \tag{3.8b}$$

where H_{-A} is the compressive modulus of a confined sample or aggregate compressive modulus, and H_{+A} is the aggregate tensile modulus.

3.3.4.b Modeling Unconfined Compression

Unconfined axial compression of a cylindrical sample, assuming frictionless contact between the platens and sample, is described by the following strain tensor

$$[\boldsymbol{E}] = \begin{bmatrix} \boldsymbol{E_{rr}} & 0 & 0 \\ 0 & \boldsymbol{E_{\theta\theta}} & 0 \\ 0 & 0 & \boldsymbol{E_{zz}} \end{bmatrix} = \begin{bmatrix} \frac{\partial u_r}{\partial r} & 0 & 0 \\ 0 & \frac{u_r}{r} & 0 \\ 0 & 0 & \frac{\partial u_z}{\partial z} \end{bmatrix} \tag{3.9}$$

where $\boldsymbol{u}$ is the displacement vector in the current configuration, and the subscripts r, θ, and z represent the three dimensions of the cylindrical coordinate system.

The stress tensor describing the solid matrix under these conditions is obtained by substituting the strain components of Equation 3.9 into Equation 3.6

$$[\boldsymbol{S^e}] = \begin{bmatrix} H_{+A}\frac{\partial u_r}{\partial r} + \lambda_2\left(\frac{u_r}{r} + \frac{\partial u_z}{\partial z}\right) & 0 & 0 \\ 0 & H_{+A}\frac{u_r}{r} + \lambda_2\left(\frac{\partial u_r}{\partial r} + \frac{\partial u_z}{\partial z}\right) & 0 \\ 0 & 0 & H_{-A}\frac{\partial u_z}{\partial z} + \lambda_2\left(\frac{u_r}{r} + \frac{\partial u_r}{\partial r}\right) \end{bmatrix} \tag{3.10}$$

Under the above assumptions of frictionless contact and axisymmetric conditions, the axial (engineering) strain imposed by the platen in a stress-relaxation experiment is independent of position and is equal to the prescribed displacement of the platens, $u_a(t)$, normalized by the thickness, h, of the sample,

$$\frac{\partial u_z(t)}{\partial z} \equiv \varepsilon(t) = -\frac{u_a(t)}{h} \tag{3.11}$$

The specific process of applying the biphasic and constitutive equations to frictionless unconfined compression of cylindrical samples has been detailed many times previously (Armstrong et al., 1984; Cohen et al., 1998; Mak, 1986; Soulhat et al., 1999). The main governing equation is the differential equation describing the radial displacement of the sample

$$\frac{\partial^2 u_r}{\partial r^2} + \frac{1}{r}\frac{\partial u_r}{\partial r} - \frac{u_r}{r^2} - \frac{1}{H_{+A}k_r}\frac{\partial u_r}{\partial t} = \frac{1}{H_{+A}k_r}\frac{r}{2}\dot{\varepsilon} \tag{3.12}$$

where the over dot ($\dot{}$) implies a time derivative. Applying the boundary conditions that enforce axisymmetry and traction-free lateral boundaries,

$$u_r\left(r=0,t\right)=0 \tag{3.13a}$$

$$S_{rr}\left(r_0,t\right) = -p\left(r_0,t\right) + S^e_{rr}\left(r_0,t\right) = 0 \tag{3.13b}$$

an analytical solution to the partial differential equation can be obtained in the Laplace domain, permitting the determination of the fluid pressure by Equation 3.3 and Equation 3.4 and a dynamic modulus that relates engineering axial stress ($\overline{\sigma}\left(\hat{s}\right) = \overline{F}(\hat{s})/\pi r_0^2$) to engineering axial strain ($\overline{\varepsilon}\left(\hat{s}\right) = \overline{u}_a(s)/h$) through material properties in a frequency-dependent manner

$$\overline{G}\left(\hat{s};A,B,C\right) = \frac{\overline{F}(\hat{s})/\pi r_0^2}{\overline{u}_a(\hat{s})/h} = \frac{\overline{\sigma}(\hat{s})}{\overline{\varepsilon}(\hat{s})} = \frac{BI_0\left(\sqrt{\hat{s}}\right) - C\frac{I_1(\sqrt{\hat{s}})}{\sqrt{\hat{s}}}}{I_0\left(\sqrt{\hat{s}}\right) - A\frac{I_1(\sqrt{\hat{s}})}{\sqrt{\hat{s}}}} \tag{3.14}$$

where

$$\hat{s} = \frac{s}{s_0} \tag{3.15a}$$

$$s_0 = \frac{H_{+A} k_r}{r_0^2} \tag{3.15b}$$

$$A\left(H_{+A}, \lambda_2\right) = 1 - \frac{\lambda_2}{H_{+A}} \tag{3.15c}$$

$$B\left(H_{-A}, H_{+A}, \lambda_2\right) = \frac{2H_{-A} - 3\lambda_2 + H_{+A}}{2} \tag{3.15d}$$

$$C\left(H_{-A}, H_{+A}, \lambda_2\right) = A\left(H_{-A} + H_{+A} - 2\lambda_2\right) \tag{3.15e}$$

In the above expressions, F is the total axial force applied to the sample, u_a is the applied axial displacement, r_0 is the sample radius, h is the sample thickness, s is the complex frequency, s_0 is a characteristic angular frequency used to nondimensionalize s, r_0 is the initial radius of the specimen, and I_0 and I_1 are modified Bessel functions of the first kind. Over bars (—) represent quantities in the Laplace domain and over hats ($\widehat{\ }$) represent nondimensionalized quantities. The nondimensionalized dynamic modulus can further be obtained by normalizing the stress and strain signals to their equilibrated values in a stress relaxation test, σ_{eq} and ε_{eq}. This dynamic modulus has a form common to most other biphasic models of unconfined compression (Armstrong et al., 1984; Cohen et al., 1998; Huang et al., 2003; Mak, 1986; Soulhat et al., 1999), with the forms of the A, B, and C parameters dependent on the choice of material model for the solid matrix.

Four material properties describe the tissue: the aggregate compressive modulus H_{-A}, aggregate tensile modulus H_{+A}, the off-diagonal modulus λ_2, and the hydraulic permeability k_r. Tensile and compressive Poisson's ratio ($v_{\pm}$) can be calculated by the relationship

$v_{\pm} = (H_{\pm A} + \lambda_2)/\lambda_2$. The shear modulus cannot be measured in these experiments due to the assumption of shear-free state of deformation. The off-diagonal modulus λ_2 can best be interpreted in the context of a confined compression experiment, where samples are physically prevented from expanding radially. If a sample were fully confined and axial compression were applied, λ_2 would represent the ratio of stress applied to the confining walls to the amount of axial strain applied (Khalsa & Eisenberg, 1997).

By taking the limit of the dynamic modulus in low frequencies, we obtain a relationship between the equilibrium unconfined compressive (Young's) modulus E_{-Y} and the other CLE constants

$$\lim_{\hat{s}\to 0} \overline{G}(\hat{s}) = E_{-Y} = \frac{2B - C}{2 - A} = H_{-A} - \frac{2\lambda_2^2}{H_{+A} + \lambda_2} \tag{3.16}$$

In an unconfined compression stress relaxation test, this modulus is directly measured as the ratio of equilibrium stress to equilibrium strain, $E_{-Y} = \sigma_{eq}/\varepsilon_{eq}$. By rearranging Equation 3.16 to isolate H_{-A}, it is convenient to reformulate B and C to be in terms of this directly determined quantity

$$B\left(E_{-Y}, H_{+A}, \lambda_2\right) = \frac{2E_{-Y} + \frac{4\lambda_2^2}{H_{+A}+\lambda_2} - 3\lambda_2 + H_{+A}}{2} \tag{3.17a}$$

$$C\left(E_{-Y}, H_{+A}, \lambda_2\right) = A\left(E_{-Y} + \frac{2\lambda_2^2}{H_{+A} + \lambda_2} + H_{+A} - 2\lambda_2\right) \tag{3.17b}$$

This modification to the formulation of the dynamic modulus allows for the direct determination of one material property from an unconfined stress relaxation experiment, whereas

prior studies using this model performed an additional confined compression experiment to determine H_{-A}, so as to reduce the dimensionality of the optimization problem when fitting the model to experimental data.

3.3.5 Data Analysis

Fitting of experimental data to determine material constants followed the following procedure:

1. Engineering stress and engineering strain were calculated by dividing the axial force, $F_z(t)$, and axial displacement, $u_a(t)$, by the reference configuration contact area (assumed identical to the internal area of the biopsy punch) and initial sample thickness, respectively. Each of the three stress-relaxation steps for each sample were analyzed independently. The final 50 seconds of each step were assumed to be fully equilibrated, and mean values of stress (σ_{eq}) and strain (ε_{eq}) over this time were used to calculate E_{-Y} at each loading step.

2. Stress and strain signals were normalized by each of their equilibrated values and represented by a linear interpolation function with an analytical Laplace transform, as defined in Huang et al (Huang et al., 2003). Due to the inherent force-controlled nature of the compression device used, the ratio of transformed strain to stress was used to create an experimental transfer function, $\widehat{\overline{\boldsymbol{Y}}}_{exp}(s) = \widehat{\overline{\varepsilon}}_{exp}(s)/\widehat{\overline{\sigma}}_{exp}(s)$, that could be used to determine the experimental gain and phase; this quantity is the reciprocal of the derived BCLE dynamic modulus (Equation 3.14).

3. The remaining three unknown material properties, H_{+A}, λ_2, and k_r, were obtained

by curve fitting the reciprocal of $\overline{G}$, $\widehat{\overline{\boldsymbol{Y}}}_{model}$, to $\widehat{\overline{\boldsymbol{Y}}}_{exp}$ over a limited frequency range (10^{-7}–10^{-1} Hz).

The frequency range was informed by previous studies in cartilage and was chosen to capture the behavior of the samples while limiting the influence of measurement noise. A differential evolution algorithm was used to cover a wide expanse of the parameter space and decrease the chance of local minima convergence during minimization of the chosen objective function (Arruda, 1992; Hu et al., 2013),

$$Obj = ln\left(1 - R\right) \tag{3.18}$$

where R is the cross-correlation between the experimental transfer function and model, given by

$$R\left(\widehat{\overline{Y}}_{exp}, \widehat{\overline{Y}}_{model}\right) = \frac{\widehat{\overline{\boldsymbol{Y}}}_{exp} \bullet \widehat{\overline{\boldsymbol{Y}}}_{model}}{\left\|\widehat{\overline{\boldsymbol{Y}}}_{exp}\right\| \left\|\widehat{\overline{\boldsymbol{Y}}}_{model}\right\|} \tag{3.19}$$

Bounds were implemented for the fitted material properties to enforce positive definiteness of the elasticity tensor

$$H_{+A} > 0 \tag{3.20a}$$

$$-\frac{H_{-A}}{2} < \lambda_2 < H_{-A} \tag{3.20b}$$

$$-\frac{H_{+A}}{2} < \lambda_2 < H_{+A} \tag{3.20c}$$

Due to the inherent dependence of permeability on compressive strain, a standard ex-

ponential model (Hatami-Marbini & Etebu, 2013; Lai & Mow, 1980) was fit to the three permeability values obtained for each sample, given by

$$k_r(\varepsilon) = k_0 e^{-M\varepsilon} \tag{3.21}$$

where ε is the compressive engineering strain, k_0 represents the in-plane permeability at 0% compressive strain, and M defines the nonlinearity of the relationship between compressive strain and permeability.

It is convenient to visualize the model stress in the time domain for various purposes. For such visualizations, the Laplace domain interpolation function describing the experimental strain was substituted into Equation 3.14, and the time domain stress signal was calculated using the De Hoog algorithm for numerical inverse Laplace transform using the mpmath Python library (Johansson et al., 2018).

3.3.6 Statistical Analysis

Goodness of fits of the models, $\widehat{\overline{\boldsymbol{Y}}}_{model}$, to the experimental transfer functions, $\widehat{\overline{Y}}_{exp}$, are reported as the nonlinear coefficient of determination, r^2, defined as (Kvalseth, 1985)

$$r^2 = 1 - \frac{\sum \left(\widehat{\overline{\boldsymbol{Y}}}_{exp,i} - \widehat{\overline{\boldsymbol{Y}}}_{model,i}\right)^2}{\sum \left(\widehat{\overline{\boldsymbol{Y}}}_{exp,i} - mean(\widehat{\overline{\boldsymbol{Y}}}_{exp,i}\right)^2} \tag{3.22}$$

The four material properties obtained from each step of each experiment were analyzed using a random-intercept generalized linear mixed effects model (GLMM) using the "lme4" package in R (Bates, Mächler, et al., 2015). Gamma distributed errors were assumed with a log link function to ensure positive fitted values, as the tensile and compressive moduli

and hydraulic conductivity are strictly positive. Due to the range of λ_2 values crossing zero, all values were translated to positive using standard transformations. The statistical model was defined as

$$DV \sim Species + Strain + Species : Strain + (1|ID) \tag{3.23}$$

where DV is one of the material properties, $Species$ is either pig or mouse, $Strain$ is the amount of compressive strain applied, $Species : Strain$ accounts for the interaction of the two fixed effects, and $(1|ID)$ is the random intercept factor that accounts for the three repeated measurements on the same sample. Likelihood ratio tests were performed between the full model (Equation 3.23) and three null models, each lacking one of the fixed effect terms, to test for significance of the factors. In the presence of significant interaction effects, Tukey post hoc tests were performed, and the adjusted p values are reported. Only the first measurement of each porcine sample was included in the analysis comparing species.

The test-retest repeatability between first and second test of porcine scleral samples were analyzed by calculating both Pearson (ρ) and Lin's concordance (ρ_c) correlation coefficients for the fitted tensile stiffness and hydraulic conductivity and the measured thickness and compressive modulus values. Perfect concordance or discordance would be represented by ρ_c values of ± 1, whereas a ρ of ± 1 would indicate perfect univariate correlation. All results are reported as the mean $\pm$ standard deviation unless otherwise noted.

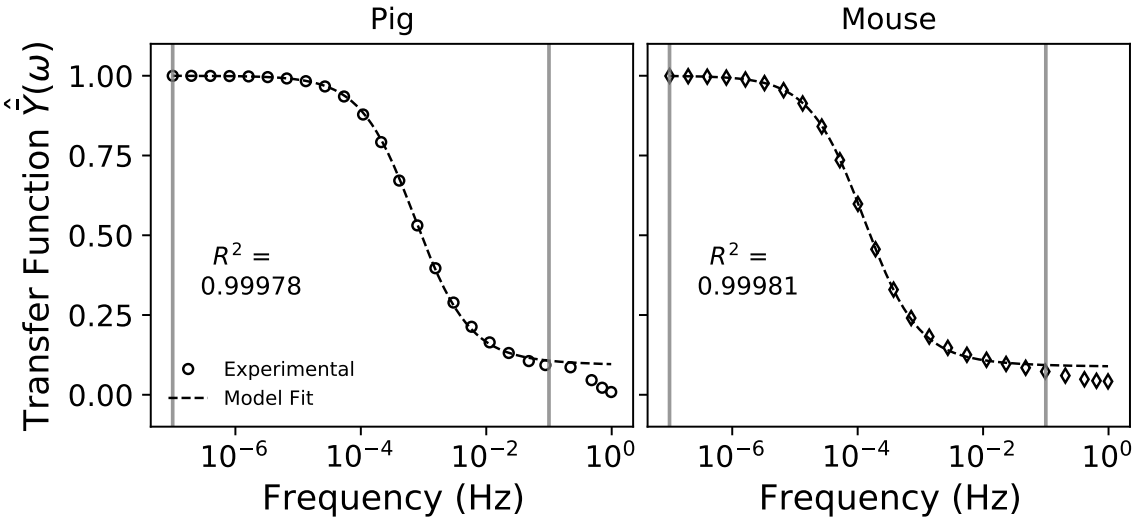

Figure 3.4: Experimental and fitted transfer functions for pig (left) and mouse (right). Vertical lines represent the bounds of the data range used for fitting. Excellent agreement was seen over fitting region as judged by the nonlinear R^2 (Equation 3.22), with deviations present at higher frequencies. The reported R^2 value refers only to fitting between the vertical lines.

3.4 Results

In total, 10 eyes were included for analysis (4 porcine, 6 mouse), which included 13 unique samples (4 porcine, 9 mouse) and 51 fitted stress relaxation steps (24 porcine, 27 mouse). Seven samples in total were excluded from analysis after testing. One sample was taken from each pig eye, and each sample was tested twice. When samples were successfully tested from multiple regions of the same mouse eye, the obtained properties were averaged. The thickness of the samples after preload was 1294±241 μm for the porcine sclera and 77.2±8.9 μm for the murine sclera.

3.4.1 Quality of Curve fitting

The biphasic CLE theory successfully fit the unconfined compression response of scleral samples from both species (Figure 3.4). The average nonlinear coefficients of determi-

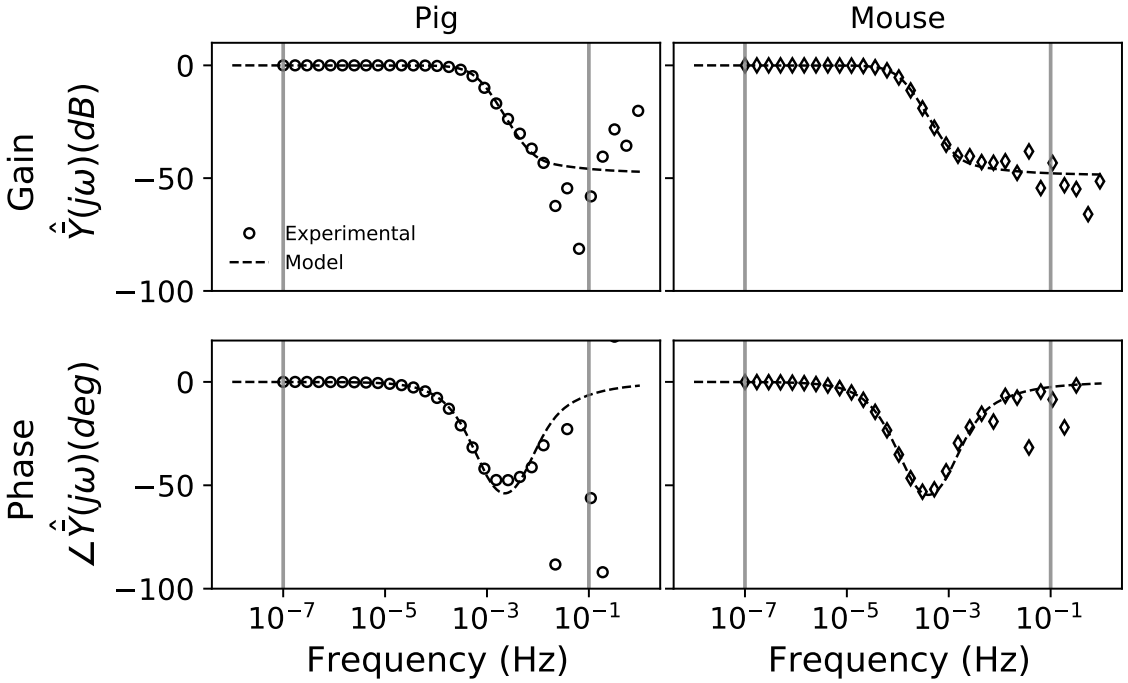

Figure 3.5: Experimental and model Bode plots for pig (left) and mouse (right) scleral samples. Top: Gain as a function of frequency. Bottom: Phase as a function of frequency. Model values were calculated using the material properties obtained by curve fitting the transfer function over a selected frequency range (represented by the vertical lines). Both species show frequency dependence for gain and phase that are matched well by the model. Noise infiltration exists at the higher frequencies primarily due to the high frequency camera noise of the device, while noise infiltrates at lower frequencies in the pig due to the slower ramp speed.

nation of the model to experimental data (Equation 3.22) in the frequency domain were 0.9989±0.0006 and 0.9982±0.0018 for samples from pig and mouse, respectively. Fitting was repeated ten times for each of the 51 strain steps using different starting populations selected by randomly seeded Latin hypercube sampling of the bounded parameter space. Of the 10 fits performed for each of the 51 steps, none converged on appreciably different sets of parameters. This translated to a small coefficient of variation for each parameter over the repeated fittings (H_{+A}: 0.562%, λ_2:2.02%, k: 2.04%).

The calculated model phase and gain components showed good agreement with the experimental components over a wide range of frequencies (Figure 3.5). Similarly, the

model time domain stress obtained by convolving the experimental strain with the impulse response function also agreed well with the experimental data, showing similar peak stresses and relaxation time between model and experiment (Figure 3.6).

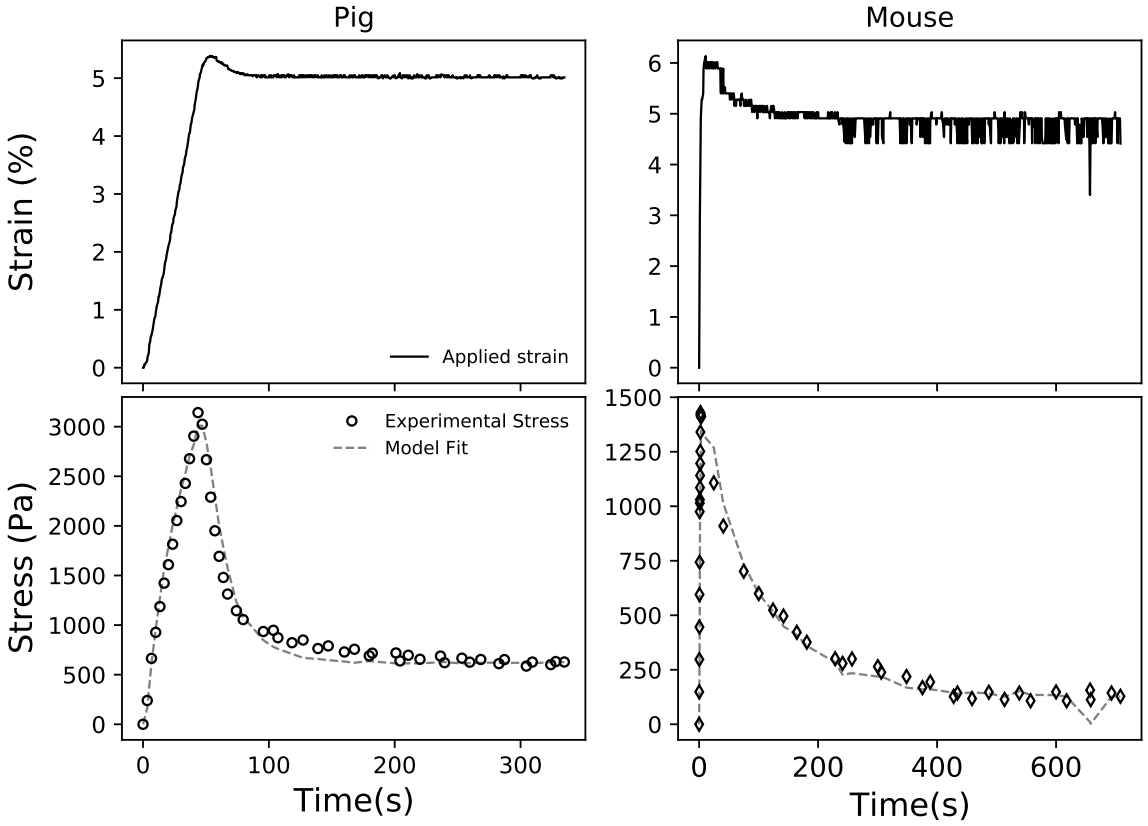

Figure 3.6: Representative strain measurements for both pig (left) and mouse (right) scleral samples at the first step (0-5% strain) and the resulting model fit. Top: Engineering compressive strain during a ramp-hold experiment at 5% compressive strain. Significant deviation from the desired strain vs. time profile is evident in both species at both ramp speeds due to limitations of the testing equipment (see text). Bottom: Time-domain experimental compressive stress and modelled stress, as determined from the applied strain for pig and mouse scleral samples. Note, significantly more noise is visible in the mouse strain signal due to the thinner sclera. The camera and beam tracking add noise to the measurements of displacement to a similar degree in both species, but the noise makes up a smaller percentage of the overall displacements in the pig sclera.

3.4.2 Material Properties

For both species, both tensile modulus and permeability were highly dependent on the state of compressive strain of the sample (Figure 3.7); the tensile modulus was seen to increase

with increasing compressive strain, while the hydraulic conductivity decreased. However, a significant interaction effect between the state of compressive strain and species were also found for both the tensile modulus and permeability (*Species:Strain*; H_{+A}: p<0.001, k: p<0.001), implying that both properties are dependent on state of compressive strain in a species-dependent manner. The porcine sclera was significantly stiffer in tension than the mouse sclera at the first two strain steps (p<0.001 for both 5 and 10% strain), with the difference vanishing at the third strain step (p=0.098). The hydraulic conductivity of the murine and porcine sclera were not different over the first two strain steps (5% strain: p=0.34; 10% strain: p=0.90), with the mouse sclera significantly less permeable than the porcine sclera at the third strain step (p<0.001). E_{-Y} and λ_2 were not observed to be species-dependent (E_{-Y}: p=0.26; λ_2: p=0.19) or change with compressive strain (E_{-Y}: p=0.06; λ_2: p= 0.29) (Table 3.1). The average tensile Poisson's ratios were 0.469±0.048 and 0.5±0.004 for pig and mouse sclerae, respectively. The average compressive Poisson's ratios were 0.028±0.007 and 0.082± 0.050 for pig and mouse sclerae, respectively, after the removal of one outlier in the mouse group.

Table 3.1: Average poroelastic properties of porcine and mouse sclera (averaged over strain steps and samples) as determined by the BCLE model. n values refer to the number of eyes tested.

Species	$\mathbf{E}_{-Y}$ [kPa]	$\mathbf{H}_{+A}$ [kPa]	$\boldsymbol{\lambda}_2$ [kPa]	**k** ($x10^{15}$) [m^4/(N s)]	$\mathbf{k}_0$ ($x10^{15}$) [m^4/(N s)]
Pig (n=4)	10.0 ± 3.2	341.4 ± 130.6	9.5 ± 3.6	8.6 ± 4.2	25± 33
Mouse (n=6)	10.1 ± 4.6	173.7 ± 118.9	12.6 ± 7.9	9.5 ± 9.7	62± 51

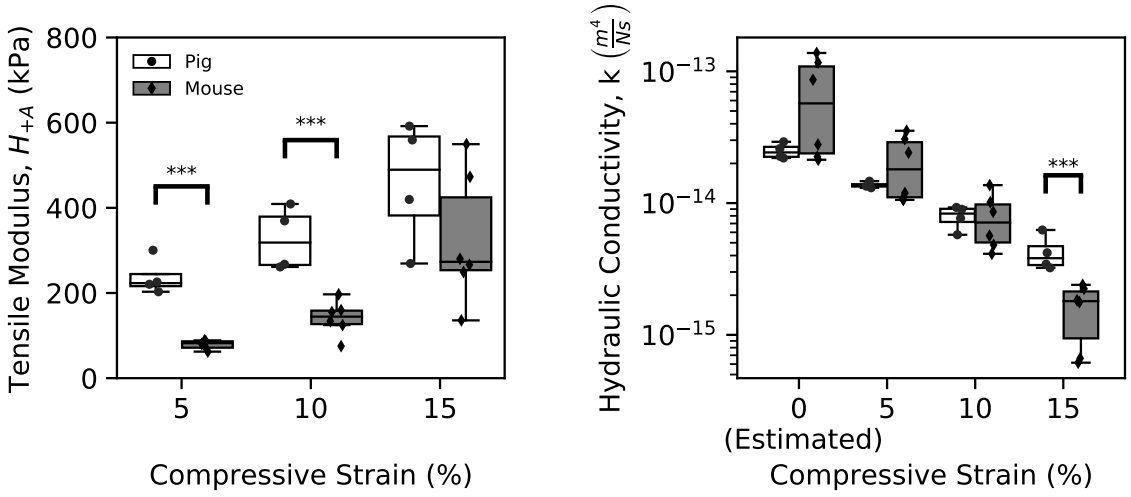

Figure 3.7: Relationship of tensile stiffness and hydraulic conductivity to compressive strain. Left: Tensile stiffness of pig and mouse sclera. Stiffness of both species' sclerae increased with increasing compressive strain, and a significant interaction effect was present (Species:Strain; $p<0.001$). Right: Hydraulic conductivity of pig and mouse sclera. Hydraulic conductivity of both species decreased with increasing compressive strain, and a significant interaction was present (Species:Strain; $p<0.001$). ***: $p<0.001$, **: $p<0.01$ by Tukey post hoc analysis with adjusted alphas for multiple comparisons.

3.4.3 Repeatability

The measured compressive moduli and thicknesses were both highly correlated (E_{-Y}: ρ_c=0.83, $p<0.001$; thickness**:** ρ_c=0.98, p=0.019); however, the concordance of the compressive moduli between experiments was only moderate (E_{-Y}: ρ_c=0.52; thickness: ρ_c=0.92), showing a general trend of increasing in stiffness from the first to second test (Figure 3.8). The fitted tensile moduli and permeabilities were both highly correlated and moderately concordant between the first and second tests (H_{+A}: ρ_c=0.82, p=0.001, ρ_c=0.76; k: ρ_c=0.83, $p<0.001$, ρ_c=0.82), not displaying any obvious trends.

3.5 Discussion

We describe here the first multiphasic biomechanical characterization of the sclera using the BCLE model and unconfined compression testing. Previous studies implementing biphasic models typically either performed both a confined and unconfined compression test on the same samples to characterize the tissue (Huang et al., 2001; Huang et al., 2003; Soltz & Ateshian, 2000) or made assumptions on the Poisson's ratio (Hatami-Marbini & Etebu, 2013; Soulhat et al., 1999). We show here that by reformulating the material properties using the limit solution of the dynamic modulus, a single unconfined compression test yields sufficient information to curve fit the model parameters consistently and yields physiologically reasonable estimates for the in plane tensile stiffness and in plane hydraulic conductivity of the tissue. This is crucial for the implementation of these methods for tissues in the mouse eye, as truly confined compression is quite challenging to achieve even in much larger samples. Importantly, good curve fitting was observed not only in porcine sclera, but also mouse sclera which was $\sim$15x thinner on average.

3.5.1 Applicability of BCLE to Sclera

The optimal scenario for determining how well a material model captures the physical characteristics of a tissue involves fitting a measured quantity to determine tissue material properties and then using the model and fitted properties to predict another simultaneously measured quantity, *e.g.*, curve fitting stress and comparing measured and model-predicted radial expansion or interstitial fluid pressure. Due to the physical size of the samples and the constraints on the compression device, this was not achievable in this study as we were not

able to simultaneously record another outcome measure. It was not possible to measure the radial expansion using the compression device's built-in camera due to the inability to keep the entire specimen in frame during the experiment. In order to achieve simultaneous measurements of a secondary outcome measure for predictive purposes, significant modifications or a custom compression set up would be necessary; however, the measurement would still not be trivial as the small specimens would lead to very small radial displacements and would make the measurement of fluid pressure quite difficult without significant deviations from the assumptions of flat, smooth platens. Future studies, potentially on much larger samples to avoid these technical challenges, may thus be necessary to fully validate the model's predictive capabilities in the sclera.

Thus, to gain an understanding of how well the model described the tissue response, we instead chose to compare the magnitude of the fitted porcine properties to the literature, while also judging the quality of the curve fitting and the repeatability and uniqueness of fitted properties. Each of these factors support the BCLE model as capable of describing the biomechanical response of the sclera under unconfined compression in a physiologically reasonable and unique manner, as detailed below.

3.5.2 Material Properties

3.5.2.a Tensile and Compressive Stiffness of Porcine Sclera

The tensile stiffness of porcine sclera has been previously characterized many times using uniaxial testing (Campbell et al., 2014); however, the nature of the loading is quite different from that used here, making comparisons challenging. The in-plane normal strains

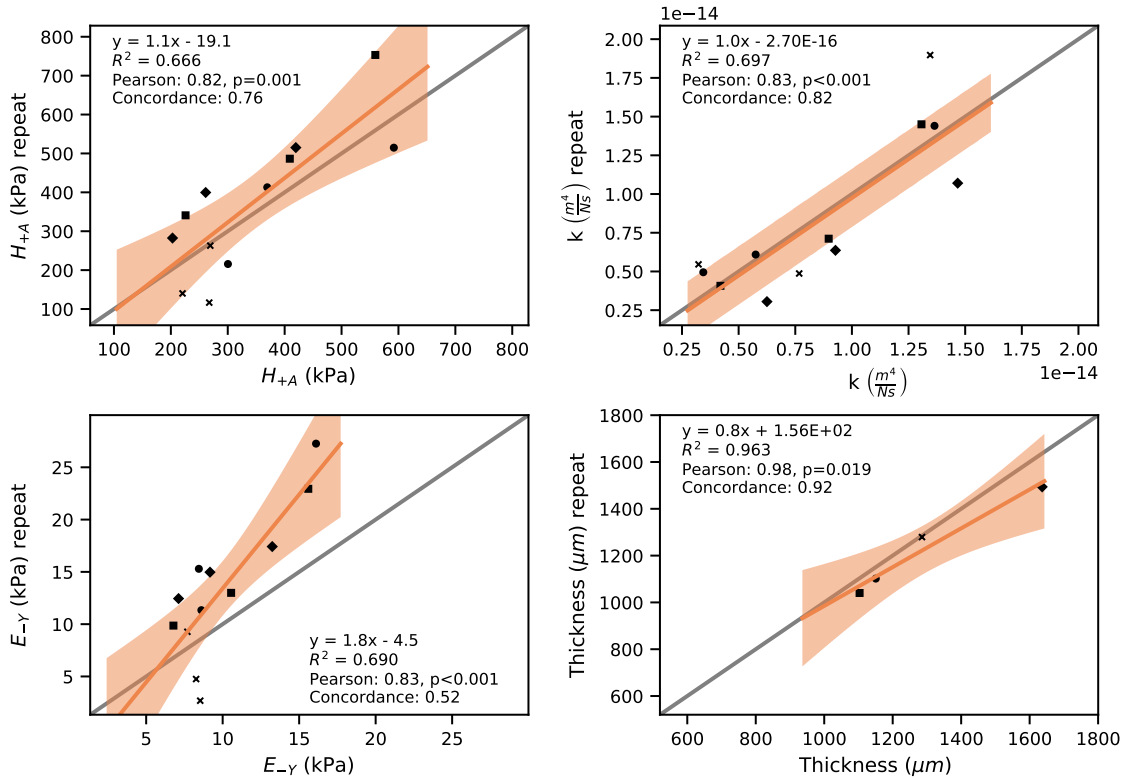

Figure 3.8: Concordance plots of first and repeated measurements on pig scleral samples. Top: Fitted properties, tensile modulus (Left) and hydraulic conductivity (Right). Both show moderate concordance and repeatability. Bottom: Directly measured properties, compressive modulus (Left) and thickness (Right). Compressive modulus is observed to change from first to second test. The identity line is represented in gray. Perfect concordance between first and second measurement would be indicated by points falling exactly on this line. Each symbol shape represents measurements coming from the same eye over the three strain steps. Orange lines show the best fit linear regression, and shaded areas show the 95% confidence bands.

generated from unconfined compression are biaxial and solely tensile in nature, whereas a uniaxial tensile test generates tensile strains in only one direction. Biaxial testing of porcine sclera has been reported by Cruz-Perez et al., who used a reduced Fung-type hyperelastic model to analyze biaxial tensile tests (Cruz Perez et al., 2014). Scleral samples in their study were stretched in-plane between 2-4% and had an average equivalent stiffness of 410.81 $\pm$ 168.58 kPa. Here, BCLE theory estimates in-plane tensile strain to be up to 2.5% for any one individual step, decreasing to 0% during stress relaxation, and an overall average stiffness

of 341.4 $\pm$ 130.6 kPa for porcine sclera. We conclude that despite the disparate handling, methodology, and analysis procedures between these two studies, the tensile stiffness values measured by unconfined compression matched the results of a well-accepted biaxial methodology reasonably well.

Studies on the compressive properties of the sclera are rare compared to those on its tensile properties, but the results obtained here are comparable in magnitude to the few previous studies performed. Mortavazi et al. used unconfined compression to measure a drained secant modulus, a conceptually similar measure of elastic stiffness to the equilibrium Young's modulus, E_{-Y}, measured in this study and found porcine peripapillary sclera to have a drained secant compressive modulus of approximately 4kPa (Mortazavi et al., 2009). Worthington et al. measured a compressive Young's modulus of porcine sclera to be $\sim$35kPa, which agrees closely to what was measured in human scleral samples by Battaglioli and Kamm (Battaglioli & Kamm, 1984; Worthington et al., 2014). However, Battaglioli and Kamm also measured scleral samples from cattle and found the compressive modulus to be in the range of 12-18kPa, closer to the measurements found in this study. The compressive stiffness of porcine sclera measured here had a mean of 10kPa, spanning $\sim$6.5 to 16kPa, which is fully contained in the range of 4-35kPa found in the literature and thus appears to be physiologically reasonable. The small differences in mean values between studies are likely to be explained by inconsistent reference configurations used for stress and strain calculations, namely differences in tare loading; however, differences in parameters used to quantify compressive stiffness (drained secant modulus, Young's modulus, and equilibrium Young's modulus) and regional variability of the compressive stiffness may also be contributing.

3.5.2.b Hydraulic Conductivity of Porcine Sclera

Through-plane permeability of sclera has been measured a few times in the literature using a falling head permeability assay, but it is known that a lack of uniformity in permeability testing methodology makes comparisons between laboratories difficult (Pennella et al., 2013). Jackson et al. measured human scleral permeability and found an average value of 8.62e-18 $\pm$ 10.42e-18 m^2 from 18 human donors (Jackson et al., 2006). Stewart et al. measured porcine scleral permeability and reported an average value of 43.3e-18 $\pm$ 23.5e-18 m^2 from 7 pigs (Stewart et al., 2009). Due to the dependence of permeability on compressive strain and the likely anisotropic nature of the quantity due to structural anisotropy of the sclera, a direct comparison to the literature is challenging. However, after converting hydraulic conductivity measurements in this study to intrinsic permeability by assuming a viscosity of 0.7MPa s for PBS at 37°C (Fluxion, 2009), the average value of porcine permeability at 5% compressive strain in this study was 9.8e-18 $\pm$ 0.50e-18 m^2, and the estimated zero-strain permeability was 17.9e-18 $\pm$ 2.9e-18 m^2. Thus, the magnitude of permeability measured here lies between the literature values, showing that this methodology produces a physiologically reasonable permeability value with less variability than the falling head methodology, which is prone to leakage, a lack of precisely controlled or measured compressive strain, and possible sample degradation/remodeling over the typical $\sim$24 hour testing times.

3.5.3 Quality of curve fitting

The model was successfully able to fit the experimental data from low frequencies up to the chosen cutoff frequency, at which point high frequency camera noise and the low sample rate of the device precluded accurate Laplace transformations (Figure 3.4). While the material properties were determined only from curve fitting the experimental transfer function, defined as the Laplace domain strain signal divided by the stress signal, on the real axis of the Laplace domain, both the gain (real) and phase (imaginary) components of the model calculated using these fitted properties aligned well with the experimental components (Figure 3.5). Finally, the material properties determined in the frequency domain led to time domain stress fits of similar quality; specifically, the model matched the peak stresses and characteristic relaxation times quite well (Figure 3.6).

3.5.4 Repeatability

The ability to curve fit data alone does not prove a model's applicability to analyzing tissue response; a model can curve fit any data given enough degrees of freedom. It is important that a model yields a unique set of parameters for any individual data set in order to characterize a tissue accurately and in the most generalizable manner. Here, we probed the uniqueness of the fits by utilizing a differential evolution algorithm to broadly interrogate the parameter space in conjunction with performing a test-retest experiment. The sets of parameters for any one experiment did not vary appreciably from one curve fit to another, implying that the optimization was consistently finding a global minimum.

Similarly, the sets of parameters obtained by curve fitting varied only slightly from the

first to second test of the porcine samples (Figure 3.8). A perfect test-retest experiment was not achievable due to the likelihood of physical changes in the samples between the first and second test, likely due to some combination of the loading experienced in the first test, the time spent in PBS overnight, and continued biological processes. Evidence for these changes are seen in the directly measured compressive modulus of the samples, which were seemingly altered from the first to second test. Yet despite these limitations, the test-retest methodology showed relatively concordant results for the fitted parameters, which would be unlikely if the biphasic model employed here did not describe the physical state of the samples in this configuration uniquely.

3.5.5 Murine vs Porcine Sclera

Both the pig and mouse sclera display the typical behavior of biphasic materials (Figure 3.7). The application of high frequency stress resulted in a dampened strain response due to the fluid pressurization within the sample, whereas low frequency loading led to strain magnitudes independent of the hydraulic properties, solely dependent on the solid matrix compressive stiffness, E_{-Y}. Fluid pressurization and permeation were also seen to cause a phase delay in the strain response from stress applied at intermediate frequencies where fluid permeation occurs on the same timescale as the loading.

Despite these qualitative similarities, we observed quantitative differences between species, consistent with previous reports on mechanical properties of sclera, including compressive stiffness, tensile stiffness, and permeability (Battaglioli & Kamm, 1984; Cruz Perez et al., 2014; Eilaghi et al., 2010; Jackson et al., 2006; Stewart et al., 2009). Here, the porcine sclera was found to be stiffer than the sclera of the mouse on average, and a minor difference in

permeability was observed as well at the third strain step. Species differences in properties are an important factor to consider in the interpretation of results of animal models of ocular conditions. While these findings may be explained by species differences in the microstructure or scleral composition, another possibility for this study is that age differences in the two groups are driving the differences. There is evidence of age-related scleral remodeling of the collagen and proteoglycan networks (Coudrillier et al., 2015; Rada, Achen, Penugonda, et al., 2000; Stewart et al., 2009). While the pigs exact age was not known, they were likely $\sim$6 months of age, compared to a mean age $\sim$ 4 months for the mice. This difference in mean age, especially when considering the different lifespans of the mouse and the pig, may be driving the differences in properties found in this study.

While the cause of the observed difference between the two species is left to future work, it is important to note that unconfined compression analyzed with BCLE was able to discern a difference between the two groups, supporting its use as a tool to detect biomechanical differences between treatment groups.

3.5.6 Limitations

3.5.6.a Infinitesimal Strain Assumption

The formulation of the model used to analyze the stress relaxation experiments includes an infinitesimal strain assumption that introduces error into the analysis. While the compressive strains were held to a maximum of 15% in the stress relaxation experiments, a tare stress of $\sim$636 Pa was applied to the samples prior to the 15% strain application. Accurately determining the corresponding amount of tare strain in these experiments is not trivial due

to the curved and small size of the samples. However, the mean compressive stiffness of 10 kPa for the porcine and mouse scleral samples can be used to estimate ∼6% strain due to the tare loading. While the total ∼20% compressive strain on the samples in this study introduces a non-negligible amount of error (∼2% strain), the associated error is generally deemed to be an acceptable trade-off for the significant simplification of the analysis in soft tissue mechanics (Cohen et al., 1998; Hatami-Marbini & Etebu, 2013; Soltz & Ateshian, 2000).

To obtain material properties for a constitutive relationship valid for large deformations, e.g. for general modeling purposes, it would be necessary to extend the approach to consider finite deformations, which was beyond the scope of this manuscript. However, we suggest that our technique is nonetheless useful for comparison of material properties between experimental groups, since the ability to obtain three material properties closely related to the microstructure of the tissue from one experiment, without the use of inverse finite element modeling, is appealing. A technique of this sort is also particularly powerful in the hard-to-work-with mouse eye, due to the multitude of readily available transgenic mouse strains.

3.5.6.b Experimental Limitations

The compression testing device had limited accuracy in applying specific strain signals due to the software feedback used to control the tip position. This is visible in the transient overshooting of applied strain (Figure 3.6 compared to Figure 3.3); however, the strain always equilibrated quite accurately on the commanded 5% strain step. The curve fitting and calculations of model time domain stress were done independent of any assumed strain

signal to account for the transient overshoot; however, Huang et al showed that the strain rate of the applied compression affected fitted properties of the solid matrix of articular cartilage due to its inherent viscoelasticity. Thus, the inconsistency of the applied strain likely added additional variability in the fitted properties.

3.5.7 Conclusion

We evaluated the applicability of unconfined compression analyzed with poroelastic theory to characterize scleral biomechanics and have shown that poroelasticity well describes the biomechanics of the sclera, an important advance in capturing the contribution of the sclera's complex microstructure to its biomechanics. We showed that by reformulating the model parameters, a single unconfined compression test can yield unique sets of parameter values that are physiologically reasonable and consistent with other testing methodologies. Using this method, we have characterized intrinsic material properties of the murine sclera for the first time and found them to be quite similar to the porcine sclera. Unconfined compression is moderately repeatable under a test-retest reliability experiment, potentially permitting comparisons within the same sample before and after an experimental treatment. These methods are also relatively insensitive to the thickness of the samples, since they can characterize porcine sclera as well as the significantly thinner murine sclera, showing that this method can likely be successfully applied to other small tissue samples. Future work should focus on more completely validating the model's ability to fully describe the tissue's biomechanics by predicting another simultaneously measured quantity and work towards a full characterization of the tissue by measuring the shear modulus and relaxing the cubic symmetry assumption. Importantly, this method will allow more focused study on the con-

tribution of the glycosaminoglycans (GAGs) to scleral biomechanics, an area of increasing interest in both glaucoma and myopia research. This study may also spur increased use of the mouse as an animal model for future ocular biomechanics studies where the sclera is a target, such as myopia and glaucoma, and permit more rigorous studies of the genetic pathways regulating scleral biomechanics.

CHAPTER 4

ALTERED STRUCTURE AND FUNCTION OF MURINE SCLERA IN FORM-DEPRIVATION MYOPIA

4.1 Submission Details

Authors: **Dillon M. Brown**, Michael A. Kowalski, Quinn M. Paulus, Jianshi Yu, Praveen Kumar, Maureen A. Kane, Jay M. Patel, C. Ross Ethier, Machelle T. Pardue

Status: Accepted for publication in *Investigative Ophthalmology & Visual Science* (November, 2022)

4.2 Introduction

Myopia is the most common refractive error and cause of visual impairment, predicted to affect over 50% of the population by 2050 (Holden et al., 2016). Myopia is typically caused by axial elongation of the eye beyond that necessitated by the eye's optical power (axial myopia) (Flitcroft et al., 2019), i.e. incoming collimated light is focused in front of the retina. This elongation not only disrupts the optics, but also the ocular biomechanical environment, which may explain why excessive axial length is a risk factor for other blinding diseases with biomechanical aspects (e.g., retinal detachment, glaucoma, optic disk abnormalities) (Lakawicz et al., 2020; Saw et al., 2005; Shen, Melles, et al., 2016). Thus, preventing myopigenesis is of great interest, yet our understanding of the mechanisms of axial elongation and myopigenesis is lacking.

The physical process of axial elongation appears to be dictated by the biomechanics of the sclera, which in turn are determined by the quantity/types of constituent components and their microstructural arrangement (Harper & Summers, 2015; Summers, 2014). Presentation of myopigenic visual stimuli causes significant and rapid scleral remodeling, including changes in sulfated GAG (sGAG) levels and an increase in extensibility (i.e., altered biomechanics) (Backhouse & Gentle, 2018; Grytz & Siegwart, 2015; Harper & Summers, 2015; Lewis et al., 2014; McBrien et al., 2009; Moring et al., 2007; Phillips et al., 2000; Siegwart & Norton, 1999). This relationship between the state of the sclera (structure and biomechanics) and axial length appears to be causal, as supported by both computational modeling (Grytz & El Hamdaoui, 2017) and studies in which the sclera is experimentally stiffened (e.g., using collagen cross-linking agents or other mechanical reinforcement) which result in altered axial length (Boote et al., 2020; Grytz, 2018). However, no proposed mechanisms linking scleral biomechanics to axial length have successfully explained the magnitude and time course of myopigenic axial elongation, indicative of the complexity of this process.

There is great interest in elucidating the mechanism by which myopigenic visual cues are able to influence scleral remodeling (Brown et al., 2022; Summers et al., 2021). Significant evidence supports the general idea of a direct retina-to-sclera (retinoscleral) signaling cascade capable of communicating information about magnitude and direction of optical defocus contained in an image (McFadden & Wildsoet, 2020; Norton et al., 1994; Troilo & Wallman, 1991; Troilo et al., 1987; Wallman et al., 1987; Wiesel & Raviola, 1977; Wildsoet & Wallman, 1995; Wildsoet & Pettigrew, 1988b; Wildsoet, 2003). However, the details behind this signaling cascade remain elusive, especially regarding how the signal is being propagated through the choroid (Brown et al., 2022; Nickla & Wallman, 2010;

Summers et al., 2021).

Retinoic acid (RA) may be an important signal capable of trans-choroidal signaling within the retinoscleral cascade. All-trans retinoic acid (atRA) concentrations and synthesis in retinal and choroidal tissue have been shown to be correlated to the refractive state and direction of blur, dependent on both tissue and species (McFadden et al., 2004; Summers, 2013). atRA has been previously shown to disproportionately concentrate in the sclera when co-cultured with choroidal tissue (McFadden et al., 2004), suggesting the existence of an active transport process, and scleral concentrations of atRA influence the remodeling processes by modulating sGAG and/or synthesis (Mertz & Wallman, 2000). Finally, exogenous atRA given to guinea pigs and chickens has been shown to promote axial elongation (McFadden et al., 2004; McFadden et al., 2006) and influence scleral remodeling (Li et al., 2010). However, it is not clear if atRA-induced elongation occurs via the same pathways as myopigenesis.

The mouse model of myopia has great potential to address questions pertaining to mechanisms of myopigenesis. Although the mouse is widely used for studying complex biological mechanisms, it is still not clear how comparable mouse myopigenesis is to other mammalian species and thus to what degree findings in mice may translate (Pardue et al., 2013; Schaeffel et al., 2004). Additionally, the small size of its eye ($\sim$3 mm) introduces significant technical challenges in measuring axial elongation, scleral biomechanics, and quantities of signaling molecules. In the mouse, axial elongation is inconsistently reported to change with myopigenic cues (Pardue et al., 2013), and neither scleral glycosaminoglycans (GAGs) nor biomechanics have been studied in respect to myopigenesis.

Here, we studied the form-deprivation (FD) model of myopia in the mouse, primarily

focusing on scleral endpoints described below. We hypothesized that myopigenesis in the mouse progresses via a retinoscleral signaling cascade similar to other mammals, and thus, that the sclera would be measurably more extensible in myopic eyes. Additionally, we hypothesized that sGAG content, shown to be rapidly altered in other species in response to myopigenic visual cues, would be decreased. Finally, we measured ocular atRA content to determine if increased retinal or choroidal atRA concentrations coincided with myopigenesis, as has been observed in other mammalian models.

4.3 Material and Methods

4.3.1 Animals

Male C57BL/6J mice (Jackson Laboratory, Bar Harbor, Maine, USA) were housed at the Atlanta Veterans Affairs Healthcare System in normal lighting conditions (12:12-hour cycles, 20-200 lux) with access to mouse chow and water ad libitum. All procedures were performed in accordance with the Association for Research in Vision and Ophthalmology (ARVO) Statement for the Use of Animals in Ophthalmic and Vision Research and approved by the relevant Institutional Animal Care and Use Committee.

4.3.2 In Vivo

4.3.2.a Ocular Measurements

At baseline and on the day of sacrifice, animals were prepared for in vivo measurements (Bergen et al., 2016; Faulkner et al., 2007). Eyes were dilated with 1% tropicamide and animals were anesthetized (ketamine: 80 mg/kg; xylazine: 16 mg/kg). Refractive error

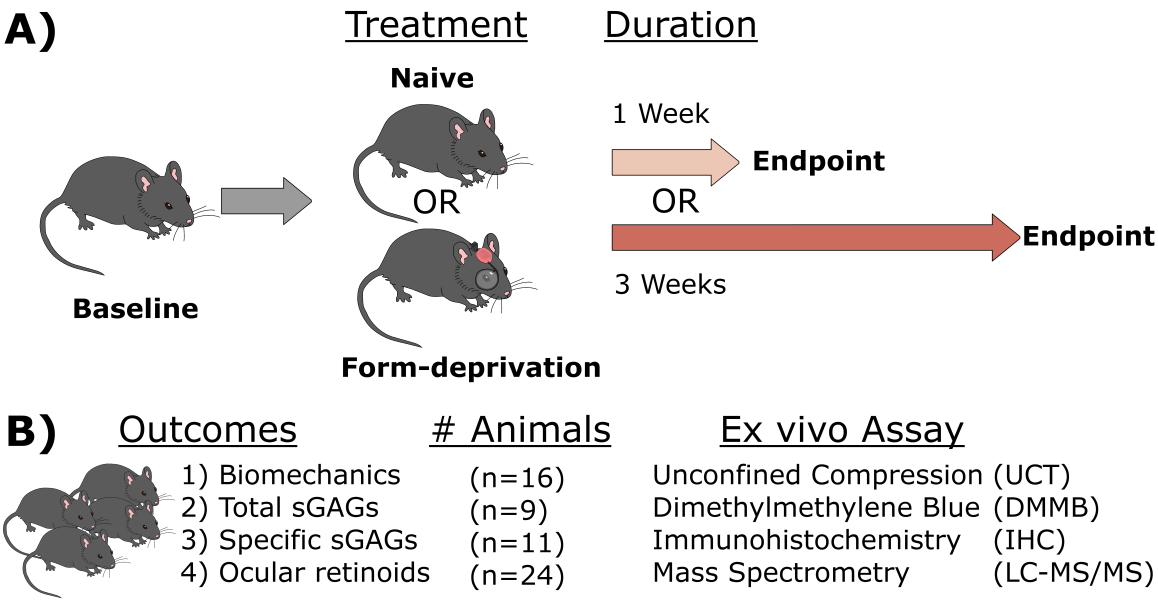

Figure 4.1: Experimental study design. A) In vivo measurements were made at baseline, after which animals were either assigned to receive monocular form deprivation (form deprivation) or remain naive controls (naive). Treatments were maintained for either 1 or 3 weeks, after which in vivo measurements were again made at the endpoint and prior to sacrifice. B) Ex vivo outcome measures were studied using different cohorts of animals.

(RE) (mouse automated infrared photorefractor), corneal curvature (CC) (infrared photokeratometry), and ocular biometry (spectral domain optical coherence tomography (OCT); Envisu R4300, Leica Microsystems, Wetzlar, Germany) were then sequentially measured, with the entire process taking ∼20 minutes (Schaeffel, 2008; Schaeffel et al., 2004). OCT volumes were registered to correct for motion artifacts, and tissue interfaces were manually marked, permitting the calculation of central corneal thickness (CCT), anterior chamber depth (ACD), lens thickness (LT), vitreous chamber depth (VCD), retinal thickness (RT), and axial length (AL) (corneal surface to retinal pigment epithelium (RPE)). To convert optical path lengths from SD-OCT to physical distances, an average refractive index of 1.39 was assumed, resulting in 4.1 µm axial resolution in tissue. In vivo measurements were excluded when significant corneal/lens opacities were observed.

4.3.2.b Induction of Form-deprivation Myopia

After the baseline in vivo ocular measurements were made at postnatal day 28 (p28), form-deprivation myopia was induced by head mounting diffuser lenses unilaterally OD, leaving OS as a naive contralateral control (Faulkner et al., 2007). Lens compliance was checked at least once daily, and no mice were eliminated from the study based on lack of lens compliance. Lenses were cleaned weekly under dim lighting and maintained for either 1 week (FD-1) or 3 weeks (FD-3).

4.3.3 Ex Vivo Protocols

Following the final in vivo measurement, animals were sacrificed, and eyes were enucleated and processed on the same day. Specifically, depending on the animal's assigned ex vivo endpoint, eyes were processed in one of three ways:

1. Biomechanical characterization using unconfined compression testing (UCT);
2. Frozen for later quantification of total scleral sGAG content by 1,9-dimethylmethylene blue (DMMB) or for later atRA measurements using liquid chromatography-tandem mass spectrometry (LC-MS/MS); or
3. Fixed for immunohistochemistry (IHC).

Both eyes from each animal were used for the same ex vivo endpoints to permit pairwise comparisons within each animal and the calculation of an interocular difference (treated - contralateral eye) (IOD) or "shift". For some endpoints, untreated, naive animals were also tested. The investigators were blinded in the DMMB and LC-MS/MS assays, and partially

blind in IHC (samples were coded by the investigator and only decoded after imaging and masking was performed). In total, 60 animals were studied between the 4 different ex vivo endpoints (Figure 4.1).

4.3.3.a Unconfined Compression Testing (UCT)

Eyes used for quantifying scleral biomechanics were enucleated and stored in phosphate-buffered saline (PBS) at 4°C until use the same day. As previously described (Brown, Pardue, et al., 2021), eyes were first dissected under PBS to remove orbital muscle, fat, and conjunctiva. Globes were divided at the limbus, and the intraocular tissues were removed to create a scleral shell. Four cuts were made to flatten the sclera and create four regions from which samples could be taken. 1 mm diameter cylindrical samples were taken from the posterior region of the scleral shell using a biopsy punch, approximately 0.5 mm from the optic nerve. Samples were taken randomly from the four regions, and when multiple samples were tested from the same eye, the results were averaged. In support of this approach, in the current study and our previous study40 detailing the methodology, we have seen no effect of region on measured mechanical properties. Samples were coated in graphite powder and submerged in a 37°C 0.1M PBS fluid bath for biomechanical testing.

UCT was performed on the cylindrical samples using a cantilever-based compression testing apparatus (Microsquisher; CellScale, Waterloo, ON, Canada). Samples were placed on the platens and a 500 μN (636 Pa engineering stress) tare load was applied to flatten the samples and keep them in place. After equilibration, the thickness of the sample was measured via the calibrated camera (resolution: 0.6155 μm/pixel). This was used as the reference configuration for stress/strain calculations. Then, an incremental 3 step stress

relaxation compression protocol was performed, applying a total of 15% compressive strain over three steps, with each step applying and maintaining an additional 5% compressive strain until stress relaxed and equilibrated. (Average relaxation time - step 1: 12 min, step 2: 22 min, step 3: 25 min). The time taken to relax increases with each incremental strain step due to the viscoelastic effects being a result of fluid exudation, and the tissue hydraulic conductivity is dependent on the state of compression, i.e., increased compression causes pores to close and resistance to fluid flow to increase. The biphasic conewise linear elastic material model was independently fit to each step of the compression experiment, permitting the calculation of an ”aggregate” tensile modulus (intrinsic material property reflecting resistance to tensile deformation once internal fluid flow has ceased; “tensile stiffness”) and hydraulic conductivity (tissue permeability to water; “permeability”) at each of the three steps (Brown, Pardue, et al., 2021; Soltz & Ateshian, 2000)(Supplementary Figure A.1).

The IOD of each material property was calculated at each step and averaged to obtain the mean IOD of each sample. However, in some cases, applied compressive strain deviated up to $\sim$1.5 percentage points from the target strain (Supplementary Figure A.1). Due to the strong dependence of the properties on the state of sample compression, we included this deviation as a factor in our statistical model (generalized linear models). IODs are presented as estimated marginal means of the fitted statistical model in which the strain deviations are corrected.

4.3.3.b Dimethylmethylene Blue Assay (DMMB)

To quantify total scleral sGAG content, eyes were enucleated and stored in PBS at 4°C until dissection the same day. The sclera was isolated from the rest of the eye while submerged in PBS, carefully removing the RPE and choroid by scraping with the tips of angled forceps. Isolated sclerae were then dehydrated in a vacuum desiccator overnight and weighed 3 times on an analytical balance (XSR205DU; Mettler Toledo, Columbus, OH, USA), with the average being taken as the dry mass of the sclera. These procedures led to good interocular agreement in tissue masses in a preliminary group of naive, untreated animals (n=8 pairs of eyes, concordance correlation coefficient ρ_c = 0.94, Supplementary Figure A.2). The isolated sclerae were frozen on dry ice in Eppendorf tubes and stored at -80°C until use.

Total sGAG content was measured via the metachromatic DMMB assay. Samples were first thawed and digested in 200µL papain (Sigma P3125, 2% v/v) in buffer (0.1M Sodium Acetate, 0.01M Cysteine Hydrochloride, 0.05M EDTA, pH 6.0) at 60°C for 1-2 days, or until completely digested. Samples were spun down every 4-6 hours to keep them immersed. 200µL of the DMMB dye mixture (8mg 1,9 dimethylmethlene blue in 2.4mL ethanol, 1g sodium formate, 1mL formic acid, diluted to 500mL with ddH2O) was added to 30µL of digested sample in a 96 well plate and absorbance was read at 525 nm, the accepted preferred wavelength for measuring sGAG content with this assay (Farndale et al., 1986). Concentration was determined by comparing absorbances to a standard curve created from shark cartilage chondroitin sulfate (Sigma C4384). DNA was also measured in each sample via the picogreen assay. 100µL of the picogreen working reagent (50µL PicoGreen Reagent, 0.5mL 20x TE buffer, 9.45mL ddH20) was added to 5µL of digested sample, and

absorbance was read using 480nm excitation and 520nm emission and compared to a standard curve created using Lambda DNA stock (Cat #: SD0011, Thermo Fisher Scientific, Waltham, MA, USA). Both assays were performed in triplicate, with the average of the three taken as the final value.

To account for variability in the amount of isolated sclera collected per eye, scleral sGAG content is reported as a mass fraction (µg sGAG/mg sclera) and a mass ratio (µg sGAG/µg DNA).

4.3.3.c Immunohistochemistry (IHC)

Immediately following sacrifice, eyes were immersion fixed in buffered zinc formalin (Z-Fix; Anatech LTD, Battle Creek, MI, USA) for approximately 1 hour. Eyes were cryoprotected in 30% sucrose solution overnight, embedded in optimal cutting temperature medium, and rapidly frozen at -60°C on the Peltier cooling element of a cryostat (CM1850; Leica Microsystems, Wetzlar, Germany). 10µm sagittal sections were taken through the optic nerve head and stored at -20°C.

For immunostaining, we used a well characterized monoclonal primary antibody (2B6) specific to chondroitinase-generated neoepitopes on both chondroitin-4-sulfate (C-4-S) and dermatan sulfate (DS) (Clone 2B6, Cat:1042009, Lot: S1605002; MD Biosciences, Oakdale, MN, USA). C-4-S and DS make up the majority of the sGAG content in the sclera (Moring et al., 2007). Additionally, they tend to associate with two separate classes of proteoglycans; DS tends to be found predominately in small leucine-rich proteoglycans that associate with collagen (e.g., decorin and biglycan), whereas the majority of C-4-S tends to be found in larger, aggregating proteoglycans (e.g., aggrecan) (Harper & Summers, 2015;

Lopez & Bonassar, 2022).

To separately label C-4-S and DS, tissue sections were deglycosylated using either chondroitinase AC (ChAC), which specifically deglycosylates chondroitin A (C-4-S) and chondroitin C (C-6-S); or chondroitinase B (ChB), which targets DS (both ChB and ChAC *from Flavobacterium heparinum*, Sigma-Aldrich, Saint Louis, MO, USA). Thus, tissue sections treated with ChAC and stained with 2B6 allow visualization of only the "stub" neoepitopes of C-4-S, and those treated with ChB and stained with 2B6 only allow visualization of DS (Table 4.1).

Table 4.1: Enzymatic deglycosylations and immunostaining outcomes. Chondroitinase enzymes deglycosylate and expose neoepitopes on specific sGAGs. Combining the different treatments with antibodies (2B6 - anti-4 sulfation stub monoclonal antibody) permit labeling of specific sGAGs. sGAG: sulfated glycosaminoglycan, ChAC: Chondroitinase AC, ChB: Chondroitinase B, C-4-S: Chondroitin-4-sulfate, C-6-S: Chondroitin-6-sulfate, DS: Dermatan Sulfate

Deglycosylation		*Immunostaining*		
Enzyme	**Exposed Neoepitope(s)**	**Antibody**	**Recognized Neoepitopes**	**Labeled GAG**
ChAC	C-4-S C-6-S	2B6	C-4-S DS	**C-4-S**
ChB	DS	2B6	C-4-S DS	**DS**

To prepare tissue for immunostaining, slides were first washed with tris-buffered saline with 0.1% Triton X-100 (TBS-T) to remove excess embedding medium. After enzymatic treatment (ChB, ChAC, or buffer-only; 0.5 U/mL, 3 hours at 24°C, 8.0 pH) sections were permeabilized (0.5% Triton X-100 in TBS, 10 minutes at 24°C) and then incubated with blocking buffer (10% normal goat serum and 1% bovine serum albumin in TBS-T, 45 minutes at 24°C). Sections were then incubated with mouse monoclonal antibody 2B6 in a humidity-controlled environment (1:100, 18 hours at 4°C). The following day, sections

were washed three times in TBS-T and incubated with Alexa Fluor-647 labeled goat anti-mouse secondary antibodies in blocking buffer (1:500, 45 minutes at 24°C in darkness; Cat # A-21244, Invitrogen). Tissue was washed, treated with DAPI (NucBlue Fixed Cell Stain ReadyProbes DAPI, Cat # R37606, Invitrogen), washed, and finally coverslipped with antifade medium (Prolong Diamond Antifade Medium, Cat # P36961, Invitrogen). All slides were stained in parallel using the same batch of working reagents.

Stained samples were imaged on a confocal microscope (Nikon A1R, Nikon, Tokyo, Japan) using an apochromatic 20X objective lens. Three images (600x600µm per field of view, 12 bits per channel) were taken per section – one centered on the optic nerve head, and one each superior and inferior to the first. Three sections were imaged per slide (ChB-treated, ChAC-treated, and buffer-only control). Microscope settings were kept constant across all samples and imaging sessions.

Images were stitched, masked, thresholded, and quantified via custom semiautomated macros using built-in analysis functions in FIJI (Schindelin et al., 2012). The sclera was manually masked from other tissues. To quantify relative GAG content, average pixel intensities were measured within the masked regions and normalized to each slide's buffer-only control.

4.3.3.d Liquid Chromatography tandem mass spectrometry (LC-MS/MS)

Eyes used to quantify retinoids were enucleated and dissected in PBS under dim red light to limit RA isomerization (KANE et al., 2005; Kane & Napoli, 2010). The extraocular tissues, optic nerve head, anterior chamber, and lens were removed from the eyes. The remaining posterior cup was divided into two groups by carefully isolating the retina. The remaining

RPE, choroid, and sclera (R/C/S) were analyzed together due to the small quantities of tissue (mean ± std sample mass; Retina: 14.6 ± 4.8 mg, R/C/S: 10.8 ± 3.3 mg). Tissues were blotted, placed into light proof Eppendorf tubes on dry ice, and stored at -80°C.

Samples were shipped from Atlanta, GA to Baltimore, MD on dry ice for LC-MS/MS characterization of retinoids using a previously detailed and rigorously characterized methodology, developed specifically for measuring endogenous RA isomers in limited tissue samples from mice (Jones et al., 2015; KANE et al., 2005; Kane, Folias, & Napoli, 2008; Kane, Folias, Wang, et al., 2008; Kane & Napoli, 2010). In brief, samples were combined, and the wet weights of the grouped samples were measured. Tissue was then homogenized in a ground glass homogenizer in 0.9% NaCl (normal saline) and extracted using a two-step acid-base extraction previously described in detail using 4,4-dimethyl-RA as an internal standard for RA and retinyl acetate as an internal standard for retinol and total retinyl esters (Kane & Napoli, 2010). Levels of RA were quantified using liquid chromatography-multistage-tandem mass spectrometry, which is an LC-MS/MS method utilizing two distinct fragmentation events for enhanced selectivity using a Prominence UFLC XR liquid chromatography system (Shimadzu, Columbia, MD) coupled to a 6500+ QTRAP hybrid triple quadrupole mass spectrometer (AB Sciex, Framingham, MA) using atmospheric chemical ionization (APCI) operated in positive ion mode as previously described (Jones et al., 2015). Levels of retinol and total retinyl esters were quantified via HPLC-UV as previously described (Kane, Folias, & Napoli, 2008; Kane & Napoli, 2010). From these procedures, atRA, retinol (ROL), and total retinyl esters (tRE) were quantified and reported. Individuals carrying out the LC-MS/MS measurements were blinded to the identities of samples.

4.3.4 Statistical Analysis

Generalized linear mixed effects models were constructed for each outcome measure. Fitting and contrasts were done using the "lme4" and "emmeans" packages in R (version 4.1.1) (Bates, Machler, et al., 2015; Lenth, 2021). When multiple contrasts were run, p values were adjusted via the multivariate t method (Westfall & Tobias, 2007). Significance of fixed effects was calculated by performing likelihood ratio tests between the full model and null models, each lacking one of the fixed effect terms. Random effects were used to account for correlated samples, e.g., two eyes from the same animal or multiple measurements on the same eyes. Outcomes were assigned a Gamma error distribution with a log link based on priors (outcomes that are strictly positive and/or ratios) and based on analysis of model residuals (Supplementary Table A.1). Significant alpha threshold was taken to be 0.05, and all results are presented as mean ± standard deviation.

4.4 Results

4.4.1 Form-deprivation induces myopic refractive errors in mice

At baseline and in the naïve animals, refractive errors displayed good interocular agreement, i.e. refractive shifts (IOD RE) were not significantly different from 0 (Baseline: -0.13±0.67D; Naive: 0.02±0.37D). Form-deprivation, initiated at 4 weeks of age, led to myopia relative to the contralateral eye by 1 week (-2.35±1.11 D, $p<0.001$) and worsened by 3 weeks (-4.07±0.72D, $p<0.001$) (Figure 4.2). Despite myopic refractive errors, no biometry measurements were significantly altered with myopia relative to their contralateral controls, including AL (Supplementary Table A.2).

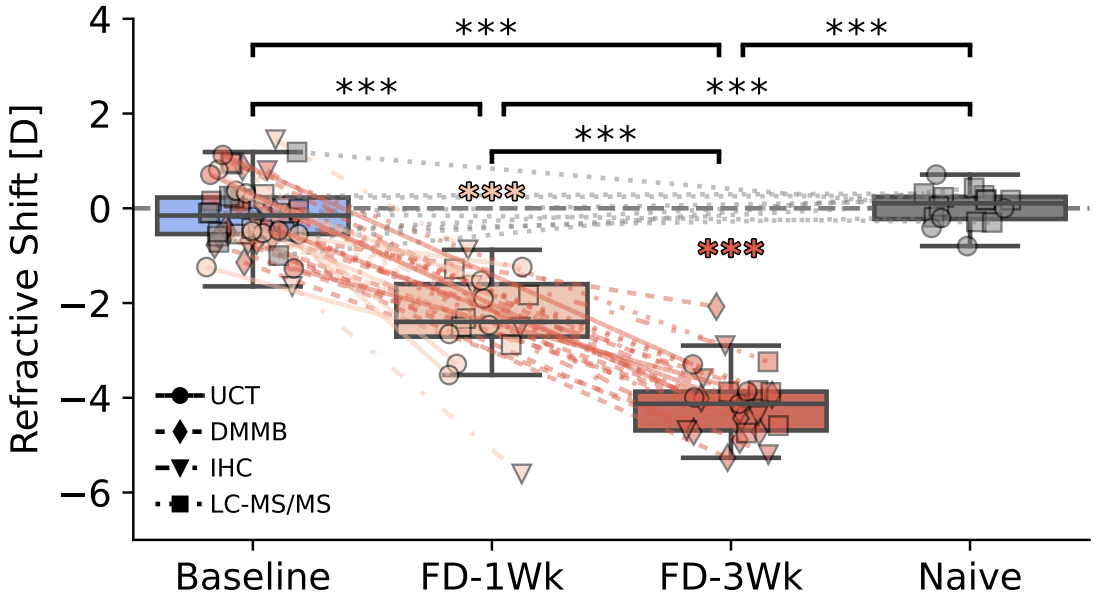

Figure 4.2: Form deprivation caused time-dependent myopigenesis in mice quantified by refractive error. Naïve animals and all animals at baseline displayed good interocular agreement in refractive error (treated – contralateral close to 0). Form deprivation caused increasingly more myopia over time relative to the contralateral eye. Different symbols represent the different outcome measures studied in each animal. Brackets denote difference between groups; filled asterisks denote an interocular difference in that group. The box contains the second and third quartiles of data, with the line indicating the median. The whiskers show the first and fourth quartiles. UCT: unconfined compression test, DMMB: dimethylmethylene blue, IHC: immunohistochemistry, LC-MS/MS: Liquid Chromatography tandem mass spectrometry. *: $p<0.05$, **: $p<0.01$, ***: $p<0.001$.

4.4.2 Scleral stiffness and permeability are altered during myopigenesis

In naïve animals, the measured tensile stiffness and permeability displayed good interocular agreement, with only minor and insignificant differences occurring. The sclerae from form-deprived eyes were less stiff (FD vs Contra; 1 week FD: -29.2%, $p<0.001$, 3 weeks FD: -39.9%, $p<0.001$) and more permeable (FD vs Contra; 1 week FD: +80.1%, $p=0.0025$, 3 weeks FD: +131.4 %, $p<0.001$) than the contralateral eyes (Figure 4.3). The interocular differences in both form-deprivation groups were significantly different from those measured in the naïve animals (Naïve vs FD-1: Stiffness, $p=0.02$; Permeability: $p=0.04$; Naïve vs FD-3: Stiffness, $p<0.001$; Permeability: $p<0.001$). Scleral biomechanical properties

did not differ between contralateral eyes of either form-deprivation group or between contralateral eyes and naïve eyes (Supplementary Figure A.1, Supplementary Table A.3).

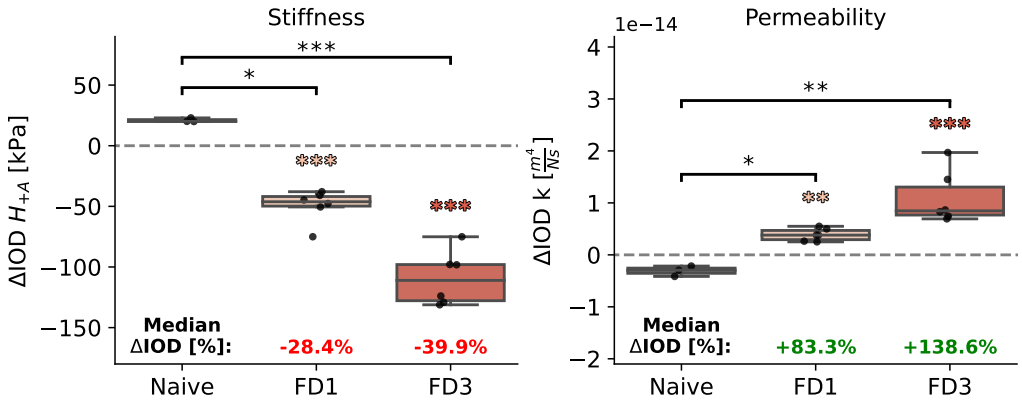

Figure 4.3: Form deprivation altered the biomechanics of the sclera, decreasing the tensile stiffness and increasing permeability as myopia develops relative to the contralateral eye. In other words, the interocular differences in scleral aggregate tensile modulus (left) and hydraulic conductivity (i.e., permeability) (right) differed from 0 due to form deprivation. Interocular differences were calculated at each step and the differences were averaged. Values plotted are the estimated marginal means derived from the fitted statistical model. The gray dashed line shows the 0 point (no interocular difference). Filled asterisks indicate a significant difference from 0. Brackets indicate differences between groups. The box contains the second and third quartiles of data, with the line indicating the median. The whiskers show the first and fourth quartiles. FD1: 1 week form deprivation, FD3: 3 weeks form deprivation, IOD: Interocular difference, H_{+A}: Aggregate tensile modulus ("stiffness"), k: hydraulic conductivity ("permeability"). *: $p<0.05$, **: $p<0.01$, ***: $p<0.001$.

4.4.3 sGAG content in the posterior sclera is decreased with myopia development

Total scleral sGAG content as quantified by the DMMB assay was not measurably altered after 3 weeks of form deprivation (Supplementary Table A.4). However, using semiquantitative immunohistological methods limited to the posterior sclera to observe the primary sGAGs, DS and C-4-S, myopic sclerae tended to have decreased sGAG content (Figure 4.4). DS content was dependent on the duration of FD (Interaction effect: animal_treatment x eye, p=0.017). DS was not changed in the FD eye relative to the contralateral eye after 1 week of treatment (p=0.871) but decreased after 3 weeks ($p<0.001$, Figure 4.4). A different

trend was observed with C-4-S, which was decreased by a similar degree after both 1 and 3 weeks of form deprivation (Main effect: eye, $p<0.001$, Supplementary Table A.5).

4.4.4 Form-deprivation alters retinoids in ocular tissues

Retinoids (atRA, tRE, and ROL) were each quantified in the retina and combined R/C/S (Figure 4.5). The bioactive retinoid, atRA, was significantly increased in the retina of eyes exposed to form deprivation for 1 week compared to contralateral controls ($p=0.037$), which returned to normal levels by 3 weeks. The concentration of atRA in the combined R/C/S was not altered with treatment. tRE in the R/C/S was decreased at 1 week of form deprivation relative to naive animals (Naïve vs FD, $p=0.028$), and a decrease was observed in the contralateral eyes at 3 weeks (Naïve vs Contra, $p=0.016$).

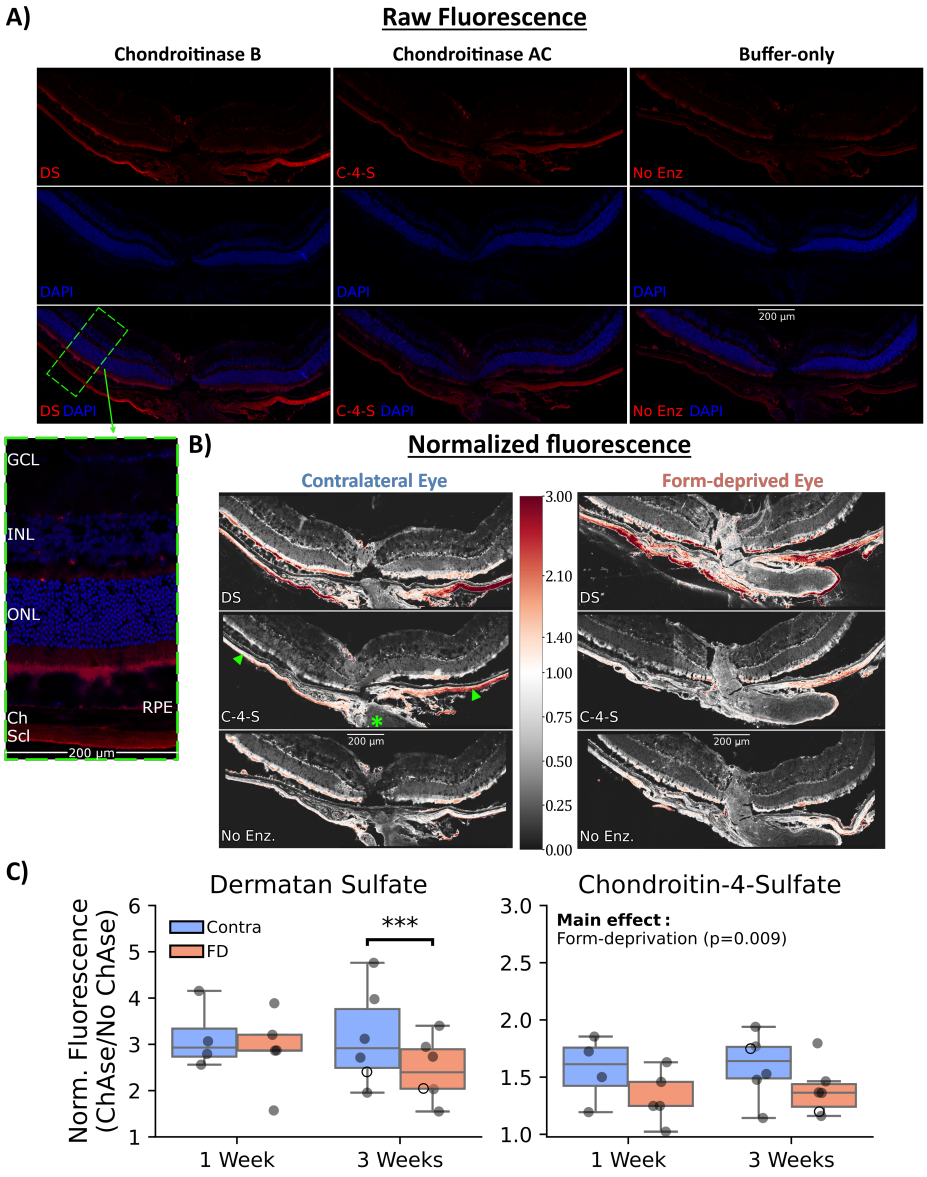

Figure 4.4: Effect of form deprivation on immunostaining of specific scleral sGAGs in the posterior sclera. A) Representative immunostaining of the posterior eye. Without chondroitinase treatment, staining was minimal (right). Deglycosylation using ChAC (middle) or ChB (left) increased the amount of labeling, primarily in the sclera. The green dashed rectangle shows an annotated/magnified 200 µm wide region and is representative of the distance from the optic nerve at which staining was quantified. B) Representative normalized fluorescence of the same sample in A) presented alongside the same animal's form-deprived eye. Fluorescence was normalized to the average intensity in the sclera of the "buffer-only" treatment to account for inter-sample differences in nonspecific staining and autofluorescence. Red coloring indicates increased staining, white indicates no change, and gray coloring indicates decreased staining relative to the sclera of the "buffer-only" treatment. Arrowheads point to the sclera and the asterisk labels the optic nerve. C) Quantification of the normalized fluorescence. DS content was significantly decreased in the sclera only after 3 weeks of form deprivation. In contrast, C-4-S content was significantly decreased in form-deprived eyes independent of the treatment duration (Main effect: Treatment, $p<0.001$). The box contains the second and third quartiles of data, with the line indicating the median. The whiskers show the first and fourth quartiles. Open markers show the spatially averaged values of the representative samples in B). *: $p<0.05$, **: $p<0.01$, ***: $p<0.001$.

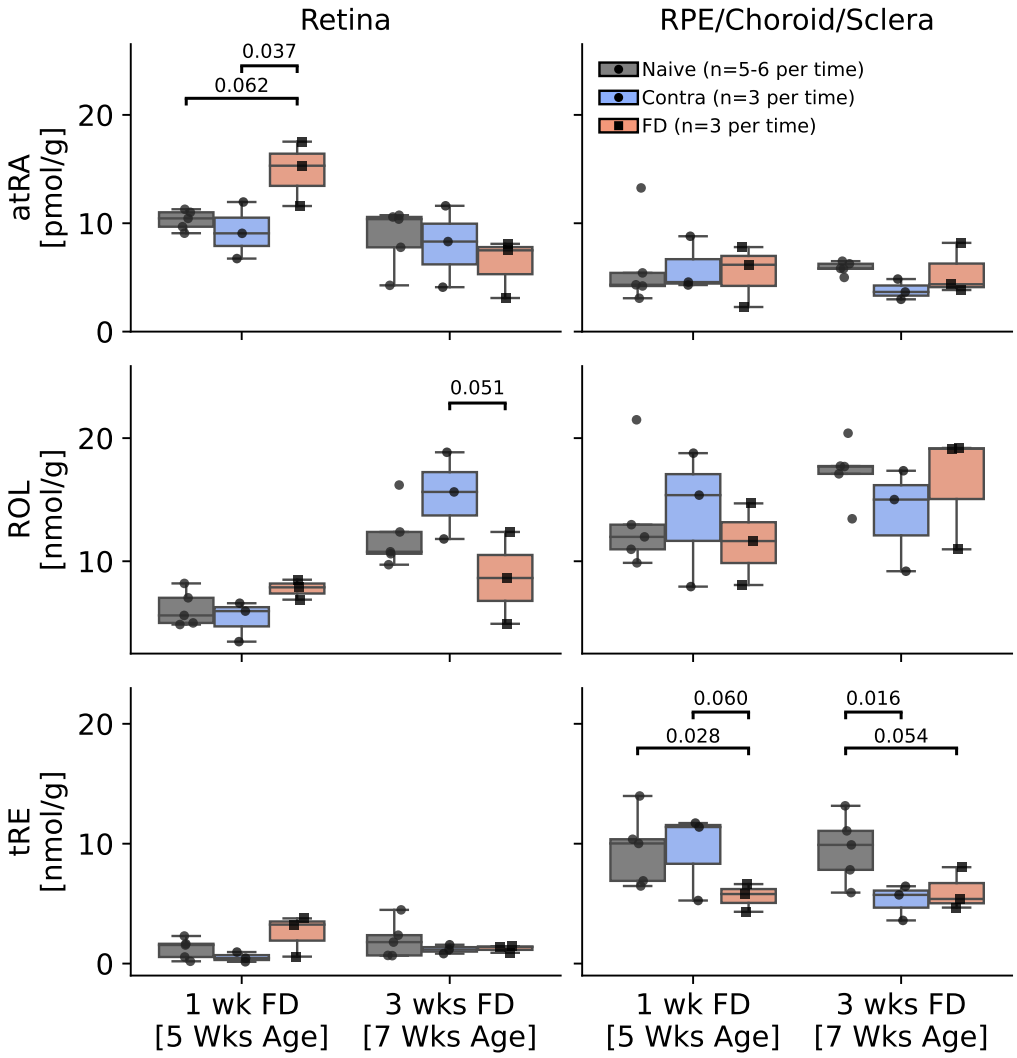

Figure 4.5: Retinoid concentrations in ocular tissues were altered with form deprivation. atRA increased in the retina of form-deprived eyes at 1 week. tRE decreased in the sclera of form-deprived animals - unilaterally after 1 week and bilaterally after 3 weeks. Each plotted point is one measurement made on grouped tissue from two eyes. Values above brackets are the adjusted p-values of the simple effect contrasts of eye treatment (Naïve, Contra, or FD). The box contains the second and third quartiles of data, with the line indicating the median. The whiskers show the first and fourth quartiles. FD: form-deprivation, Contra: contralateral, atRA: all-trans retinoic acid, tRE: total retinyl esters, ROL: retinol.

4.5 Discussion

The present study has established that the sclera of the mouse is significantly altered during visually mediated myopigenesis. A myopigenic visual cue (form deprivation) presented to the retina leads to both myopic refractive errors and altered scleral biomechanics. The myopic mouse sclera is more extensible, consistent with studies in other species using disparate mechanical testing methods and measures of stiffness (Grytz & Siegwart, 2015; Lewis et al., 2014; Phillips et al., 2000; Siegwart & Norton, 1999), and more permeable, a finding not previously reported. In our efforts to quantify degradation of sGAGs, results from semi-quantitative IHC suggests that the two major scleral sGAGs, C-4-S and DS, are decreased in the posterior sclera. Interestingly, DS was only reduced after 3 weeks of form deprivation, while significant myopia, altered biomechanics, and reduced C-4-S were found even at 1 week of form deprivation, suggesting that C-4-S, but not DS, may be involved in the early process of axial elongation. Finally, we present an exploratory overview of retinoid concentrations in ocular tissues of mice, which appear to vary throughout the posterior eye wall in response to form deprivation. These findings together, despite having not measured an increase in axial length, support the hypothesis that the mouse develops axial myopia via a retinoscleral signaling pathway, with largely conserved scleral endpoints to those reported in other mammalian species.

4.5.1 The mouse sclera becomes more extensible and permeable during myopigenesis

In contrast to the large variability of axial length (standard deviation of interocular difference $\sim$25 μm, or an estimated $\sim$5 D in the mouse), the effects of form deprivation on the

scleral material properties are large and consistent. One week of FD resulted in ∼2 D of myopia and corresponded with a 30% increase in the median extensibility of the myopic sclera, relative to the contralateral eye. By 3 weeks, the amount of myopia nearly doubled to ∼4D and myopic sclerae were ∼40% more extensible. Without any adjustments from the statistical model, 1 week of FD caused 5/6 animals to have more extensible myopic sclerae, increasing to 6/6 animals by 3 weeks of FD. The trend of a more extensible sclera in myopic eyes is consistent with previous findings of tensile stiffness changes in the chicken and tree shrew sclera, measured using a variety of approaches (Grytz & Siegwart, 2015; Lewis et al., 2014). While it is still not clear how exactly stiffness relates to axial length or what specific remodeling processes influence stiffness, these findings support the idea that the elongation is not driven by strictly elastic deformations of the corneoscleral shell.

The permeability of the mouse sclera was also altered in response to form deprivation, a finding not previously reported in any species. The tissue permeability of hydrated tissues accounts for a significant amount of viscoelasticity (time-dependent responses to loading) under certain modes of deformation (Huang et al., 2001; Huang et al., 2003), and the eye is constantly experiencing pulsatile, time-varying loading via the intraocular pressure and normal eye movements (Campbell et al., 2014). Thus, while it is feasible that scleral permeability could have important implications for scleral deformations, it is not obvious what role, if any, permeability may play in the proper functioning of the sclera and regulation of eye size. We note though that permeability appeared to track myopia better than tensile stiffness in this study; both myopic refractive errors and median permeability increased by about 70% between 1 and 3 weeks (-2.4D to -4.1D, +83% to +139% relative to the contralateral eye), whereas median tensile stiffness decreased by only ∼40% (-28% to -40%).

Despite lacking a clear understanding of this functional relationship, measurements of the scleral permeability may serve as a useful proxy for characterizing scleral microstructure, specifically its sGAG content. Tissue permeability has been most extensively studied in articular cartilage, where permeability is directly tied to function, i.e., in the lubrication of joints (Roughley & Mort, 2014). Theoretical and experimental results support a negative correlation between permeability and sGAG content (Gu et al., 1993; Rotter et al., 2002), i.e., decreased sGAG content results in increased permeability. If a similar relationship is demonstrated in the sclera, the measured increase of permeability in this study would be consistent with the widely replicated finding that scleral sGAGs decrease during myopigenesis (Moring et al., 2007; Norton & Rada, 1995).

4.5.2 Specific scleral glycosaminoglycans are decreased with different time courses

To study aspects of remodeling that occur in the mouse sclera during myopigenesis, we characterized sGAG content using two assays: DMMB (quantitative) and IHC (semiquantitative). While total sGAG content was not found to change after 3 weeks of form deprivation using the DMMB assay, the two most abundant sGAGs in the sclera, DS and C-4-S, appeared to be altered due to form deprivation when studied using IHC.

We report that C-4-S content is decreased in the myopic mouse sclera, occurring by 1 week and persisting through 3 weeks. This decrease in response to form deprivation agrees with a study by Moring et al., in which C-4-S was found to decrease at 4 days of lens defocus myopia in the tree shrew (Moring et al., 2007). C-4-S is primarily found on large, aggregating proteoglycans, e.g., aggrecan (Lopez & Bonassar, 2022; Rada et al., 1997), and aggrecan production has been shown to be rapidly downregulated while aggrecanases

are upregulated in the sclera in response to myopigenic visual cues (Guo et al., 2013; Guo et al., 2014; Siegwart & Norton, 2005). Thus, the semiquantitative results of the IHC are consistent with other methods and species.

Additionally, we found that scleral DS was decreased, but only after 3 weeks of form deprivation. DS has been shown to associate closely with, and influence, collagen, with DS concentrations being correlated to the amount of collagen (Junqueira et al., 1981; Keene et al., 2000; Moring et al., 2007; Orgel et al., 2009; Raspanti et al., 2007; Robinson et al., 2017; Svensson et al., 1995). Thus, this decrease in DS may be indicative of longer-term decreases in type I collagen content, a conserved finding across species (McBrien, Cornell, et al., 2001).

The apparent contradictory results obtained from the DMMB and IHC assays may be reconciled in several ways. First, the two assays measured different regions/amounts of the sclera. It was not feasible to isolate and measure a specific scleral region for the DMMB assay due to the very limited amount of scleral tissue from each mouse eye ($\sim$150μg of total, dehydrated tissue). Thus, whereas total scleral samples were used in the DMMB assay, we limited the IHC to the posterior sclera, where changes in scleral remodeling during myopigenesis have been most commonly shown (Moring et al., 2007; Norton & Rada, 1995). Other possible explanations could include lack of sensitivity of the DMMB assay to relatively small changes in total GAG and/or variability in the processing of the small tissue samples.

4.5.3 A speculative mechanism linking scleral sGAGs to biomechanics

By incorporating results from the present study with those from studies of cartilage biomechanics and scleral remodeling in myopia, it is possible to construct a speculative but self-consistent mechanism linking scleral sGAGs to biomechanics. In cartilage, permeability affects fluid pressurization in the tissue, hydration, and the loading imposed on collagen fibrils (Mow et al., 1984), all of which may influence collagen crimp and/or recruitment (Andrews et al., 2015; Mattson et al., 2017; Michalek et al., 2018). During myopigenesis, aggrecan and sGAGs appear to be the most rapidly altered component in the sclera (Moring et al., 2007), and other work shows evidence of collagen crimp being rapidly increased in the myopic sclera (Grytz & Siegwart, 2015). We hypothesize that loss of sGAGs in the sclera is causal to the increased tissue permeability, subsequently decreasing fluid pressurization and loading of the collagen fibrils, resulting in increased crimping of collagen fibrils that translates to a decrease in the tissue-level tensile modulus. We emphasize that results from cartilage are not guaranteed to hold in the sclera, since the relative proportion of sGAGs/proteoglycans to other extracellular components in the sclera is different from cartilage by approximately an order of magnitude. However, sGAGs and collagen crimp have also been shown to be related in tendon, which is more comparable to the sclera in terms of sGAG content ($\sim$10% in articular cartilage, $\sim$2.5% in tendon, $\sim$1% in the sclera) and other anatomical features (Atta et al., 2022; Michalek et al., 2018).

A logical outcome of the above proposed mechanism is that the scleral tensile modulus and sGAGs content are positively correlated, where sGAG content causally influences tensile stiffness. Attempts to study this structure-function question have utilized ex vivo

methods to degrade sGAGs and measure changes in biomechanics; however, there no consensus has been reached, with studies showing that degrading sGAGs increases (Murienne et al., 2016; Murienne et al., 2015), decreases (Murienne et al., 2016; Zhuola et al., 2018), or has no effect on (Hatami-Marbini & Pachenari, 2020) the tensile stiffness of the sclera. However, these studies digested significantly more GAGs, in quantity and type, than are altered with myopigenesis. Short-term decreases in scleral GAGs in myopia appear to be restricted to those associated with the aggregating proteoglycans (hyaluronan and C-4-S) that typically reside between the collagen lamellae; the above-referenced studies nearly completely digested all scleral sGAGs, including DS, which are typically attached to small leucine-rich proteoglycans that associate closely with and regulate collagen fibrils (Junqueira et al., 1981; Keene et al., 2000; Orgel et al., 2009; Raspanti et al., 2007; Robinson et al., 2017; Svensson et al., 1995). Additionally, the sclera was loaded under tension via different methods in these studies; perhaps sGAGs differentially contribute to the biomechanical response to a directly applied tensile load (Hatami-Marbini & Pachenari, 2020) versus tension resulting from compression or inflation (Murienne et al., 2016; Murienne et al., 2015; Zhuola et al., 2018). Further study of the solid/fluid biphasic mechanics of the sclera (as studied here), along with extending this work to study the sclera as a triphasic material (solid/fluid/ions), are warranted to elucidate these relationships.

4.5.4 Ocular retinoids are altered during myopigenesis

One possible mechanism by which a visual cue may be propagated to the sclera is via retinoids, including atRA, the bioactive form of retinoic acid. Previous studies have shown myopigenesis in mammals is accompanied by increased concentrations of atRA in the retina

and choroid. Here, we measured retinal and R/C/S concentrations of atRA, as well as ROL and tRE, atRA precursors typically understood to be used for transport and storage (Theodosiou et al., 2010). Our results indicate that all three retinoids were influenced by form deprivation, with potentially interesting and unexpected temporal characteristics. Specifically, after 1 week, we observed increases in retinal atRA consistent with previous findings in guinea pigs, chickens, and marmosets (McFadden et al., 2004; McFadden et al., 2006; Troilo et al., 2006). However, this difference was not seen after three weeks of form deprivation. The data in this study suggests that retinoids in the retina and at least one of the RPE, choroid, and/or sclera are being influenced by visual cues; however, future work using a larger cohorts of animals will be necessary to draw stronger conclusions about the role of atRA in mouse myopigenesis.

4.5.5 Technical challenges of the mouse model of myopia

Significant effort was spent in the present study aligning, positioning, and processing OCT images to reduce extrinsic variability in biometric measurements, yet we were unable to measure an overall effect of form deprivation on axial length. This negative finding is common in the mouse (Pardue et al., 2013; Schaeffel et al., 2004), raising concerns over whether the mouse develops axial myopia consistent with other mammals.

It is possible that the mouse does not undergo axial myopigenesis; however, the axial elongation could also be falling below the threshold of detection. Schematic models of the mouse eye have suggested that 1 D of myopia only requires about 5μm of elongation (Schmucker & Schaeffel, 2004b). The axial resolution of a typical OCT system (∼4μm) thus corresponds to ∼1D of myopia. In practice, biological variability (e.g., in eye

size, refractive index, cataracts, astigmatism) and noise inherent to the measurements (e.g., breathing artifacts, acute corneal/lens opacities, intersession/interocular alignment variability, magnification variability in non-telecentric lenses, manual segmentation errors) will further raise the threshold of detection above the resolution.

While there are reports of axial elongation in the myopic mouse eye (Bergen et al., 2016; Schaeffel et al., 2004; Tkatchenko et al., 2010), it is difficult to weight the positive and negative findings in an unbiased manner. Experimental studies reporting positive findings are not consistent in the amount of axial elongation per diopter of myopia (ranging from 5-40 μm/D), thus generally also inconsistent with the 5μm/D estimate from modeling studies (Pardue et al., 2013). Lacking a replicable, consistent effect and/or additional positive findings causal to elongation (e.g., scleral remodeling/biomechanics), it is difficult to conclude whether these studies show true positive findings or type I errors, possibly due to bias either at the level of the researchers (e.g., "lack of blinding" bias) or literature (e.g., "positive result bias").

4.5.6 Conclusions

The present study clearly shows the sclera undergoes remodeling that results in significantly altered biomechanics, in a manner facilitating axial elongation. When compared to axial length as an outcome measure of myopia, scleral biomechanics show a greater effect size and consistency, readily detectable even with modest amounts of myopia (∼2 D). This suggests that, at least at present, scleral biomechanics may be a more reliable measure of axial myopigenesis than biometry in the mouse. It also supports the idea that negative axial elongation findings are type II errors arising from the small magnitudes of elongation.

With the knowledge that retinoids are changing throughout the eye in a time dependent manner, future studies should focus on more thoroughly elucidating the spatial and temporal characteristics. Additionally, transgenic mice could help to better understand the causal impact of these retinoids and specific proteoglycans (aggrecan) on the mouse sclera.

4.5.7 Acknowledgements

Funding: Supported by the National Institutes of Health [NIH R01 EY016435 (MTP), NIHP30 EY006360 (MTP), T32 EY007092 (D.M.B.), Department of Veterans Affairs [Rehabilitation R&D Service Research Career Scientist Award IK6 RX003134 (MTP), CDA1 IK1 RX003208 (JMP), CDA2 IK2 RX003928 (JMP)], University of Maryland Baltimore, School of Pharmacy Mass Spectrometry Center (SOP1841-IQB2014 (MAK)), and the Georgia Research Alliance (CRE).

Disclosures: **D.M. Brown**, None, **M.A. Kowalski**, None, **Q.M. Palus**, None, **J. Yu**, None, **P. Kumar**, None, **M.A. Kane**, None, **J.M. Patel**, None, **C.R. Ethier**, None, **M.T. Pardue**, None

CHAPTER 5

EXOGENOUS ALL-TRANS RETINOIC ACID INDUCES MYOPIA AND ALTERS SCLERAL BIOMECHANICS IN MICE

5.1 Submission Details

Authors: **Dillon M. Brown**, Jianshi Yu, Praveen Kumar, Quinn M. Paulus, Michael A. Kowalski, Jay M. Patel, Maureen A. Kane, C. Ross Ethier, Machelle T. Pardue

Status: In Review at *Investigative Ophthalmology & Visual Science* (Submitted October, 2022)

5.2 Abstract

Purpose: Ocular all-trans retinoic acid (atRA) levels are influenced by visual cues, and exogenous atRA has been shown to increase eye size in chickens and guinea pigs. However, it is not clear whether atRA induces myopic axial elongation via scleral changes. Here, we test the hypothesis that exogenous atRA will induce myopia and alter scleral biomechanics in the mouse.

Methods: Male C57BL/6J mice were trained to voluntarily ingest atRA+vehicle (1% atRA in sugar, 25 mg/kg) (RA: n=16 animals) or vehicle-only (Ctrl: n=14 animals). Refractive error (RE) and ocular biometry were measured at baseline and after 1 and 2 weeks of daily atRA treatment. Eyes were used in ex vivo assays to measure: scleral biomechanics (un-confined compression: n=18), total scleral sulfated glycosaminoglycan (sGAG) content

(dimethylmethylene blue: n=23), and specific sGAGs (immunohistochemistry: n=18).

Results: Exogenous atRA caused myopic RE and larger vitreous chamber depth (VCD) to develop by 1 week (RE: -3.7 ± 2.2 D, $p<0.001$; VCD: +20.7 ± 15.1 μm, $p<0.001$), becoming more severe by 2 weeks (RE: -5.7 ± 2.2 D, $p<0.001$; VCD: +32.3 ± 25.8 μm, $p<0.001$). The anterior eye biometry was unaffected. While scleral sGAG content was not measurably affected, scleral biomechanics were significantly altered (Tensile stiffness: -30 ± 19.5%, $p<0.001$; Permeability: +60 ± 95.3%, $p<0.001$).

Conclusions: In mice, atRA treatment results in an axial myopia phenotype. Eyes developed myopic RE and larger VCD without the anterior eye being affected. The decrease in stiffness and increase in permeability of the sclera is consistent with the form-deprivation myopia phenotype.

5.3 Introduction

The eye's refractive state is jointly determined by its optical power and axial length, with deviations in either causing a refractive error that decreases visual acuity. In the healthy eye, refractive errors are minimized by a complex, homeostatic process (emmetropization) that couples regulation of axial elongation to visual cues (Flitcroft, 2013; Troilo et al., 2019). This coupling is achieved via a retinoscleral signaling cascade that propagates the sign and magnitude of visual blur from the retina, through the retinal pigment epithelium and choroid, ultimately influencing tissue remodeling in the sclera. While it is straightforward to optically correct a refractive error, such corrections do not address the underlying alterations in scleral structure, biomechanics, and eye shape, which can predispose to blinding diseases

(Lakawicz et al., 2020; Saw et al., 2005; Shen, Melles, et al., 2016).

For the eye size to increase, the sclera as the outermost layer must either grow (increasing in total tissue volume) or remodel (reorganizing/degrading constituent components to change tissue material properties). While the sclera grows early in life, the elongation of the eye throughout adolescence appears to be facilitated predominately by scleral remodeling that is increased in myopic eyes (Harper & Summers, 2015). The sclera from myopic eyes has reduced extracellular matrix content (primarily collagen and glycosaminoglycans) that results in a more extensible and thinner sclera than that from a control eye (Boote et al., 2020; Harper & Summers, 2015). Correspondingly, preventing or reversing such changes to the sclera has been demonstrated to protect against myopigenesis, e.g., by reinforcing the scleral collagen network (Grytz, 2018) or reducing collagen degradation (Zhao et al., 2018). However, scleral changes in myopigenesis are complex, with the sclera demonstrating both visually mediated (Grytz & Siegwart, 2015; Harper & Summers, 2015) and load-dependent remodeling (Campbell et al., 2014; Girard et al., 2011; Grytz et al., 2012). Further, as the eye elongates, the loading imparted to the sclera likely changes. Thus, it is not clear whether changes in scleral collagen are the cause or result of myopia. Proteoglycans (PGs)/glycosaminoglycans (GAGs) appear to be more tightly coupled to visual cues, with myopigenic cues decreasing expression and concentration of PGs/GAGs within hours (Summers Rada & Hollaway, 2011). However, their influence on scleral biomechanics is still disputed.

Retinoic acid, specifically all-trans retinoic acid (atRA), has been proposed to be involved in the retinoscleral signaling cascade (Mertz & Wallman, 2000; Seko et al., 1998; Seko et al., 1996). atRA is produced in the retina, RPE, and choroid, and visual cues have

been shown to influence ocular atRA concentrations (Brown et al., 2022). While the sclera does not synthesize atRA, visual cues influence the scleral expression of retinoid receptors (Guo et al., 2013; Guo et al., 2014; Guo et al., 2019; Seko et al., 1996). By co-culturing choroid and sclera ex vivo, Mertz and Wallman found that the choroid is particularly leaky to atRA, and the sclera was able to concentrate atRA beyond that which would be predicted by passive diffusion (Mertz & Wallman, 2000). Additionally, they measured a significant effect of atRA on sulfated GAG (sGAG) synthesis in culture that is supported by in vivo work in the guinea pig (Li et al., 2010), that may indicate an important scleral remodeling endpoint of retinoscleral signaling.

Emmetropization appears to function by modulating the rate of axial elongation to minimize refractive errors as the eye's optical power develops (Brown et al., 2022), and when emmetropization fails, the resulting eye tends to be longer, with a myopic refractive error, but little difference in anterior biometry (Grytz, 2018). While experimentally increasing ocular atRA concentrations causes an increase in eye size (Li et al., 2010; McFadden et al., 2004; McFadden et al., 2006), there are some apparent differences in the resulting phenotype than in visually-mediated models of myopia. Some differences, such as an altered anterior segment and more rapid axial elongation, could be due to the specifics of the treatment, e.g., systemic drug delivery at supraphysiological concentrations (Grytz, 2018; McFadden et al., 2004; McFadden et al., 2006). However, most puzzling are the findings that atRA-induced axial elongation mostly occurred without corresponding myopic refractive errors (McFadden et al., 2004; McFadden et al., 2006). Thus, it is still unclear how atRA is exerting its effects on eye size and if such changes are consistent with typical myopic axial elongation.

Here, we studied the influence of exogenous atRA on the refractive development of the mouse eye starting at 4 weeks of age. We hypothesized that increasing ocular atRA would be myopigenic, resulting in features of axial myopia such as an elongated posterior segment and altered scleral biomechanics. Scleral sGAG concentrations were measured as a possible mediator between the atRA treatment and scleral biomechanics.

5.4 Materials and Methods

5.4.1 Animals

Mice (C57BL/6J; Jackson Laboratory, Bar Harbor, Maine, USA) were housed at the Atlanta Veterans Affairs Healthcare System. Animals were reared with littermates in normal lighting (12:12-hour cycles, 20-200 lux) with access to mouse chow and water ad libitum, except during the periods of atRA or vehicle feeding. Procedures were approved by the relevant Institutional Animal Care and Use Committee and adhered to the Association for Research in Vision and Ophthalmology (ARVO) Statement for the Use of Animals in Ophthalmic and Vision Research.

5.4.2 Daily Voluntary Feeding of atRA

Male C57BL/6J mice were trained to voluntarily eat sugar pellets, which were then used as a vehicle for daily oral delivery of atRA (Cadot et al., 2012). Sugar pellets (98% sucrose, water, corn syrup, maltodextrin, cornstarch; Signature Brands, LLC) were formed and allowed to set at 4°C. Pellets used as a vehicle were mixed with 1% atRA ($\geq$98% pure, Cat # R2625, CAS: 302- 79-4; Sigma-Aldrich, Saint Louis, MO, USA) by weight prior to form-

ing and setting. Pellets with atRA were stored for up to a week in a lightproof container at 4°C.

Voluntary feeding was carried out by first weighing each animal and placing them into individual cages without bedding. Animals were allowed to adjust to this environment while the appropriate doses of sugar pellets or sugar+atRA were weighed out (2.5 mg pellet/g yielding 25 mg/kg atRA). Pellets were placed into each cage after wiping the cage with a paper towel. After 1-2 days of training (using only sugar pellets), animals voluntarily and quickly ingested the pellets (typically <5 minutes, always within 1 hour). Cages were checked every few minutes, and once a mouse ate the pellet, it was returned to its regular cage. All procedures involving atRA were performed in darkness or under dim, red/yellow light to prevent excessive isomerization.

To confirm that orally delivered atRA was reaching the eye, a small cohort of animals (n=6) were fed atRA (RA: n=3) or sugar (Ctrl: n=3) for two weeks. After their final treatment, animals were placed in the dark for 1-2 hours prior to sacrifice by cervical dislocation. Eyes were enucleated, and retinas and the combined RPE, choroid, and sclera (R/C/S) were collected from each eye and stored in light-proof Eppendorf tubes at -80°C until use for retinoid quantification via liquid chromatography-tandem mass spectrometry (LC-MS/MS).

5.4.2.a Liquid Chromatography tandem mass spectrometry (LC-MS/MS)

Characterization of retinoids in the ocular tissues were performed as previously described (Brown et al, in review). In brief, the same tissue from left and right eyes of each animal were combined and weighed prior to homogenizing in 0.9% NaCl (normal saline). A two-step acid-base extraction was performed, including internal standards (RA: 4,4-

dimethyl-RA; retinol, total retinyl esters: retinyl acetate) (Kane & Napoli, 2010). Liquid chromatography-multistage-tandem mass spectrometry was used to quantify RA and its isomers (9-cis-RA, 13-cis-RA, 9,13-di-cis-RA) (Jones et al., 2015). HPLC-UV was used to quantify retinol and total retinyl esters (Kane, Folias, & Napoli, 2008; Kane, Folias, Wang, et al., 2008; Kane & Napoli, 2010). All experimenters handling samples after tissue was collected were blinded to the identities/treatments of the animals.

5.4.3 In Vivo Ocular Measurements

Mice at 4 weeks of age were fed daily with atRA or vehicle for 2 weeks (Ctrl: n=14, atRA: n=16) Several outcomes were measured in eyes prior to and after 1 and 2 weeks of daily feeding. Eyes were dilated with 1% topical tropicamide and animals were anesthetized (intraperitoneal injection of ketamine: 80 mg/kg; xylazine: 16 mg/kg) (Bergen et al., 2016; Faulkner et al., 2007). Measurements were then made of the cycloplegic refractive error (RE) using a mouse-specific automated infrared photorefractor, corneal curvature (CC) using infrared photokeratometry, and axial ocular biometry using spectral domain optical coherence tomography (OCT) (4.1 μm axial resolution; Envisu R4300, Leica Microsystems, Wetzlar, Germany) (Schaeffel, 2008; Schaeffel et al., 2004). Registration (phase-correlation) was performed on adjacent B-scans (Guizar-Sicairos et al., 2008), and eye-specific spatial and temporal averaging was performed to obtain a representative B-scan with the best possible signal-to-noise ratio, as judged by the annotator. Tissue interfaces were manually delimited, from which central corneal thickness (CCT), anterior chamber depth (ACD), lens thickness (LT), vitreous chamber depth (VCD), retinal thickness (RT), and axial length (AL) (corneal surface to retinal pigment epithelium (RPE)) were calculated.

Optical path lengths of the SD-OCT were converted to physical distances by assuming an average refractive index of 1.39 (Chakraborty et al., 2022; Landis et al., 2020). Eyes were excluded when significant opacities were seen in the cornea or lens, and animals were included if at least one eye was measured.

In vivo measurements are presented as either values relative to the control group at each timepoint t_n ("shifts" $\equiv x_i^{t_n} - \bar{x}_{Ctrl}^{t_n}$) or as a change from baseline ($\Delta^t x_i \equiv x_i^{t_n} - x_i^{t_0}$), where x_i is the average of the two eyes from mouse i, $\bar{x}_{Ctrl}$ is the mean of the Ctrl group, and superscript t_n denotes the timepoint. t_0 denotes the baseline timepoint.

5.4.4 Ex Vivo Endpoints

Ex vivo endpoints were assigned to each eye pseudo randomly prior to the 1-week timepoint, typically assigning two different endpoints to each animal. After the two-week treatment period, animals were sacrificed, and eyes were enucleated and processed the same day according to the chosen ex vivo endpoint, as listed below:

1. Kept fresh for biomechanical measurements via unconfined compression testing (UCT);
2. Frozen for quantification of total scleral sGAG/DNA content by 1,9-dimethylmethylene blue (DMMB)/PicoGreen; or
3. Fixed for semiquantitative immunohistochemistry (IHC).

In total, 59 eyes from 30 animals were studied across the 3 ex vivo endpoints, in addition to 12 eyes used for confirming oral atRA reached the ocular tissues (Figure 5.1).

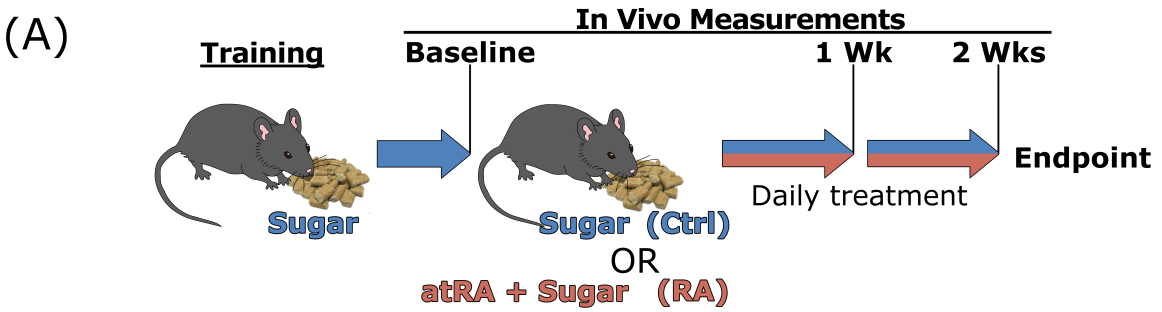

(B)

Outcomes	# Eyes	Ex vivo Assay	
1) Ocular retinoids	(n=12)	Mass Spectrometry	(LC-MS/MS)
2) Biomechanics	(n=18)	Unconfined Compression	(UCT)
3) Total sGAGs	(n=23)	Dimethylmethylene Blue	(DMMB)
4) Specific sGAGs	(n=18)	Immunohistochemistry	(IHC)

Figure 5.1: Experimental study design. A) In vivo measurements were made at baseline, after which animals were either assigned to daily feeding of atRA in sugar pellets (RA; 25 mg/kg) or sugar pellets-only (Ctrl). Treatments were maintained for 2 weeks, with body mass recorded daily and ocular measurements made weekly (3 times total). B) The outcomes studied are presented alongside their associated ex vivo assays and the number of eyes sampled.

5.4.4.a Unconfined Compression Testing (UCT)

Eyes were stored in phosphate-buffered saline (PBS) at 4°C after enucleation and scleral biomechanical properties were characterized the same day as previously described (Brown, Pardue, et al., 2021). Posterior eye cups were obtained as described above for LC-MS/MS measurements (under normal lighting). The retina was removed from the posterior eye cup. Four cuts were made to flatten the posterior eye, and the choroid and RPE were removed. A biopsy punch was used to obtain 1 mm diameter cylindrical samples from the posterior region of the scleral shell (~0.5 mm from the optic nerve). A small amount of graphite powder was applied to samples to minimize friction between samples and compressive platens. Samples were then placed into a 37°C PBS fluid bath, in which biomechanical testing was carried out.

A compression testing apparatus designed for small samples (Microsquisher; CellScale,

Waterloo, ON, Canada) was used to perform unconfined compression stress relaxation experiments on scleral samples. A tare load (500 μN) was applied to flatten the samples and ensure samples were in contact with the platens. After equilibrating, 3 compressive strain steps were incrementally applied (5% strain per step, 15% maximum compressive strain). At each step, strain was rapidly applied and maintained until stress relaxed and equilibrated, after which the next step was started. The biphasic conewise linear elastic model was independently fit to each step, whose parameters include the aggregate tensile modulus H_{+A} (i.e., in-plane tensile stiffness) and hydraulic conductivity k (i.e. permeability to water) (Brown, Pardue, et al., 2021). One estimate of each parameter was obtained at each of the three strain steps, yielding 3 measurements of each parameter per sample over the test.

Due to the variability in the strain applied at each step and the dependence of the material properties on compressive strain, both the raw values and estimated marginal means obtained from the fitted statistical model are reported, in which strains are adjusted to exactly the target strains (5%, 10%, and 15%).

5.4.4.b Dimethylmethylene Blue Assay (DMMB)

Eyes were stored in PBS at 4°C until dissection the same day, following the same procedures described for unconfined compression. Isolated sclerae were dehydrated overnight in a vacuum desiccator and weighed 3 times on an analytical balance (XSR205DU; Mettler Toledo, Columbus, OH, USA), with the average being taken as the dry mass of the sclera. The isolated sclerae were stored at -80°C until use.

Total scleral sGAG and DNA content were quantified via spectrophotometric assays, the DMMB assay and PicoGreen assay, respectively (Brown et al., in review). In brief,

samples were thawed and digested in 200microiter papain solution (0.1M Sodium Acetate (anhydrous), 10mM Cysteine Hydrochloride, 50mM EDTA, pH 6, 2% v/v papain), distributing the digestate between the two assays. For the DMMB assay, absorbance was read at 525 nm immediately following the addition of the DMMB dye mixture. To measure DNA, the PicoGreen working reagent was added and absorbance was read using 480 nm excitation and 520 nm emission.

Concentrations of each were then determined by comparing absorbances to a standard curve. Absorbances from the DMMB assay were compared to shark cartilage chondroitin sulfate (working range 0-25 µg sGAG/µL, 8 measured standards; Sigma C4384). Absorbances from the PicoGreen assay were compared to Lambda DNA stock (working range 0-4 µg DNA/µL, 8 measured standards; Sigma Cat #: SD0011, Thermo Fisher Scientific, Waltham, MA, USA). Both assays were performed in triplicate, with the average of the three readings taken as the final value. Scleral sGAG content is reported as a mass fraction (µg sGAG/mg sclera) and as a mass ratio (µg sGAG/µg DNA) to account for differences in quantity of collected tissue.

5.4.4.c Immunohistochemistry (IHC)

Eyes were enucleated and immersion fixed in buffered zinc formalin (Z-Fix; Anatech LTD, Battle Creek, MI, USA) for 1 hour immediately following sacrifice. Extraocular tissue, cornea, and lens were removed after fixation. Prior to cryosectioning, eyes were allowed to equilibrate in 30% sucrose solution overnight, following which they were embedded in optimal cutting temperature medium and frozen on the Peltier cooling element of a cryostat (CM1850; Leica Microsystems, Wetzlar, Germany). Sagittal sections were taken through

the optic nerve head (10μm), applied to charged slides (Superfrost Plus; Thermo Fisher Scientific, Waltham, MA, USA), and stored at -20°C.

A monoclonal primary antibody (Clone 2B6, Cat:1042009, Lot: S1605002; MD Biosciences, Oakdale, MN, USA) was used to stain specific sGAGs. 2B6 is specific to neoepitopes generated by chondroitinase digestion of chondroitin-4-sulfate (C-4-S) and dermatan sulfate (DS), but not chondroitin-6-sulfate (C-6-S). C-4-S and DS were separately labeled by treating tissue sections with one of two chondroitinases: either chondroitinase AC (ChAC), which specifically deglycosylates chondroitin A (C-4-S) and chondroitin C (C-6-S); or chondroitinase B (ChB), which targets chondroitin B (DS) (both from Flavobacterium heparinum, Sigma-Aldrich, Saint Louis, MO, USA). Thus, one antigen site recognized by 2B6 will be exposed per C-4-S chain when tissue is treated with ChAC; similarly, one site recognized by 2B6 will be exposed per DS chain when treated with ChB.

Tissue was prepared for immunostaining by first washing the samples with tris-buffered saline with 0.1% Triton X-100 (TBS-T) to remove embedding medium and then samples were treated with chondroitinase (3 hours at 24°C; ChB, ChAC, or buffer-only; 0.5 U/mL, 8.0 pH). Sections were then permeabilized (10 minutes at 24°C; 0.5% Triton X-100 in TBS), blocked (45 minutes at 24°C; 10% normal goat serum, 1% bovine serum albumin in TBS-T), and incubated with primary antibody overnight (18 hours at 4°C; mouse monoclonal antibody 2B6 in blocking buffer, 1:100). The next day, sections were washed and incubated with secondary antibodies (45 minutes at 24°C in darkness; 1:500; Alexa Fluor-647 conjugated goat anti-mouse antibodies in blocking buffer, Cat # A-21244, Invitrogen). Samples were washed, treated with DAPI (NucBlue Fixed Cell Stain ReadyProbes DAPI, Cat # R37606, Invitrogen), washed, and coverslipped with antifade medium (Prolong Di-

amond Antifade Medium, Cat # P36961, Invitrogen). Staining was done using the same batch of working reagents on all slides in parallel, and each slide had sections from the same eye treated with each of the chondroitinase conditions (ChB-treated, ChAC-treated, and buffer-only control).

A confocal microscope (Nikon A1R, Nikon, Tokyo, Japan) with an apochromatic 20X objective lens was used to image immunolabeled tissue, keeping all settings the same across all samples. Three images (600x600μm each, 2 channels, 12 bits per channel) were taken per section, centered around the optic nerve head as a reference location. Semiautomated macros in FIJI (Schindelin et al., 2012) were used to stitch, mask, threshold, and quantify images. The sclera was manually masked from the adjacent choroid and the region directly surrounding the optic nerve. For regional analysis, the masked regions were split at the optic nerve to divide the superior and inferior sclera.

On each slide, average pixel intensities within the masked sclera were calculated for a ChB-treated section, a ChAC-treated section, and a buffer-only section. Normalized fluorescence is reported as a semiquantitative measure of the specific sGAGs (DS = Intensity of ChB-treated section/Intensity of buffer-only; C-4-S = Intensity of ChAC-treated section/Intensity of buffer-only), and is related to the number of GAG attachment sites on proteoglycans.

5.4.5 Statistical Analysis

Each outcome measure was analyzed by constructing a generalized linear mixed model reflecting the experimental design. Outcomes were assigned a Gamma error distribution with a log link when this led to reasonable predictions (e.g., strictly positive quantities) and based

on analysis of the model residuals (Supplementary Table B.1). Significance of fixed effects was calculated by performing likelihood ratio tests between the full model and null models, each lacking one of the fixed effect terms. Random intercepts were included to account for inter-sample correlation, such as multiple measurements of the same animals/eyes. Fitting, contrasts, and p value calculations were done using the "lme4" and "emmeans" packages in R (version 4.1.1) (Bates, Machler, et al., 2015; Lenth, 2021). The significant alpha threshold was set to 0.05, and when multiple contrasts were run, adjusted p values are reported (multivariate t method) (Westfall & Tobias, 2007).

5.5 Results

5.5.1 Effects of orally delivered atRA on the mouse

Animals treated with atRA daily for 2 weeks displayed no obvious changes in behavior or health; no animals were lost due to treatment. Animals consumed food/water normally, and treatment did not affect the normal body mass development (Interaction: treatment:duration, $p=0.06$, Supplementary Figure B.1). Animals voluntarily ingested the drug for the entire treatment period.

Oral ingestion of atRA significantly increased ocular atRA levels (atRA vs Ctrl: $p<0.001$ for both retina and combined R/C/S) without affecting the levels of other retinoids (Figure 5.2). On average, isomerization of atRA to all measured cis forms (combined) was approximately 7%, which is the amount expected when atRA is in the presence of biological tissue matrix (KANE et al., 2005), and there were no signs of significant isomerization in the internal standards.

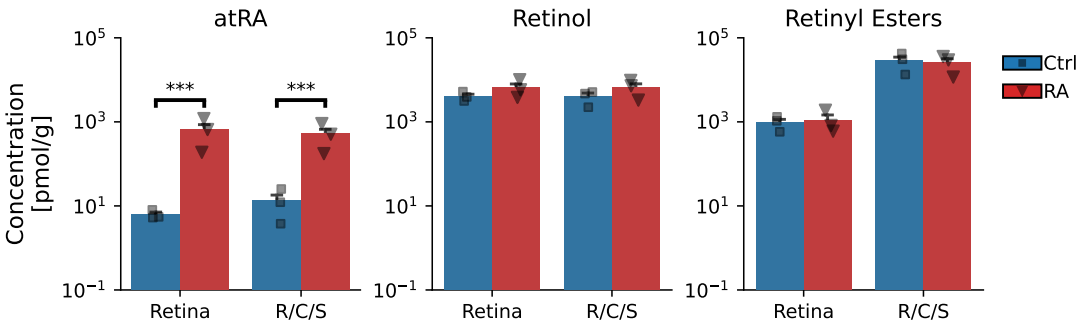

Figure 5.2: Oral delivery of atRA significantly increased the concentration of atRA in the retina and R/C/S without influencing levels of other retinoids. Similar tissue from the two eyes from each animal were grouped and measured together. R/C/S: combined RPE, choroid, and sclera; Ctrl: Vehicle-treated group (n=3 animals/6 eyes); RA: atRA-treated group (n=3 animals/6 eyes). *: $p<0.05$, **: $p<0.01$, ***: $p<0.001$.

5.5.2 Increasing ocular atRA induces axial myopia in the mouse

Prior to treatment, animals in both groups had similar refractive errors (RE shift; 0.12 $\pm$ 1.1 D, p=0.72). Treatment with atRA for both 1 and 2 weeks caused animals to develop significant myopic shifts in refractive error (RE shift; 1 week: -3.7 $\pm$ 2.2 D, $p<0.001$; 2 weeks: -5.7 $\pm$ 2.2 D, $p<0.001$). Every animal treated with atRA was relatively myopic compared to the mean of the littermate controls after 2 weeks (Figure 5.3a).

Measurements of AL and VCD were consistent with the development of refractive errors. At baseline, neither VCD nor AL were different between treatment groups (VCD: p=0.72, AL: p=0.55, Supplementary Table B.2). VCD decreased with age in both groups but less in the atRA-treated animals than controls (VCD $\Delta^t x_i$; 1 week: Ctrl: -25.2 $\pm$ 24.2 µm, RA: -2.2 $\pm$ 25.8 µm, $p<0.001$; 2 weeks: -45.1 $\pm$ 32.1 µm, RA: -18.2 $\pm$ 37.3 µm, $p<0.001$, Supplementary Figure B.2b), resulting in atRA-treated animals having deeper vitreous chambers at both timepoints (VCD shift; 1 week: +20.7 $\pm$ 15.1 µm, $p<0.001$; 2 weeks: +32.3 $\pm$ 24.8 µm, $p<0.001$; Figure 5.3b). The VCD decreases with age due to the

growth of the lens overtaking the rate of elongation. In other words, because the lens development is not affected by treatment, the shift in VCD is consistent with excess posterior elongation of the eye.

A similar but more variable trend was observed in axial length (Figure 5.3c). While the mean axial lengths were not significantly different at any timepoint (AL shift; 1 week: 13.7 ± 42.5 µm, p=0.42; 2 weeks: 19.1 ± 34.5 µm, p=0.14), atRA-treated eyes elongated more than control eyes after both 1 and 2 weeks (AL $\Delta^t x_i$; 1 week: Ctrl: 82.6 ± 14.7 µm, RA: 90.9 ± 17.5 µm, p=0.024; 2 weeks: Ctrl: 132.1 ± 15.1 µm, RA: 145.0 ± 16.6 µm, $p<0.001$).

Treatment with atRA did not cause any significant shifts in anterior eye biometry outcomes that influence optical power (anterior corneal curvature, corneal thickness, lens thickness, anterior chamber depth) (Supplementary Table B.2). However, atRA treatment had a minor but significant effect on the development of the anterior chamber depth. Specifically, the anterior chamber depth increased over time in both groups, but less so in the atRA-treated animals (ACD $\Delta^t x_i$; 1 week: Ctrl: +19.9 ± 7.5 µm, RA: +11.1 ± 8.8 µm, $p<0.001$; 2 weeks: +35.7 ± 9.1 µm, RA: +26.7 ± 7.1 µm, $p<0.001$, Supplementary Figure B.2e), but this did not result in a significant shift at either timepoint (ACD shift; baseline: 2.5 ± 11.7 µm, p=0.97; 1 week: -7.0 ± 12.8 µm, p=0.29; 2 weeks: -7.7 ± 12.0 µm, p=0.22, Figure 5.3e).

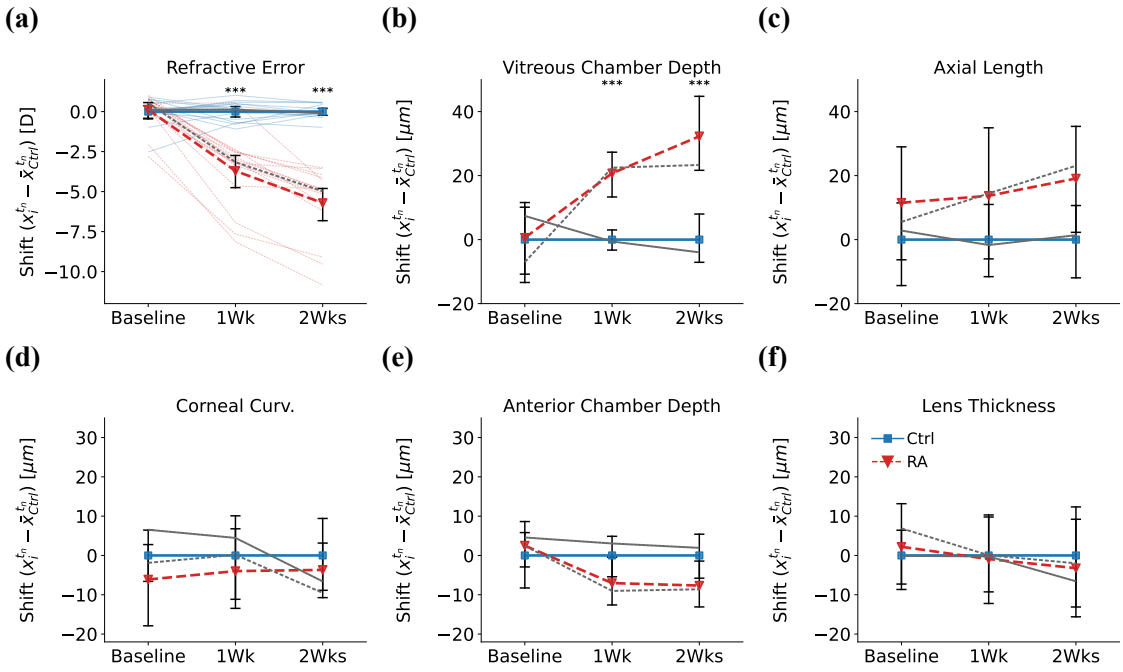

Figure 5.3: Treatment with atRA caused significant changes in refractive state and ocular biometry. Plots show the "shifts" of each outcome (shift = $x_i^{t_n} - \bar{x}_{Ctrl}^{t_n}$), where $x_i^{t_n}$ represents the measured value in animal i at timepoint t_n, and $\bar{x}_{Ctrl}^{t_n}$ is the mean of the control group at timepoint t_n. A) Control and atRA-treated animals had very similar refractive errors at baseline prior to treatment. 1 and 2 weeks of daily atRA caused significant myopia to develop. B) Vitreous chamber depth (VCD) increased with atRA feeding, consistent with a myopic refractive error. (C-F) Other measurements of optical biometry were unaffected by atRA, including those in the anterior chamber. Individual animals are shown with fainter lines in A). Solid blue (gray) lines are the mean (median) of the control group, dashed red (gray) lines are the mean (median) of the atRA-treated group. Error bars show the 95% confidence intervals. Ctrl: Vehicle-treated group (n=14 animals); RA: atRA-treated group (n=16 animals). *: $p<0.05$, **: $p<0.01$, ***: $p<0.001$, adjusting for deviations in age and multiple comparisons.

5.5.3 Scleral stiffness and permeability are both altered as a result of increased ocular atRA.

Scleral biomechanical properties were altered by atRA feeding. Averaged across all strain steps, sclerae from atRA-treated animals were less stiff (atRA: 104 ± 47 kPa, Ctrl: 160 ± 96 kPa, Main effect: treatment, $p<0.001$) and more permeable (atRA: 0.96E-14 $m^4/(Pa\,s)$, Ctrl: 0.73E-14 $m^4/(Pa\,s)$, Main effect: treatment, $p=0.02$) (Figure 5.4). When compared to the mean of the control group at the same strain step, the sclerae from atRA-treated

animals were ∼30% less stiff and ∼60% more permeable compared to control animals (Supplementary Table B.5).

These differences were more pronounced with increasing compressive strain (Interactions: Stiffness:strain: $p<0.001$, Permeability:strain: $p=0.03$). Specifically, with increasing compressive loads, sclerae from atRA treated animals stiffened less ($p<0.001$) and permeability decreased less ($p=0.03$) than was the case for control sclerae (Figure 5.4). For example, sclerae from atRA treated eyes were approximately half as stiff and twice as permeable than those from control eyes at 15% compressive strain (Supplementary Table B.5). Using the fitted statistical model to estimate properties at 0% compressive strain, there were no differences between atRA and control eyes in either outcome.

5.5.4 Scleral sGAGs and DNA content were not measurably altered with atRA treatment.

No effect of atRA was seen on the DNA content of the total sclera, indicating no large influence on the proliferation of resident cells (Ctrl: 1.19±0.16 μg DNA/mg sclera, RA: 1.29±0.21 μg DNA/mg sclera). Two measurements of sGAGs in the sclera were performed: total concentration in the sclera (via DMMB assay) and fluorescence intensity of immunolabelling in the posterior sclera (via IHC as a semiquantitative proxy for number of sGAG attachment sites). Neither sGAG concentration nor fluorescence intensity were affected by atRA treatment (Figure 5.5, Table 5.1). An additional regional analysis was performed on the IHC images, in which the regions superior and inferior to the optic nerve were analyzed separately, and no regional differences were observed (Supplementary Figure B.3).

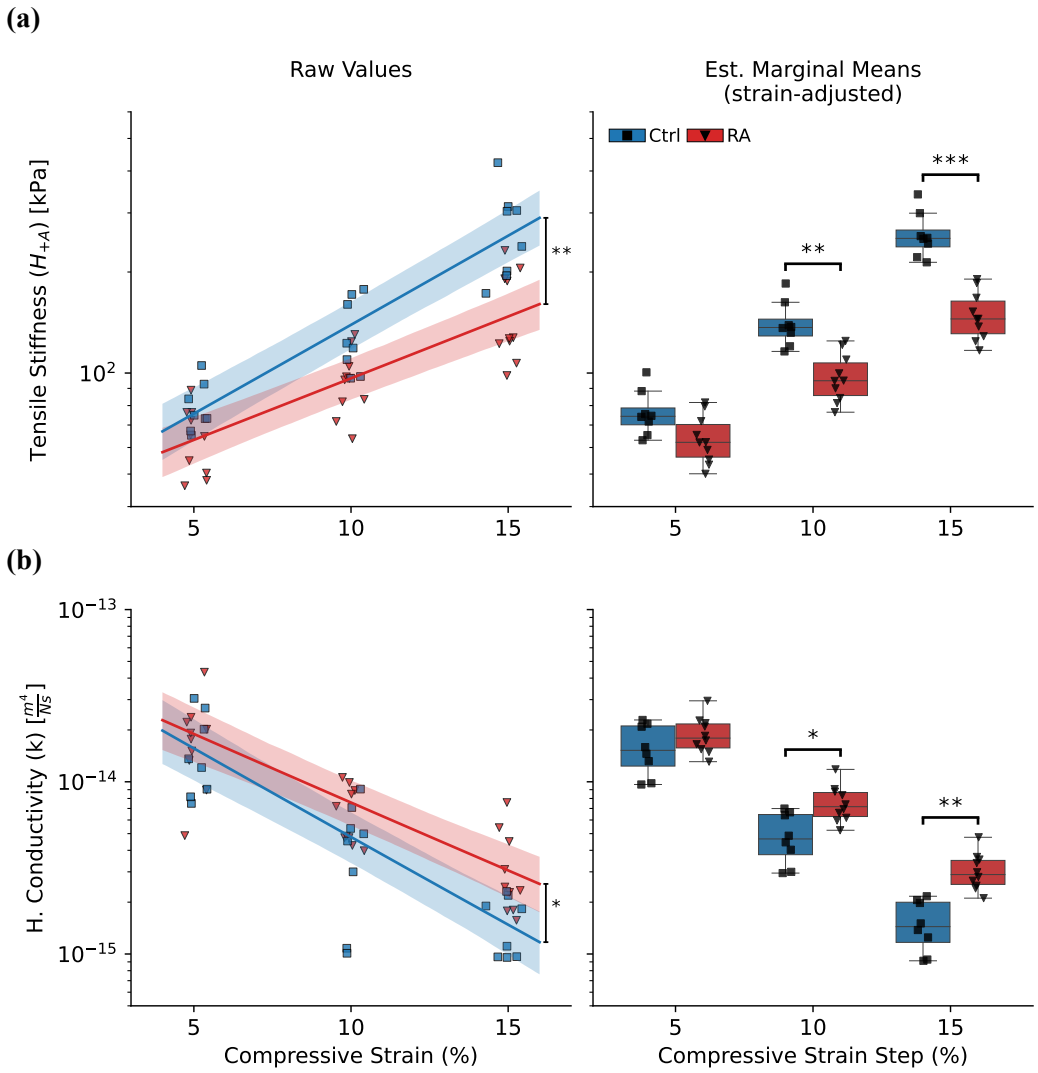

Figure 5.4: Scleral biomechanics were altered in response to atRA treatment. A) In-plane aggregate tensile modulus (H_{+A}), i.e., stiffness and B) hydraulic conductivity (k), i.e., permeability were altered in response to treatment. Plots show the raw values obtained from fitting the poroelastic material model, regressions, and 95% credible intervals obtained from the statistical model (left) and the estimated marginal means obtained from the statistical model (right), both plotted as a function of the applied compressive strain. Ctrl: Vehicle-treated group (n=8 animals/eyes); RA: atRA-treated group (n=10 animals/eyes). *: $p<0.05$, **: $p<0.01$, ***: $p<0.001$.

Table 5.1: Biochemical makeup of the sclera was not measurably changed with atRA treatment. Tabulated quantities are mean ± standard deviation (# eyes). Scleral DNA was quantified by the PicoGreen assay, and sGAGs were quantified by both the DMMB assay (total) and immunostaining of chondroitinase-treated samples (specific sGAGs). sGAG: sulfated Glycosaminoglycans; AU: Arbitrary units (normalized fluorescence); C-4-S: Chondroitin-4-sulfate; DS: Dermatan Sulfate; Ctrl: Vehicle-treated group (n=14 animals); RA: atRA-treated group (n=16 animals).

Group	**Body Weight** [g]	**Sclera mass (dry)** [µg]	**DNA Conc.** [µg/mg]	**GAG Conc.** [µg/mg]	**GAG/DNA** [µg/µg]	**C-4-S** [AU]	**DS** [AU]
Ctrl	22.89±1.65 (9)	140.22±21.94 (9)	1.19±0.16 (9)	7.18±2.10 (9)	5.97±1.30 (9)	1.48±0.28 (7)	3.69±1.31 (7)
RA	20.21±2.33 (14)	135.33±16.93 (14)	1.29±0.21 (14)	8.70±1.98 (14)	6.81±1.43 (14)	1.52±0.32 (11)	3.91±1.42 (11)

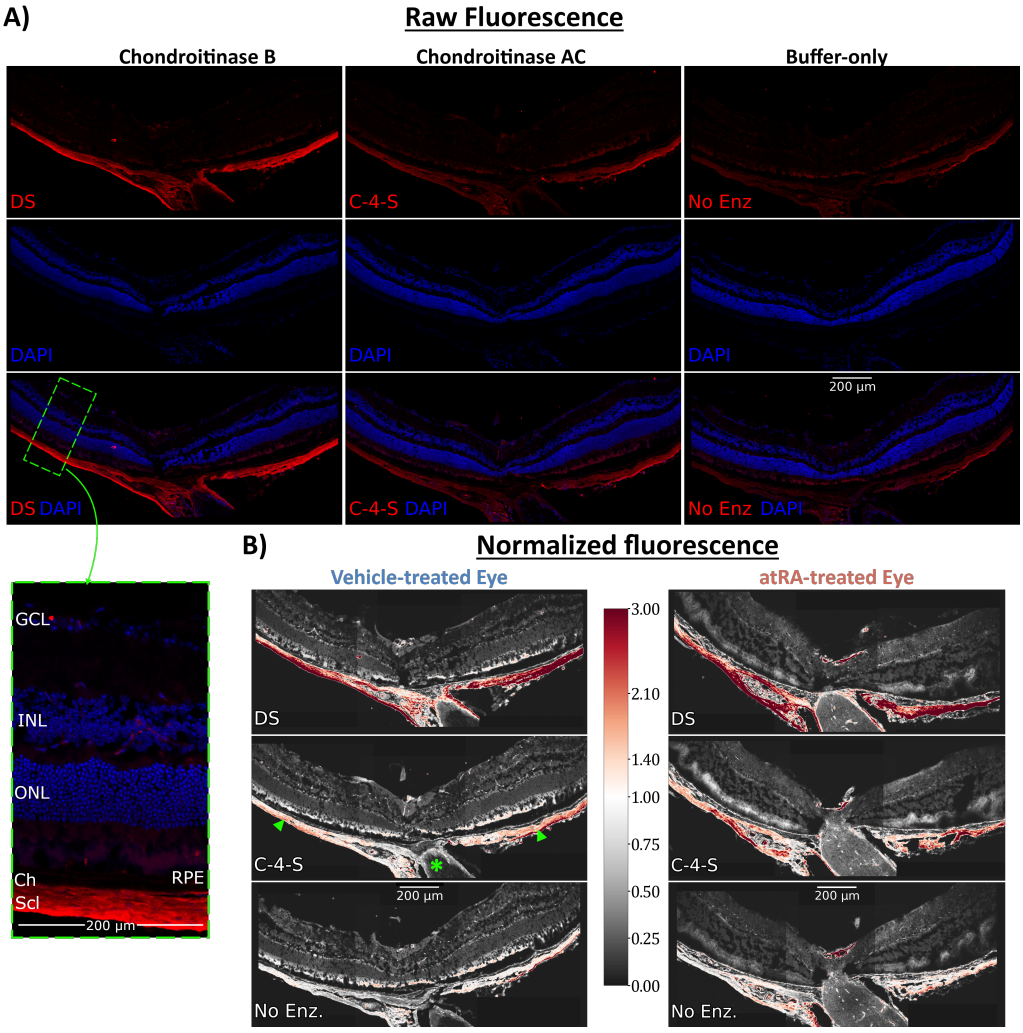

Figure 5.5: Effect of oral atRA on immunostaining of specific scleral sGAGs. A) Representative immunostaining of the posterior eye subjected to the different chondroitinase treatments. Staining was minimal in the absence of chondroitinase during incubation (top right). When samples were incubated with either ChAC (top middle) or ChB (top left), labeling increased, primarily in the sclera. The green dashed rectangle outlines a 200 µm wide region and its magnified/annotated view. B) From the immunostaining in A), normalized fluorescence is obtained for ChB and ChAC conditions by normalizing to the average intensity in the sclera of the buffer-only condition. There were no quantifiable differences between the control and atRA-treated animals. Red pixels indicate increased staining, white indicates no change, and gray indicates decreased staining relative to the sclera of the same eye's "buffer-only" treatment, as shown in the colorbar. Arrowheads label the sclera; the asterisk denotes the optic nerve. ChAC: Chondroitinase AC, ChB: Chondroitinase B, sGAG: sulfated glycosaminoglycan

5.6 Discussion

The present study demonstrates a causal link between increased ocular atRA levels and myopic axial elongation in the mouse. Systemic delivery of atRA specifically increased the concentration of atRA in the eye, without increasing other retinoic acid isomers, and resulted in mice developing myopic refractive errors. Treatment with atRA minimally affected the biometry of the anterior eye but led to significantly increased axial elongation and correspondingly longer vitreous chambers than control animals, indicating an elongation of the posterior eye that is consistent with axial myopia in other species. We have also established that the myopic phenotype induced by atRA is accompanied by altered scleral biomechanics, with the sclera becoming more extensible and permeable, an effect consistent with that seen in visually-mediated myopia in other species (Grytz & Siegwart, 2015; Phillips et al., 2000; Siegwart & Norton, 1999; Westfall & Tobias, 2007), including our previous report in the mouse (Brown et al., in review). The overall impact of atRA on the eye appeared to be limited entirely to the posterior eye, except for a minor effect on anterior chamber depth that was also observed to occur in chickens (McFadden et al., 2006). We did not identify changes in scleral sGAGs or obvious signs of systemic or ocular toxicity. Together, these findings support a role for atRA in myopigenic retinoscleral signaling by influencing both axial length and scleral biomechanics similarly to visually-mediated myopigenesis.

5.6.1 atRA causes axial myopia in the mouse

The results of this study are consistent with the results of previous studies in guinea pigs and chickens (Li et al., 2010; McFadden et al., 2004; McFadden et al., 2006) demonstrating that

experimentally elevating atRA levels causes an increase in eye size; however, it is not clear by what mechanism this occurs. In the studies by McFadden et al. (McFadden et al., 2004), atRA caused increases in eye size but did not induce refractive errors, indicating that the optical power of the eyes was also affected in a manner that kept the focal point of light on the retina. Additional significant changes uncharacteristic of axial myopia were observed by McFadden et al., e.g., a thinner lens and shorter anterior chamber, even with atRA doses as small as 2 mg/kg (McFadden et al., 2006). While Li et al. reported myopic refractive errors, axial elongation, and changes in scleral proteoglycans in response to atRA in guinea pigs (Li et al., 2010), other ocular biometry was not reported, and scleral proteoglycans were not quantified (Li et al., 2010), making comparison to the other studies difficult. Thus, most previous studies suggest that atRA causes the eye to enlarge in a manner disparate from what occurs in axial myopia.

In agreement with previous studies, we have demonstrated a causal connection between ocular atRA and the size of the eye (McFadden et al., 2004; McFadden et al., 2006). However, the present study has shown that increasing ocular atRA levels caused mice to develop myopic refractive errors; notably, eyes elongated more over the treatment period and had longer vitreous chambers on average than the control animals, and the anterior segment was only minimally affected. Additionally, while remodeling outcomes were not measurably different, the biomechanics of the sclera were significantly altered, resulting in a biomechanical phenotype in close agreement with the outcomes of form-deprivation models of myopia (Brown et al., in review); specifically, atRA caused the sclera to become more extensible and more permeable.

While we measured no effect of atRA on lens thickness, we did observe a mild short-

ening of the anterior chamber similar to that observed in the guinea pig (McFadden et al., 2004). McFadden et al. speculated that the effect on ACD could be the result of a flattened cornea; however, we observed no changes in the anterior corneal curvature with atRA treatment. Whatever the cause of the change in ACD, the effect was relatively small when compared to the axial elongation. Estimates from simple ray tracing would suggest the $\sim$8µm decrease in ACD seen here would be responsible for $<$1 D of myopia (Lewis et al., 2014). In contrast, the $\sim$30µm longer vitreous chamber is estimated to cause 6 D of myopia in the mouse, which closely agrees with the measured $\sim$-5.7 D refractive error (Schmucker & Schaeffel, 2004a). Thus, while atRA may have a minor impact on the anterior ocular tissues, the effects in the mouse are predominately in the posterior eye and characteristic of myopic axial elongation.

The present study has significant phenotypic differences from those reported previously by McFadden et al., and comparison could be informative. Two primary methodological differences between the present study and those of McFadden are in the means of drug delivery (voluntary feeding here vs. gavage by McFadden et al.) and the age of the animals at the onset of treatment. While gavage and feeding both deliver the drug systemically via the gastrointestinal tract, it has been previously shown that there are differences in the effect of atRA when the two methods are compared directly (Cadot et al., 2012). Perhaps more relevant to myopigenesis is the choice of age of the animals. Here, treatment was initiated at 4 weeks of age, when the mouse eye has already reached 90-95% of its mature size but is still emmetropizing (Lewis et al., 2014; Schmucker & Schaeffel, 2004b). In the studies by McFadden et al., both guinea pigs and chickens were treated starting at 1 week of age (McFadden et al., 2004; McFadden et al., 2006), when the eye is still elongating rapidly and

is only approximately 60-80% of its mature size (Schaeffel et al., 1986; Tkatchenko et al., 2010). Considering that atRA is centrally involved in developmental processes in many organs, influencing the transcription of c. 100 genes and displaying precise spatiotemporal regulation (Howlett & McFadden, 2007), it is not unreasonable to speculate that atRA may be involved in modulating both eye growth and myopigenic axial elongation, with the relative contribution to these processes depending on the age of the animal. However, to date no studies have directly explored this hypothesized dual role.

5.6.2 Form-deprivation compared to atRA-induced myopigenesis in the mouse

We have previously reported that form-deprivation in the mouse results in altered scleral biomechanics and decreased scleral sGAGs levels (Brown et al., in review). Specifically, after 3 weeks of form-deprivation, mice developed 4.1D of myopia, and the sclera was 40% more extensible and 140% more permeable compared to the contralateral control eyes. Here, daily atRA treatment for 2 weeks caused 5.7D of myopia, and an average 30% and 60% increase in scleral extensibility and permeability compared to the control group. Considering the difference in how these percentages were calculated (pairwise within each animal in the form-deprivation study, compared to mean of the control group in the current study) and the fact that the minor effects of atRA on ACD may be responsible for $\sim$1D of refractive myopia, the degree of myopigenesis and associated scleral biomechanical changes agree reasonably well.

However, whereas we previously measured a decrease in C-4-S and DS in the sclera of form-deprived eyes, here, using identical methodologies, we saw no measurable change in scleral sGAG content with atRA treatment. While this difference could be indicative

of disparate remodeling and myopigenesis mechanisms, it could also be an artifact of the treatment. One obvious difference between form deprivation and atRA as delivered in this study is the different temporal characteristics of the stimuli. To induce form-deprivation myopia, a diffuser lens is maintained over the eyes of animals, which presumably yields a roughly steady-state retinoscleral signal. However, the bioavailability of orally-ingested atRA will vary with time, as it is uptaken and eventually metabolized. In chickens, atRA delivery caused a day of rapid growth before a rebound the following day (McFadden et al., 2006). Both scleral biomechanics and sGAG synthesis have been demonstrated to respond rapidly to visual stimuli, on the timescale of hours to days (Moring et al., 2007; Summers, 2019). Thus, it is possible that by the time animals were sacrificed ($\sim$24 hours after their last dose of atRA), sGAG content had rebounded back to or above the control level.

However, there is also precedent in the literature showing that periods of myopigenic stimuli followed by periods of normal vision can prevent certain aspects of the myopic phenotype, from axial elongation to choroidal changes (Mertz & Wallman, 2000). The bolus delivery of atRA in this study possibly mimics this type of signaling to some degree and perhaps sGAGs are not reduced unless scleral atRA is maintained above normal levels for longer periods of time. Further studies on the short-term effects of atRA are warranted to help elucidate these potential confounders and better understand the timescales of the scleral response to atRA.

5.6.3 Altered scleral biomechanics without altered sGAGs

GAG content has been demonstrated to influence the hydraulic conductivity of biological tissues. Consistent with such data, we previously reported that both scleral hydraulic con-

ductivity and C-4-S levels changed in the mouse model of form deprivation myopia (Brown et al., in review). However, in the present study, treatment with atRA caused changes to the hydraulic conductivity without a measurable effect on sGAG content. One explanation for this apparent "decoupling" between conductivity and sGAG levels may be that another unmeasured scleral constituent that influences the hydraulic conductivity was altered, such as another GAG (e.g., heparin sulfate) or the architecture of the collagen network was changed. A second possible explanation is that the physical distribution/configuration of sGAGs changed at the cellular level without a change in overall scleral sGAG concentration, since such changes are known to affect hydraulic conductivity in other tissues (Levick, 1987; Quinn et al., 2001). In particular, if sGAG configuration were to be affected by the biomechanical environment (strain levels), this could also explain why neither hydraulic conductivity nor stiffness estimated at 0% compressive strain were significantly different between the atRA-treated and control sclera.

5.7 Conclusion

We have demonstrated that orally delivered atRA is highly myopigenic in mice, causing myopic refractive errors. In contrast to previous studies, the anterior eye was largely unaffected, whereas the posterior eye was significantly elongated, both consistent with a typical axial myopia phenotype. For the first time, the effect of atRA on scleral biomechanics was studied, where atRA treatment led to a more extensible and permeable sclera, comparable to what is seen in the sclerae of form-deprived eyes. Together, this study supports a role for atRA in visually-mediated myopigenesis; future work examining the effects of atRA, both

in animals of different ages and studying effects at different times after atRA administration, are warranted to better understand the myopic phenotype.

5.8 Acknowledgements

5.8.1 Funding

This project was supported by the National Institutes of Health [NIH R01 EY033361 (MTP,CRE) NIH R01 EY016435 (MTP), NIH P30 EY006360 (MTP), T32 EY007092 (DMB)], Department of Veterans Affairs [Rehabilitation R&D Service Research Career Scientist Award IK6 RX003134 (MTP), CDA1 IK1 RX003208 (JMP), CDA2 IK2 RX003928 (JMP)], University of Maryland Baltimore, School of Pharmacy Mass Spectrometry Center (SOP1841-IQB2014 (MAK)), and the Georgia Research Alliance (CRE).

5.8.2 Disclosures

D.M. Brown, None, **J. Yu**, None, **P. Kumar**, None, **Q.M. Paulus**, None, **M.A. Kowalski**, None, **J.M. Patel**, None, **M.A. Kane**, None, **C.R. Ethier**, None, **M.T. Pardue**, None

CHAPTER 6

CONCLUSIONS AND FUTURE DIRECTIONS

In a recent series of whitepapers, the International Myopia Institute (IMI) emphasized the need to discriminate axial myopia from refractive myopia, as most clinical cases of myopia appear to be axial in nature, with the excessive axial elongation driving an increase in the risk of other blinding conditions (Tideman et al., 2016). Axial myopia is driven by retinoscleral signaling that transforms visual cues from the retina into remodeling of the sclera, and a deeper mechanistic understanding of this signaling cascade would aid in the development of more effective interventions.

The mouse has been introduced and slowly adopted as an animal model for myopia over the last two decades, potentially facilitating the study of these mechanistic questions. However, despite having accumulated an unparalleled collection of general knowledge and genetic infrastructure/tools specific to the mouse, technical challenges associated with the small mouse eye have made even the confirmation of myopic phenotypes quite challenging, whereas in most species this is easily confirmed. The purpose of this dissertation was multifaceted: In Aim 1 we developed new methods for studying the biomechanics of the mouse sclera, applicable outside of myopia research; while in Aims 2 and 3 we applied these techniques to the study of a classical model of myopia and a potential molecule implicated in myopigenic retinoscleral signaling. Below, I summarize my conclusions, limitations, and future directions for each aim.

6.1 Aim 1: Evaluate the efficacy of poroelastic theory for characterizing scleral biomechanics.

6.1.1 Conclusions

In Chapter 3 of this dissertation, we presented the first quantification of the intrinsic material properties of the mouse sclera. Compression as a mode of testing is more suitable for small samples than tensile tests, as stretching a sample requires an interface between the tissue and device that invariably introduces stress concentrations and significant error unless a large enough sample is used (Choi & Horgan, 1977; Ng et al., 2005). We demonstrated that the sclera can be successfully analyzed as a biphasic material, allowing us to more comprehensively characterize its biomechanics than is typical; notably, a through-plane compressive modulus can be directly calculated from unconfined compression experiments, while an in-plane tensile modulus and a hydraulic conductivity can be obtained from fitting a biphasic model to the experimental data. The mechanical testing was repeatable (both when testing a sample twice and in fitting the model to the data) and fitted properties were highly comparable to values obtained through more direct measurements on large samples. The benefit of our new approach is that it can be performed on small samples of mouse sclera.

Importantly, the tensile modulus of the mouse sclera was comparable to that of the pig sclera. While not immediately obvious, this suggests that the biomechanical properties of the sclera do not scale significantly with the size of the eye. This subtle point has important implications for the use of scleral biomechanical properties as an outcome measure in the study of myopia. Unlike axial elongation, which scales with eye size and often falls below

the noise threshold in the mouse eye, scleral biomechanical changes in the mouse model of myopia should be of a similar magnitude as changes in larger eyes. In other words, while 1 D of myopia will cause different magnitudes of axial elongation in the mouse versus larger animals, it is feasible that the same 1 D myopic shift should cause comparable changes in biomechanical properties between eyes from mice and larger animals.

6.1.2 Limitations

The chosen poroelastic model included an infinitesimal strain assumption that introduces a non-negligible amount of error into the results. Additionally, the linear elastic properties that result are clearly dependent on the amount of compressive strain applied to the sample, which confirms that the sclera is not a linear elastic material. The sclera is known to have significant viscoelasticity intrinsic to the collagen itself, and this model only accounts for the viscoelasticity due to solid-fluid interaction. Together, these limitations mean that our quantification of scleral biomechanical properties are not fully separated from the testing conditions, i.e., derived material properties will be influenced by the amount of tare loading applied, the degree of loading chosen, the rate at which the loads are applied, etc. While these limitations do not influence the utility for comparative studies, they do raise concerns about using the resulting properties for general modeling purposes intended to accurately model the response of the sclera.

Additionally, there were significant experimental limitations involving the device used for the compression testing. Specifically, experimental control over the strain applied by the compression device was poor for these small/thin samples. Together, this not only introduced additional variability into the results, but also limited the amount of information

that could be obtained, e.g., measuring differential responses to varying strain rates could in principle be used to obtain viscoelastic properties of the collagen matrix (Huang et al., 2001; Huang et al., 2003), but we were unable to do so because we could not precisely control the strain rate. Finally, the experiments themselves required a well-trained individual and were technically demanding.

6.1.3 Future Work

Although multiphasic material models have been primarily developed and used in the context of biomechanical testing of articular cartilage, they have been demonstrated to be widely applicable to other biological tissues (Atkinson et al., 1997; Cowin, 1999; Ehret et al., 2017; Hatami-Marbini & Etebu, 2013; Yang & Taber, 1991). We showed that the sclera is a biphasic material under compression, displaying significant frequency-dependence to loading and showed that a commercial compression device is accurate enough to obtain biphasic material properties of the sclera. However, with more accurate or specialized compression testing devices, or by testing sclera from larger eyes, this approach could be extended to measure the viscoelasticity of the collagen matrix (Huang et al., 2001; Huang et al., 2003), which may be more directly responsible for axial elongation (Ku & Greene, 1981; Levy et al., 2018; Moring et al., 2007; Phillips et al., 2000). Additionally, extension to a triphasic model that includes ions as a third phase (Mow et al., 2002) would permit the inclusion of the effect of fixed charge density on tissue biomechanics, which could possibly allow glycosaminoglycan changes to be determined.

With or without these modeling extensions, the effects of glycosaminoglycans on scleral poroelastic material properties should be further explored. Ex vivo biomechanical studies

in which specific glycosaminoglycans were degraded or collagen was degraded/crosslinked and the biomechanics characterized using poroelastic models would lead to a clearer understanding of the structure/function relationship between scleral microstructure and biomechanics. As of now, it is assumed that tensile stiffness is largely dominated by collagen, and permeability largely dominated by glycosaminoglycans. However, as described in Chapters 1 and 4, there is a logical mechanism that may connect glycosaminoglycans to scleral in-plane tensile stiffness via influences on collagen (Figure A.3).

The current study developed an experimental method for use in comparative studies; however, finite element modeling of inflation testing could be impactful. The eye is often idealized as a thin-walled pressure vessel, in which tension is generated throughout the sclera. From this perspective, compressive properties are at least an order of magnitude less influential and thus largely secondary to tensile properties (Sinclair & Helms, 2015). Yet, the eye is not truly a thin-walled pressure vessel, and the sclera is not a passive, uniphasic material. Sensitivity studies on the effects of biphasic (or triphasic) properties on global eye deformations/shape/size under inflation would help connect the biomechanics to scleral function. Glycosaminoglycans have been shown to influence permeability of certain tissues (Gu et al., 1993; Rotter et al., 2002), and proteoglycans concentrate and fix charges within the tissue matrix. Modeling inflation of a biphasic scleral shell with a dynamic intraocular pressure and varying permeability/fixed charge density could help lead to a better understanding of how the fluid phase influences ocular globe deformations and how glycosaminoglycans may influence eye shape and size. Additionally, such work could allow detailed studies of the effects of intraocular pressure pulsations on time-dependent global eye deformations (Ku & Greene, 1981).

6.2 Aim 2: Quantify biomechanical and related biochemical changes in myopic murine sclera.

6.2.1 Conclusions

After developing the unconfined compression testing in Aim 1, we conducted a study of form-deprivation myopia in the mouse. The primary results of this study suggest that the mouse sclera is profoundly altered in response to form deprivation. Notably, we showed that mouse scleral biomechanics were altered significantly and rapidly in response to myopigenic visual cues, and confirmed that scleral biomechanical properties quantified via compression testing are useful for comparative studies. As has been shown in other species, the tensile modulus of the sclera was decreased compared to the contralateral eye that was not subjected to myopigenic visual cues. However, we also showed for the first time that the hydraulic conductivity of the myopic sclera was increased. Correspondingly, we also determined that glycosaminoglycans in the myopic sclera were likely decreased, agreeing with results from other species (Moring et al., 2007; Norton & Rada, 1995; Rada, Nickla, et al., 2000; Troilo et al., 2006). Results in other tissues predict that permeability will increase in response to a decrease in glycosaminoglycans, which demonstrates an internal consistency in our results. Finally, retinoid concentrations appear to be changing throughout the eye in response to myopigenic visual cues, which lays the groundwork for more detailed studies of specific retinoid receptors that are currently most feasible in the mouse.

6.2.2 Limitations

The obvious limitations to this work are related to sampling. Only male mice from one strain were used. Both eyes from each animal were used in their entirety for a single assay, i.e., sclera from left and right eyes were both used for unconfined compression testing, and leftover tissue was not used for any other assay, which precluded correlations between different endpoints within the same animals or eyes.

The retinoid characterization is one of the most detailed analyses to date applied to the myopic eye, measuring many different retinoids and retinoic acid isomers. While it appears that retinoids are changing, it is difficult to draw more conclusive results from this data. For one, the method necessitated combining tissue from multiple animals, reducing our statistical power. Additionally, dissections were performed submerged in PBS. Tissues were separated as quickly as possible during dissection, and medium was changed and surfaces/tools bleached between eyes/animals to prevent contamination; however, the choroid has previously been shown to be particularly ”leaky” to atRA and thus it is possible that a significant fraction of the retinoids were lost to the medium used during dissection.

6.2.3 Future Work

We have demonstrated that scleral biomechanics are altered in a time-dependent manner due to form-deprivation in the mouse. However, the methods and experimental design used here could be used to gain a deeper mechanistic understanding of the structure-function relationships of the sclera by studying additional timepoints. It has been reported that scleral biomechanics and glycosaminoglycan synthesis can be changed rapidly, on the order of

hours to days (Moring et al., 2007; Siegwart & Norton, 1999). While the results of this study are consistent with the idea that glycosaminoglycans are driving a biomechanical change in the sclera, the results of the 1-week timepoint in this chapter would be bolstered by measurements at <24 hour and 1-2 days of treatment. For example, if biomechanical changes were shown to be uncoupled from changes in glycosaminoglycans, it would imply that an additional remodeling outcome may be driving the changes, e.g., instead of glycosaminoglycans driving changes in collagen crimp, perhaps the opposite is occurring.

Additionally, the results of the retinoid quantification show an intriguing trend that could form the basis for many future studies - in the retina, atRA is increased at 1 week, but returns to baseline at 3 weeks. Adding earlier timepoints and potentially a 2-week timepoint, and/or starting the form-deprivation treatment at a different baseline age (e.g., 3 weeks or 5 weeks) could help discern the origins of this effect. Additionally, repeating the current study with different powered lenses could show whether atRA levels return to baseline after myopigenesis is complete, i.e., after the mouse has fully emmetropized to the lens.

A working hypothesis of this thesis is that the number of distinct signaling pathways involved in retinoscleral signaling are reduced as signaling propagates from the retina to the sclera, i.e., pathways merge. Whereas different visual cues (lens defocus, chromatic aberrations, form deprivation) have been noted to cause different retinal signaling (Bartmann et al., 1994; Kee et al., 2001; Schaeffel et al., 1994), no stark differences have been observed in the sclera (Guo et al., 2013). The biphasic characterization introduced here is more informative than other tests, and thus, it would be of interest to study the scleral outcomes of these different visual cues. If the scleral biomechanics change similarly with disparate visual cues, this would support the idea that the various retinal signaling converges

into a limited, perhaps singular, signaling molecule/pathway in order to influence scleral remodeling, which would thus make it a clinically relevant point to target pharmacological interventions.

6.3 Aim 3: Determine the effect of retinoic acid on refractive development and scleral biomechanics.

6.3.1 Conclusions

Our study of the effects of exogenous atRA on refractive development included the most complete ocular characterization among studies that have treated animals with atRA, and our results overwhelmingly show that mice develop axial myopia after atRA administration. Notably, treatment with atRA caused an increase in axial elongation, and resulted in eyes with longer vitreous chambers and altered scleral biomechanics with very minimally altered anterior segments. The manner by which the sclera was altered was very similar to that seen in form deprivation, namely decreased in-plane tensile stiffness and increased permeability.

6.3.2 Limitations

atRA influences the transcription of c. 100 genes, and thus, systemic atRA treatment is most likely not only affecting the eyes/sclerae of the animals. In addition to the primary outcomes of Chapter 5, we measured body mass, scleral DNA content, and retinal thickness/general retinal health via spectral domain optical coherence tomography (OCT); while none were obviously affected by the atRA treatment, in the case that they had been, the interpretation of our results would change. Thus, it is conceivable, albeit unlikely, that atRA was influ-

encing some unknown latent variables that caused the myopic phenotype. Smaller doses of atRA, or more targeted treatments directly to the eye (e.g., lipid nanoparticles, transgenic approaches), would help to strengthen our results and implicate ocular atRA as the source of the measured effects.

Interestingly, while biomechanics of the form-deprived sclera were similar to that seen after treatment with exogenous atRA, scleral glycosaminoglycans were not found to be altered with atRA treatment. We speculate that the timing and type of treatment, along with the timing of sacrifice, may have led to a rebound in glycosaminoglycan levels. Previous studies have shown the effects of orally delivered atRA to last on the order of $\sim$1 day, while glycosaminoglycans and scleral biomechanics have been shown to change on a similar timescale. While measurements were typically done $<$24 hours after the last atRA dose, it is possible that glycosaminoglycans had already rebounded to normal or above normal values at the time of measurement.

6.3.3 Future Work

There are many studies motivated by our results. Studies should be performed to obtain a dose-response curve of atRA on ocular development and scleral remodeling. Previous studies have shown effects at concentrations as low as 0.5-2 mg/kg (compared to the 25 mg/kg used here) (McFadden et al., 2006). Lowering the dose, in conjunction with collecting serum and additional tissues (liver, brain) could be useful in understanding how specifically atRA concentrates in the eye relative to other tissues and lower the chances of an off-target effect confounding the results.

Additionally, there remain discrepancies between existing studies related to atRA and

axial elongation. In our work, axial myopia clearly and conclusively developed due to exogenous atRA, whereas this was not necessarily the case in other studies. A difference between our study and others is the age at which atRA treatment was started (4 weeks here, 1 week in both chicken and guinea pig). Beginning atRA treatment earlier in the mouse or later in other species would help determine whether the discrepancy is a species-dependent effect or whether it perhaps relates to an age-dependent effect of atRA on ocular development.

Along with an earlier timepoint for starting the treatment, earlier ex vivo timepoints should be considered. For example, repeating our experiments only a few hours or 1 day after atRA feeding could help discern the timescale of the effects of atRA on the sclera. Further, in vivo fluorescent imaging (e.g. confocal scanning laser ophthalmology) and a fluorescent retinoid could be used to monitor how long it takes atRA to reach the eye, where the atRA comes from (presumably the choroid), and whether atRA travels from the choroid into the retina/sclera.

Finally, emmetropization has been demonstrated to be possible without a connection between the eye and the brain; however, there is still dispute over how much of an effect the brain can have on the eye's development and scleral remodeling. An informative study motivated by our results would be to deliver atRA after transecting the optic nerve, which would identify whether the effect of atRA on the eye originate in the brain.

6.4 Final Thoughts

This dissertation has demonstrated that the mouse can be a useful model for ocular biomechanics and the study of myopia, despite its small eye size. We introduced a methodology that, while more complex than the average tensile test, yields information-dense results that can be applied successfully to compare phenotypes using a commercially available biomechanical testing device. Using this detailed biomechanical characterization in parallel with other ocular measurements, we have provided evidence that the mouse develops axial myopia in response to visual cues, despite not measuring axial elongation. The structure and function of the mouse sclera changes significantly with form-deprivation in a manner that is consistent with other species, with specific glycosaminoglycans decreasing and the sclera becoming more extensible. Additionally, while the implications are not understood, the increased permeability of the myopic sclera is consistent with results in cartilage showing glycosaminoglycans and permeability are correlated. Finally, while minor differences were observed between the observed phenotypes, myopia due to exogenous atRA caused scleral biomechanical changes that were strikingly similar to those due to form-deprivation. Considering that decades of research have yielded minimal candidate molecules that may be capable of retinoscleral signaling, the causal impacts of exogenous atRA and the similarity in the biomechanical phenotypes together warrant increased attention on retinoid signaling in the mammalian eye.

CHAPTER 7

GRANTS, PUBLICATIONS, AND CONFERENCE PRESENTATIONS ARISING FROM THE PHD

7.1 Funded Grants Related to Thesis Work:

1. 1R01EY033361-01: *"Mechanisms of axial elongation in myopia" (2022)*
   PIs: Machelle T. Pardue, C. Ross Ethier, Maureen A. Kane

7.2 Refereed Journal Publications Related to Thesis Work:

1. **Brown, D. M.**, Mazade, R., Clarkson-Townsend, D., Hogan, K., Datta Roy, P. M., Pardue, M. T. Candidate pathways for retina to scleral signaling in refractive eye growth. Experimental Eye Research 219, 109071 (2022).

2. **Brown, D. M.**, Pardue, M. T., Ethier, C. R. A biphasic approach for characterizing tensile, compressive and hydraulic properties of the sclera. Journal of The Royal Society Interface 18, (2021).

3. **Brown, D. M.**, Kowalski, M. A., Paulus, Q. M., Yu, J., Kumar, P., Kane, M. A., Patel, J. M., Ethier, C. R., Pardue, M. T., Altered structure and function of murine sclera in form-deprivation myopia. IOVS, (Accepted for publication)

4. **Brown, D. M.**, Yu, J., Kumar, P., Paulus, Q. M., Kowalski, M. A., Patel, J. M., Kane, M. A., Ethier, C. R., Pardue, M. T.Exogenous all-trans retinoic acid induces myopia and alters scleral biomechanics in mice. IOVS, (In Review)

7.3 Refereed Journal Publications Not Directly Related to Thesis Work:

1. Goyal, V., Read, A. T., Ritch, M. D., Hannon, B. G., G. Sanchez-Rodriguez, **Brown, D. M.**, Feola, A. J., A. Hedberg-Buenz, Cull, G. A., Reynaud, J., Garvin, M. K., Anderson, M. G., Burgoyne, C. F., Ethier, C. R. Axonet 2.0: A deep learning-based tool for Morphometric Analysis of Retinal Ganglion Cell Axons. TVST. (In Review)

2. Goyal, V., Read, A. T., **Brown, D. M.**, Brawer, L., Bateh, K., Hannon, B. G., Feola, A. J., Ethier, C. R. Morphometric Analysis of Retinal Ganglion Cell Axons in Glaucomatous Brown Norway Rats. TVST. (Accepted for publication)

3. Gerberich, B. G., Hannon, B. G., **Brown, D. M.**, Read, A. T., Ritch, M. D., Echeverri, E. S., Nichols, L., Potnis, C., Sridhar, S., Toothman, M. G., Schwaner, S. A., Winger,

E. J., Huang, H., Gershon, G. S., Feola, A. J., Pardue, M. T., Prausnitz, M. R., Ethier, C. R. Evaluation of Spatially Targeted Scleral Stiffening on Neuroprotection in a Rat Model of Glaucoma. Translational Vision Science & Technology 11, 7 (2022).

4. Liu, A. S., **Brown, D. M.**, Conn, R. E., McNabb, R. P., Pardue, M. T., Kuo, M. N. Topography and pachymetry maps for mouse corneas using optical coherence tomography. Experimental Eye Research 190, 107868 (2020).

5. Landis, E. G., Yang, V., **Brown, D. M.**, Pardue, M. T., Read, S. A. Dim Light Exposure and Myopia in Children. Invest. Ophthalmol. Vis. Sci. 59, 4804 (2018).

7.4 Conference Presentations

7.4.1 Podium Presentations

1. **Brown, D. M.**, Kowalski, M. A., Paulus, Q. M., Yu, J., Kumar, P., Kane, M. A., Patel, J. M., Ethier, C. R., Pardue, M. T., Form deprivation (FD) and exogenous all-trans retinoic acid (atRA) result in similar myopigenesis and scleral phenotypes in mice. Talk presented May, 2022 at ARVO in Denver, CO. *Awarded Knights Templar Eye Foundation Travel Grant.*

2. **Brown, D. M.**, Yu, J., Kumar, P., Kane, M. A., Ethier, C. R., Pardue, M. T., Increasing Ocular All-trans Retinoic Acid Alters Scleral Biomechanics and Induces Myopia in Mice. Talk presented July, 2021 at FASEB Retinoids (Virtual). *Awarded Best Trainee Talk.*

3. **Brown, D.M.**, Ethier, C.R., Pardue, M.T. Oral All-trans Retinoic Acid Treatment Alters Scleral Biomechanics and Induces Myopia in Mice. Talk presented June, 2021 at SB3C (Virtual)

4. **Brown, D.M.**, Ethier, C.R., Pardue, M.T. Oral All-trans Retinoic Acid Treatment Induces Myopia and Alters Scleral Biomechanics in Mice. Talk presented May, 2021 at ARVO (Virtual). *Awarded Josh Wallman Travel Grant.*

5. **Brown, D.M.**, Ethier, C.R., Pardue, M.T. Form Deprivation Myopia in the Mouse involves Altered Scleral Biomechanics. Talk presented November, 2020 at Southeastern Vision Research Conference (Virtual)

6. **Brown, D.M.**, Ethier, C.R., Pardue, M.T. Altered Tensile Stiffness And Permeability Of Myopic Mouse Sclera As Determined By Compression Testing. Lightning Talk presented June, 2020 at SB3C (Virtual)

7. **Brown, D.M.**, Ethier, C.R., Pardue, M.T. Altered Scleral Biomechanics Accompany Early Myopia Development in Mice. Talk presented May, 2020 at ARVO (Virtual).

8. **Brown, D.M.**, Strickland, R.G., Landis, E.G., Ethier, C.R., Pardue, M.T. Decreased Stiffness and Increased Permeability in Sclera of Myopic Mice. Talk presented September, 2019 at International Myopia Conference in Tokyo, Japan

7.4.2 Poster Presentations

1. **Brown, D.M.**, Strickland, R.G., Landis, E.G., Pardue, M.T., Ethier, C.R. Altered Scleral Biomechanics in the Mouse Model of Myopia. Poster presented May, 2019 at ARVO in Vancouver, Canada

2. **Brown, D.M.**, Landis, E.G., Pardue, M.T., Ethier, C.R. Using Biphasic Theory to Analyze Unconfined Compression of Murine Sclera and Cornea. Poster presented October, 2018 at BMES in Atlanta, GA

3. **Brown, D.M.**, Landis, E.G., Pardue, M.T., Ethier, C.R. Biomechanical Properties of Murine Sclera and Cornea Tested By Unconfined Compression and Interpreted Using Biphasic Theory. Poster presented July, 2018 at World Congress of Biomechanics in Dublin, Ireland.

Appendices

Table 1: Aggrecan antibodies tested.

Antigen	Supplier	Cat. Num	RRID	Host Species	Clonality	Clone ID	Isotype
Aggrecan	GeneTex	GTX03179		Rabbit	Monoclonal	GT1267	IgG
Aggrecan	Boster Bio	M04655-1		Rabbit	Monoclonal	17A33	IgG
Aggrecan	St John's Laboratory	STJ11101391		Rabbit	Monoclonal	ARC0678	IgG
Aggrecan	Santa Cruz	sc-33695		Mouse	Monoclonal	4F4	IgG
Aggrecan	Santa Cruz	sc-166951		Mouse	Monoclonal	D-4	IgM κ
Aggrecan	Boster Bio	A04655-1		Rabbit	Polyclonal		IgG
Aggrecan	Abcam	ab216965		Rabbit	Polyclonal		IgG
Aggrecan	EMD Millipore	ABT1373		Rabbit	Polyclonal		IgG
NITIGE	Thermo Fisher Scientific	PA1-1746	AB_2242021	Rabbit	Polyclonal		IgG

APPENDIX A

SUPPLEMENTARY INFORMATION FOR CHAPTER 4

Table A.1: Summary of statistical models used to analyze outcome measures. Covariates identify continuous predictors set to 0 during analysis. Covariate days_deviation is the difference from timepoint in the in vivo measurements (4 weeks, 5 weeks, 7 weeks) or the mean age at the time of sacrifice. "*": full interaction operator indicating inclusion of all main effects and interactions, "1|animal_id": random intercept for each animal. UCT: unconfined compression test, DMMB: dimethylmethylene blue assay, PG: picogreen assay, IHC: immunohistochemistry, LC-MS/MS: Liquid chromatography tandem mass spectrometry, DVs: Dependent variables, RE: Refractive error, AL: Axial length, H_{+A}: Aggregate tensile modulus (tensile stiffness), k: permeability, GAG: glycosaminoglycan, atRA: all-trans retinoic acid, tRE: total retinyl esters, ROL: Retinol.

Outcomes	DVs	Fixed Effects	Covariates	Random Effects	Family	Link
In Vivo	RE, AL	~ age*animal_treatment*eye	days_deviation	1|animal_id	Gaussian	Identity
UCT	H_{+A}, k	~ animal_treatment*eye*strain	days_deviation	1|animal_id	Gamma	Log
DMMB/PG	GAG/mass, GAG/DNA	~ eye		1|animal_id	Gamma	Log
IHC	NormIntensity	~ animal_treatment*eye		1|animal_id	Gamma	Log
LC-MS/MS	atRA, tRE, ROL	~ age*eye_treatment*tissue			Gaussian	Identity

Table A.2: Effect of form deprivation on ocular biometry. Tabulated data are the mean ± standard deviation of interocular differences for each outcome. Bolded values are significantly different from 0 ($p<0.05$). RE: Refractive error, CC: Corneal curvature, CT: corneal thickness, ACD: Anterior chamber depth, LT: Lens thickness, VCD: Vitreous chamber depth, AL: Axial length

Group	RE [D]	CC [μm]	CT [μm]	ACD [μm]	LT [μm]	VCD [μm]	RT [μm]	AL [μm]
Baseline (53)	-0.13±0.67	-2.52±12.90	-1.31±6.86	-1.65±10.04	-3.50±13.90	2.83±16.12	0.06±10.73	-3.10±27.01
Naive (16)	0.02±0.37	-2.07±5.81	-1.56±2.58	1.61±6.97	-3.19±14.58	3.58±13.22	3.76±5.59	5.27±24.41
1 Week FD (17)	**-2.35±1.11**	-4.52±7.80	-1.28±4.48	-0.20±11.19	-4.40±12.40	3.48±16.62	-1.29±8.57	-0.89±27.29
3 Weeks FD (27)	**-4.07±0.72**	1.53±16.43	0.00±6.31	3.39±9.65	2.61±17.17	4.74±16.52	-2.96±10.15	9.87±25.05

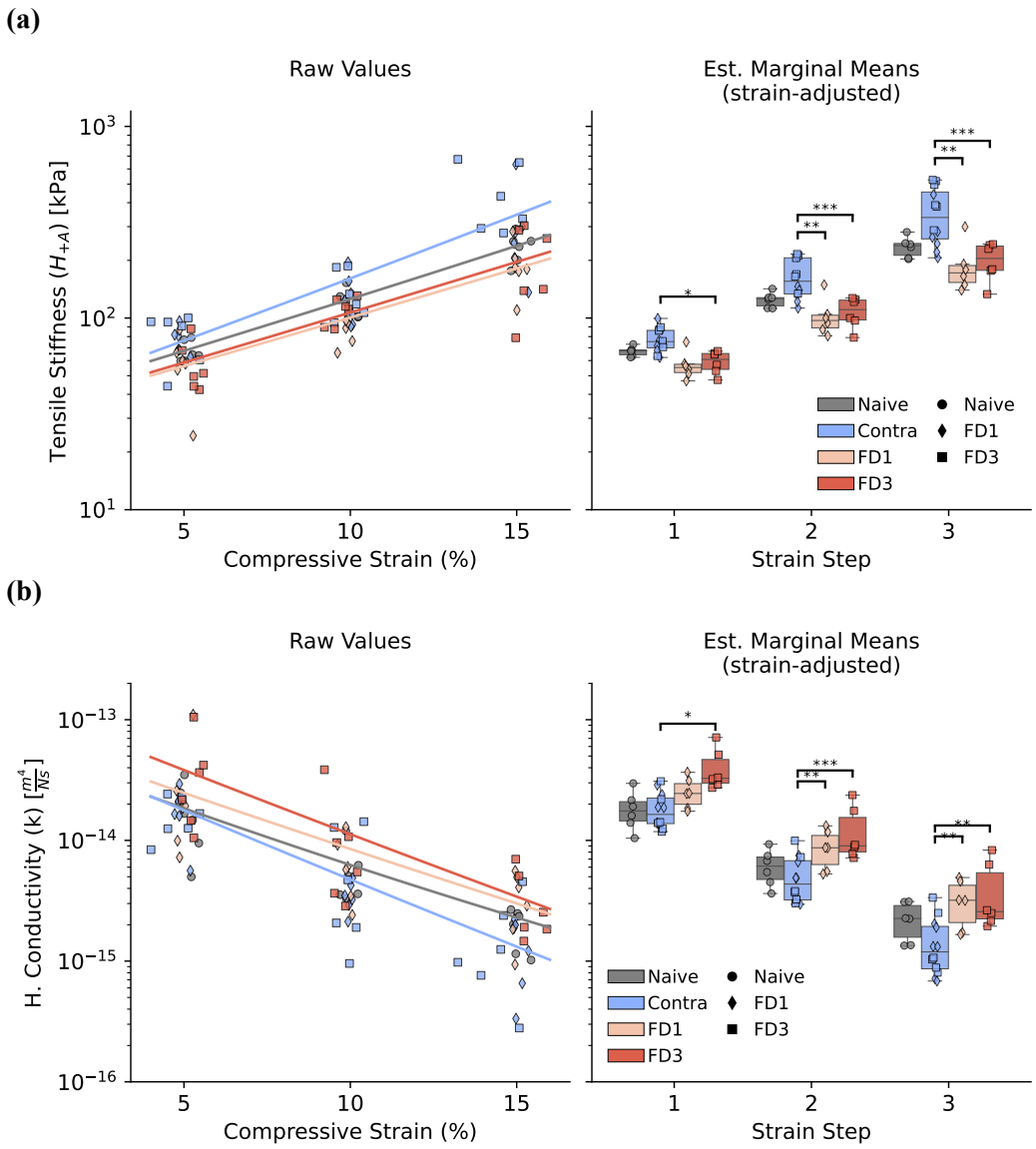

Figure A.1: The biomechanical material properties of the sclera were altered as a result of form deprivation. Specifically, aggregate tensile modulus (i.e., stiffness) (top) and hydraulic conductivity (i.e., permeability) (bottom) were both altered relative to the contralateral control eyes. Plots show the raw values obtained from fitting the poroelastic material model and the regressions obtained from the statistical model (left) and the estimated marginal means obtained from the statistical model (right), both plotted as a function of the compressive strain magnitude (strain steps). The box contains the second and third quartiles of data, with the line indicating the median. The whiskers show the first and fourth quartiles. FD1: 1 Week form deprivation, FD3: 3 weeks form deprivation. *: $p<0.05$, **: $p<0.01$, ***: $p<0.001$.

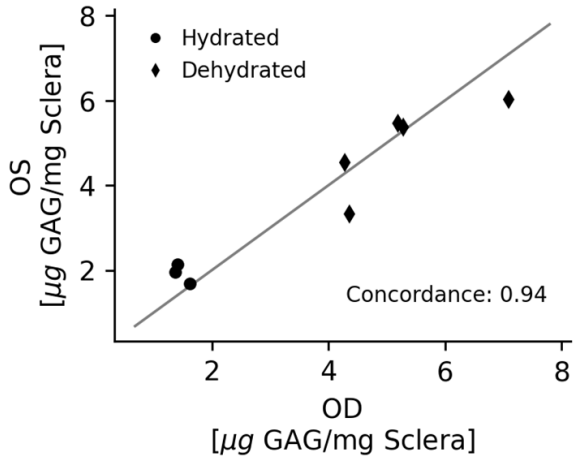

Figure A.2: Preliminary experiments demonstrate high concordance in GAG measurements made within control animals using the DMMB assay protocol. Each data point represents measurements of the scleral GAGs in the left (OS) and right (OD) eyes of an individual animal. Some samples were blotted (diamonds, hydrated) and others were dehydrated (circles, dehydrated). The DMMB assay measured differences in the two treatments and had high concordance across the entire range of concentrations (concordance = 0.94). The solid line represents the identity line (OD = OS). Perfect concordance (Concordance=1) would occur if every point fell on the identity line. DMMB: dimethylmethylene blue, GAG: glycosaminoglycans.

Table A.3: Material properties obtained from 3 step unconfined compression testing of the mouse sclera. Tabulated values are the mean ± standard deviation of unadjusted, fitted material properties at each step, and averaged over the three-step protocol (5%, 10%, 15% compressive strain). H_{+A}: Aggregate tensile modulus, k: permeability, FD1: 1 week FD, FD3: 3 weeks FD, Contra: Contralateral eye.

	H_{+A} [kPa]				k $[m^4/Pa \cdot s]$ (x10^{14})			
Group (# eyes)	**Step 1**	**Step 2**	**Step 3**	**Average**	**Step 1**	**Step 2**	**Step 3**	**Average**
Naive (6)	67.31±8.60	118.61±20.42	234.65±41.00	140.19±76.34	1.76±1.08	0.56±0.33	0.19±0.07	0.84±0.92
Contra (12)	78.75±17.82	132.21±38.85	371.23±182.99	194.06±166.53	1.72±0.68	0.48±0.43	0.15±0.12	0.78±0.82
FD1 (6)	58.10±20.21	92.72±23.70	189.32±55.90	113.38±66.85	3.18±3.89	0.66±0.39	0.34±0.18	1.39±2.49
FD3 (6)	57.18±17.55	109.83±17.86	201.74±93.63	122.92±80.88	3.84±3.49	1.18±1.35	0.33±0.22	1.78±2.55

Table A.4: Effect of form deprivation on total scleral sulfated GAG content as measured by the DMMB assay. Total sulfated GAG content was not significantly altered after 3 weeks of form deprivation when compared to contralateral control eyes ($p>0.05$ for all). GAG: glycosaminoglycans, DMMB: dimethylmethylene blue assay.

Group	**Scleral mass (dry)** [μg]	**Total GAG** [μg]	**GAG Conc.** [μg/mg]	**GAG/DNA** [μg/μg]
Contralateral (n=9)	161.78 ± 16.85	1.04 ± 0.10	6.54 ± 1.21	8.50 ± 0.94
Form-deprived (n=9)	167.78 ± 16.01	1.16 ± 0.17	7.01 ± 1.40	9.30 ± 1.72
Interocular Difference (n=9)	6.00 ± 26.05	0.12 ± 0.21	0.48 ± 2.33	0.80 ± 1.95

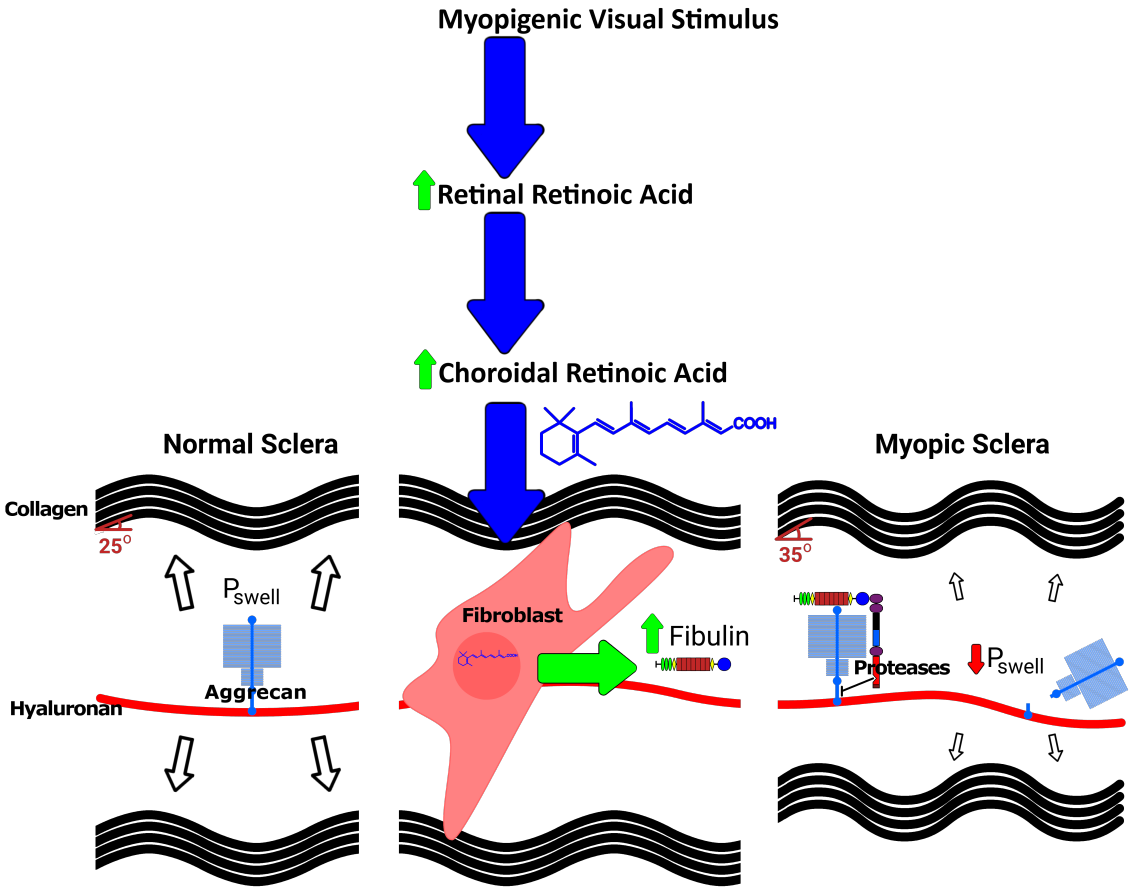

Figure A.3: Hypothesized mechanism connecting scleral remodeling to altered biomechanics

Table A.5: Effect of form-deprivation on scleral sGAGs as measured by immunostaining of chondroitinase-treated samples. Chondroitin-4-sulfate content was significantly decreased in form-deprived eyes, independent of the duration of form-deprivation treatment. Dermatan sulfate content was only significantly decreased after 3 weeks of form-deprivation. Tabulated quantities are mean ± standard deviation. Groups are presented as Treatment-Duration (# eyes). Durations (1 and 3) are weeks of form-deprivation treatment. Bolded values are significantly different from the contralateral groups ($p<0.05$). Contra: contralateral eye, FD: form-deprivation, sGAG: sulfated Glycosamino-glycans, AU: Arbitrary units (ratio of pixel intensities).

Group	**Chondroitin-4-Sulfate** [AU]	**Dermatan Sulfate** [AU]
Contra-1 (4)	1.50±0.20	3.09±0.53
FD-1 (5)	**1.34±0.25**	3.09±0.89
Contra-3 (6)	1.68±0.25	3.11±0.85
FD-3 (6)	**1.39±0.27**	**2.31±0.56**

APPENDIX B

SUPPLEMENTARY INFORMATION FOR CHAPTER 5

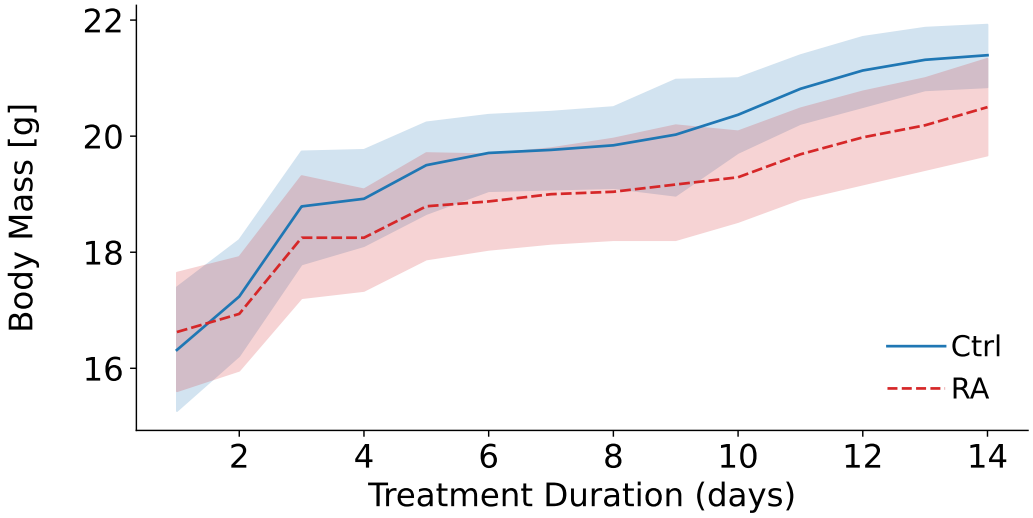

Figure B.1: Body mass was not significantly affected by two-weeks of atRA treatment. Lines are the mean body masses of the control (solid, blue) and atRA-treated (dashed, red) animals. Shaded regions show the 95% confidence intervals. Ctrl: Vehicle-treated group (n=14 animals); RA: atRA-treated group (n=16 animals).

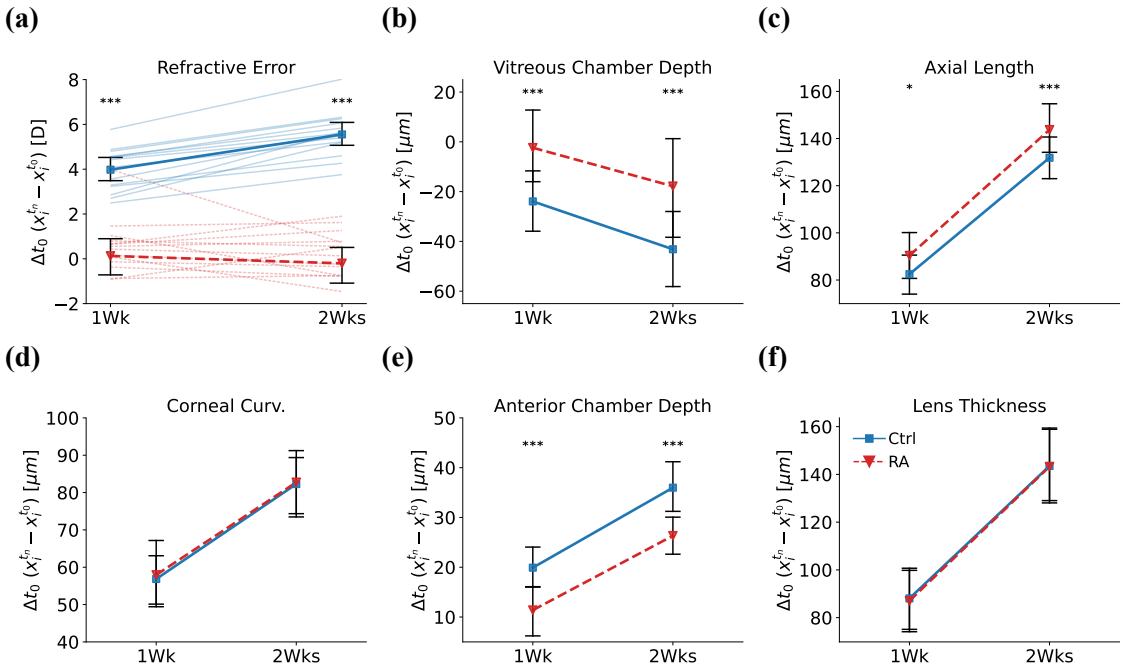

Figure B.2: Treatment with atRA significantly alters the development of refractive state and ocular biometry. Plots show the changes from baseline (t_0) of each outcome ($\Delta^t x_i$; $x_i^{t_n} - x_i^{t_0}$), where $x_i^{t_n}$ represents the measured quantity in animal i at timepoint t_n. A) Development of refractive error was significantly influenced by atRA, with 1 and 2 weeks of daily atRA causing significant myopia to develop relative to the control animals. B) VCD and C) axial length increased more over the treatment period in the atRA-treated animals vs. controls. D-F) Biometry of the anterior eye was largely unaffected, except for a small shrinkage of the anterior chamber. Individual animals are shown with fainter lines in A). Solid (blue) lines are the mean of the control group, dashed (red) lines are the mean of the atRA-treated group. Error bars show the 95% confidence intervals. Ctrl: Vehicle-treated group (n=14 animals); RA: atRA-treated group (n=16 animals). *: $p<0.05$, **: $p<0.01$, ***: $p<0.001$, adjusting for deviations in age and multiple comparisons

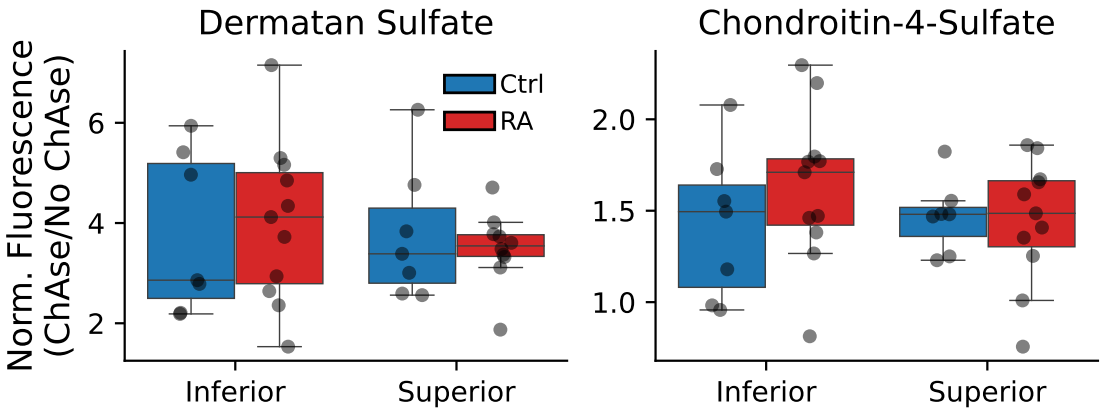

Figure B.3: Immunolabeling of glycosaminoglycans was not measurably changed by atRA treatment or different between the superior and inferior sclera.

Table B.1: Summary of statistical models used to analyze study outcomes. Covariate "days deviation" adjusts for deviations in age at the time of a measurement. "*": full interaction operator (indicating both main effects and their interaction), "1|animal id": random intercept for each animal. unconfined compression testing (UCT): unconfined compression test; 1,9-dimethylmethylene blue (DMMB): dimethylmethylene blue assay; PG: picogreen assay; immunohistochemistry (IHC): immunohistochemistry; liquid chromatography-tandem mass spectrometry (LC-MS/MS): Liquid chromatography tandem mass spectrometry; DVs: Dependent variables; refractive error (RE): Refractive error; axial length (AL): Axial length; H_{+A}: Aggregate tensile modulus (tensile stiffness); k: hydraulic conductivity (permeability); GAG: glycosaminoglycan; all-trans retinoic acid (atRA): all-trans retinoic acid; tRE: total retinyl esters; ROL: Retinol.

Outcomes	DVs	Fixed Effects	Covariates	Random Effects	Family	Link
In Vivo	RE, AL, etc.	$\sim$ timepoint*treatment	days_deviation	1|animal_id	Gaussian	Identity
	body_mass	$\sim$ treatment*log(days)			Gamma	Log
LCMSMS	atRA, tRE, ROL	$\sim$ treatment*tissue			Gaussian	Identity
UCT	H_{+A}, k	$\sim$ treatment*strain		1|animal_id	Gamma	Log
DMMB/PG	GAG/mass, GAG/DNA	$\sim$ treatment		1|animal_id	Gamma	Log
IHC	NormIntensity	$\sim$ treatment		1|animal_id	Gamma	Log

Table B.2: Raw ocular biometry at each timepoint of the study. Groups are presented as "Group (# animals)". Tabulated data are the mean $\pm$ standard deviation of the outcome. Bolded values are significantly different from the controls at the same timepoint ($p<0.05$), using the regression models and adjusting for deviations in age. RE: Refractive error; corneal curvature (CC): Corneal curvature; central corneal thickness (CCT): central corneal thickness; anterior chamber depth (ACD): Anterior chamber depth; lens thickness (LT): Lens thickness; vitreous chamber depth (VCD): Vitreous chamber depth; AL: Axial length; Ctrl: Vehicle-treated group; RA: atRA-treated group.

Timepoint	Group (n)	RE [D]	CC [mm]	CCT [µm]	ACD [µm]	LT [mm]	VCD [µm]	RT [µm]	AL [mm]
Baseline	Ctrl (14)	0.90±0.87	1.41±0.01	92.80±3.06	335.99±13.91	1.78±0.01	669.57±21.59	181.71±9.28	3.09±0.03
	RA (16)	1.02±1.05	1.40±0.02	**95.36±3.51**	338.49±11.74	1.78±0.02	670.15±24.40	184.25±7.06	3.10±0.03
1 Week	Ctrl (14)	4.88±0.65	1.46±0.02	95.60±2.21	354.99±10.85	1.87±0.02	645.46±6.02	176.98±7.08	3.17±0.02
	RA (16)	**1.17±2.20**	1.46±0.02	96.39±3.28	347.96±12.78	1.87±0.02	**666.18±15.14**	176.16±5.33	3.19±0.04
2 Weeks	Ctrl (14)	6.45±0.43	1.49±0.02	94.61±2.53	370.67±11.76	1.92±0.02	625.71±15.16	175.54±4.80	3.22±0.02
	RA (16)	**0.74±2.20**	1.48±0.01	94.49±3.72	363.01±12.04	1.92±0.03	**657.99±24.83**	173.01±10.26	3.24±0.03

Table B.3: Shift in ocular biometry over the atRA treatment period. Groups are presented as "Group (# animals)". Tabulated data are the mean ± standard deviation of the shift in outcomes ("Shift"; $x_i^{t_n} - x_{Ctrl}^{t_n}$), where $x_i^{t_n}$ represents animal i at timepoint t_n. Bolded values are significantly different from the controls at the same timepoint ($p<0.05$), using the regression models and adjusting for deviations in age. RE: Refractive error; CC: Corneal curvature; CCT: central corneal thickness; ACD: Anterior chamber depth; LT: Lens thickness; VCD: Vitreous chamber depth; AL: Axial length; Ctrl: Vehicle-treated group; RA: atRA-treated group

Timepoint	Group (n)	RE [D]	CC [μm]	CCT [μm]	ACD [μm]	LT [μm]	VCD [μm]	RT [μm]	AL [μm]
Baseline	RA-Ctrl	0.12±1.05	-6.12±19.87	**2.56±3.51**	2.50±11.74	2.20±20.46	0.58±24.40	2.53±7.06	11.52±34.43
1 Week	RA-Ctrl	**-3.71±2.20**	-3.98±21.36	0.79±3.28	-7.04±12.78	-0.92±22.93	**20.72±15.14**	-0.82±5.33	13.69±42.49
2 Weeks	RA-Ctrl	**-5.71±2.20**	-3.68±14.98	-0.11±3.72	-7.67±12.04	-3.23±27.18	**32.28±24.83**	-2.53±10.26	19.09±34.53

Table B.4: Change from baseline of ocular biometry over the atRA treatment period. Groups are presented as "Group (# animals)". Tabulated data are the mean ± standard deviation of the change from baseline (t_0) of each animal ($\Delta^t x_i$; $x_i^{t_n} - x_i^{t_0}$), where $x_i^{t_n}$ represents the measured quantity in animal i at timepoint t_n. Bolded values are significantly different from the controls at the same timepoint ($p<0.05$), using the regression models and adjusting for deviations in age. RE: Refractive error; CC: Corneal curvature; CCT: central corneal thickness; ACD: Anterior chamber depth; LT: Lens thickness; VCD: Vitreous chamber depth; AL: Axial length; Ctrl: Vehicle-treated group; RA: atRA-treated group.

Timepoint	Group (n)	RE [D]	CC [μm]	CCT [μm]	ACD [μm]	LT [μm]	VCD [μm]	RT [μm]	AL [μm]
1 week	Ctrl (14)	3.98±0.97	56.85±12.28	3.01±3.58	19.86±7.45	89.05±25.12	-25.16±24.19	-4.84±8.60	82.58±14.72
	RA (16)	**0.14±1.57**	59.06±16.73	0.61±3.25	**11.13±8.78**	86.74±24.14	**-2.16±25.80**	-6.85±6.75	**90.86±17.45**
2 week	Ctrl (14)	5.55±1.02	82.28±15.13	2.21±3.51	35.68±9.13	144.91±30.33	-45.08±32.07	-6.37±8.50	132.05±15.14
	RA (16)	**-0.27±1.64**	82.71±17.18	0.02±4.11	**26.69±7.12**	143.36±28.67	**-18.17±37.29**	-7.59±7.53	**145.01±16.64**

Table B.5: Material properties of the sclera obtained from unconfined compression. Groups are presented as "Group (# animals)". Tabulated values are the mean ± standard deviation of unadjusted, fitted material properties at each step (5%, 10%, 15% compressive strain) and the average over the steps. Bolded values are significantly different from the controls ($p<0.05$), using the regression models and adjusting for deviations in applied compressive strain. H+A: Aggregate in-plane tensile modulus (stiffness); k: Hydraulic conductivity (permeability); RA: atRA-treated animals; Ctrl: vehicle-treated animals.

	$\boldsymbol{H_{+A}}$ [kPa]				$\boldsymbol{k}$ $[m^4/Pa \cdot s]$ (x10^{14})			
Group (# eyes)	**Step 1**	**Step 2**	**Step 3**	**Average**	**Step 1**	**Step 2**	**Step 3**	**Average**
Ctrl (8)	79.42±13.70	131.81±33.02	269.12±83.27	160.12±95.79	1.60±0.88	0.45±0.28	0.15±0.06	0.73±0.82
RA (10)	64.34±14.32	**94.94±21.12**	**152.29±46.99**	**103.86±47.56**	1.89±1.04	**0.68±0.25**	**0.33±0.20**	**0.96±0.91**

APPENDIX C

ASSAYS

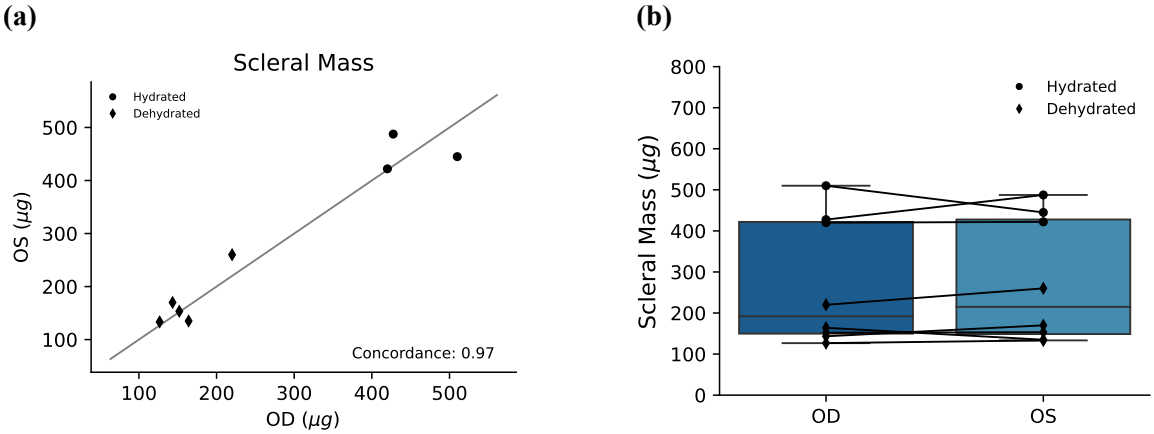

Figure C.1: Interocular concordance of collected scleral tissue.

C.1 DMMB Assay

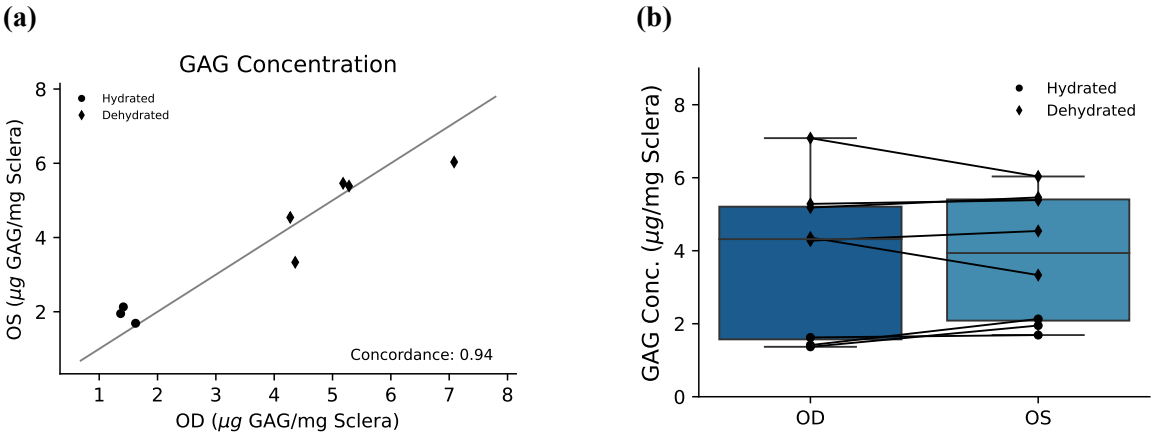

Figure C.2: Interocular concordance of DMMB assay.

C.2 Picogreen Assay

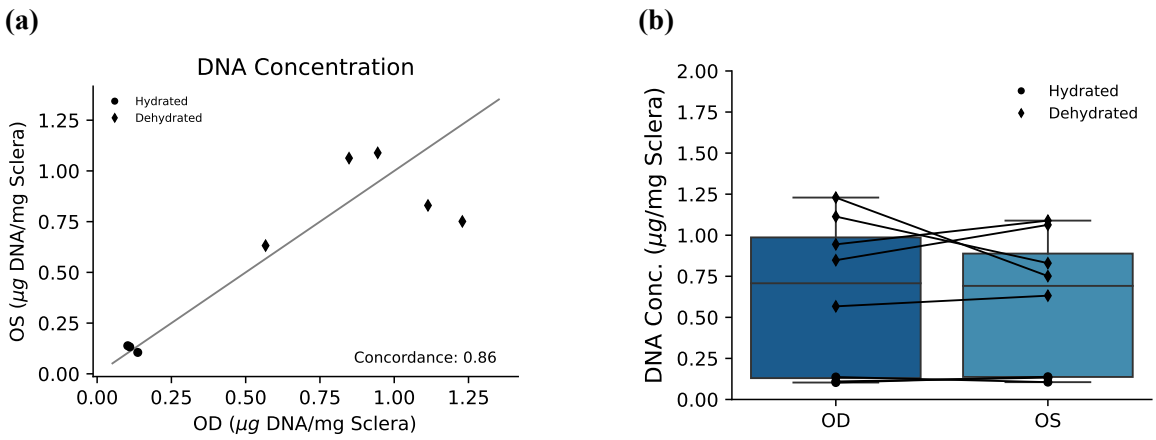

Figure C.3: Interocular concordance of Picogreen assay.

BIBLIOGRAPHY

Aleman, A. C., Wang, M., & Schaeffel, F. (2018). Reading and myopia: Contrast polarity matters. *Scientific Reports*, *8*(1), 10840.

André, E., Conquet, F., Steinmayr, M., Stratton, S. C., Porciatti, V., & Becker-André, M. (1998). Disruption of retinoid-related orphan receptor β changes circadian behavior, causes retinal degeneration and leads to vacillans phenotype in mice. *The EMBO Journal*, *17*(14), 3867–3877.

Andrews, S. H. J., Rattner, J. B., Shrive, N. G., & Ronsky, J. L. (2015). Swelling significantly affects the material properties of the menisci in compression. *Journal of Biomechanics*, *48*(8), 1485–1489.

Antonioli, L., Pacher, P., Vizi, E. S., & Haskó, G. (2013). CD39 and CD73 in immunity and inflammation. *Trends in Molecular Medicine*, *19*(6), 355–367.

Armstrong, C. G., Lai, W. M., & Mow, V. C. (1984). An analysis of the unconfined compression of articular cartilage. *Journal of Biomechanical Engineering*, *106*(2), 165.

Arruda, J. R. F. (1992). Objective functions for the nonlinear curve fit of frequency response functions. *AIAA Journal*, *30*(3), 855–857.

Arslan, G., Kull, B., & Fredholm, B. B. (2002). Anoxia redistributes adenosine a(2a) receptors in PC12 cells and increases receptor-mediated formation of cAMP. *Naunyn-Schmiedeberg's Archives of Pharmacology*, *365*(2), 150–157.

Ashby, R., McCarthy, C. S., Maleszka, R., Megaw, P., & Morgan, I. G. (2007). A muscarinic cholinergic antagonist and a dopamine agonist rapidly increase ZENK mRNA expression in the form-deprived chicken retina [Number: 1]. *Experimental Eye Research*, *85*(1), 15–22.

Ashby, R., Ohlendorf, A., & Schaeffel, F. (2009). The effect of ambient illuminance on the development of deprivation myopia in chicks. *Investigative Opthalmology & Visual Science*, *50*(11), 5348.

Ashby, R. S., & Schaeffel, F. (2010). The effect of bright light on lens compensation in chicks [Number: 10]. *Investigative Opthalmology & Visual Science*, *51*(10), 5247.

Atkinson, T. S., Haut, R. C., & Altiero, N. J. (1997). A poroelastic model that predicts some phenomenological responses of ligaments and tendons. *Journal of Biomechanical Engineering*, *119*(4), 400–405.

Atta, G., Tempfer, H., Kaser-Eichberger, A., Traweger, A., Heindl, L. M., & Schroedl, F. (2022). Is the human sclera a tendon-like tissue? a structural and functional comparison. *Annals of Anatomy - Anatomischer Anzeiger*, *240*, 151858.

Baba, K., DeBruyne, J. P., & Tosini, G. (2017). Dopamine 2 receptor activation entrains circadian clocks in mouse retinal pigment epithelium [Number: 1 Publisher: Nature Publishing Group]. *Scientific Reports*, *7*(1), 5103.

Backhouse, S., & Gentle, A. (2018). Scleral remodelling in myopia and its manipulation: A review of recent advances in scleral strengthening and myopia control. *Annals of Eye Science*, *3*, 5–5.

Balmer, J. E., & Blomhoff, R. (2002). Gene expression regulation by retinoic acid. *Journal of Lipid Research*, *43*(11), 1773–1808.

Bartmann, M., & Schaeffel, F. (1994). A simple mechanism for emmetropization without cues from accommodation or colour. *Vision Research*, *34*(7), 873–876.

Bartmann, M., Schaeffel, F., Hagel, G., & Zrenner, E. (1994). Constant light affects retinal dopamine levels and blocks deprivation myopia but not lens-induced refractive errors in chickens. *Visual Neuroscience*, *11*(2), 199–208.

Bates, D., Machler, M., Bolker, B., & Walker, S. (2015). Fitting linear mixed-effects models using lme4. *Journal of Statistical Software*, *67*(1), 1–48.

Bates, D., Mächler, M., Bolker, B., & Walker, S. (2015). Fitting linear mixed-effects models using lme4. *Journal of Statistical Software*, *67*(1), 1–48.

Battaglioli, J. L., & Kamm, R. D. (1984). Measurements of the compressive properties of scleral tissue. *Investigative Ophthalmology and Visual Science*, *25*(1), 59–65.

Bauer, B., Ehinger, B., & Aberg, L. (1980). [3h]-dopamine release from the rabbit retina. *Albrecht von Graefes Archiv fur Klinische und Experimentelle Ophthalmologie*, *215*(2), 71–78.

Beach, K. M., Hung, L.-F., Arumugam, B., Smith, E. L., & Ostrin, L. A. (2018). Adenosine receptor distribution in rhesus monkey ocular tissue. *Experimental Eye Research*, *174*, 40–50.

Bergen, M. A., Park, H. n., Chakraborty, R., Landis, E. G., Sidhu, C., He, L., Iuvone, P. M., & Pardue, M. T. (2016). Altered refractive development in mice with reduced levels of retinal dopamine [Number: 10]. *Investigative Opthalmology & Visual Science*, *57*(10), 4412.

Bertrand, E., Fritsch, C., Diether, S., Lambrou, G., Müller, D., Schaeffel, F., Schindler, P., Schmid, K. L., van Oostrum, J., & Voshol, H. (2006). Identification of apolipoprotein a-i as a "STOP" signal for myopia. *Molecular & cellular proteomics : MCP*, *5*(11), 2158–2166.

Bitzer, M., Feldkaemper, M., & Schaeffel, F. (2000). Visually induced changes in components of the retinoic acid system in fundal layers of the chick. *Experimental Eye Research*, *70*(1), 97–106.

Boelen, M. K., Boelen, M. G., & Marshak, D. W. (1998). Light-stimulated release of dopamine from the primate retina is blocked by l -2-amino-4-phosphonobutyric acid (APB). *Visual Neuroscience*, *15*(1), 97–103.

Bonassar, L. J., Sandy, J. D., Lark, M. W., Plaas, A. H. K., Frank, E. H., & Grodzinsky, A. J. (1997). Inhibition of cartilage degradation and changes in physical properties induced by IL-1β and retinoic acid using matrix metalloproteinase inhibitors. *Archives of Biochemistry and Biophysics*, *344*(2), 404–412.

Boote, C., Sigal, I. A., Grytz, R., Hua, Y., Nguyen, T. D., & Girard, M. J. A. (2020). Scleral structure and biomechanics. *Progress in retinal and eye research*, *74*, 100773.

Bowrey, H. E., Metse, A. P., Leotta, A. J., Zeng, G., & Mcfadden, S. A. (2015). The relationship between image degradation and myopia in the mammalian eye [Publisher: Taylor & Francis _eprint: https://doi.org/10.1111/cxo.12316]. *Clinical and Experimental Optometry*, *98*(6), 555–563.

Brambilla, D., Chapman, D., & Greene, R. (2005). Adenosine mediation of presynaptic feedback inhibition of glutamate release. *Neuron*, *46*(2), 275–283.

Brown, D., Ethier, C. R., & Pardue, M. T. (2021). Oral all-trans retinoic acid treatment induces myopia and alters scleral biomechanics in mice [Publisher: The Association for Research in Vision and Ophthalmology]. *Investigative Ophthalmology & Visual Science*, *62*(8), 2876–2876.

Brown, D. M., Mazade, R., Clarkson-Townsend, D., Hogan, K., Datta Roy, P. M., & Pardue, M. T. (2022). Candidate pathways for retina to scleral signaling in refractive eye growth. *Experimental Eye Research*, *219*, 109071.

Brown, D. M., Pardue, M. T., & Ethier, C. R. (2021). A biphasic approach for characterizing tensile, compressive and hydraulic properties of the sclera [Number: 174 Publisher: Royal Society]. *Journal of The Royal Society Interface*, *18*(174).

Brundege, J. M., & Dunwiddie, T. V. (1998). Metabolic regulation of endogenous adenosine release from single neurons. *Neuroreport*, *9*(13), 3007–3011.

Cadot, S., Frenz, D., & Maconochie, M. (2012). A novel method for retinoic acid administration reveals differential and dose-dependent downregulation of fgf3 in the developing inner ear and anterior CNS [Number: 4]. *Developmental Dynamics*, *241*(4), 741–758.

Campbell, I. C., Coudrillier, B., & Ross Ethier, C. (2014). Biomechanics of the posterior eye: A critical role in health and disease. *Journal of biomechanical engineering*, *136*(2), 021005.

Chakraborty, R., Landis, E. G., Mazade, R., Yang, V., Strickland, R., Hattar, S., Stone, R. A., Iuvone, P. M., & Pardue, M. T. (2022). Melanopsin modulates refractive development and myopia. *Experimental Eye Research*, *214*, 108866.

Chakraborty, R., Park, H. n., Aung, M. H., Tan, C. C., Sidhu, C. S., Iuvone, P. M., & Pardue, M. T. (2014). Comparison of refractive development and retinal dopamine in OFF pathway mutant and c57bl/6j wild-type mice. *Molecular Vision*, *20*, 1318–1327.

Chakraborty, R., Park, H. n., Hanif, A. M., Sidhu, C. S., Iuvone, P. M., & Pardue, M. T. (2015). ON pathway mutations increase susceptibility to form-deprivation myopia. *Experimental Eye Research*, *137*, 79–83.

Chakraborty, R., Read, S. A., & Vincent, S. J. (2020). Understanding myopia: Pathogenesis and mechanisms. In M. Ang & T. Y. Wong (Eds.), *Updates on myopia: A clinical perspective* (pp. 65–94). Springer Singapore.

Chen, S., Zhi, Z., Ruan, Q., Liu, Q., Li, F., Wan, F., Reinach, P. S., Chen, J., Qu, J., & Zhou, X. (2017). Bright light suppresses form-deprivation myopia development with activation of dopamine d1 receptor signaling in the ON pathway in retina [Number: 4]. *Investigative Opthalmology & Visual Science*, *58*(4), 2306.

Cheng, C.-Y., Schache, M., Ikram, M. K., Young, T. L., Guggenheim, J. A., Vitart, V., MacGregor, S., Verhoeven, V. J. M., Barathi, V. A., Liao, J., Hysi, P. G., Bailey-Wilson, J. E., St. Pourcain, B., Kemp, J. P., McMahon, G., Timpson, N. J., Evans, D. M., Montgomery, G. W., Mishra, A., … Baird, P. N. (2013). Nine loci for ocular axial length identified through genome-wide association studies, including shared loci with refractive error. *The American Journal of Human Genetics*, *93*(2), 264–277.

Choi, I., & Horgan, C. O. (1977). Saint-Venant's Principle and End Effects in Anisotropic Elasticity. *Journal of Applied Mechanics*, *44*(3), 424–430.

Cohen, B., Lai, W. M., & Mow, V. C. (1998). A transversely isotropic biphasic model for unconfined compression of growth plate and chondroepiphysis. *120*, 491–496.

Cohen, J., Hadjiconstantinou, M., & Neff, N. H. (1983). Activation of dopamine-containing amacrine cells of retina: Light-induced increase of acidic dopamine metabolites. *Brain Research*, *260*(1), 125–127.

Cohen, Y., Peleg, E., Belkin, M., Polat, U., & Solomon, A. S. (2012). Ambient illuminance, retinal dopamine release and refractive development in chicks. *Experimental Eye Research*, *103*, 33–40.

Cotrina, M. L., Lin, J. H., Alves-Rodrigues, A., Liu, S., Li, J., Azmi-Ghadimi, H., Kang, J., Naus, C. C., & Nedergaard, M. (1998). Connexins regulate calcium signaling by controlling ATP release. *Proceedings of the National Academy of Sciences of the United States of America*, *95*(26), 15735–15740.

Coudrillier, B., Boote, C., Quigley, H. A., & Nguyen, T. D. (2012). Scleral anisotropy and its effects on the mechanical response of the optic nerve head. *Biomechanics and Modeling in Mechanobiology*, *12*(5), 941–963.

Coudrillier, B., Pijanka, J., Jefferys, J., Sorensen, T., Quigley, H. A., Boote, C., & Nguyen, T. D. (2015). Collagen structure and mechanical properties of the human sclera: Analysis for the effects of age. *Journal of biomechanical engineering*, *137*(4), 041006.

Cowin, S. C. (1999). Bone poroelasticity. *Journal of Biomechanics*, *32*(3), 217–238.

Crewther, S. G., Liang, H., Junghans, B. M., & Crewther, D. P. (2006). Ionic control of ocular growth and refractive change. *Proceedings of the National Academy of Sciences of the United States of America*, *103*(42), 15663–15668.

Crewther, S. G., Murphy, M. J., & Crewther, D. P. (2008). Potassium channel and NKCC cotransporter involvement in ocular refractive control mechanisms. *PloS One*, *3*(7), e2839.

Cruz Perez, B., Tang, J., Morris, H. J., Palko, J. R., Pan, X., Hart, R. T., & Liu, J. (2014). Biaxial mechanical testing of posterior sclera using high-resolution ultrasound speckle tracking for strain measurements. *Journal of Biomechanics*, *47*(5), 1151–1156.

Cui, D., Trier, K., Chen, X., Zeng, J., Yang, X., Hu, J., & Ge, J. (2008). Distribution of adenosine receptors in human sclera fibroblasts. *Molecular Vision*, *14*, 523–529.

Cui, D., Trier, K., Zeng, J., Wu, K., Yu, M., & Ge, J. (2010). Adenosine receptor protein changes in guinea pigs with form deprivation myopia [_eprint: https://onlinelibrary.wiley.com/doi/pdf/10.1111/j.1755-3768.2009.01559.x]. *Acta Ophthalmologica*, *88*(7), 759–765.

Cui, D., Trier, K., Zeng, J., Wu, K., Yu, M., Hu, J., Chen, X., & Ge, J. (2011). Effects of 7-methylxanthine on the sclera in form deprivation myopia in guinea pigs. *Acta Ophthalmologica*, *89*(4), 328–334.

Curnier, A., He, Q.-C., & Zysset, P. (1995). Conewise linear elastic materials. *Journal of Elasticity*, *37*(1), 1–38.

Cvekl, A., & Wang, W.-L. (2009). Retinoic acid signaling in mammalian eye development [Number: 3]. *Experimental Eye Research*, *89*(3), 280–291.

Dacey, D. M. (1990). The dopaminergic amacrine cell. *Journal of Comparative Neurology*, *301*(3), 461–489.

de Jong, P. T. V. M. (2018). Myopia: Its historical contexts [Number: 8]. *British Journal of Ophthalmology*, *102*(8), 1021–1027.

Diether, S., & Schaeffel, F. (1997). Local changes in eye growth induced by imposed local refractive error despite active accommodation. *Vision Research*, *37*(6), 659–668.

Ding, X., Hu, Y., Guo, X., Guo, X., Morgan, I., & He, M. (2018). Possible causes of discordance in refraction in monozygotic twins: Nearwork, time outdoors and stochastic variation [Publisher: The Association for Research in Vision and Ophthalmology]. *Investigative Ophthalmology & Visual Science*, *59*(13), 5349–5354.

Dirani, M., Tong, L., Gazzard, G., Zhang, X., Chia, A., Young, T. L., Rose, K. A., Mitchell, P., & Saw, S.-M. (2009). Outdoor activity and myopia in singapore teenage children [Number: 8]. *British Journal of Ophthalmology*, *93*(8), 997–1000.

Dolgin, E. (2015). The myopia boom [Bandiera_abtest: a Cg_type: Nature Research Journals Number: 7543 Primary_atype: News Publisher: Nature Publishing Group Subject_term: Epidemiology;Health care;Medical research;Sensory systems Subject_term_id: epidemiology;health-care;medical-research;sensory-systems]. *Nature*, *519*(7543), 276–278.

Dong, F., Zhi, Z., Pan, M., Xie, R., Qin, X., Lu, R., Mao, X., Chen, J.-F., Willcox, M. D. P., Qu, J., & Zhou, X. (2011). Inhibition of experimental myopia by a dopamine agonist: Different effectiveness between form deprivation and hyperopic defocus in guinea pigs. *Molecular Vision*, *17*, 2824–2834.

Doyle, S. E., Grace, M. S., McIVOR, W., & Menaker, M. (2002). Circadian rhythms of dopamine in mouse retina: The role of melatonin. *Visual Neuroscience*, *19*(5), 593–601.

Drury, A. N., & Szent-Györgyi, A. (1929). The physiological activity of adenine compounds with especial reference to their action upon the mammalian heart. *The Journal of Physiology*, *68*(3), 213–237.

Dumitrescu, O. N., Pucci, F. G., Wong, K. Y., & Berson, D. M. (2009). Ectopic retinal ON bipolar cell synapses in the OFF inner plexiform layer: Contacts with dopaminergic amacrine cells and melanopsin ganglion cells [Number: 2]. *The Journal of Comparative Neurology*, *517*(2), 226–244.

Edwards, R. B., Adler, A. J., Dev, S., & Claycomb, R. C. (1992). Synthesis of retinoic acid from retinol by cultured rabbit müller cells. *Experimental Eye Research*, *54*(4), 481–490.

Ehret, A. E., Bircher, K., Stracuzzi, A., Marina, V., Zündel, M., & Mazza, E. (2017). Inverse poroelasticity as a fundamental mechanism in biomechanics and mechanobiology [Bandiera_abtest: a Cc_license_type: cc_by Cg_type: Nature Research Journals Number: 1 Primary_atype: Research Publisher: Nature Publishing Group Subject_term: Biomedical engineering;Tissues Subject_term_id: biomedical-engineering;tissues]. *Nature Communications*, *8*(1), 1002.

Eilaghi, A., Flanagan, J. G., Tertinegg, I., Simmons, C. A., Wayne Brodland, G., & Ross Ethier, C. (2010). Biaxial mechanical testing of human sclera. *Journal of Biomechanics*, *43*(9), 1696–1701.

Eltzschig, H. K. (2013). Extracellular adenosine signaling in molecular medicine. *Journal of molecular medicine (Berlin, Germany)*, *91*(2), 141–146.

Fan, Q., Verhoeven, V. J. M., Wojciechowski, R., Barathi, V. A., Hysi, P. G., Guggenheim, J. A., Höhn, R., Vitart, V., Khawaja, A. P., Yamashiro, K., Hosseini, S. M., Lehtimäki, T., Lu, Y., Haller, T., Xie, J., Delcourt, C., Pirastu, M., Wedenoja, J., Gharahkhani, P., … Saw, S.-M. (2016). Meta-analysis of gene–environment-wide association scans accounting for education level identifies additional loci for refractive error [Bandiera_abtest: a Cc_license_type: cc_by Cg_type: Nature Research Journals Number: 1 Primary_atype: Research Publisher: Nature Publishing Group Subject_term: Education;Genetic variation;Genome-wide association studies;Refractive errors Subject_term_id: education;genetic-variation;genome-wide-association-studies;refractive-errors]. *Nature Communications*, *7*(1), 11008.

Farndale, R. W., Buttle, D. J., & Barrett, A. J. (1986). Improved quantitation and discrimination of sulphated glycosaminoglycans by use of dimethylmethylene blue. *Biochimica et Biophysica Acta (BBA) - General Subjects*, *883*(2), 173–177.

Faulkner, A. E., Kim, M. K., Iuvone, P. M., & Pardue, M. T. (2007). Head-mounted goggles for murine form deprivation myopia. *Journal of Neuroscience Methods*, *161*(1), 96–100.

Feldkaemper, M., & Schaeffel, F. (2013). An updated view on the role of dopamine in myopia. *Experimental Eye Research*, *114*, 106–119.

Fledelius, H. C., & Christensen, A. C. (1996). Reappraisal of the human ocular growth curve in fetal life, infancy, and early childhood. *British Journal of Ophthalmology*, *80*(10), 918–921.

Fledelius, H. C., Christensen, A. S., & Fledelius, C. (2014). Juvenile eye growth, when completed? an evaluation based on IOL-master axial length data, cross-sectional and longitudinal. *Acta Ophthalmologica*, *92*(3), 259–264.

Flitcroft, D. I. (2013). Is myopia a failure of homeostasis? *Experimental Eye Research*, *114*, 16–24.

Flitcroft, D. I., Harb, E. N., & Wildsoet, C. F. (2020). The spatial frequency content of urban and indoor environments as a potential risk factor for myopia development. *Investigative Opthalmology & Visual Science*, *61*(11), 42.

Flitcroft, D. I., He, M., Jonas, J. B., Jong, M., Naidoo, K., Ohno-Matsui, K., Rahi, J., Resnikoff, S., Vitale, S., & Yannuzzi, L. (2019). IMI – defining and classifying myopia: A proposed set of standards for clinical and epidemiologic studies. *Investigative Opthalmology & Visual Science*, *60*(3), M20.

Fluxion. (2009). Understanding effects of viscosity in the BioFlux system. *Technical Note*, 1–2.

Fredholm, B. B. (2007). Adenosine, an endogenous distress signal, modulates tissue damage and repair. *Cell Death and Differentiation*, *14*(7), 1315–1323.

Fredholm, B. B. (2014). Adenosine–a physiological or pathophysiological agent? *Journal of Molecular Medicine (Berlin, Germany)*, *92*(3), 201–206.

Fredholm, B. B., Bättig, K., Holmén, J., Nehlig, A., & Zvartau, E. E. (1999). Actions of caffeine in the brain with special reference to factors that contribute to its widespread use. *Pharmacological Reviews*, *51*(1), 83–133.

Fredholm, B. B., Chern, Y., Franco, R., & Sitkovsky, M. (2007). Aspects of the general biology of adenosine a2a signaling. *Progress in Neurobiology*, *83*(5), 263–276.

French, A. N., Ashby, R. S., Morgan, I. G., & Rose, K. A. (2013). Time outdoors and the prevention of myopia. *Experimental Eye Research*, *114*, 58–68.

Fricke, T. R., Jong, M., Naidoo, K. S., Sankaridurg, P., Naduvilath, T. J., Ho, S. M., Wong, T. Y., & Resnikoff, S. (2018). Global prevalence of visual impairment associated with myopic macular degeneration and temporal trends from 2000 through 2050:

Systematic review, meta-analysis and modelling [Publisher: BMJ Publishing Group Ltd Section: Global issues]. *British Journal of Ophthalmology*, *102*(7), 855–862.

Gallemore, R. P., & Steinberg, R. H. (1990). Effects of dopamine on the chick retinal pigment epithelium. membrane potentials and light-evoked responses. *Investigative Ophthalmology & Visual Science*, *31*(1), 67–80.

Galvis, V., Tello, A., Parra, M. M., Merayo-Lloves, J., Larrea, J., Julian Rodriguez, C., & Camacho, P. A. (2016). Topical atropine in the control of myopia. *Medical Hypothesis, Discovery & Innovation Ophthalmology Journal*, *5*(3), 78–88.

Gao, Q., Liu, Q., Ma, P., Zhong, X., Wu, J., & Ge, J. (2006). Effects of direct intravitreal dopamine injections on the development of lid-suture induced myopia in rabbits [Number: 10]. *Graefe's Archive for Clinical and Experimental Ophthalmology = Albrecht Von Graefes Archiv Fur Klinische Und Experimentelle Ophthalmologie*, *244*(10), 1329–1335.

Gawne, T. J., Siegwart, J. T., Ward, A. H., & Norton, T. T. (2017). The wavelength composition and temporal modulation of ambient lighting strongly affect refractive development in young tree shrews. *Experimental Eye Research*, *155*, 75–84.

Gervois, P., Torra, I. P., Fruchart, J. C., & Staels, B. (2000). Regulation of lipid and lipoprotein metabolism by PPAR activators. *Clinical Chemistry and Laboratory Medicine*, *38*(1), 3–11.

Ghorbani Mojarrad, N., Plotnikov, D., Williams, C., Guggenheim, J. A., & UK Biobank Eye and Vision Consortium. (2020). Association between polygenic risk score and risk of myopia. *JAMA ophthalmology*, *138*(1), 7–13.

Girard, M. J. A., Suh, J.-K. F., Bottlang, M., Burgoyne, C. F., & Downs, J. C. (2011). Biomechanical changes in the sclera of monkey eyes exposed to chronic IOP elevations. *Investigative Ophthalmology & Visual Science*, *52*(8), 5656–5669.

Godley, B. F., & Wurtman, R. J. (1988). Release of endogenous dopamine from the superfused rabbit retina in vitro: Effect of light stimulation. *Brain Research*, *452*(1), 393–395.

Gogola, A., Jan, N.-J., Lathrop, K. L., & Sigal, I. A. (2018). Radial and circumferential collagen fibers are a feature of the peripapillary sclera of human, monkey, pig, cow, goat, and sheep. *Investigative Ophthalmology & Visual Science*, *59*(12), 4763–4774.

Goldschmidt, E., & Jacobsen, N. (2014). Genetic and environmental effects on myopia development and progression [Bandiera_abtest: a Cg_type: Nature Research Journals Number: 2 Primary_atype: Research Publisher: Nature Publishing Group Sub-

ject_term: Epidemiology;Pathogenesis;Refractive errors Subject_term_id: epidemiology;pathogenesis;refractive-errors]. *Eye*, *28*(2), 126–133.

Gordon, R. A., & Donzis, P. B. (1985). Refractive development of the human eye. *Archives of Ophthalmology*, *103*(6), 785–789.

Gottlieb, M. D., Joshi, H. B., & Nickla, D. L. (1990). Scleral changes in chicks with form-deprivation myopia. *Current eye research*, *9*(12), 1157–1165.

Greene, P. R., & McMahon, T. A. (1979). Scleral creep vs. temperature and pressure in vitro. *Experimental Eye Research*, *29*(5), 527–537.

Grytz, R. (2018, April 20). Scleral remodeling in myopia [Google-Books-ID: TDNjDwAAQBAJ]. In C. J. Roberts, W. J. Dupps, & J. C. Downs (Eds.), *Biomechanics of the eye* (pp. 383–403). Kugler Publications.

Grytz, R., & El Hamdaoui, M. (2017). Multi-scale modeling of vision-guided remodeling and age-dependent growth of the tree shrew sclera during eye development and lens-induced myopia. [Number: 1-2]. *Journal Of Elasticity*, *129*(1), 171–195.

Grytz, R., Girkin, C. A., Libertiaux, V., & Downs, J. C. (2012). Perspectives on biomechanical growth and remodeling mechanisms in glaucoma. *Mechanics Research Communications*, *42*, 92–106.

Grytz, R., & Siegwart, J. T. J. (2015). Changing material properties of the tree shrew sclera during minus lens compensation and recovery. *Investigative ophthalmology & visual science*, *56*(3), 2065–2078.

Grytz, R., Yang, H., Hua, Y., Samuels, B. C., & Sigal, I. A. (2020). Connective tissue remodeling in myopia and its potential role in increasing risk of glaucoma. *Current Opinion in Biomedical Engineering*, *15*, 40–50.

Gu, W. Y., Lai, W. M., & Mow, V. C. (1993). Transport of fluid and ions through a porous-permeable charged-hydrated tissue, and streaming potential data on normal bovine articular cartilage. *Journal of Biomechanics*, *26*(6), 709–723.

Guizar-Sicairos, M., Thurman, S. T., & Fienup, J. R. (2008). Efficient subpixel image registration algorithms [Publisher: Optica Publishing Group]. *Optics Letters*, *33*(2), 156–158.

Guo, L., Frost, M. R., He, L., Siegwart, J. T. J., & Norton, T. T. (2013). Gene expression signatures in tree shrew sclera in response to three myopiagenic conditions. *Investigative ophthalmology & visual science*, *54*(10), 6806–6819.

Guo, L., Frost, M. R., Siegwart, J. T., & Norton, T. T. (2014). Scleral gene expression during recovery from myopia compared with expression during myopia development in tree shrew. *Molecular Vision*, *20*, 1643–1659.

Guo, L., Frost, M. R., Siegwart, J. T. J., & Norton, T. T. (2019). Gene expression signatures in tree shrew sclera during recovery from minus-lens wear and during plus-lens wear. *Molecular vision*, *25*, 311–328.

Guo, S. S., Sivak, J. G., Callender, M. G., & Diehl-Jones, B. (1995). Retinal dopamine and lens-induced refractive errors in chicks. *Current Eye Research*, *14*(5), 385–389.

Hagen, L. A., Gilson, S. J., Akram, M. N., & Baraas, R. C. (2019). Emmetropia is maintained despite continued eye growth from 16 to 18 years of age. *Investigative Opthalmology & Visual Science*, *60*(13), 4178.

Harper, A. R., & Summers, J. A. (2015). The dynamic sclera: Extracellular matrix remodeling in normal ocular growth and myopia development. *Experimental eye research*, *133*, 100–111.

Haskó, G., Antonioli, L., & Cronstein, B. N. (2018). Adenosine metabolism, immunity and joint health. *Biochemical Pharmacology*, *151*, 307–313.

Hatami-Marbini, H., & Etebu, E. (2013). An experimental and theoretical analysis of unconfined compression of corneal stroma. *Journal of Biomechanics*, *46*(10), 1752–1758.

Hatami-Marbini, H., & Pachenari, M. (2020). The contribution of sGAGs to stress-controlled tensile response of posterior porcine sclera [Publisher: Public Library of Science]. *PLOS ONE*, *15*(2), e0227856.

He, L., Frost, M. R., Siegwart, J. T., & Norton, T. T. (2014). Gene expression signatures in tree shrew choroid in response to three myopiagenic conditions. *Vision Research*, *102*, 52–63.

He, W., Sun, T., Yang, J., Qin, G., Wu, Z., Zhu, X., & Lu, Y. (2017). Analysis of factors associated with the ocular features of congenital cataract children in the shanghai pediatric cataract study. *Journal of Ophthalmology*, *2017*, 1–7.

Holden, B. A., Fricke, T. R., Wilson, D. A., Jong, M., Naidoo, K. S., Sankaridurg, P., Wong, T. Y., Naduvilath, T. J., & Resnikoff, S. (2016). Global prevalence of myopia and high myopia and temporal trends from 2000 through 2050 [Number: 5]. *Ophthalmology*, *123*(5), 1036–1042.

Howlett, M. H. C., & McFadden, S. A. (2007). Emmetropization and schematic eye models in developing pigmented guinea pigs. [Number: 9]. *Vision research*, *47*(9), 1178–1190.

Howlett, M. H., & McFadden, S. A. (2006). Form-deprivation myopia in the guinea pig (cavia porcellus). *Vision Research*, *46*(1), 267–283.

Hu, Z., Xiong, S., Su, Q., & Zhang, X. (2013). Sufficient conditions for global convergence of differential evolution algorithm. *Journal of Applied Mathematics*, *2013*.

Huang, C.-Y., Mow, V. C., & Ateshian, G. A. (2001). The role of flow-independent viscoelasticity in the biphasic tensile and compressive responses of articular cartilage. *Journal of Biomechanical Engineering*, *123*(5), 410.

Huang, C.-Y., Soltz, M. A., Kopacz, M., Mow, V. C., & Ateshian, G. A. (2003). Experimental verification of the roles of intrinsic matrix viscoelasticity and tension-compression nonlinearity in the biphasic response of cartilage. *Journal of Biomechanical Engineering*, *125*(1), 84.

Huang, F., Shu, Z., Huang, Q., Chen, K., Yan, W., Wu, W., Yang, J., Wang, Q., Wang, F., Zhang, C., Qu, J., & Zhou, X. (2022). Retinal dopamine d2 receptors participate in the development of myopia in mice. *Investigative Opthalmology & Visual Science*, *63*(1), 24.

Huang, F., Wang, Q., Yan, T., Tang, J., Hou, X., Shu, Z., Wan, F., Yang, Y., Qu, J., & Zhou, X. (2020). The role of the dopamine d2 receptor in form-deprivation myopia in mice: Studies with full and partial d2 receptor agonists and knockouts. *Investigative Ophthalmology & Visual Science*, *61*(6), 47.

Huang, F., Yan, T., Shi, F., An, J., Xie, R., Zheng, F., Li, Y., Chen, J., Qu, J., & Zhou, X. (2014). Activation of dopamine d2 receptor is critical for the development of form-deprivation myopia in the c57bl/6 mouse. *Investigative Opthalmology & Visual Science*, *55*(9), 5537.

Huang, F., Zhang, L., Wang, Q., Yang, Y., Li, Q., Wu, Y., Chen, J., Qu, J., & Zhou, X. (2018). Dopamine d1 receptors contribute critically to the apomorphine-induced inhibition of form-deprivation myopia in mice [Number: 6]. *Investigative Opthalmology & Visual Science*, *59*(6), 2623.

Huang, H.-M., Chang, D. S.-T., & Wu, P.-C. (2015). The association between near work activities and myopia in children—a systematic review and meta-analysis (V. Jhanji, Ed.) [Number: 10]. *PLOS ONE*, *10*(10), e0140419.

Huang, J., Qu, X.-M., & Chu, R.-Y. (2011). Expressions of cellular retinoic acid binding proteins i and retinoic acid receptor-β in the guinea pig eyes with experimental myopia. *International Journal of Ophthalmology*, *4*(2), 131–136.

Hung, L.-F., Arumugam, B., Ostrin, L., Patel, N., Trier, K., Jong, M., & Iii, E. L. S. (2018). The adenosine receptor antagonist, 7-methylxanthine, alters emmetropizing responses in infant macaques [Number: 1]. *Investigative Opthalmology & Visual Science*, *59*(1), 472.

Huo, L., Cui, D., Yang, X., Gao, Z., Trier, K., & Zeng, J. (2013). All-trans retinoic acid modulates mitogen-activated protein kinase pathway activation in human scleral fibroblasts through retinoic acid receptor beta. *Molecular Vision*, *19*, 1795–1803.

Hysi, P. G., Choquet, H., Khawaja, A. P., Wojciechowski, R., Tedja, M. S., Yin, J., Simcoe, M. J., Patasova, K., Mahroo, O. A., Thai, K. K., Cumberland, P. M., Melles, R. B., Verhoeven, V. J. M., Vitart, V., Segre, A., Stone, R. A., Wareham, N., Hewitt, A. W., Mackey, D. A., … Hammond, C. J. (2020). Meta-analysis of 542,934 subjects of european ancestry identifies new genes and mechanisms predisposing to refractive error and myopia [Bandiera_abtest: a Cg_type: Nature Research Journals Number: 4 Primary_atype: Research Publisher: Nature Publishing Group Subject_term: Diseases;Genetic association study;Genomics;Population genetics Subject_term_id: diseases;genetic-association-study;genomics;population-genetics]. *Nature Genetics*, *52*(4), 401–407.

I. Papastergiou, G., F. Schmid, G., M. Laties, A., Pendrak, K., Lin, T., & A. Stone, R. (1998). Induction of axial eye elongation and myopic refractive shift in one-year-old chickens. *Vision Research*, *38*(12), 1883–1888.

Iuvone, P., Galli, C., Garrison-Gund, C., & Neff, N. (1978). Light stimulates tyrosine hydroxylase activity and dopamine synthesis in retinal amacrine neurons. *Science*, *202*(4370), 901–902.

Iuvone, P. M., Tigges, M., Stone, R. A., Lambert, S., & Laties, A. M. (1991). Effects of apomorphine, a dopamine receptor agonist, on ocular refraction and axial elongation in a primate model of myopia. *Investigative Ophthalmology & Visual Science*, *32*(5), 1674–1677.

Iuvone, P. M., Tigges, M., Fernandes, A., & Tigges, J. (1989). Dopamine synthesis and metabolism in rhesus monkey retina: Development, aging, and the effects of monocular visual deprivation. *Visual Neuroscience*, *2*(5), 465–471.

Jackson, T. L., Hussain, A., Hodgetts, A., Morley, A. M., Hillenkamp, J., Sullivan, P. M., & Marshall, J. (2006). Human scleral hydraulic conductivity: Age-related changes, topographical variation, and potential scleral outflow facility. *Investigative Ophthalmology and Visual Science*, *47*(11), 4942–4946.

Jia, L., Oh, E. C. T., Ng, L., Srinivas, M., Brooks, M., Swaroop, A., & Forrest, D. (2009). Retinoid-related orphan nuclear receptor RORβ is an early-acting factor in rod photoreceptor development [Publisher: National Academy of Sciences Section: Biological Sciences]. *Proceedings of the National Academy of Sciences*.

Jiang, X., Pardue, M. T., Mori, K., Ikeda, S.-I., Torii, H., D'Souza, S., Lang, R. A., Kurihara, T., & Tsubota, K. (2021). Violet light suppresses lens-induced myopia via neuropsin (OPN5) in mice. *Proceedings of the National Academy of Sciences of the United States of America*, *118*(22).

Jin, J.-X., Hua, W.-J., Jiang, X., Wu, X.-Y., Yang, J.-W., Gao, G.-P., Fang, Y., Pei, C.-L., Wang, S., Zhang, J.-Z., Tao, L.-M., & Tao, F.-B. (2015). Effect of outdoor activity on myopia onset and progression in school-aged children in northeast china: The sujiatun eye care study. *BMC Ophthalmology*, *15*(1), 73.

Johansson, F. et al. (2018). Mpmath: A python library for arbitrary-precision floating-point arithmetic (version 1.1).

Johnson, M., & Tarbell, J. M. (2001). A biphasic, anisotropic model of the aortic wall. *Journal of Biomechanical Engineering*, *123*(1), 52–57.

Jones, J. W., Pierzchalski, K., Yu, J., & Kane, M. A. (2015). Use of fast HPLC multiple reaction monitoring cubed for endogenous retinoic acid quantification in complex matrices. *Analytical Chemistry*, *87*(6), 3222–3230.

Jones, L. A., Mitchell, G. L., Mutti, D. O., Hayes, J. R., Moeschberger, M. L., & Zadnik, K. (2005). Comparison of ocular component growth curves among refractive error groups in children. *Investigative Ophthalmology & Visual Science*, *46*(7), 2317–2327.

Jones-Jordan, L. A., Sinnott, L. T., Cotter, S. A., Kleinstein, R. N., Manny, R. E., Mutti, D. O., Twelker, J. D., & Zadnik, K. (2012). Time outdoors, visual activity, and myopia progression in juvenile-onset myopes [Number: 11]. *Investigative Opthalmology & Visual Science*, *53*(11), 7169.

Junqueira, L. C. U., Toledo, O. M. S., & Montes, G. S. (1981). Correlation of specific sulfated glycosaminoglycans with collagen types i, II, and III. *Cell and Tissue Research*, *217*(1), 171–175.

KANE, M. A., CHEN, N., SPARKS, S., & NAPOLI, J. L. (2005). Quantification of endogenous retinoic acid in limited biological samples by LC/MS/MS. *Biochemical Journal*, *388*(1), 363–369.

Kane, M. A., Folias, A. E., & Napoli, J. L. (2008). HPLC/UV quantitation of retinal, retinol, and retinyl esters in serum and tissues. *Analytical Biochemistry*, *378*(1), 71–79.

Kane, M. A., Folias, A. E., Wang, C., & Napoli, J. L. (2008). Quantitative profiling of endogenous retinoic acid in vivo and in vitro by tandem mass spectrometry. *Analytical Chemistry*, *80*(5), 1702–1708.

Kane, M. A., & Napoli, J. L. (2010). Quantification of endogenous retinoids. *Methods in Molecular Biology (Clifton, N.J.)*, *652*, 1–54.

Kee, C. S., Marzani, D., & Wallman, J. (2001). Differences in time course and visual requirements of ocular responses to lenses and diffusers. *Investigative ophthalmology & visual science*, *42*(3), 575–583.

Keene, D. R., Antonio, J. D. S., Mayne, R., McQuillan, D. J., Sarris, G., Santoro, S. A., & Iozzo, R. V. (2000). Decorin binds near the c terminus of type i collagen * [Publisher: Elsevier]. *Journal of Biological Chemistry*, *275*(29), 21801–21804.

Khalsa, P. S., & Eisenberg, S. R. (1997). Compressive behavior of articular cartilage is not completely explained by proteoglycan osmotic pressure. *Journal of Biomechanics*, *30*(6), 589–594.

Khanal, S., Norton, T. T., & Gawne, T. (2020). 7-methylxanthine does not prevent induced myopia in tree shrews [Number: 7 Publisher: The Association for Research in Vision and Ophthalmology]. *Investigative Ophthalmology & Visual Science*, *61*(7), 1136–1136.

Kiani, C., Chen, L., Wu, Y. J., Yee, A. J., & Yang, B. B. (2002). Structure and function of aggrecan [Number: 1 Publisher: Nature Publishing Group]. *Cell Research*, *12*(1), 19–32.

Kiefer, A. K., Tung, J. Y., Do, C. B., Hinds, D. A., Mountain, J. L., Francke, U., & Eriksson, N. (2013). Genome-wide analysis points to roles for extracellular matrix remodeling, the visual cycle, and neuronal development in myopia [Publisher: Public Library of Science]. *PLOS Genetics*, *9*(2), e1003299.

Klooster, J., Beckers, H., Tusscher, T., Vrensen, G., van der Want, J., & Lamers, W. (1996). Sympathetic innervation of the rat choroid: An autoradiographic tracing and immunohistochemical study. *Ophthalmic Research*, *28*(1), 36–43.

Kong, T., Westerman, K. A., Faigle, M., Eltzschig, H. K., & Colgan, S. P. (2006). HIF-dependent induction of adenosine a2b receptor in hypoxia. *FASEB journal: official publication of the Federation of American Societies for Experimental Biology*, *20*(13), 2242–2250.

Kramer, S. G. (1971). Dopamine: A retinal neurotransmitter. i. retinal uptake, storage, and light-stimulated release of h3-dopamine in vivo. *Investigative Ophthalmology*, *10*(6), 438–452.

Kröger, R. H. H., Hirt, B., & Wagner, H.-J. (1999). Effects of retinal dopamine depletion on the growth of the fish eye. *Journal of Comparative Physiology A: Sensory, Neural, and Behavioral Physiology*, *184*(4), 403–412.

Krutmann, J., Béhar-Cohen, F., Baillet, G., de Ayguavives, T., Ortega Garcia, P., Peña-García, P., Remé, C., & Wolffsohn, J. (2014). Towards standardization of UV eye protection: What can be learned from photodermatology? *Photodermatology, Photoimmunology & Photomedicine*, *30*(2), 128–136.

Ku, D. N., & Greene, P. R. (1981). Scleral creep in vitro resulting from cyclic pressure pulses: Applications to myopia. *American journal of optometry and physiological optics*, *58*(7), 528–535.

Kvalseth, T. O. (1985). Cautionary note about r2. *The American Statistician*, *39*(4), 279–285.

Lai, W. M., & Mow, V. C. (1980). Drag-induced compression of articular cartilage during a permeation experiment. *Biorheology*, *17*(1), 111–123.

Lakawicz, J. M., Bottega, W. J., Fine, H. F., & Prenner, J. L. (2020). On the mechanics of myopia and its influence on retinal detachment. [Number: 2]. *Biomechanics and modeling in mechanobiology*, *19*(2), 603–620.

Landis, E., Chrenek, M., Chakraborty, R., Strickland, R., Bergen, M., Yang, V., Iuvone, P., & Pardue, M. (2020). Increased endogenous dopamine prevents myopia in mice. *Experimental Eye Research*, *193*, 107956.

Landis, E. G., Park, H. N., Chrenek, M., He, L., Sidhu, C., Chakraborty, R., Strickland, R., Iuvone, P. M., & Pardue, M. T. (2021). Ambient light regulates retinal dopamine signaling and myopia susceptibility. *Investigative Ophthalmology & Visual Science*, *62*(1), 28.

Landis, E. G., Yang, V., Brown, D. M., Pardue, M. T., & Read, S. A. (2018). Dim light exposure and myopia in children [Number: 12]. *Investigative Opthalmology & Visual Science*, *59*(12), 4804.

Legerlotz, K., Riley, G. P., & Screen, H. R. C. (2010). Specimen dimensions influence the measurement of material properties in tendon fascicles. *Journal of Biomechanics*, *43*(12), 2274–2280.

Lenth, R. V. (2021). *Emmeans: Estimated marginal means, aka least-squares means* [R package version 1.7.0].

Lepack, A. E., Werner, C. T., Stewart, A. F., Fulton, S. L., Zhong, P., Farrelly, L. A., Smith, A. C. W., Ramakrishnan, A., Lyu, Y., Bastle, R. M., Martin, J. A., Mitra, S., O'Con-

nor, R. M., Wang, Z.-J., Molina, H., Turecki, G., Shen, L., Yan, Z., Calipari, E. S., … Maze, I. (2020). Dopaminylation of histone h3 in ventral tegmental area regulates cocaine seeking [Number: 6487]. *Science (New York, N.Y.)*, *368*(6487), 197–201.

Levick, J. R. (1987). Flow through interstitium and other fibrous matrices. *Quarterly Journal of Experimental Physiology (Cambridge, England)*, *72*(4), 409–437.

Levy, A. M., Fazio, M. A., & Grytz, R. (2018). Experimental myopia increases and scleral crosslinking using genipin inhibits cyclic softening in the tree shrew sclera. *Ophthalmic and Physiological Optics*, *38*(3), 246–256.

Lewis, J. A., Garcia, M. B., Rani, L., & Wildsoet, C. F. (2014). Intact globe inflation testing of changes in scleral mechanics in myopia and recovery. *Experimental eye research*, *127*, 42–48.

Lewis, T. L., & Maurer, D. (2005). Multiple sensitive periods in human visual development: Evidence from visually deprived children. *Developmental Psychobiology*, *46*(3), 163–183.

Li, C., McFadden, S. A., Morgan, I., Cui, D., Hu, J., Wan, W., & Zeng, J. (2010). All-trans retinoic acid regulates the expression of the extracellular matrix protein fibulin-1 in the guinea pig sclera and human scleral fibroblasts. *Molecular Vision*, *16*, 689–697.

Li, H., Zhang, Z., Blackburn, M. R., Wang, S. W., Ribelayga, C. P., & O'Brien, J. (2013). Adenosine and dopamine receptors coregulate photoreceptor coupling via gap junction phosphorylation in mouse retina. *Journal of Neuroscience*, *33*(7), 3135–3150.

Li, W., Lan, W., Yang, S., Liao, Y., Xu, Q., Lin, L., & Yang, Z. (2014). The effect of spectral property and intensity of light on natural refractive development and compensation to negative lenses in guinea pigs. *Investigative Opthalmology & Visual Science*, *55*(10), 6324.

Li, X.-X., Schaeffel, F., Kohler, K., & Zrenner, E. (1992). Dose-dependent effects of 6-hydroxy dopamine on deprivation myopia, electroretinograms, and dopaminergic amacrine cells in chickens. *Visual Neuroscience*, *9*(5), 483–492.

Liang, H., Crewther, S. G., Crewther, D. P., & Junghans, B. M. (2004). Structural and elemental evidence for edema in the retina, retinal pigment epithelium, and choroid during recovery from experimentally induced myopia. *Investigative Opthalmology & Visual Science*, *45*(8), 2463.

Lim, L. S., Yang, X., Gazzard, G., Lin, X., Sng, C., Saw, S.-M., & Qiu, A. (2011). Variations in eye volume, surface area, and shape with refractive error in young children by magnetic resonance imaging analysis. *Investigative Opthalmology & Visual Science*, *52*(12), 8878.

Lin, X., Naidu, R. K., Dai, J., Zhou, X., Qu, X., & Zhou, H. (2019). Scleral cross-linking using glyceraldehyde for the prevention of axial elongation in the rabbit: Blocked axial elongation and altered scleral microstructure. *Current eye research*, *44*(2), 162–171.

Lingham, G., Mackey, D. A., Lucas, R., & Yazar, S. (2020). How does spending time outdoors protect against myopia? a review. *British Journal of Ophthalmology*, *104*(5), 593–599.

Liu, H., Schaeffel, F., Trier, K., & Feldkaemper, M. (2020). Effects of 7-methylxanthine on deprivation myopia and retinal dopamine release in chickens [Number: 3 Publisher: Karger Publishers]. *Ophthalmic Research*, *63*(3), 347–357.

Liu, Y., Wang, L., Xu, Y., Pang, Z., & Mu, G. (2021). The influence of the choroid on the onset and development of myopia: From perspectives of choroidal thickness and blood flow. *Acta Ophthalmologica*.

Lopez, S. G., & Bonassar, L. J. (2022). The role of SLRPs and large aggregating proteoglycans in collagen fibrillogenesis, extracellular matrix assembly, and mechanical function of fibrocartilage [Publisher: Taylor & Francis _eprint: https://doi.org/10.1080/03008207.2021.1
Connective Tissue Research, *63*(3), 269–286.

Lovatt, D., Xu, Q., Liu, W., Takano, T., Smith, N. A., Schnermann, J., Tieu, K., & Nedergaard, M. (2012). Neuronal adenosine release, and not astrocytic ATP release, mediates feedback inhibition of excitatory activity. *Proceedings of the National Academy of Sciences of the United States of America*, *109*(16), 6265–6270.

Mak, A. F. (1986). UNCONFINED COMPRESSION OF HYDRATED VISCOELASTIC TISSUES : A BIPHASIC POROVISCOELASTIC ANALYSIS. *Biorheology*, *23*, 371–383.

Mao, J., & Liu, S. (2017). Different roles of retinal dopamine in albino guinea pig myopia. *Neuroscience Letters*, *639*, 94–97.

Mao, J.-F., Liu, S.-Z., & Dou, X.-Q. (2012). Retinoic acid metabolic change in retina and choroid of the guinea pig with lens-induced myopia. *International Journal of Ophthalmology*, *5*(6), 670–674.

Mao, J., Liu, S., & Fu, C. (2016). Citicoline retards myopia progression following form deprivation in guinea pigs [Number: 11]. *Experimental Biology and Medicine*, *241*(11), 1258–1263.

Mao, J., Liu, S., Qin, W., Li, F., Wu, X., & Tan, Q. (2010). Levodopa inhibits the development of form-deprivation myopia in guinea pigs [Number: 1]. *Optometry and Vision Science: Official Publication of the American Academy of Optometry*, *87*(1), 53–60.

Marzani, D., & Wallman, J. (1997). Growth of the two layers of the chick sclera is modulated reciprocally by visual conditions. *Investigative Ophthalmology & Visual Science*, *38*(9), 1726–1739.

Mathis, U., Feldkaemper, M., Wang, M., & Schaeffel, F. (2020). Studies on retinal mechanisms possibly related to myopia inhibition by atropine in the chicken. *Graefe's Archive for Clinical and Experimental Ophthalmology = Albrecht Von Graefes Archiv Fur Klinische Und Experimentelle Ophthalmologie*, *258*(2), 319–333.

Mattson, J. M., Turcotte, R., & Zhang, Y. (2017). Glycosaminoglycans contribute to extracellular matrix fiber recruitment and arterial wall mechanics [Num Pages: 213-225 Place: Dordrecht, Netherlands Publisher: Springer Nature B.V.]. *Biomechanics and Modeling in Mechanobiology*, *16*(1), 213–225.

McBrien, N. A., Cottriall, C. L., & Annies, R. (2001). Retinal acetylcholine content in normal and myopic eyes: A role in ocular growth control? *Visual Neuroscience*, *18*(4), 571–580.

McBrien, N. A., Cornell, L. M., & Gentle, A. (2001). Structural and ultrastructural changes to the sclera in a mammalian model of high myopia. *Investigative Ophthalmology & Visual Science*, *42*(10), 2179–2187.

McBrien, N. A., Jobling, A. I., & Gentle, A. (2009). Biomechanics of the sclera in myopia: Extracellular and cellular factors. *Optometry and Vision Science*, *86*(1), E23.

McCaffery, P., Mey, J., & Drager, U. C. (1996). Light-mediated retinoic acid production. *Proceedings of the National Academy of Sciences*, *93*(22), 12570–12574.

McCarthy, C. S., Megaw, P., Devadas, M., & Morgan, I. G. (2007). Dopaminergic agents affect the ability of brief periods of normal vision to prevent form-deprivation myopia [Number: 1]. *Experimental Eye Research*, *84*(1), 100–107.

McFadden, S. A., Howlett, M. H. C., & Mertz, J. R. (2004). Retinoic acid signals the direction of ocular elongation in the guinea pig eye. *Vision Research*, *44*(7), 643–653.

McFadden, S. A., Howlett, M. H. C., Mertz, J. R., & Wallman, J. (2006). Acute effects of dietary retinoic acid on ocular components in the growing chick. *Experimental Eye Research*, *83*(4), 949–961.

McFadden, S. A., & Wildsoet, C. (2020). The effect of optic nerve section on form deprivation myopia in the guinea pig. *The Journal of Comparative Neurology*, *528*(17), 2874–2887.

Megaw, P., Morgan, I., & Boelen, M. (2001). Vitreal dihydroxyphenylacetic acid (DOPAC) as an index of retinal dopamine release: Vitreal DOPAC reflects dopamine release. *Journal of Neurochemistry*, *76*(6), 1636–1644.

Mertz, J. R., & Wallman, J. (2000). Choroidal retinoic acid synthesis: A possible mediator between refractive error and compensatory eye growth. *Experimental eye research*, *70*(4), 519–527.

Michalek, A. J., Kuxhaus, L., Jaremczuk, D., & Zaino, N. L. (2018). Proteoglycans contribute locally to swelling, but globally to compressive mechanics, in intact cervine medial meniscus. *Journal of Biomechanics*, *74*, 86–91.

Midgett, D. E., Jefferys, J. L., Quigley, H. A., & Nguyen, T. D. (2018). The contribution of sulfated glycosaminoglycans to the inflation response of the human optic nerve head. *Investigative Ophthalmology & Visual Science*, *59*(7), 3144–3154.

Milam, A. H., Possin, D. E., Huang, J., Fariss, R. N., Flannery, J. G., & Saari, J. C. (1997). Characterization of aldehyde dehydrogenase-positive amacrine cells restricted in distribution to the dorsal retina. *Visual Neuroscience*, *14*(3), 601–608.

Milam, A. H., Leeuw, A. M. D., Gaur, V. P., & Saari, J. C. (1990). Immunolocalization of cellular retinoic acid binding protein to müller cells and/or a subpopulation of GABA□positive amacrine cells in retinas of different species. *Journal of Comparative Neurology*, *296*(1).

Miyake, M., Yamashiro, K., Tabara, Y., Suda, K., Morooka, S., Nakanishi, H., Khor, C.-C., Chen, P., Qiao, F., Nakata, I., Akagi-Kurashige, Y., Gotoh, N., Tsujikawa, A., Meguro, A., Kusuhara, S., Polasek, O., Hayward, C., Wright, A. F., Campbell, H., … Yoshimura, N. (2015). Identification of myopia-associated WNT7b polymorphisms provides insights into the mechanism underlying the development of myopia [Bandiera_abtest: a Cg_type: Nature Research Journals Number: 1 Primary_atype: Research Publisher: Nature Publishing Group Subject_term: Disease genetics;Epidemiology;Genome-wide association studies;Refractive errors Subject_term_id: disease-genetics;epidemiology;genome-wide-association-studies;refractive-errors]. *Nature Communications*, *6*(1), 6689.

Morgan, I. G., Ohno-Matsui, K., & Saw, S.-M. (2012). Myopia. *The Lancet*, *379*(9827), 1739–1748.

Moring, A. G., Baker, J. R., & Norton, T. T. (2007). Modulation of glycosaminoglycan levels in tree shrew sclera during lens-induced myopia development and recovery [Publisher: The Association for Research in Vision and Ophthalmology]. *Investigative Ophthalmology & Visual Science*, *48*(7), 2947–2956.

Mortazavi, A. M., Simon, B. R., Stamer, W. D., & Vande Geest, J. P. (2009). Drained secant modulus for human and porcine peripapillary sclera using unconfined compression testing. *Experimental Eye Research*, *89*(6), 892–897.

Mow, V. C., Mak, A. F., Lai, W. M., Rosenberg, L. C., & Tang, L. .-. (1984). Viscoelastic properties of proteoglycan subunits and aggregates in varying solution concentrations. *Journal of Biomechanics*, *17*(5), 325–338.

Mow, V. C., Sun, D. D., Guo, X. E., Likhitpanichkul, M., & Lai, W. M. (2002). Fixed negative charges modulate mechanical behaviours and electrical signals in articular cartilage under unconfined compression — a triphasic paradigm. In W. Ehlers & J. Bluhm (Eds.), *Porous media: Theory, experiments and numerical applications* (pp. 227–247). Springer.

Mow, V. C., Wang, C. C., & Hung, C. T. (1999). The extracellular matrix, interstitial fluid and ions as a mechanical signal transducer in articular cartilage. *Osteoarthritis and Cartilage*, *7*(1), 41–58.

Murienne, B. J., Chen, M. L., Quigley, H. A., & Nguyen, T. D. (2016). The contribution of glycosaminoglycans to the mechanical behaviour of the posterior human sclera. [Number: 119]. *Journal of the Royal Society, Interface*, *13*(119).

Murienne, B. J., Jefferys, J. L., Quigley, H. A., & Nguyen, T. D. (2015). The effects of glycosaminoglycan degradation on the mechanical behavior of the posterior porcine sclera. *Acta biomaterialia*, *12*, 195–206.

Mutti, D. O., Mitchell, G. L., Jones, L. A., Friedman, N. E., Frane, S. L., Lin, W. K., Moeschberger, M. L., & Zadnik, K. (2005). Axial growth and changes in lenticular and corneal power during emmetropization in infants. *Investigative Opthalmology & Visual Science*, *46*(9), 3074.

Myers, K. M., Cone, F. E., Quigley, H. A., Gelman, S., Pease, M. E., & Nguyen, T. D. (2010). The in vitro inflation response of mouse sclera. *Experimental eye research*, *91*(6), 866–875.

Naidoo, K. S., Fricke, T. R., Frick, K. D., Jong, M., Naduvilath, T. J., Resnikoff, S., & Sankaridurg, P. (2019). Potential Lost Productivity Resulting from the Global Burden of Myopia: Systematic Review, Meta-analysis, and Modeling. *Ophthalmology*, *126*(3), 338–346.

Ng, B. H., Chou, S. M., & Krishna, V. (2005). The Influence of Gripping Techniques on the Tensile Properties of Tendons [Publisher: IMECHE]. *Proceedings of the Institution of Mechanical Engineers, Part H: Journal of Engineering in Medicine*, *219*(5), 349–354.

Nguyen, C., Cone, F. E., Nguyen, T. D., Coudrillier, B., Pease, M. E., Steinhart, M. R., Oglesby, E. N., Jefferys, J. L., & Quigley, H. A. (2013). Studies of scleral biomechanical behavior related to susceptibility for retinal ganglion cell loss in experimental mouse glaucoma. *Investigative Ophthalmology and Visual Science*, *54*(3), 1767–1780.

Nickla, D. L., Jordan, K., Yang, J., & Singh, P. (2019). Effects of time-of-day on inhibition of lens-induced myopia by quinpirole, pirenzepine and atropine in chicks. *Experimental Eye Research*, *181*, 5–14.

Nickla, D. L., & Totonelly, K. (2011). Dopamine antagonists and brief vision distinguish lens-induced- and form-deprivation-induced myopia. *Experimental Eye Research*, *93*(5), 782–785.

Nickla, D. L., Totonelly, K., & Dhillon, B. (2010). Dopaminergic agonists that result in ocular growth inhibition also elicit transient increases in choroidal thickness in chicks [Number: 5]. *Experimental Eye Research*, *91*(5), 715–720.

Nickla, D. L., & Wallman, J. (2010). The multifunctional choroid [Number: 2]. *Progress in Retinal and Eye Research*, *29*(2), 144–168.

Nie, H.-H., Huo, L.-J., Yang, X., Gao, Z.-Y., Zeng, J.-W., Trier, K., & Cui, D.-M. (2012). Effects of 7-methylxanthine on form-deprivation myopia in pigmented rabbits [Number: 2]. *International Journal of Ophthalmology*, *5*(2), 133–137.

Norman, R. E., Flanagan, J. G., Rausch, S. M. K., Sigal, I. A., Tertinegg, I., Eilaghi, A., Portnoy, S., Sled, J. G., & Ethier, C. R. (2010). Dimensions of the human sclera: Thickness measurement and regional changes with axial length. *Experimental Eye Research*, *90*(2), 277–284.

Norman, R. E., Flanagan, J. G., Sigal, I. A., Rausch, S. M. K., Tertinegg, I., & Ethier, C. R. (2011). Finite element modeling of the human sclera: Influence on optic nerve head biomechanics and connections with glaucoma. *Experimental Eye Research*, *93*(1), 4–12.

Norton, T. T., Essinger, J. A., & McBrien, N. A. (1994). Lid-suture myopia in tree shrews with retinal ganglion cell blockade. *Visual Neuroscience*, *11*(1), 143–153.

Norton, T. T., & Siegwart, J. T. (1995). Animal models of emmetropization: Matching axial length to the focal plane. *Journal of the American Optometric Association*, *66*(7), 405–414.

Norton, T. T. (2016). What do animal studies tell us about the mechanism of myopia—protection by light?: *Optometry and Vision Science*, *93*(9), 1049–1051.

Norton, T. T., & Rada, J. A. (1995). Reduced extracellular matrix in mammalian sclera with induced myopia. *Vision Research*, *35*(9), 1271–1281.

Norton, T. T., & Siegwart, J. T. (2013). Light levels, refractive development, and myopia – a speculative review. *Experimental Eye Research*, *114*, 48–57.

Ohngemach, S., Hagel, G., & Schaeffel, F. (1997). Concentrations of biogenic amines in fundal layers in chickens with normal visual experience, deprivation, and after reserpine application. *Visual Neuroscience*, *14*(3), 493–505.

Orgel, J. P. R. O., Eid, A., Antipova, O., Bella, J., & Scott, J. E. (2009). Decorin core protein (decoron) shape complements collagen fibril surface structure and mediates its binding [Publisher: Public Library of Science]. *PLOS ONE*, *4*(9), e7028.

Pan, M., Guan, Z., Reinach, P. S., Kang, L., Cao, Y., Zhou, D., Srinivasalu, N., Zhao, F., Qu, J., & Zhou, X. (2021). PPARγ modulates refractive development and form deprivation myopia in guinea pigs. *Experimental Eye Research*, *202*, 108332.

Pan, M., Jiao, S., Reinach, P. S., Yan, J., Yang, Y., Li, Q., Srinivasalu, N., Qu, J., & Zhou, X. (2018). Opposing effects of PPARα agonism and antagonism on refractive development and form deprivation myopia in guinea pigs [Publisher: The Association for Research in Vision and Ophthalmology]. *Investigative Ophthalmology & Visual Science*, *59*(15), 5803–5815.

Pandey, S., Blanks, J. C., Spee, C., Jiang, M., & Fong, H. K. W. (1994). Cytoplasmic retinal localization of an evolutionary homolog of the visual pigments. *Experimental Eye Research*, *58*(5), 605–613.

Pardue, M. T., Faulkner, A. E., Fernandes, A., Yin, H., Schaeffel, F., Williams, R. W., Pozdeyev, N., & Iuvone, P. M. (2008). High susceptibility to experimental myopia in a mouse model with a retinal on pathway defect [Number: 2]. *Investigative Ophthalmology & Visual Science*, *49*(2), 706–712.

Pardue, M. T., Stone, R. A., & Iuvone, P. M. (2013). Investigating mechanisms of myopia in mice. *Experimental Eye Research*, *114*, 96–105.

Park, H. n., Jabbar, S. B., Tan, C. C., Sidhu, C. S., Abey, J., Aseem, F., Schmid, G., Iuvone, P. M., & Pardue, M. T. (2014). Visually-driven ocular growth in mice requires functional rod photoreceptors [Number: 10]. *Investigative Opthalmology & Visual Science*, *55*(10), 6272.

Pascual, O., Casper, K. B., Kubera, C., Zhang, J., Revilla-Sanchez, R., Sul, J.-Y., Takano, H., Moss, S. J., McCarthy, K., & Haydon, P. G. (2005). Astrocytic purinergic signaling coordinates synaptic networks. *Science (New York, N.Y.)*, *310*(5745), 113–116.

Pennella, F., Cerino, G., Massai, D., Gallo, D., Falvo D'Urso Labate, G., Schiavi, A., Deriu, M. A., Audenino, A., & Morbiducci, U. (2013). A survey of methods for the evaluation of tissue engineering scaffold permeability. *Annals of Biomedical Engineering*, *41*(10), 2027–2041.

Phillips, J. R., Khalaj, M., & McBrien, N. A. (2000). Induced myopia associated with increased scleral creep in chick and tree shrew eyes. *Investigative ophthalmology & visual science*, *41*(8), 2028–2034.

Phillips, J. R., & McBrien, N. A. (1995). Form deprivation myopia: Elastic properties of sclera. *Ophthalmic & physiological optics : the journal of the British College of Ophthalmic Opticians (Optometrists)*, *15*(5), 357–362.

Phillips, J. R., & McBrien, N. A. (2004). Pressure-Induced Changes in Axial Eye Length of Chick and Tree Shrew: Significance of Myofibroblasts in the Sclera. *Investigative Ophthalmology & Visual Science*, *45*(3), 758–763.

Pijanka, J. K., Kimball, E. C., Pease, M. E., Abass, A., Sorensen, T., Nguyen, T. D., Quigley, H. A., & Boote, C. (2014). Changes in scleral collagen organization in murine chronic experimental glaucoma. *Investigative ophthalmology & visual science*, *55*(10), 6554–6564.

Pottek, M., & Weiler, R. (2000). Light-adaptive effects of retinoic acid on receptive field properties of retinal horizontal cells: Light-adaptive effects of retinoic acid. *European Journal of Neuroscience*, *12*(2), 437–445.

Prigge, C. L., Yeh, P.-T., Liou, N.-F., Lee, C.-C., You, S.-F., Liu, L.-L., McNeill, D. S., Chew, K. S., Hattar, S., Chen, S.-K., & Zhang, D.-Q. (2016). M1 ipRGCs influence visual function through retrograde signaling in the retina [Number: 27]. *Journal of Neuroscience*, *36*(27), 7184–7197.

Proll, M. A., Kamp, C. W., & Morgan, W. W. (1982). Use of liquid chromatography with electrochemistry to measure effects of varying intensities of white light on DOPA accumulation in rat retinas. *Life Sciences*, *30*(1), 11–19.

Puopolo, M., Hochstetler, S. E., Gustincich, S., Wightman, R. M., & Raviola, E. (2001). Extrasynaptic release of dopamine in a retinal neuron: Activity dependence and transmitter modulation. *Neuron*, *30*(1), 211–225.

Qiao, S.-N., Zhang, Z., Ribelayga, C. P., Zhong, Y.-M., & Zhang, D.-Q. (2016). Multiple cone pathways are involved in photic regulation of retinal dopamine [Number: 1]. *Scientific Reports*, *6*(1), 28916.

Qiu, C., Chen, M., Yao, J., Sun, X., Xu, J., Zhang, R., Wang, X., Li, G., & Qian, S. (2018). Mechanical strain induces distinct human scleral fibroblast lineages: Differential

roles in cell proliferation, apoptosis, migration, and differentiation. [Number: 6]. *Investigative ophthalmology & visual science*, *59*(6), 2401–2410.

Quinn, T. M., Dierickx, P., & Grodzinsky, A. J. (2001). Glycosaminoglycan network geometry may contribute to anisotropic hydraulic permeability in cartilage under compression. *Journal of Biomechanics*, *34*(11), 1483–1490.

Rada, J. A., Achen, V. R., Perry, C. A., & Fox, P. W. (1997). Proteoglycans in the human sclera. evidence for the presence of aggrecan. *Investigative Ophthalmology & Visual Science*, *38*(9), 1740–1751.

Rada, J. A., Nickla, D. L., & Troilo, D. (2000). Decreased proteoglycan synthesis associated with form deprivation myopia in mature primate eyes. *Investigative ophthalmology & visual science*, *41*(8), 2050–2058.

Rada, J. A., Achen, V. R., Penugonda, S., Schmidt, R. W., & Mount, B. A. (2000). Proteoglycan composition in the human sclera during growth and aging. *Investigative Ophthalmology and Visual Science*, *41*(7), 1639–1648.

Rada, J. A. S., Hollaway, L. R., Lam, W., Li, N., & Napoli, J. L. (2012). Identification of RALDH2 as a visually regulated retinoic acid synthesizing enzyme in the chick choroid [Publisher: The Association for Research in Vision and Ophthalmology]. *Investigative Ophthalmology & Visual Science*, *53*(3), 1649–1662.

Rada, J. A. S., Shelton, S., & Norton, T. T. (2006). The sclera and myopia. *Experimental eye research*, *82*(2), 185–200.

Ramessur, R., Williams, K. M., & Hammond, C. J. (2015). Risk factors for myopia in a discordant monozygotic twin study [_eprint: https://onlinelibrary.wiley.com/doi/pdf/10.1111/opo.122
Ophthalmic and Physiological Optics, *35*(6), 643–651.

Raspanti, M., Viola, M., Sonaggere, M., Tira, M. E., & Tenni, R. (2007). Collagen fibril structure is affected by collagen concentration and decorin [Publisher: American Chemical Society]. *Biomacromolecules*, *8*(7), 2087–2091.

Read, S. A., Collins, M. J., & Vincent, S. J. (2014). Light exposure and physical activity in myopic and emmetropic children: *Optometry and Vision Science*, 1.

Reitsamer, H. A., Zawinka, C., & Branka, M. (2004). Dopaminergic vasodilation in the choroidal circulation by d1/d5 receptor activation. *Investigative Ophthalmology & Visual Science*, *45*(3), 900–905.

Ribelayga, C., & Mangel, S. C. (2005). A circadian clock and light/dark adaptation differentially regulate adenosine in the mammalian retina [Publisher: Society for Neu-

roscience Section: Behavioral/Systems/Cognitive]. *Journal of Neuroscience*, *25*(1), 215–222.

Robinson, K. A., Sun, M., Barnum, C. E., Weiss, S. N., Huegel, J., Shetye, S. S., Lin, L., Saez, D., Adams, S. M., Iozzo, R. V., Soslowsky, L. J., & Birk, D. E. (2017). Decorin and biglycan are necessary for maintaining collagen fibril structure, fiber realignment, and mechanical properties of mature tendons. *Matrix Biology*, *64*, 81–93.

Rohrer, B., Spira, A. W., & Stell, W. K. (1993). Apomorphine blocks form-deprivation myopia in chickens by a dopamine d 2 -receptor mechanism acting in retina or pigmented epithelium. *Visual Neuroscience*, *10*(3), 447–453.

Rose, K. A., Morgan, I. G., Ip, J., Kifley, A., Huynh, S., Smith, W., & Mitchell, P. (2008). Outdoor activity reduces the prevalence of myopia in children [Number: 8]. *Ophthalmology*, *115*(8), 1279–1285.

Rotter, N., Tobias, G., Lebl, M., Roy, A. K., Hansen, M. C., Vacanti, C. A., & Bonassar, L. J. (2002). Age-related changes in the composition and mechanical properties of human nasal cartilage. *Archives of Biochemistry and Biophysics*, *403*(1), 132–140.

Roughley, P. J., & Mort, J. S. (2014). The role of aggrecan in normal and osteoarthritic cartilage. *Journal of Experimental Orthopaedics*, *1*(1), 8.

Roy, S., & Field, G. D. (2019). Dopaminergic modulation of retinal processing from starlight to sunlight [Number: 1]. *Journal of Pharmacological Sciences*, *140*(1), 86–93.

Rucker, F. (2019). Monochromatic and white light and the regulation of eye growth. *Experimental Eye Research*, *184*, 172–182.

Rymer, J., & Wildsoet, C. F. (2005). The role of the retinal pigment epithelium in eye growth regulation and myopia: A review. *Visual neuroscience*, *22*(3), 251–261.

Saari, J. C., Champer, R. J., Asson-Batres, M. A., Garwin, G. G., Huang, J., Crabb, J. W., & Milam, A. H. (1995). Characterization and localization of an aldehyde dehydrogenase to amacrine cells of bovine retina. *Visual Neuroscience*, *12*(2), 263–272.

Sato, T., Yoneyama, T., Kim, H. K., & Suzuki, T. A. (1987). Effect of dopamine and haloperidol on the c-wave and light peak of light-induced retinal responses in chick eye. *Documenta Ophthalmologica. Advances in Ophthalmology*, *65*(1), 87–95.

Saw, S.-M., Gazzard, G., Shih-Yen, E. C., & Chua, W.-H. (2005). Myopia and associated pathological complications [_eprint: https://onlinelibrary.wiley.com/doi/pdf/10.1111/j.1475-1313.2005.00298.x]. *Ophthalmic and Physiological Optics*, *25*(5), 381–391.

Schaeffel, F., Hagel, G., Bartmann, M., Kohler, K., & Zrenner, E. (1994). 6-hydroxy dopamine does not affect lens-induced refractive errors but suppresses deprivation myopia. *Vision research*, *34*(2), 143–149.

Schaeffel, F. (2008). Test systems for measuring ocular parameters and visual function in mice. *Frontiers in Bioscience: A Journal and Virtual Library*, *13*, 4904–4911.

Schaeffel, F., Bartmann, M., Hagel, G., & Zrenner, E. (1995). Studies on the role of the retinal dopamine/melatonin system in experimental refractive errors in chickens. *Vision Research*, *35*(9), 1247–1264.

Schaeffel, F., Burkhardt, E., Howland, H. C., & Williams, R. W. (2004). Measurement of refractive state and deprivation myopia in two strains of mice. *Optometry and Vision Science*, *81*(2), 99–110.

Schaeffel, F., & Feldkaemper, M. (2015). Animal models in myopia research. *Clinical and Experimental Optometry*, *98*(6), 507–517.

Schaeffel, F., Glasser, A., & Howland, H. C. (1988). Accommodation, refractive error and eye growth in chickens. *Vision Research*, *28*(5), 639–657.

Schaeffel, F., Howland, H. C., & Farkas, L. (1986). Natural accommodation in the growing chicken. *Vision Research*, *26*(12), 1977–1993.

Schindelin, J., Arganda-Carreras, I., Frise, E., Kaynig, V., Longair, M., Pietzsch, T., Preibisch, S., Rueden, C., Saalfeld, S., Schmid, B., Tinevez, J.-Y., White, D. J., Hartenstein, V., Eliceiri, K., Tomancak, P., & Cardona, A. (2012). Fiji: An open-source platform for biological-image analysis [Number: 7 Publisher: Nature Publishing Group]. *Nature Methods*, *9*(7), 676–682.

Schmid, K. L., & Wildsoet, C. F. (2004). Inhibitory effects of apomorphine and atropine and their combination on myopia in chicks. *Optometry and Vision Science*, *81*(2), 137–147.

Schmucker, C., & Schaeffel, F. (2004a). In vivo biometry in the mouse eye with low coherence interferometry. *Vision Research*, *44*(21), 2445–2456.

Schmucker, C., & Schaeffel, F. (2004b). A paraxial schematic eye model for the growing c57bl/6 mouse. *Vision Research*, *44*(16), 1857–1867.

Seko, Y., Shimokawa, H., Pang, J., & Tokoro, T. (2000). Disturbance of electrolyte balance in vitreous of chicks with form-deprivation myopia. *Japanese Journal of Ophthalmology*, *44*(1), 15–19.

Seko, Y., Shimizu, M., & Tokoro, T. (1998). Retinoic acid increases in the retina of the chick with form deprivation myopia. *Ophthalmic Research*, *30*(6), 361–367.

Seko, Y., Shimokawa, H., & Tokoro, T. (1996). In vivo and in vitro association of retinoic acid with form-deprivation myopia in the chick. *Experimental Eye Research*, *63*(4), 443–452.

Shen, L., Melles, R. B., Metlapally, R., Barcellos, L., Schaefer, C., Risch, N., Herrinton, L. J., Wildsoet, C., & Jorgenson, E. (2016). The association of refractive error with glaucoma in a multiethnic population. *Ophthalmology*, *123*(1), 92–101.

Shen, L., You, Q. S., Xu, X., Gao, F., Zhang, Z., Li, B., & Jonas, J. B. (2016). SCLERAL AND CHOROIDAL THICKNESS IN SECONDARY HIGH AXIAL MYOPIA. *Retina (Philadelphia, Pa.)*, *36*(8), 1579–1585.

Shen, W., Vijayan, M., & Sivak, J. G. (2005). Inducing form-deprivation myopia in fish. *Investigative Opthalmology & Visual Science*, *46*(5), 1797.

Shen, Z. L., Kahn, H., Ballarini, R., & Eppell, S. J. (2011). Viscoelastic properties of isolated collagen fibrils. *Biophysical Journal*, *100*(12), 3008–3015.

Shi, D., & Daly, J. W. (1999). Chronic effects of xanthines on levels of central receptors in mice. *Cellular and Molecular Neurobiology*, *19*(6), 719–732.

Siegwart, J. T., & Norton, T. T. (1999). Regulation of the mechanical properties of tree shrew sclera by the visual environment. *Vision Research*, *39*(2), 387–407.

Siegwart, J. T. J., & Norton, T. T. (2005). Selective regulation of MMP and TIMP mRNA levels in tree shrew sclera during minus lens compensation and recovery. *Investigative ophthalmology & visual science*, *46*(10), 3484–3492.

Siegwart, J. T. J., & Strang, C. E. (2007). Selective modulation of scleral proteoglycan mRNA levels during minus lens compensation and recovery. *Molecular vision*, *13*, 1878–1886.

Sinclair, G. B., & Helms, J. E. (2015). A review of simple formulae for elastic hoop stresses in cylindrical and spherical pressure vessels: What can be used when. *International Journal of Pressure Vessels and Piping*, *128*, 1–7.

Smith, E. L., Hung, L.-F., & Arumugam, B. (2014). Visual regulation of refractive development: Insights from animal studies. *Eye (London, England)*, *28*(2), 180–188.

Smith, E. L., Huang, J., Hung, L.-F., Blasdel, T. L., Humbird, T. L., & Bockhorst, K. H. (2009). Hemiretinal form deprivation: Evidence for local control of eye growth and

refractive development in infant monkeys. *Investigative Ophthalmology & Visual Science*, *50*(11), 5057–5069.

Smith, E. L., & Hung, L.-F. (2000). Form-deprivation myopia in monkeys is a graded phenomenon. *Vision Research*, *40*(4), 371–381.

Smith, E. L., Hung, L.-F., Arumugam, B., Holden, B. A., Neitz, M., & Neitz, J. (2015). Effects of long-wavelength lighting on refractive development in infant rhesus monkeys. *Investigative Ophthalmology & Visual Science*, *56*(11), 6490–6500.

Smith, E. L., Hung, L.-F., Arumugam, B., & Huang, J. (2013). Negative lens–induced myopia in infant monkeys: Effects of high ambient lighting. *Investigative Opthalmology & Visual Science*, *54*(4), 2959.

Smith, E. L., Hung, L.-F., & Huang, J. (2012). Protective effects of high ambient lighting on the development of form-deprivation myopia in rhesus monkeys. *Investigative Opthalmology & Visual Science*, *53*(1), 421.

Smith, E. L., Hung, L.-F., Huang, J., Blasdel, T. L., Humbird, T. L., & Bockhorst, K. H. (2010). Effects of optical defocus on refractive development in monkeys: Evidence for local, regionally selective mechanisms [Publisher: The Association for Research in Vision and Ophthalmology]. *Investigative Ophthalmology & Visual Science*, *51*(8), 3864–3873.

Smith, M. J., & Walline, J. J. (2015). Controlling myopia progression in children and adolescents. *Adolescent Health, Medicine and Therapeutics*, *6*, 133–140.

Smith, T. S. T., Frick, K. D., Holden, B. A., Fricke, T. R., & Naidoo, K. S. (2009). Potential lost productivity resulting from the global burden of uncorrected refractive error. *Bulletin of the World Health Organization*, *87*(6), 431–437.

Solouki, A. M., Verhoeven, V. J. M., van Duijn, C. M., Verkerk, A. J. M. H., Ikram, M. K., Hysi, P. G., Despriet, D. D. G., van Koolwijk, L. M., Ho, L., Ramdas, W. D., Czudowska, M., Kuijpers, R. W. A. M., Amin, N., Struchalin, M., Aulchenko, Y. S., van Rij, G., Riemslag, F. C. C., Young, T. L., Mackey, D. A., … Klaver, C. C. W. (2010). A genome-wide association study identifies a susceptibility locus for refractive errors and myopia at 15q14 [Bandiera_abtest: a Cg_type: Nature Research Journals Number: 10 Primary_atype: Research Publisher: Nature Publishing Group Subject_term: Comparative genomics;Eye manifestations;Gene regulation;Genome-wide association studies Subject_term_id: comparative-genomics;eye-manifestations;gene-regulation;genome-wide-association-studies]. *Nature Genetics*, *42*(10), 897–901.

Soltz, M. A., & Ateshian, G. A. (2000). A conewise linear elasticity mixture model for the analysis of tension-compression nonlinearity in articular cartilage. *Journal of Biomechanical Engineering*, *122*(6), 576–586.

Song, Y., Zhang, F., Zhao, Y., Sun, M., Tao, J., Liang, Y., Ma, L., Yu, Y., Wang, J., & Hao, J. (2016). Enlargement of the axial length and altered ultrastructural features of the sclera in a mutant lumican transgenic mouse model. [Number: 10]. *PloS one*, *11*(10), e0163165.

Soulhat, J., Buschmann, M. D., & Shirazi-Adl, A. (1999). A fibril-network-reinforced biphasic model of cartilage in unconfined compression. *Journal of Biomechanical Engineering*, *121*(3), 340.

Spinozzi, E., Baldassarri, C., Acquaticci, L., Del Bello, F., Grifantini, M., Cappellacci, L., & Riccardo, P. (2021). Adenosine receptors as promising targets for the management of ocular diseases. *Medicinal Chemistry Research*, *30*(2), 353–370.

Stewart, J. M., Schultz, D. S., Lee, O. T., & Trinidad, M. L. (2009). Exogenous collagen cross-linking reduces scleral permeability: Modeling the effects of age-related cross-link accumulation. *Investigative Ophthalmology and Visual Science*, *50*(1), 352–357.

Stone, R. A., Lin, T., Laties, A. M., & Iuvone, P. M. (1989). Retinal dopamine and form-deprivation myopia. *Proceedings of the National Academy of Sciences*, *86*(2), 704–706.

Stone, R. A., Cohen, Y., McGlinn, A. M., Davison, S., Casavant, S., Shaffer, J., Khurana, T. S., Pardue, M. T., & Iuvone, P. M. (2016). Development of experimental myopia in chicks in a natural environment. *Investigative Opthalmology & Visual Science*, *57*(11), 4779.

Stone, R. A., Pendrak, K., Sugimoto, R., Lin, T., Gill, A. S., Capehart, C., & Liu, J. (2006). Local patterns of image degradation differentially affect refraction and eye shape in chick. *Current Eye Research*, *31*(1), 91–105.

Strauss, O. (2005). The retinal pigment epithelium in visual function. *Physiological Reviews*, *85*(3), 845–881.

Strickland, R., Landis, E. G., & Pardue, M. T. (2020). Short-wavelength (violet) light protects mice from myopia through cone signaling. *Investigative Opthalmology & Visual Science*, *61*(2), 13.

Summers, J. A. (2013). The choroid as a sclera growth regulator. *Experimental Eye Research*, *114*, 120–127.

Summers, J. A. (2014). The sclera and its role in regulation of the refractive state. In R. F. Spaide, K. Ohno-Matsui, & L. A. Yannuzzi (Eds.), *Pathologic myopia* (pp. 87–104). Springer International Publishing.

Summers, J. A. (2019, May 15). *Retinoic acid in ocular growth regulation* [Publication Title: Vitamin A]. IntechOpen.

Summers, J. A., Cano, E. M., Kaser-Eichberger, A., & Schroedl, F. (2020). Retinoic acid synthesis by a population of choroidal stromal cells. *Experimental Eye Research*, *201*, 108252.

Summers, J. A., Harper, A. R., Feasley, C. L., Van-Der-Wel, H., Byrum, J. N., Hermann, M., & West, C. M. (2016). Identification of apolipoprotein a-i as a retinoic acid-binding protein in the eye. [Number: 36]. *The Journal of biological chemistry*, *291*(36), 18991–19005.

Summers, J. A., Schaeffel, F., Marcos, S., Wu, H., & Tkatchenko, A. V. (2021). Functional integration of eye tissues and refractive eye development: Mechanisms and pathways. *Experimental Eye Research*, *209*, 108693.

Summers Rada, J. A., & Hollaway, L. R. (2011). Regulation of the biphasic decline in scleral proteoglycan synthesis during the recovery from induced myopia. *Experimental Eye Research*, *92*(5), 394–400.

Sun, Y., Zhao, N., Liu, W., Liu, M., Ju, Z., Li, J., Cheng, Z., & Liu, X. (2018). Study of vesicular monoamine transporter 2 in myopic retina using [18f]FP-(+)-DTBZ [Number: 5]. *Molecular Imaging and Biology*, *20*(5), 771–779.

Svensson, L., Heineg, D., & Oldberg. (1995). Decorin-binding sites for collagen type i are mainly located in leucine-rich repeats 4-5 (□) [Publisher: Elsevier]. *Journal of Biological Chemistry*, *270*(35), 20712–20716.

Swiatczak, B., & Schaeffel, F. (2021). Emmetropic, but not myopic human eyes distinguish positive defocus from calculated blur. *Investigative Opthalmology & Visual Science*, *62*(3), 14.

Tao, Y., Pan, M., Liu, S., Fang, F., Lu, R., Lu, C., Zheng, M., An, J., Xu, H., Zhao, F., Chen, J.-f., Qu, J., & Zhou, X. (2013). cAMP level modulates scleral collagen remodeling, a critical step in the development of myopia [Publisher: Public Library of Science]. *PLOS ONE*, *8*(8), e71441.

Tedja, M. S., Haarman, A. E. G., Meester-Smoor, M. A., Kaprio, J., Mackey, D. A., Guggenheim, J. A., Hammond, C. J., Verhoeven, V. J. M., Klaver, C. C. W., & for the CREAM Consortium. (2019). IMI – myopia genetics report [Number: 3]. *Investigative Opthalmology & Visual Science*, *60*(3), M89.

Tedja, M. S., Wojciechowski, R., Hysi, P. G., Eriksson, N., Furlotte, N. A., Verhoeven, V. J. M., Iglesias, A. I., Meester-Smoor, M. A., Tompson, S. W., Fan, Q., Khawaja, A. P., Cheng, C.-Y., Höhn, R., Yamashiro, K., Wenocur, A., Grazal, C., Haller, T.,

Metspalu, A., Wedenoja, J., … Klaver, C. C. W. (2018). Genome-wide association meta-analysis highlights light-induced signaling as a driver for refractive error [Bandiera_abtest: a Cg_type: Nature Research Journals Number: 6 Primary_atype: Research Publisher: Nature Publishing Group Subject_term: Diseases;Genome-wide association studies;Medical research Subject_term_id: diseases;genome-wide-association-studies;medical-research]. *Nature Genetics*, *50*(6), 834–848.

Theodosiou, M., Laudet, V., & Schubert, M. (2010). From carrot to clinic: An overview of the retinoic acid signaling pathway. *Cellular and Molecular Life Sciences*, *67*(9), 1423–1445.

Thomson, K., Karouta, C., & Ashby, R. (2020a). Form-deprivation and lens-induced myopia are similarly affected by pharmacological manipulation of the dopaminergic system in chicks [Number: 12]. *Investigative Ophthalmology & Visual Science*, *61*(12), 4.

Thomson, K., Karouta, C., & Ashby, R. (2020b). Topical application of dopaminergic compounds can inhibit deprivation myopia in chicks. *Experimental Eye Research*, *200*, 108233.

Thomson, K., Morgan, I., Karouta, C., & Ashby, R. (2020). Levodopa inhibits the development of lens-induced myopia in chicks [Number: 1 Publisher: Nature Publishing Group]. *Scientific Reports*, *10*(1), 13242.

Thomson, K., Morgan, I., Kelly, T., Karouta, C., & Ashby, R. (2021). Coadministration with carbidopa enhances the antimyopic effects of levodopa in chickens [Number: 4 Publisher: The Association for Research in Vision and Ophthalmology]. *Investigative Ophthalmology & Visual Science*, *62*(4), 25–25.

Thorne, H. C., Jones, K. H., Peters, S. P., Archer, S. N., & Dijk, D.-J. (2009). Daily and seasonal variation in the spectral composition of light exposure in humans [Publisher: Taylor & Francis _eprint: https://doi.org/10.1080/07420520903044315]. *Chronobiology International*, *26*(5), 854–866.

Tideman, J. W. L., Snabel, M. C. C., Tedja, M. S., van Rijn, G. A., Wong, K. T., Kuijpers, R. W. A. M., Vingerling, J. R., Hofman, A., Buitendijk, G. H. S., Keunen, J. E. E., Boon, C. J. F., Geerards, A. J. M., Luyten, G. P. M., Verhoeven, V. J. M., & Klaver, C. C. W. (2016). Association of Axial Length With Risk of Uncorrectable Visual Impairment for Europeans With Myopia. *JAMA Ophthalmology*, *134*(12), 1355–1363.

Tkatchenko, T. V., Shen, Y., & Tkatchenko, A. V. (2010). Mouse experimental myopia has features of primate myopia. *Investigative Ophthalmology & Visual Science*, *51*(3), 1297–1303.

Tkatchenko, T. V., Troilo, D., Benavente-Perez, A., & Tkatchenko, A. V. (2018). Gene expression in response to optical defocus of opposite signs reveals bidirectional mechanism of visually guided eye growth [Publisher: Public Library of Science]. *PLOS Biology*, *16*(10), e2006021.

Torii, H., Kurihara, T., Seko, Y., Negishi, K., Ohnuma, K., Inaba, T., Kawashima, M., Jiang, X., Kondo, S., Miyauchi, M., Miwa, Y., Katada, Y., Mori, K., Kato, K., Tsubota, K., Goto, H., Oda, M., Hatori, M., & Tsubota, K. (2017). Violet light exposure can be a preventive strategy against myopia progression. *EBioMedicine*, *15*, 210–219.

Tran, N., Chiu, S., Tian, Y., & Wildsoet, C. F. (2008). The significance of retinal image contrast and spatial frequency composition for eye growth modulation in young chicks. *Vision Research*, *48*(15), 1655–1662.

Trier, K., Olsen, E. B., Kobayashi, T., & Ribel-Madsen, S. M. (1999). Biochemical and ultrastructural changes in rabbit sclera after treatment with 7-methylxanthine, theobromine, acetazolamide, or l-ornithine. *The British Journal of Ophthalmology*, *83*(12), 1370–1375.

Trier, K., Munk Ribel-Madsen, S., Cui, D., & Brøgger Christensen, S. (2008). Systemic 7-methylxanthine in retarding axial eye growth and myopia progression: A 36-month pilot study. *Journal of Ocular Biology, Diseases, and Informatics*, *1*(2), 85.

Troilo, D., & Wallman, J. (1991). The regulation of eye growth and refractive state: An experimental study of emmetropization. *Vision Research*, *31*(7), 1237–1250.

Troilo, D., Gottlieb, M. D., & Wallman, J. (1987). Visual deprivation causes myopia in chicks with optic nerve section. *Current Eye Research*, *6*(8), 993–999.

Troilo, D., & Nickla, D. L. (2005). The response to visual form deprivation differs with age in marmosets. *Investigative Opthalmology & Visual Science*, *46*(6), 1873.

Troilo, D., Nickla, D. L., Mertz, J. R., & Rada, J. A. S. (2006). Change in the synthesis rates of ocular retinoic acid and scleral glycosaminoglycan during experimentally altered eye growth in marmosets [Publisher: The Association for Research in Vision and Ophthalmology]. *Investigative Ophthalmology & Visual Science*, *47*(5), 1768–1777.

Troilo, D., Smith, E. L., Nickla, D. L., Ashby, R., Tkatchenko, A. V., Ostrin, L. A., Gawne, T. J., Pardue, M. T., Summers, J. A., Kee, C.-s., Schroedl, F., Wahl, S., & Jones, L. (2019). IMI – report on experimental models of emmetropization and myopia [Publisher: The Association for Research in Vision and Ophthalmology]. *Investigative Ophthalmology & Visual Science*, *60*(3), M31–M88.

Upadhyay, A., & Beuerman, R. W. (2020). Biological mechanisms of atropine control of myopia. *Eye & Contact Lens*, *46*(3), 129–135.

Verhoeven, V. J. M., Hysi, P. G., Wojciechowski, R., Fan, Q., Guggenheim, J. A., Höhn, R., MacGregor, S., Hewitt, A. W., Nag, A., Cheng, C.-Y., Yonova-Doing, E., Zhou, X., Ikram, M. K., Buitendijk, G. H. S., McMahon, G., Kemp, J. P., Pourcain, B. S., Simpson, C. L., Mäkelä, K.-M., … Hammond, C. J. (2013). Genome-wide meta-analyses of multiancestry cohorts identify multiple new susceptibility loci for refractive error and myopia. *Nature Genetics*, *45*(3), 314–318.

Vishweswaraiah, S., Swierkowska, J., Ratnamala, U., Mishra, N. K., Guda, C., Chettiar, S. S., Johar, K. R., Mrugacz, M., Karolak, J. A., Gajecka, M., & Radhakrishna, U. (2019). Epigenetically dysregulated genes and pathways implicated in the pathogenesis of non-syndromic high myopia [Bandiera_abtest: a Cc_license_type: cc_by Cg_type: Nature Research Journals Number: 1 Primary_atype: Research Publisher: Nature Publishing Group Subject_term: DNA methylation;Predictive markers Subject_term_id: dna-methylation;predictive-markers]. *Scientific Reports*, *9*(1), 4145.

Vitale, S., Sperduto, R. D., & Ferris, F. L. (2009). Increased prevalence of myopia in the united states between 1971-1972 and 1999-2004 [Number: 12]. *Archives of Ophthalmology (Chicago, Ill.: 1960)*, *127*(12), 1632–1639.

Wagner, E., McCaffery, P., Mey, J., Farhangfar, F., Applebury, M. L., & Dräger, U. C. (1997). Retinoic aid increases arrestin mRNA levels in the mouse retina. *The FASEB Journal*, *11*(4), 271–275.

Wallman, J., Gottlieb, M. D., Rajaram, V., & Fugate-Wentzek, L. A. (1987). Local retinal regions control local eye growth and myopia. *Science (New York, N.Y.)*, *237*(4810), 73–77.

Wallman, J., Turkel, J., & Trachtman, J. (1978). Extreme myopia produced by modest change in early visual experience. *Science*, *201*(4362), 1249–1251.

Wallman, J., Wildsoet, C., Xu, A., Gottlieb, M. D., Nickla, D. L., Marran, L., Krebs, W., & Christensen, A. M. (1995). Moving the retina: Choroidal modulation of refractive state. *Vision Research*, *35*(1), 37–50.

Wang, G., & Chen, W. (2012). Effects of mechanical stimulation on viscoelasticity of rabbit scleral fibroblasts after posterior scleral reinforcement. *Experimental biology and medicine (Maywood, N.J.)*, *237*(10), 1150–1154.

Wang, K., Read, A. T., Sulchek, T., & Ethier, C. R. (2017). Trabecular meshwork stiffness in glaucoma. *Experimental Eye Research*, *158*, 3–12.

Wang, M., Aleman, A. C., & Schaeffel, F. (2019). Probing the potency of artificial dynamic ON or OFF stimuli to inhibit myopia development. *Investigative Opthalmology & Visual Science*, *60*(7), 2599.

Wang, M., Schaeffel, F., Jiang, B., & Feldkaemper, M. (2018). Effects of light of different spectral composition on refractive development and retinal dopamine in chicks. *Investigative Opthalmology & Visual Science*, *59*(11), 4413.

Wang, S., Liu, S., Mao, J., & Wen, D. (2014). Effect of retinoic acid on the tight junctions of the retinal pigment epithelium-choroid complex of guinea pigs with lens-induced myopia in vivo [Publisher: Spandidos Publications]. *International Journal of Molecular Medicine*, *33*(4), 825–832.

Wang, S., & Larin, V. K. (2014). Shear wave imaging optical coherence tomography (SWI-OCT) for ocular tissue biomechanics. *Optics Letters*, *39*(1), 41.

Ward, A. H., Norton, T. T., Huisingh, C. E., & Gawne, T. J. (2018). The hyperopic effect of narrow-band long-wavelength light in tree shrews increases non-linearly with duration. *Vision Research*, *146-147*, 9–17.

Ward, A. H., Siegwart, J. T., Frost, M. R., & Norton, T. T. (2017). Intravitreally-administered dopamine d2-like (and d4), but not d1-like, receptor agonists reduce form-deprivation myopia in tree shrews. *Visual Neuroscience*, *34*, E003.

Watanabe, S., Yamashita, T., & Ohba, N. (1999). A longitudinal study of cycloplegic refraction in a cohort of 350 japanese schoolchildren. cycloplegic refraction. *Ophthalmic & Physiological Optics: The Journal of the British College of Ophthalmic Opticians (Optometrists)*, *19*(1), 22–29.

Watson, P. G., & Young, R. D. (2004). Scleral structure, organisation and disease. A review. *Experimental Eye Research*, *78*(3), 609–623.

Weiler, R., He, S., & Vaney, D. I. (1999). Retinoic acid modulates gap junctional permeability between horizontal cells of the mammalian retina: Retinoic acid and gap junction coupling. *European Journal of Neuroscience*, *11*(9), 3346–3350.

Weiler, R., Pottek, M., He, S., & Vaney, D. I. (2000). Modulation of coupling between retinal horizontal cells by retinoic acid and endogenous dopamine. *Brain Research Reviews*, *32*(1), 121–129.

Weiler, R., Schultz, K., Pottek, M., Tieding, S., & Janssen-Bienhold, U. (1998). Retinoic acid has light-adaptive effects on horizontal cells in the retina. *Proceedings of the National Academy of Sciences*, *95*(12), 7139–7144.

Westfall, P. H., & Tobias, R. D. (2007). Multiple testing of general contrasts [Publisher: Taylor & Francis _eprint: https://doi.org/10.1198/016214506000001338]. *Journal of the American Statistical Association*, *102*(478), 487–494.

Wiesel, T. N., & Raviola, E. (1977). Myopia and eye enlargement after neonatal lid fusion in monkeys [Number: 5597 Publisher: Nature Publishing Group]. *Nature*, *266*(5597), 66–68.

Wildsoet, C., & Wallman, J. (1995). Choroidal and scleral mechanisms of compensation for spectacle lenses in chicks. *Vision Research*, *35*(9), 1175–1194.

Wildsoet, C. F., & Pettigrew, J. D. (1988a). Kainic acid-induced eye enlargement in chickens: Differential effects on anterior and posterior segments. | IOVS | ARVO Journals. *Investigative Ophthalmology & Visual Science*, *29*(2), 311–319.

Wildsoet, C., & Pettigrew, J. (1988b). Experimental myopia and anamalous eye growth patterns unaffected by optic nerve section in chickens: Evidence for local control of eye growth. *Clinical Vision Sciences*, *3*(2), 99–107.

Wildsoet, C. (2003). Neural pathways subserving negative lens-induced emmetropization in chicks–insights from selective lesions of the optic nerve and ciliary nerve. *Current Eye Research*, *27*(6), 371–385.

Wildsoet, C. F., Chia, A., Cho, P., Guggenheim, J. A., Polling, J. R., Read, S., Sankaridurg, P., Saw, S.-M., Trier, K., Walline, J. J., Wu, P.-C., & Wolffsohn, J. S. (2019). IMI – interventions for controlling myopia onset and progression report. *Investigative Opthalmology & Visual Science*, *60*(3), M106.

Wioland, N., Rudolf, G., & Bonaventure, N. (1990). Electrooculographic and electroretinographic study in the chicken after dopamine and haloperidol. *Documenta ophthalmologica*, *75*(2), 175–180.

Witkovsky, P. (2004). Dopamine and retinal function. *Documenta Ophthalmologica*, *108*(1), 17–39.

Worthington, K. S., Wiley, L. A., Bartlett, A. M., Stone, E. M., Mullins, R. F., Salem, A. K., Guyman, C. A., & Tucker, B. A. (2014). Mechanical properties of murine and porcine ocular tissues in compression. *Experimental Eye Research*, *46*(2), 220–231.

Wu, H., Chen, W., Zhao, F., Zhou, Q., Reinach, P. S., Deng, L., Ma, L., Luo, S., Srinivasalu, N., Pan, M., Hu, Y., Pei, X., Sun, J., Ren, R., Xiong, Y., Zhou, Z., Zhang, S., Tian, G., Fang, J., … Zhou, X. (2018). Scleral hypoxia is a target for myopia control. *Proceedings of the National Academy of Sciences of the United States of America*, *115*(30), E7091–E7100.

Wu, P.-C., Tsai, C.-L., Wu, H.-L., Yang, Y.-H., & Kuo, H.-K. (2013). Outdoor activity during class recess reduces myopia onset and progression in school children. *Ophthalmology*, *120*(5), 1080–1085.

Wu, X.-H., Li, Y.-Y., Zhang, P.-P., Qian, K.-W., Ding, J.-H., Hu, G., Weng, S.-J., Yang, X.-L., & Zhong, Y.-M. (2015). Unaltered retinal dopamine levels in a c57bl/6 mouse model of form-deprivation myopia [Number: 2 Publisher: The Association for Research in Vision and Ophthalmology]. *Investigative Ophthalmology & Visual Science*, *56*(2), 967–977.

Wu, X.-H., Qian, K.-W., Xu, G.-Z., Li, Y.-Y., Ma, Y.-Y., Huang, F., Wang, Y.-Q., Zhou, X., Qu, J., Yang, X.-L., Zhong, Y.-M., & Weng, S.-J. (2016). The role of retinal dopamine in c57bl/6 mouse refractive development as revealed by intravitreal administration of 6-hydroxydopamine [Number: 13]. *Investigative Opthalmology & Visual Science*, *57*(13), 5393.

Yan, T., Xiong, W., Huang, F., Zheng, F., Ying, H., Chen, J.-F., Qu, J., & Zhou, X. (2015). Daily injection but not continuous infusion of apomorphine inhibits form-deprivation myopia in mice [Number: 4]. *Investigative Ophthalmology & Visual Science*, *56*(4), 2475–2485.

Yan, Z., Wang, C., Chen, W., & Song, X. (2010). Biomechanical considerations: Evaluating scleral reinforcement materials for pathological myopia. *Canadian journal of ophthalmology. Journal canadien d'ophtalmologie*, *45*(3), 252–255.

Yang, M., & Taber, L. A. (1991). The possible role of poroelasticity in the apparent viscoelastic behavior of passive cardiac muscle. *Journal of Biomechanics*, *24*(7), 587–597.

Yang, X., Liu, X., Peng, J., Zheng, H., Lu, F., Gong, B., Zhao, G., Meng, Y., Guan, H., Ning, M., Yang, Z., & Shi, Y. (2014). Evaluation of MYOC, ACAN, HGF, and MET as candidate genes for high myopia in a han chinese population [Publisher: Mary Ann Liebert, Inc., publishers]. *Genetic Testing and Molecular Biomarkers*, *18*(6), 446–452.

Yasmin, Maskari, R. A., McEniery, C. M., Cleary, S. E., Li, Y., Siew, K., Figg, N. L., Khir, A. W., Cockcroft, J. R., Wilkinson, I. B., & O'Shaughnessy, K. M. (2018). The matrix proteins aggrecan and fibulin-1 play a key role in determining aortic stiffness [Bandiera_abtest: a Cc_license_type: cc_by Cg_type: Nature Research Journals Number: 1 Primary_atype: Research Publisher: Nature Publishing Group Subject_term: Genetics research;Medical research Subject_term_id: genetics-research;medical-research]. *Scientific Reports*, *8*(1), 8550.

Yu, M., Liu, W., Wang, B., & Dai, J. (2021). Short wavelength (blue) light is protective for lens-induced myopia in guinea pigs potentially through a retinoic acid–related

mechanism [Publisher: The Association for Research in Vision and Ophthalmology]. *Investigative Ophthalmology & Visual Science*, *62*(1), 21–21.

Zhang, D.-Q., Belenky, M. A., Sollars, P. J., Pickard, G. E., & McMahon, D. G. (2012). Melanopsin mediates retrograde visual signaling in the retina [Publisher: Public Library of Science]. *PLOS ONE*, *7*(8), e42647.

Zhang, D.-Q., Wong, K. Y., Sollars, P. J., Berson, D. M., Pickard, G. E., & McMahon, D. G. (2008). Intraretinal signaling by ganglion cell photoreceptors to dopaminergic amacrine neurons [Number: 37]. *Proceedings of the National Academy of Sciences of the United States of America*, *105*(37), 14181–14186.

Zhang, H., Wong, C. L., Shan, S. W., Li, K. K., Cheng, A. K., Lee, K. L., Ge, J., To, C. H., & Do, C. W. (2011). Characterisation of cl transporter and channels in experimentally induced myopic chick eyes. *Clinical & Experimental Optometry*, *94*(6), 528–535.

Zhang, S., Yang, J., Reinach, P. S., Wang, F., Zhang, L., Fan, M., Ying, H., Pan, M., Qu, J., & Zhou, X. (2018). Dopamine receptor subtypes mediate opposing effects on form deprivation myopia in pigmented guinea pigs [Number: 11]. *Investigative Opthalmology & Visual Science*, *59*(11), 4441.

Zhang, Y., & Wildsoet, C. F. (2015). RPE and choroid mechanisms underlying ocular growth and myopia. *Progress in molecular biology and translational science*, *134*, 221–240.

Zhang, Y., Hu, D.-N., Zhu, Y., Sun, H., Gu, P., Zhu, D., & Zhou, J. (2017). Regulation of matrix metalloproteinase-2 secretion from scleral fibroblasts and retinal pigment epithelial cells by miR-29a. *BioMed research international*, *2017*, 2647879.

Zhao, F., Zhang, D., Zhou, Q., Zhao, F., He, M., Yang, Z., Su, Y., Zhai, Y., Yan, J., Zhang, G., Xue, A., Tang, J., Han, X., Shi, Y., Zhu, Y., Liu, T., Zhuang, W., Huang, L., Hong, Y., … Zhou, X. (2020). Scleral HIF-1α is a prominent regulatory candidate for genetic and environmental interactions in human myopia pathogenesis. *EBioMedicine*, *57*, 102878.

Zhao, F., Zhou, Q., Reinach, P. S., Yang, J., Ma, L., Wang, X., Wen, Y., Srinivasalu, N., Qu, J., & Zhou, X. (2018). Cause and effect relationship between changes in scleral matrix metallopeptidase-2 expression and myopia development in mice. *The American Journal of Pathology*, *188*(8), 1754–1767.

Zhao, X., Wong, K. Y., & Zhang, D.-Q. (2017). Mapping physiological inputs from multiple photoreceptor systems to dopaminergic amacrine cells in the mouse retina [Number: 1 Publisher: Nature Publishing Group]. *Scientific Reports*, *7*(1), 7920.

Zhou, X., Huang, Q., An, J., Lu, R., Qin, X., Jiang, L., Li, Y., Wang, J., Chen, J., & Qu, J. (2010). Genetic deletion of the adenosine a2a receptor confers postnatal development of relative myopia in mice [Publisher: The Association for Research in Vision and Ophthalmology]. *Investigative Ophthalmology & Visual Science*, *51*(9), 4362–4370.

Zhou, X., Pardue, M. T., Iuvone, P. M., & Qu, J. (2017). Dopamine signaling and myopia development: What are the key challenges. *Progress in Retinal and Eye Research*, *61*, 60–71.

Zhou, X., Zhang, S., Yang, F., Yang, Y., Huang, Q., Huang, C., Qu, J., & Zhou, X. (2021). Decreased choroidal blood perfusion induces myopia in guinea pigs. *Investigative Ophthalmology & Visual Science*, *62*(15), 30.

Zhu, S.-Q., Pan, A.-P., Zheng, L.-Y., Wu, Y., & Xue, A.-Q. (2018). Posterior scleral reinforcement using genipin-cross-linked sclera for macular hole retinal detachment in highly myopic eyes. *The British journal of ophthalmology*, *102*(12), 1701–1704.

Zhuola, Z., Barrett, S., Kharaz, Y. A., & Akhtar, R. (2018). Nanostructural and mechanical changes in the sclera following proteoglycan depletion [Number: 2]. *Modeling and Artificial Intelligence in Ophthalmology*, *2*(2), 14–17.